

# Universidade de Vigo

**Escuela Internacional de Doctorado**

Rogert Sorí Gómez

TESIS DE DOCTORADO

Atmospheric moisture transport: the bridge between ocean  
evaporation and hydrological extremes in major tropical river  
basins

Dirigida por:

Dr. Luis Gimeno Presa  
Dra. Raquel Olalla Nieto Muñiz

2018

“Mención Internacional”

# Universidade de Vigo

## Escola Internacional de Doutoramento

Luis Gimeno Presa y Raquel-Olalla Nieto Muñiz

FAI CONSTAR que o presente traballo, titulado “*Atmospheric moisture transport: the bridge between ocean evaporation and hydrological extremes in major tropical river basins*” que presenta Rogert Sorí Gómez para a obtención do título de Doutor, foi elaborado baixo a súa dirección no programa de doutoramento “*Marine Sciences, Technology and Management (DO\*MAR)*” interuniversitario das Universidades de Vigo, Santiago de Compostela, e da Coruña de España, e as Universidades de Aveiro, Minho e Tras os Montes e Alto Douro de Portugal.

Ourense, 10 de setembro de 2018

O/A Director/a da tese de doutoramento

Dr. Luis Gimeno Presa

Dra. Raquel Olalla Nieto Muñiz

## **Agradecimientos / Acknowledgements**

Agradezco en primer lugar al Dr. Luis Gimeno por confiar en mí y darme la oportunidad de comenzar este proyecto de Doctorado. A él y a la Dra. Raquel Nieto agradezco también por su orientación, comprensión, confianza y conocimientos aportados a lo largo de estos más de tres años de trabajo.

Mi agradecimiento es también para aquellos con quienes he compartido cada día en la Universidad y fuera de ella: Marta, Milica, Iago, Dejanira, Danica, Lucía, Victor, Xurxo, Mojtaba, Zeinab, Jorge, Aleksander y Elham. Cada uno ha contribuido de una forma u otra en mi trabajo, así como han hecho de mi estancia en Ourense una experiencia excepcional. Un especial agradecimiento a la Dra. Anita Drumond por su amistad, consejos y ayuda para la realización de cada trabajo. Agradezco también a: Orlando, Ángel, al Dr. Moncho y la Dra. Maite por su cordialidad y apoyo; a todo el grupo EPhysLab, donde he trabajado estos años.

Durante mi estancia en España he recibido ayuda de varias personas. Dos imprescindibles por su amistad y cariño han sido Mari Carmen Rivela y Mirna González.

Doy gracias a mis padres Concepción y Rogelio, a mi hermano Robert y a mis abuelos, en especial Conchita y Armando, por su cariño y apoyo absoluto. A mis tíos, tías, primos-hermanos y en general a toda mi familia.

Este trabajo se ha ejecutado gracias al financiamiento recibido de la Xunta de Galicia a través del Plan galego de investigación, innovación e crecemento 2011–2015 (Plan I2C). De igual forma se recibió apoyo del Campus Internacional do Mar de la Universidad de Vigo; del proyecto ED413C 2017/64 “Programa de Consolidacion e Estructuracion de Unidades de Investigacion Competitivas (Grupos de Referencia Competitiva)” co-funded by European Regional Development Fund (FEDER) y el proyecto SETH CGL2014-60849-JIN financiado por el Gobierno de España y el Fondo Regional Europea para el Desarrollo de la Comisión Europea (FEDER).

# CONTENTS

<b>ABSTRACT .....</b>	<b>i</b>
<b>LIST OF FIGURES.....</b>	<b>xii</b>
<b>LIST OF TABLES.....</b>	<b>xiv</b>
<b>LIST OF ACRONYMS .....</b>	<b>xv</b>
<b>INTRODUCTION .....</b>	<b>1</b>
1.1 The Hydrological Cycle in the Climate System .....	1
1.1.1 The Hydrological Cycle in humid tropics.....	3
1.2 Problem overview .....	6
<b>2. OBJECTIVES.....</b>	<b>8</b>
<b>3. METHODOLOGY .....</b>	<b>10</b>
3.1 The model FLEXPART.....	10
3.1.1 Identification of moisture sources and sinks with FLEXPART.....	12
3.1.2 Methods for diagnosing the atmospheric branch of the hydrological cycle: FLEXPART advantages .....	15
3.2 Identification of the onset and demise of the rainy season.....	18
3.3 Identification of dry and wet conditions.....	19
3.3.1 Meteorological drought Indices.....	19
3.3.1.1 The Standardized Precipitation-Evapotranspiration Index (SPEI).....	21
3.3.1.2 Computation of the SPEI.....	21
3.3.2 Hydrological Drought Indices .....	23
3.3.2.1 The Standardised Streamflow Index (SSI).....	24
3.3.2.2 Computation of the Standardised Streamflow Index (SSI).....	25
3.4 Tropical River Basins analysed in this Study.....	25
3.5 Datasets.....	26

3.5.1 FLEXPART inputs .....	26
3.5.2 SPEI inputs .....	27
3.5.3 Other datasets .....	27
<b>4.SET OF PUBLICATIONS.....</b>	<b>30</b>
<b>5.CONCLUSIONS.....</b>	<b>140</b>
<b>APPENDIX A: SUPPLEMENTARY MATERIAL .....</b>	<b>146</b>
<b>REFERENCES .....</b>	<b>147</b>

## **RESUMEN/ABSTRACT**

El ciclo hidrológico o ciclo del agua, constituye una sucesión de fases por las que pasa el agua en su movimiento de la atmósfera a la Tierra y en su retorno a la misma: evaporación del agua del suelo, del mar y de las aguas continentales, condensación en forma de nubes, precipitación, acumulación en el suelo o en masas de agua y reevaporación (WMO, 2012). El transporte de humedad en la atmósfera constituye la rama atmosférica del ciclo hidrológico y es considerado el puente entre la evaporación oceánica y la precipitación sobre continentes. Sin embargo, estudios locales, regionales y globales demuestran la importancia de la evaporación terrestre para la precipitación continental mediante procesos de reciclaje de humedad. El estudio de la rama atmosférica del ciclo hidrológico permite identificar el origen de la humedad que contribuye a la precipitación sobre una determinada región. De esta forma, numerosos estudios han investigado el origen de la precipitación continental e identificado las regiones fuentes de humedad más importantes. La identificación de regiones fuentes de humedad constituye un reto para las ciencias atmosféricas y un paso inicial para comprender mejor la variabilidad de la precipitación y la ocurrencia de eventos extremos como sequías e inundaciones Gimeno et al., (2010). El objetivo de este trabajo, consistió en investigar el rol de la rama atmosférica del ciclo hidrológico en la relación fuente – sumidero de humedad en grandes cuencas de ríos tropicales como las cuencas de los ríos Congo y Níger en África, los ríos Negro y Madeira en la región amazónica de América del Sur, e Indus, Ganges y Brahmaputra en el sudeste de Asia. Localizadas a lo largo de la región ecuatorial-tropical, la circulación atmosférica que controla el clima en estas cuencas se caracteriza por una inversión estacional de la dirección del viento debido al calentamiento asimétrico entre los continentes y los océanos. Esto provoca un régimen de clima monzónico que se identifica por intensas lluvias durante la estación lluviosa con respecto a las precipitaciones sobre otras cuencas de ríos localizadas a lo largo de las mismas latitudes durante esta estación. De igual forma, se propuso investigar el impacto de la variabilidad de la contribución de humedad desde regiones fuentes en la ocurrencia de condiciones húmedas y/o secas en las cuencas.

La sequía meteorológica es consecuencia de la ausencia prolongada o escasez acusada de precipitación (WMO, 2012) que pueden afectar zonas de gran extensión. Su ocurrencia, que está determinada por parámetros como la duración, severidad e intensidad, da origen

a restantes tipos de sequía como la sequía hidrológica, agrícola y socioeconómica, siendo uno de los fenómenos climáticos más complejos que afectan el planeta. Una preparación efectiva contra sus impactos requiere una capacidad adecuada para monitorear, entender y predecir este complejo fenómeno. La magnitud de sus impactos en regiones como las grandes cuencas de ríos tropicales, constituye un peligro para millones de habitantes que en ellas habitan y precisan de sus recursos.

En la metodología utilizada se utilizaron salidas globales del modelo de transporte lagrangiano FLEXPART v9.0 para rastrear hacia detrás o delante en el tiempo las masas de aire sobre las cuencas en estudio. FLEXPART utiliza datos del reanálisis ERA-Interim del Centro Europeo de Previsiones Meteorológicas a Plazo Medio (ECMWF, por sus siglas en inglés). Para ello se consideró la atmósfera homogéneamente distribuida en parcelas de 1° de longitud y latitud, aproximadamente 2 millones. Una ventaja de este modelo es que permite calcular a lo largo de las trayectorias y cada  $t$  estimados aquí establecidos de 6 horas, los cambios en la humedad específica en las parcelas a través del balance de evaporación ( $E$ ) menos precipitación ( $P$ ):  $(E - P)$ . En el análisis hacia detrás en el tiempo, la integración de  $(E - P)$  en la vertical desde 1000 hPa hasta 0.1 hPa permitió obtener el balance total de humedad, y con ello identificar las regiones donde la ganancia de humedad de una masa de aire era superior a la pérdida ( $(E - P) > 0$ ). Estas regiones se consideraron como fuentes de humedad para las cuencas. El método estadístico de percentiles se utilizó para determinar las regiones con valores de  $(E - P) > 0$  más intensos. Las fuentes se dividieron en oceánicas y continentales teniendo en cuenta la definición de áreas geográficas. Una vez definidas las principales fuentes de humedad para cada cuenca, se rastreó hacia delante en el tiempo las masas de aire sobre cada fuente para finalmente calcular sobre cada cuenca respectiva el balance de humedad integrado en la vertical. En este experimento, los valores de  $(E - P) < 0$  están asociados a una contribución de humedad desde la región de origen para la precipitación sobre las cuencas. Los valores de  $(E - P) < 0$  fueron correlacionados con valores de precipitación en busca de determinar las mejores asociaciones. FLEXPART ha sido utilizado con el mismo objetivo para estudios en diversas regiones del planeta.

Las condiciones húmedas y/o secas se determinaron mediante el Índice Estandarizado de Precipitación – Evapotranspiración (SPEI por sus siglas en inglés) (Vicente-Serrano et al., 2012). Basado en la misma metodología que el Índice Estandarizado de Precipitación

(SPI, por sus siglas en inglés) propuesto por McKee et al., (1993), el SPEI posibilita obtener un balance hidrológico para varias escalas temporales. Esto permite determinar la escala temporal que mejor se ajusta al sistema en estudio. En la selección del SPEI, se tuvo en cuenta una gran ventaja sobre otros índices de sequía multiescalar como el SPI, y es que considera la influencia en la evapotranspiración potencial. Esta característica resultó crucial teniendo en cuenta la presencia de amplias extensiones de bosques húmedos tropicales en estas cuencas. La Amazonía, por ejemplo, es el bosque tropical más extenso del mundo seguido de la selva del Congo. En el conjunto de ecosistemas de estas cuencas los altos balances de energía influyen a favor de una interacción decisiva en la regulación del ciclo hidrológico. Algunos de los ríos más extensos de planeta: Los ríos Negro y Madeira, ambos afluentes del río Amazonas, y el Congo, Niger, Indus, Ganges y Brahmaputra fluyen a través de las cuencas en estudio. En este trabajo se ha utilizado un índice de sequía hidrológico, el Índice Estandarizado de Corriente Fluvial (SSI por sus siglas en inglés) (Vicente-Serrano et al., 2011), que permite monitorizar y cuantificar la intensidad de las sequías fluviales.

Una vez obtenidas las condiciones secas y/o húmedas en las cuencas, se determinaron las anomalías en la contribución de humedad desde las fuentes con el fin de determinar la región (o regiones) cuya disminución en la contribución de humedad estuvo asociada al déficit de precipitaciones sobre la cuenca. Un enfoque similar ha sido implementado por otros autores para objetivos similares. Para su implementación se consideró su utilidad para comprender mejor el ciclo hidrológico, pero fundamentalmente la novedad de que brinda para diagnosticar las causas de la ocurrencia de sequías o precipitaciones intensas.

Los resultados indicaron que la ganancia de humedad por masas de aire rastreadas hacia atrás en el tiempo desde cada cuenca, se produce fundamentalmente en los días 1 y 2 anteriores y especialmente sobre las propias cuencas. Este resultado está en consonancia con múltiples estudios que describen la importancia de los procesos de reciclaje de humedad en las regiones húmedas tropicales. La identificación de las fuentes se realizó a escala anual o estacional teniendo en cuenta el ciclo anual de la precipitación en cada cuenca. Para la cuenca del Congo se identificaron nueve regiones fuentes fundamentales, cuatro oceánicas y cinco terrestres. Las fuentes continentales se ubican en el centro y noreste de África, en la región continental al oeste de la cuenca dividida en dos por la desembocadura del río Congo, la región continental al este de la cuenca y que se extiende

desde el norte de Somalia y Etiopía hasta aproximadamente los 20°S, y la propia cuenca. En los océanos las fuentes resultaron delimitadas en el este del océano Atlántico Sur Tropical, en el oeste del océano Indico Sur tropical y el Mar Arábico además del Mar Rojo. Para las cuencas asiáticas, las fuentes de humedad más importantes para la precipitación son: en el continente asiático la región ubicada al oeste de las cuencas, la región de la India y las propias cuencas. Desde el océano estas cuencas reciben humedad desde el Océano Índico, particularmente desde el Mar Arábico y la Bahía de Bengala. La contribución de humedad desde el Mar Arábico y en su conjunto el Océano Indico occidental está asociada al incremento de la precipitación en el periodo monzónico.

Para la cuenca del Níger, las fuentes fueron identificadas para las estaciones seca y lluviosa. En el periodo seco (noviembre – abril) las fuentes oceánicas son: el océano Atlántico Norte Tropical adyacente a las costas occidentales de África, el océano Atlántico Sur al sur de la cuenca, el Mar Mediterráneo e incluso parte del Mar Rojo. En tierra, fueron delimitadas las regiones fuentes al oeste de la cuenca, al sur, al este y la propia cuenca se consideró como fuente de humedad para sí misma. La posición de las fuentes cambia poco en la estación lluviosa, aunque destaca el incremento en la extensión de la fuente oceánica del Atlántico Sur y la contribución desde el centro-ecuatorial de África y el océano Indico.

Las principales fuentes de la cuenca Negro en el norte de la cuenca Amazonas, recibe humedad desde el océano Atlántico tropical al norte y sur del Ecuador. Desde el continente recibe humedad desde la propia cuenca, el resto de la cuenta del Amazonas y el noreste de la cuenca. La cuenca Madeira recibe humedad igualmente desde las mismas regiones oceánicas y en el continente desde ella misma, el resto de la cuenca del Amazonas, y la región continental al sudeste de la cuenca y la región de los Andes.

Las masas de aire sobre las fuentes antes mencionadas se rastrearon hacia delante en el tiempo para calcular finalmente las pérdidas de humedad ( $(E - P) < 0$ ) sobre cada cuenca. Los valores obtenidos mostraron elevados valores de correlación con la precipitación sobre las cuencas. Una cuantificación de la contribución de humedad de las fuentes y las propias cuencas reveló que generalmente esta está vinculada a la distancia de transporte. En el caso particular de la cuenca del Congo, más del 50% del total de la contribución de humedad que recibe la cuenca proviene de sí misma; destacando la importancia del

reciclaje de humedad en esta zona del centro ecuatorial de África. La eficiencia de las fuentes que proporcionan humedad a esta cuenca depende de la tasa de evaporación terrestre y oceánica e influye en la cantidad de vapor de agua que se transporta hacia la cuenca, haciendo que las fuentes sean más o menos efectivas en términos de precipitación sobre la cuenca. De hecho, la variabilidad espacial en los patrones  $(E - P) < 0$  sobre la cuenca del Congo, obtenido en las masas de aire desde cada fuente independientemente, confirmó el vínculo entre la ubicación geográfica de las fuentes y la localización de los mayores sumideros de humedad sobre la cuenca, que están asociados con la circulación atmosférica. Estos patrones espaciales mostraron una buena correlación con la distribución de precipitación sobre la cuenca, lo que demuestra la capacidad de FLEXPART para reproducir la variabilidad temporal y espacial de la precipitación. En el resto de las cuencas y de acuerdo a las referencias consultadas se confirmó el importante papel del reciclaje de humedad en las regiones ecuatoriales tropicales. Los resultados también revelaron las escalas características concluyentes del transporte de humedad atmosférica asociadas a la circulación de los monzones de verano en América del Sur, el oeste de África y el sudeste asiático.

En la cuenca del Níger la influencia del transporte de humedad por vientos de región sur desde el Atlántico Sur durante el periodo monzónico (mayo-octubre) es determinante. Sin embargo, durante el periodo seco, la región noroeste del Atlántico Norte, África y el Mediterráneo juegan además un rol fundamental. Para las cuencas asiáticas el experimento de masas de aire rastreadas hacia delante reveló el importante papel de las regiones continentales en la contribución de humedad a la precipitación sobre la cuenca Indus y Ganges durante el periodo monzónico; durante el cual las fuentes oceánicas más importantes para la cuenca del río Brahmaputra son, la región del Mar Arábico y la Bahía de Bengala. Sin embargo, durante este periodo la principal fuente de humedad es el océano Indico para todas estas cuencas.

Las condiciones secas y húmedas en las cuencas identificadas mediante el SPEI fueron categorizadas de acuerdo al criterio de Mckee et al., (1993). En la cuenca del Congo se seleccionaron los años afectados por condiciones severamente y extremadamente secas para investigar la contribución de humedad desde las fuentes. Las anomalías de divergencia VIMF se calcularon como información complementaria para evaluar las condiciones dinámicas en la atmósfera. En el periodo 1980-2010, los años 1995 y 1996

fueron afectados por condiciones de sequía severa y extrema respectivamente, mientras que 1982 se caracterizó por condiciones severamente húmedas. El estado de la sequía hidrológica se evaluó en la estación hidrológica de Kinshasa y se determinó la escala temporal de mayor impacto de la sequía meteorológica en el régimen hidrológico del río Congo en esta localidad. El papel de las fuentes que proporcionaron humedad durante años con condiciones severa y extremadamente secas y húmedas confirmó el papel clave de la cuenca del Congo en la modulación del equilibrio hídrico en sí misma. Los resultados mostraron que durante los años húmedos (secos), la contribución de humedad de la propia cuenca a la precipitación sobre sí misma aumentó (disminuyó). En promedio, el balance de agua en la atmósfera sobre la cuenca no fue homogéneo durante estos años. Este resultado sugiere que la investigación del ciclo hidrológico no debería realizarse para toda la cuenca en su conjunto.

En la Cuenca del río Níger, condiciones secas prevalecieron durante los periodos 1982-1988, 1998-2002, y 2009-2011. Las estaciones bajo condiciones severas y extremadamente secas fueron afectadas al azar por la contribución de la humedad del Océano Atlántico Sur, que es la fuente oceánica más importante. La posición de la Zona de Convergencia Intertropical y su influencia en el tiempo de residencia del vapor de agua en la atmósfera pueden ser responsables de la respuesta desigual de la fuente del Atlántico Sur en estos casos extremos. Las anomalías en el flujo vertical integrado de humedad (VIMF, por sus siglas en inglés) y la radiación de onda larga saliente (OLR, por sus siglas en inglés) para cada caso apoyan los resultados previos.

El rol de las fuentes en la contribución de humedad para la ocurrencia de precipitación durante condiciones severas y extremadamente secas y húmedas en las cuencas del Indus, Ganges y Brahmaputra (IRB, GRB y BRB respectivamente), se evaluaron para los periodos (noviembre-abril) y (de mayo a octubre), este último asociado a la ocurrencia del monzón del sudeste asiático. Se confirmó el papel crucial de las fuentes de humedad más importantes (por ejemplo, la región de la India, el Océano Índico, la Bahía de Bengala y las propias cuencas) en proporcionar menos (más) humedad durante condiciones secas (húmedas) en los periodos (noviembre-abril) y (mayo a octubre). La contribución de humedad desde el Océano Indico es determinante para en el inicio del monzón, después del cual la contribución de humedad de las fuentes de humedad continentales se destaca.

Las condiciones secas y húmedas en la cuenca del río Amazonas no ocurrieron simultáneamente en toda su extensión durante el período de estudio. Sin embargo, la cuenca del río Negro y del río Madeira fueron simultáneamente afectadas por condiciones secas intensas en el periodo 2015-2016. Aquí se analizó el impacto de la sequía meteorológica en el nivel del agua de los ríos Negro y Madeira. A lo largo de los cinco episodios secos más severos en la cuenca del río Negro, las anomalías en la contribución del Océano Atlántico Norte Tropical principalmente, y el Océano Atlántico Sur Tropical, parecieron estar asociadas con la evolución temporal del SPEI. Esto también se observó para la cuenca del río Madeira, donde tanto las fuentes oceánicas como terrestres desempeñaron un papel importante. En promedio, los episodios estuvieron asociados a una reducción en la contribución de la humedad atmosférica desde las fuentes, y en anomalías positivas de divergencia del VIMF sobre las cuencas. La contribución de la humedad de las fuentes oceánicas modula el inicio y fin de la estación lluviosa. Sin embargo, para la cuenca del río Madeira, el transporte de humedad atmosférica desde el resto de la cuenca del Amazonas es crucial para la duración de la estación lluviosa. Durante "El Niño", generalmente ocurre una reducción (aumento) de la contribución de humedad a la cuenca del río Negro (cuenca del río Madeira; principalmente de abril a agosto) desde casi todas las fuentes, causando una disminución en la precipitación. En general, ocurre lo contrario durante "La Niña".

Este estudio investigó el papel del transporte de humedad atmosférica, como puente entre la evaporación en los océanos y la tierra, y finalmente la precipitación y etapas posteriores en el ciclo hidrológico en grandes cuencas fluviales tropicales afectadas por un régimen de clima monzónico. El enfoque de lagrangiano permitió el establecimiento de la relación fuente-sumidero de humedad atmosférica. Resultados y explicaciones más detalladas para cada cuenca hidrográfica se encuentran en los manuscritos. Este método resultó útil para comprender mejor el ciclo hidrológico y esencialmente, para diagnosticar las causas de las sequías.

El conjunto de resultados obtenidos como parte del trabajo de investigación desarrollado durante la realización de esta Tesis Doctoral se estructura en este documento de la siguiente forma. El Capítulo 1 describe una introducción general sobre el estado del arte de las investigaciones relativas al ciclo hidrológico y específicamente el transporte de humedad en la atmósfera. En el Capítulo 2 se plantean los objetivos. En el capítulo 3 se

describen los métodos y técnicas utilizados, pero además se citan, explican y comparan diferentes técnicas y métodos utilizados con los mismos fines por otros autores a nivel global. En el Capítulo 4 se incluye un compendio de cinco manuscritos redactados durante el periodo de doctorando. Finalmente, en el Capítulo 5 se exponen las Conclusiones seguido de los Apéndices y Referencias.

## ABSTRACT

The transport of moisture in the atmosphere is considered the bridge between the ocean and land evaporation and later the precipitation. This work aimed to investigate the role of the atmospheric branch of the hydrological cycle in the source-sink of moisture relationships for major tropical river basins, namely, the Congo and Niger in Africa, the Negro and Madeira in the Amazon region in South America, and the Indus, Ganges, and Brahmaputra in Southeast Asia. Besides their location along the tropical region, the atmospheric circulation controlling the climate in these basins is characterised by seasonal wind reversals due to asymmetric heating between the land and oceans causing a monsoonal regime that results in the heavy rainy season with respect to other tropical river basins.

For modelling the air masses trajectories, the Lagrangian particle dispersion model FLEXPART v9.0 was used with data from the reanalysis product ERA-Interim of the European Centre for Medium-range Weather Forecast (ECMWF). FLEXPART allow us to track backward in time atmospheric air masses over the basins while calculating changes in the specific humidity through the budget of evaporation minus precipitation ( $E - P$ ). This permitted the identification of the regions where the air masses uptake humidity before arriving at the basins. The spatial pattern of the ( $E - P$ ) provides the transport distance, but also the most important moisture sources according to the intensity of the ( $E - P$ )  $> 0$  values. The results indicated that moisture uptake principally occurs in the basins themselves, surrounding continental regions, and the oceanic regions in the Atlantic for the basins in the Amazon, in the Atlantic and the Indian Ocean for the African basins, and in the Indian Ocean for Asian River Basins. The Vertically Integrated Moisture Flux (VIMF) supports these results.

Once the sources were identified, the air masses over them were tracked forward in time to finally compute moisture loses ( $(E - P) < 0$ ) over the target basin that were considered to contribute to the precipitation. The moisture contribution from the sources and basins themselves revealed that the contribution is generally linked to the transport distance and supports documented information regarding the important role of moisture recycling in

tropical-equatorial regions. The results also revealed the conclusive characteristic scales of the atmospheric moisture transport for the South American, West African, and Indian Summer Monsoons.

Dry and wet conditions in the basins were identified through the Standardised Precipitation-Evapotranspiration Index (SPEI). We selected a few years affected by severe and extremely dry and/or wet conditions to investigate the moisture contribution from the sources. The VIMF divergence anomalies were calculated as complementary values to assess the dynamic conditions in the atmosphere. In the Congo River Basin (CRB), the hydrological drought conditions were quantified at the Kinshasa gauging station using the Standardised Streamflow Index (SSI) (Vicente-Serrano et al., 2012). Here was analysed the impact of meteorological drought on the hydrological regime. The role of the sources that provided moisture during years with extreme and severe conditions confirmed the key role of the Congo River Basin in modulating the water balance within itself. The results showed that during wet (dry) years, the contribution of moisture ( $(E-P)_{10} < 0$ ) from the CRB to precipitation over itself increased (decreased). On average, the water balance in the atmosphere over the CRB was not homogenous during these years, indicating a distinct role within itself. This result confirmed that research on the hydrological cycle should not be conducted for the entire basin as a whole.

In the Niger River Basin (NRB), seasons under severe and extremely dry conditions were randomly affected by the contribution of humidity from the South Atlantic Ocean, which is the most important oceanic source. The position of the Intertropical Convergence Zone and its influence on the residence time of the water vapour in the atmosphere may be responsible for the unequal response of the eastern South Atlantic Ocean for these extreme cases. Anomalies in the VIMF and the Outgoing Longwave Radiation (OLR) for each case support the previous results.

The roles of the sources in the moisture contribution to precipitation during severe and extremely dry and wet conditions in the Indus, Ganges, and Brahmaputra River Basins were assessed through the Westerly Precipitation Regime (WPR) (November–April) and Monsoonal Precipitation Regime (MPR) (May–October) composites. This confirmed the crucial role of the most important moisture sources (e.g., Indian region (IR); Indian Ocean (IO); Bay of Bengal (BB), and the basins themselves) in providing less (more) humidity

during dry (wet) conditions in both the WPR and MPR periods. The IO plays a crucial role on the Monsoon onset, after which the moisture contribution from continental moisture sources commence to play a fundamental role.

Dry and wet conditions within the Amazon River Basin did not typically occur simultaneously during the study period. However, the Negro River Basin (NeRB) and the Madeira River Basin (MRB) were simultaneously affected by intense dry conditions in 2015–2016. Here was analysed the impact of meteorological drought on the water level of Negro and Madeira rivers. Throughout the five most severe dry episodes in the NeRB, the anomalies in the contribution from the Tropical North Atlantic Ocean (TNA) principally, and the Tropical South Atlantic Ocean (TSA), seemed to be associated with the SPEI temporal evolution. This was also observed in the MRB, but both oceanic and terrestrial sources played an important role. On average, the episodes were associated with a reduction in atmospheric moisture contribution from the sources, and subsidence based on predominantly positive VIMF divergence anomalies over the basins. The moisture contribution from the oceanic sources modulates the rainy season onset and demise. However, for the MRB the atmospheric moisture transport from the rest of the Amazon basin is crucial for the rainy season length.

This study investigated the role of atmospheric moisture transport, as a bridge between evaporation in the oceans and the earth, and finally the precipitation and subsequent stages in the hydrological cycle in large tropical river basins affected by a monsoon climate regime. The Lagrangian approach allowed the establishment of the source-sink relationship of atmospheric moisture. The results and more detailed explanations for each river basin are found in the manuscripts. This method was useful to understand better the hydrological cycle and, essentially, to diagnose the causes of droughts.

## LIST OF FIGURES

**Figure 1.** The hydrological cycle. Estimates of the observed main water reservoirs (black numbers, in  $10^3 \text{ km}^3$ ) and the flow of moisture through the system (red numbers, in  $10^3 \text{ km}^3 \text{ yr}^{-1}$ ) for the period 2002–2008. Figure from Gimeno et al., (2012) adjusted from Trenberth et al., (2007, 2011)..... 2

**Figure 2.** Estimated values of the observed hydrological cycle using eight reanalyses for 2002–2008, with the exception of ERA-40 that began from 1990 (colour coded as given at the bottom of the figure). For the ocean-to-land water vapour transport, the three estimates given for each are (1) the actual transport estimated from the moisture budget (based on analysed winds and moisture), (2) E-P from the ocean, and (3) P-E from the land that should be identical. Units:  $1000 \text{ km}^3 \text{ yr}^{-1}$ . Figure from Gimeno et al., (2012), adapted from Trenberth et al., (2011)..... 3

**Figure 3.** a): Tropical regions of the world (from Peel et al., 2007) superimposed on the drainage basins (by Syvitski et al., 2014). b): The regional monsoon precipitation domains (green) defined by the regions in which the annual range of precipitation rates exceed  $2 \text{ mm/day}$  (or  $300 \text{ mm}$  per season), and the local summer precipitation exceeds 55 % of the total annual rainfall (adapted from Wang et al., 2012). The annual range is defined as May through September (MJJAS) precipitation minus the November through March (NDJFM) precipitation in the Northern Hemisphere, and the NDJFM minus the MJJAS precipitation in the Southern Hemisphere. Rectangular domains in black define the common areas for regional studies of monsoon areas and their names: North American Monsoon (NAM), South American Monsoon (SAM), West African Monsoon (WAM), and the Indian Summer Monsoon (ISM). The threshold value used in this map to distinguish the monsoon climates from the adjacent dry regions where the local summer precipitation was less than  $1 \text{ mm/day}$  (stippled, orange)..... 4

**Figure 4.** Schematic representation of the precipitation (P), evaporation (E), transpiration (T), runoff (R), groundwater flow (GF), and water level (WL) at the onset of the rainy season (time,  $t$ ) and after the demise ( $t = t + 1$ ) in a humid river basin..... 6

**Figure 5.** Schematic illustration of an air parcel that gains and loses moisture during its spatial and temporal journey (black dots) along with its trajectory (black line). The specific humidity content of the air parcel is given in blue for each time step. An identified evaporation event is illustrated in green and two precipitation events in red. Based on the time between the evaporation event and the final precipitation event (weighted by the effective contribution of the evaporated moisture to the final precipitation), the residence time can be calculated. From Läderach and Sodemann (2016)..... 13

**Figure 6.** Geographical location and extension of the Negro (red), Madeira (blue) within the Amazon (in grey), Congo (light green), Niger (orange), Indus (purple), Ganges (yellow), and Brahmaputra (pink) River Basins..... 26

## LIST OF TABLES

<b>Table 1.</b> Summary of the main strengths and weaknesses of the Numerical Eulerian and Lagrangian Water Vapour Tracer methods. Adapted from Gimeno et al., (2012).....	17
<b>Table 2.</b> Strengths and weaknesses of the three most popular meteorological drought indices. Adapted from Zargar et al., (2011) and from WMO & GWP (2016).....	20
<b>Table 3.</b> Drought classification based on the SPEI according to the initial definition of Mckee et al., (1993) for the SPI.....	23
<b>Table 4.</b> Strengths and weaknesses of popular hydrological drought indices. Adapted from WMO & GWP (2016).....	24
<b>Table 5.</b> Collection of datasets, sources, period and spatial resolution.....	28
<b>Table 6.</b> List of articles.....	32
<b>Table 7.</b> Summary of the impact and quality of the Journals.....	32

# LIST OF ACRONYMS

**The following abbreviations are used in this manuscript:**

AED	Atmospheric Evaporative Demand
BMF	Best Monthly Fit
BRB	Brahmaputra River Basin
CHIRPS	Climate Hazards Group InfraRed Precipitation with Station data
COSMO	Consortium for Small-scale Modeling
CRB	Congo River Basin
ECMWF	European Center for Medium-Range Weather Forecast
ENSO	El Niño Southern Oscillation
EPhysLAB	Environmental Physics Laboratory
FLEXPART	FLEXible PARTicle dispersion model
GRB	Ganges River Basin
GFS	Global Forecast System
GLEAM	Global Land Evaporation Amsterdam Model
GRDC	Global Runoff Data Centre
GWP	Global Water Partnership
IPCC	Intergovernmental Panel on Climate Change
IRB	Indus River Basin
ISM	Indian Summer Monsoon
ITCZ	Intertropical Convergence Zone
MD	Minimum Orthogonal Distance
MM5	Fifth-Generation Penn State/NCAR Mesoscale Model
MPR	Monsoonal Precipitation Regime
MRB	Madeira River Basin
NAM	North American Monsoon
NCEP	National Center for Environmental Prediction
NeRB	Negro River Basin
NOAA	National Oceanic Administration Agency
NRB	Niger River Basin
OAFLUX	Objectively Analyzed air-sea Fluxes

OLR	Outgoing Longwave Radiation
P	Precipitation
PDSI	Palmer Drought Severity Index
PET	Potential Evapotranspiration
PHDI	Palmer Hydrological Drought Index
SAM	South American Monsoon
SPEI	Standardized Precipitation-Evapotranspiration Index
SPI	Standardized Precipitation Index
SSI	Standardized Streamflow Index
SST	Sea Surface Temperature
WAM	West African Monsoon
VIMF	Vertical Integrated Moisture Flux
WMO	World Meteorological Organization
WRF	Weather Research Forecast
WPR	Westerly Precipitation Regime

# 1

## Introduction

### 1.1 The Hydrological Cycle in the Climate System

Water plays a crucial role in all aspects of life on Earth. A component of the climate system, the global hydrosphere consists of various reservoirs (subsystems) connected by a succession of stages through which water passes from the atmosphere to the Earth and returns to the atmosphere. This occurs through evaporation from the land, sea, or inland water, condensation to form clouds, precipitation, interception, infiltration, percolation, runoff, accumulation in the soil, or in bodies of water, and re-evaporation (World Meteorological Organization (WMO), 2012)). This complex scheme is called the “water cycle” or the “hydrological cycle” (Peixoto and Oort, 1992; WMO, 2012, Palazzi and Provenzale, 2016). The essence of the hydrological cycle overall is that water evaporates in one place(s) and precipitates in another. Generally, evaporation exceeds precipitation over the oceans allowing moisture to be transported by atmospheric winds onto land where the precipitation exceeds evapotranspiration and the runoff flows into rivers which discharges into the ocean, completing the cycle (Figure 1) (Trenberth et al., 2011). The importance of the oceans is unquestionable because they hold approximately 97% of the world’s water reserves (Baumgartner and Reichel, 1975). According to global climate dataset reanalyses, the majority of evaporation and also precipitation occurs over the oceans (Figure 2). Thus, oceans play a key role in the precipitation moisture supply over the continents (Gimeno et al., 2010). However, on average, 40% of the terrestrial precipitation originates from land evaporation (van der Ent et al., 2010). According to these authors, high regional recycling ratios occur over very wet areas such as the tropical forests of South America, Africa, and Southeast Asia.

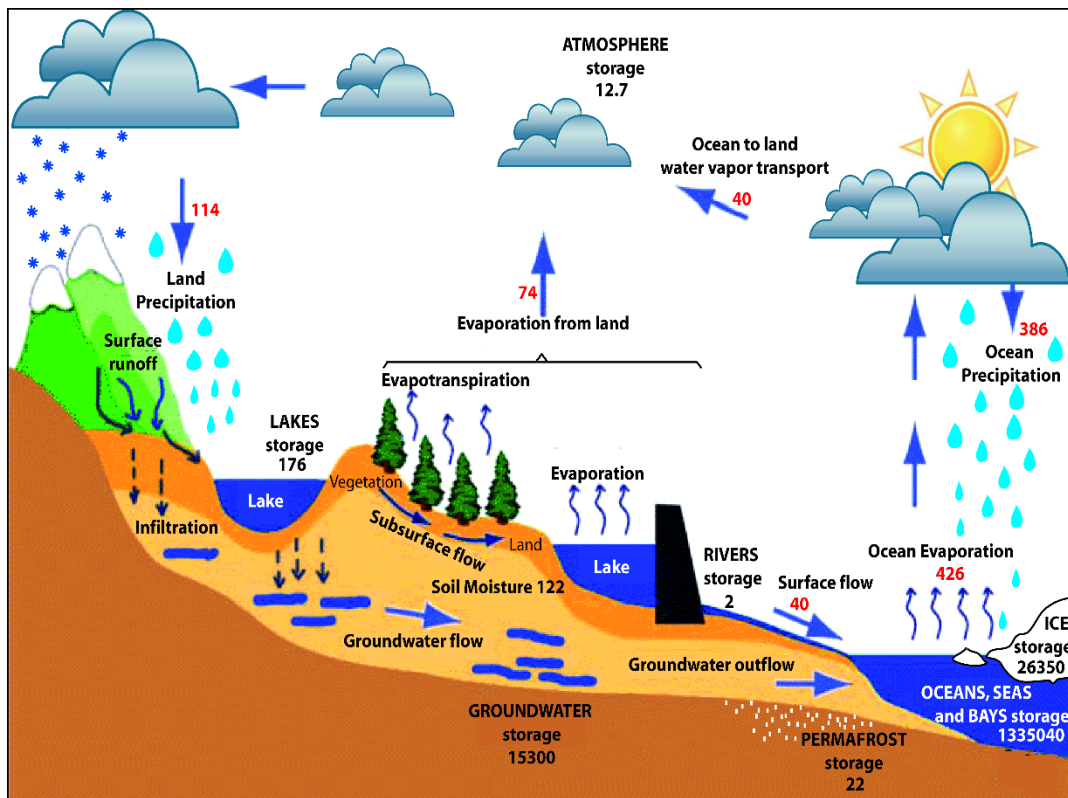


**Figure 1.** The hydrological cycle. Estimates of the observed main water reservoirs (black numbers, in 103 km<sup>3</sup>) and the flow of moisture through the system (red numbers, in 103 km<sup>3</sup> yr<sup>-1</sup>) for the period 2002–2008. Figure from Gimeno et al., (2012) adjusted from Trenberth et al., (2007, 2011).

Gimeno (2013) considered the identification of moisture sources a challenge for the atmospheric sciences. The atmospheric branch of the hydrological cycle transports the vapour, liquid, and solid water phases of the clouds by the general circulation of the atmosphere, and the terrestrial branch of the hydrological cycle is responsible for the surface and subterranean runoff (Peixoto and Oort, 1992). The atmospheric branch contains just a minor fraction of the Earth’s total water reserves and presents a crucial interface between the physical climate (such as large-scale rainfall patterns) and the ecosystems upon which human societies ultimately depend (Alan and Liepert, 2010). The interface is considered the bridge between the ocean evaporation and precipitation. Thus, researchers usually attempt to investigate the atmospheric branch of the hydrological cycle to establish the source-sink relationship of atmospheric moisture (e.g. Stohl and

James, 2004, 2005; Dirmeyer et al., 2009; Sodemann and Stohl, 2009; Gimeno et al., 2010, 2012; van der Ent et al., 2010).

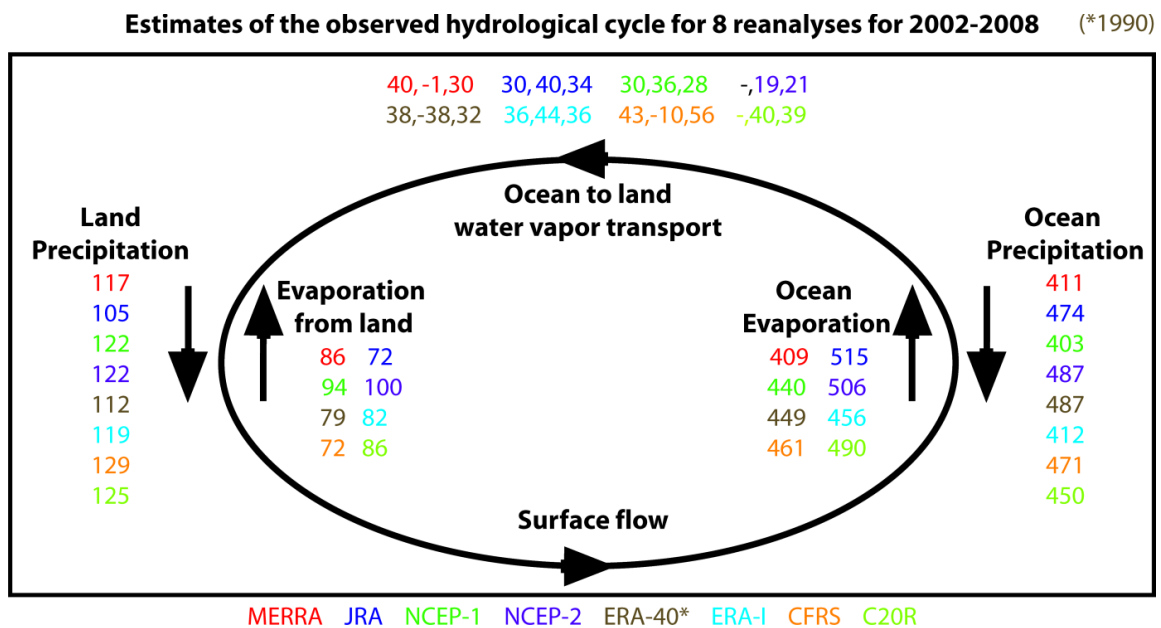


**Figure 2.** Estimated values of the observed hydrological cycle using eight reanalyses for 2002–2008, with the exception of ERA-40 that began from 1990 (colour coded as given at the bottom of the figure). For the ocean-to-land water vapour transport, the three estimates given for each are (1) the actual transport estimated from the moisture budget (based on analysed winds and moisture), (2) E-P from the ocean, and (3) P-E from the land that should be identical. Units: 1000 km<sup>3</sup> yr<sup>-1</sup>. Figure from Gimeno et al., (2012), adapted from Trenberth et al., (2011).

### 1.1.1 The Hydrological Cycle in humid tropics

The hydrological cycle in humid tropical regions differs from other regions by having greater energy inputs and faster rates of change, including human-induced change (Wohl et al., 2012). The hydrological characteristics of humid tropical climates are determined by rainfall, runoff, soil water storage, and evapotranspiration (Lal, 1993). The humid tropics lie between the Equator and 25° in both the Northern and Southern Hemispheres and include areas where the precipitation exceeds evaporation for at least 270 days per year (Wohl et al., 2012). However, the tropical zone encompasses some of the wettest locations on Earth, as well as some of the world’s driest deserts (Trewin, 2014). Figure 3a shows three types of climates in the tropical region, according to the

Köppen-Geiger climate classification (Köppen, 1936) and river basin boundaries. A river basin (or 'catchment') is the entire area having a common outlet for its surface runoff (WMO, 2012). The tropical rainforest zones mainly cover the northwest of the Amazon River Basin, Central Equatorial Africa, and Oceania. The major areas are characterised by tropical monsoon and savannah climates. Tropical river systems, wherein much of the drainage basin experiences a tropical climate are strongly influenced by the annual and inter-annual variations of the Intertropical Convergence Zone (ITCZ) and its derivative monsoonal winds (Syvitski et al., 2014). The regional monsoon precipitation location domains according to Wang et al., (2012) are shown in Figure 3b. Some of the major tropical river basins in the world, such as the Amazon, Congo, and Ganges are positioned within these monsoon climate regions.

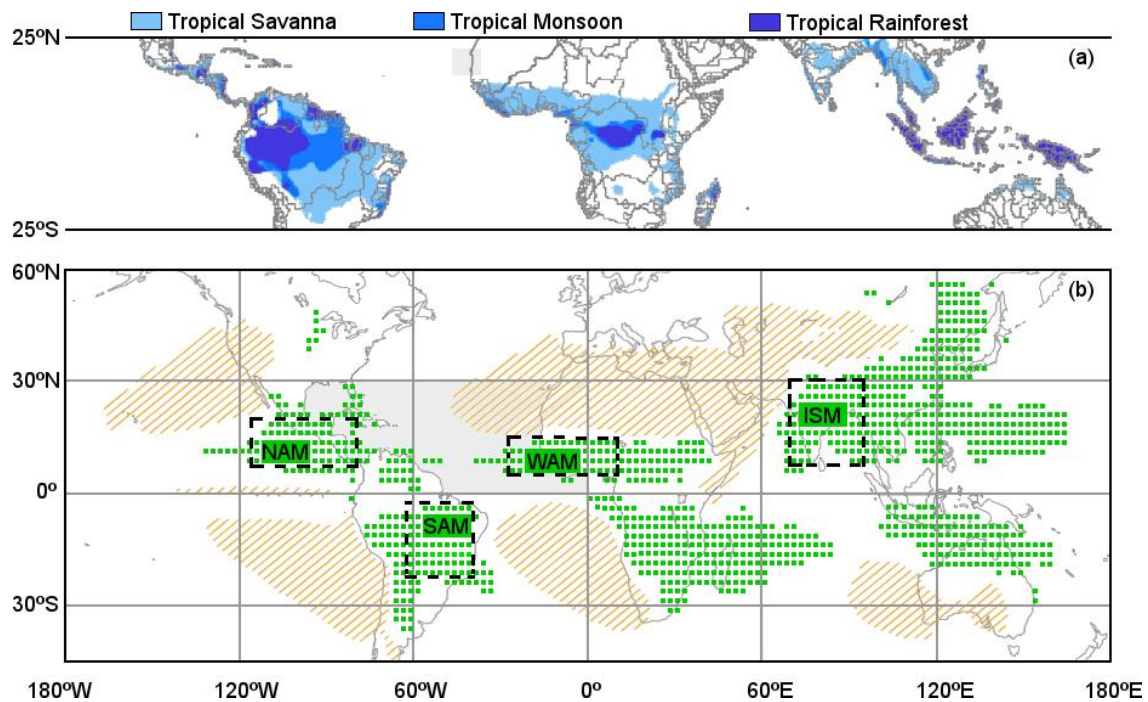


**Figure 3.** a): Tropical regions of the world (from Peel et al., 2007) superimposed on the drainage basins (by Syvitski et al., 2014). b): The regional monsoon precipitation domains (green) defined by the regions in which the annual range of precipitation rates exceed 2 mm/day (or 300 mm per season), and the local summer precipitation exceeds 55 % of the total annual rainfall (adapted from Wang et al., 2012). The annual range is defined as May through September (MJJAS) precipitation minus the November through March (NDJFM) precipitation in the Northern Hemisphere, and the NDJFM minus the MJJAS precipitation in the Southern Hemisphere. Rectangular domains in black define the common areas for regional studies of monsoon areas and their names: North American Monsoon (NAM), South American Monsoon (SAM), West African

Monsoon (WAM), and the Indian Summer Monsoon (ISM). The threshold value used in this map to distinguish the monsoon climates from the adjacent dry regions where the local summer precipitation was less than 1 mm/day (stippled, orange).

Forests play a key role in local, regional, and global climate regulation due to their influence on the water cycle. Some of the densest forests are distributed in major humid tropical river basins like the Amazon, Congo, and the Ganges and Brahmaputra in Southeast Asia. Tropical forests cool the climate due to their very high transpiration rates where the moisture transferred to the atmosphere forms large clouds that reflect the incoming solar energy and induce further cooling (Betts, 2006). The primary results of Brooks (1928) indicated that two-thirds of the rainfall over land is due to water vapour evaporated from land and therefore, changes in vegetation cover may affect the total rainfall, but not immensely. In contrast, recent studies suggest that forest cover plays a higher role in determining rainfall than previously recognised (Sheil and Murdiyarso, 2009) particularly in monsoonal regions (Notaro et al., 2011) like West Africa (Zheng and Eltahir, 1998; Douville et al., 2007; Marsham et al., 2013), the Indian Subcontinent (Dutta et al., 2009; Pathak et al., 2014, Paul et al., 2016), and the Amazon region (Tavares, J.P.N, 2012; Hilker et al., 2014; Wright et al., 2017). Pathak et al., (2014) described how monsoons enhance the soil moisture and vegetation cover in the Indian region, increasing evapotranspiration and recycled precipitation. According to Eltahir (1998), the soil moisture conditions over any large region should be associated with relatively large moist static energy in the boundary layer that favours the occurrence of additional rainfall. The most intense monsoons use more local sources of water than the least intense monsoons, but only after onset of the event (Bosilovich et al., 2003). Figure 4 presents a schematic representation of the interactions discussed above.

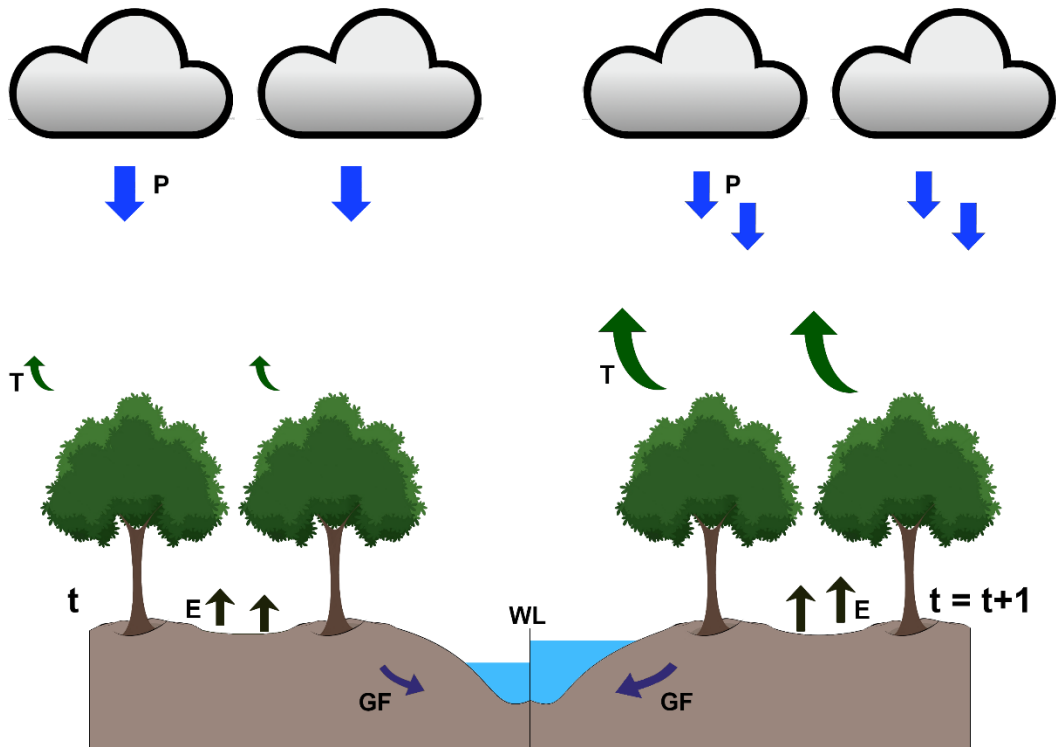


**Figure 4.** Schematic representation of the precipitation (P), evaporation (E), transpiration (T), runoff (R), groundwater flow (GF), and water level (WL) at the onset of the rainy season (time,  $t$ ) and after the demise ( $t = t + 1$ ) in a humid river basin.

## 1.2 Problem overview

Variations in freshwater availability is one of the most limiting parameters for sustaining life, agriculture, and other activities. Extremes events linked to the hydrological cycle, such as droughts and floods, have been more frequent and intense during the last decades, causing substantial damage throughout the world (Haines et al., 2006; Sheffield et al., 2012; Intergovernmental Panel on Climate Change (IPCC), 2014; Herrera-Estrada et al., 2017), particularly in humid tropical regions such as the Amazon region (Marengo et al., 2012; Jiménez-Muñoz et al., 2016), Central Equatorial Africa (Aguilar et al., 2009), the Sahel (Zeng, 2003, Tschakert et al., 2010), and the Indo Gangetic region in Southeast Asia (Hartmann and Buchanan, 2014; Priya et al., 2017). Such events are expected to increase in severity and frequency modifying the regional distribution of freshwater, thereby causing serious impacts on natural ecosystems, economies, and social development (Trenberth, 2005; Sohoulane-Djebou and Singh,

2016; IPCC, 2014). In general, experts agree that the best approach to conserving the world's freshwater resources is through the sustainable management of river basins (Sushant et al., 2015). Better management of water resources and adaptation to the expected changes requires reliable hydrological cycle predictions. However, such predictions must be grounded in the changes already observed in the data (Hegerl et al., 2015). Usually, events like droughts and floods in humid tropical regions are associated with Sea Surface Temperature (SST) variability (e.g. Erfanian et al., 2017; Lima and AghaKouchak, 2017; Hua et al., 2016; Pervez and Henebry, 2015; Roxy et al., 2015, Bian and Lu, 2013) and changes in atmospheric circulation (e.g. Chowdhury and Ward, 2004; Dezfuli and Nicholson., 2013; Lu et al., 2014; Paeth et al., 2011; Marengo et al., 2013) sometimes related to climate variability events such as the El Niño-Southern Oscillation (ENSO) (e.g. Marengo and Espinoza, 2016; Ndehedehe et al., 2017), the Atlantic Multidecadal Oscillation (AMO) (e.g. Knight et al., 2006; Joshi and Rai, 2015), and the Indian Ocean Dipole (IO) (e.g. Pervez and Henebry, 2015). Nevertheless, the related mechanisms and feedbacks on the hydrological cycle are still not well understood, particularly those operating at multiple scales or during extremes events in humid tropical river basins where forests play a key role in the hydrological cycle.

# 2

## Objectives

As was stated in the introduction, precipitation in the humid tropics is determined by moisture supplies from the oceans and continents through intense precipitation-evapotranspiration recycling. Gimeno et al., (2010) considered the identification of moisture sources as a challenge for the Atmospheric Sciences and a necessary initial step to further understanding of precipitation variability and events such as floods and droughts. Considering this, and the problem overview, a better understanding of the atmospheric branch of the hydrological cycle could clarify the origin of precipitation and the role of moisture inputs during extreme dry and/or wet conditions in the major tropical humid river basins. To introduce the objectives and results of the study, the initial objective was to describe the state-of-the-art hydrological cycle at the target river basins.

The main objective of the work was to:

**Identify the moisture sources for seven major tropical river basins.**

Once identified, the listed set of specific objectives were used to drive the study:

- Describe the annual cycle of the precipitation, potential evapotranspiration, river discharge, and/or river water levels.
- Quantify separately the moisture contribution from the oceanic and continental sources to each basin.
- Assess the role of the moisture contribution from the sources on the onset/demise of the rainy season in the Negro and Madeira River Basins in the Amazon, Indus, Ganges, and Brahmaputra River Basins in South East Asia.

- Identify the dry and wet conditions in the basins.
- Identify the dry and wet hydrological conditions at the main rivers.
- Assess the time responses from meteorological to hydrological droughts.
- Assess the moisture contribution anomalies from the sources to the basins during the seasons, and/or years affected by severely dry, extremely dry, and/or wet conditions or dry episodes.

# 3

## Methodology

### 3.1 The model FLEXPART

Build on the code base of the FLEXible TRAjectory model (FLEXTRA) (Stohl et al., 1995, 1998), the FLEXible PARTicle dispersion model (FLEXPART) is an open source Lagrangian model originally designed in 1998 for calculating long-range and mesoscale dispersion of air pollutants from point sources (Stohl et al., 2005). Since then, numerous versions of the model have been released implementing a number of technical changes and bugfixes as well as improved representation of physical processes. The model has even been adapted for meteorological input data produced by limited area meteorological models such as the Weather Research Forecast (WRF), the Consortium for Small-scale Modelling (COSMO), and the Fifth-Generation Penn State/NCAR Mesoscale Model (MM5). It has been used for modelling a large range of atmospheric transport processes such as air pollutants at the micro (Cécé et al., 2016), meso (Brioude et al., 2012; 2013), and synoptic scales (James et al. 2003; Stohl et al., 2003), the stratosphere-troposphere exchange (Stohl et al., 2003b; James et al., 2003), and the global water cycle (Stohl and James, 2004, 2005; Gimeno et al., 2010, 2012).

FLEXPART tracks a set of tracer particles (not necessarily representing real particles, but infinitesimally small air parcels) either forward in time from a source region or backward in time from a measurement location (receptor) (Stohl et al., 2005; Hegarty et al., 2013) allowing the identification of linear source-receptor relationships. Each particle is assumed to be transported by advective wind fields. Thus, FLEXPART requires the three-dimensional fields such as the horizontal and vertical wind components, and additionally temperature and specific humidity data. Reanalysis datasets from the European Centre for

Medium-Range Weather Forecast (ECMWF) and the National Centre for Environmental Prediction (NCEP), along with outputs from models like the Global Forecast System (GFS), WRF, and MM5, can be used if they are defined by a hybrid coordinate system. FLEXPART also requires the two-dimensional fields such as those for the surface pressure, total cloud cover, 10 m horizontal wind components, 2 m temperature and dew point temperature, large-scale and convective precipitation, sensible heat flux, east/west and north/south surface stress, topography, Landsea-mask and the sub-grid standard deviation of topography.

The parametrisations of turbulence and convection are implemented in FLEXPART are particularly important to simulate the effects of moisture (i.e., clouds). A Gaussian turbulence is used in FLEXPART that is strictly valid only for stable and neutral conditions. Under convective conditions, the turbulence in the vertical direction is highly inhomogeneous and skewed, that is, the downdrafts occupy larger areas than the updrafts. In the boundary layer, such turbulent convective motions can be parameterised by a Lagrangian technique by solving the Langevin equations (Forster et al., 2007). The parameterisation scheme for convective transports by Emanuel and Zivkovic-Rothman (1999) relies on the grid-scale temperature and humidity fields and calculates a displacement matrix providing the necessary mass flux information for particle redistribution was introduced into the FLEXPART model by Seibert et al., (2001, 2002). The transition probabilities are given in a discrete form in a so-called redistribution matrix that is calculated from the temperature and humidity profiles. Because convection manifests as concentrated updrafts with a high vertical velocity and weak compensating subsidence occupying a larger area, the redistribution matrix is not symmetric. In a backward run, particles must be redistributed from the destination level back to the initial level. Thus, the transposed redistribution matrix has to be used. This means that the probability of a particle arriving at its present level from another level is considered (Seibert and Frank, 2004). Stohl and James (2004, 2005) investigated the atmospheric branch of the hydrological cycle using FLEXPART and argued that global datasets do not resolve individual convective cells, although they can reproduce the large-scale effects of convection, for example, the slantwise convection in extratropical cyclones. These authors did not use the convection scheme developed by Emanuel and Zivkovic-

Rothman (1999) because it redistributes particles only within a single column that conserves the precipitable water and, thus, does not affect the evaporation minus precipitation budget.

Further improvements in new versions of FLEXPART have been made (e.g. improvements in the input/output handling). More details of the model are given by Stohl et al., (2005) and several technical notes are currently unpublished but available at: <https://www.flexpart.eu/>. In this forum, the model community creates and shares tickets with the development team inclusive of bug reports, proposals for enhancements, and other information.

### **3.1.1 Identification of moisture sources and sinks with FLEXPART**

FLEXPART has multiple options for how particles are generated and what they represent (air, or a certain trace gas that might be emitted during the simulation). During the study period, the atmosphere was considered homogeneously “filled” with particles, each representing a fraction of the total atmospheric mass. This representation was used as an extensive global air mass transport climatology scenario obtained from a backward time experiment. The experiment was provided by the Environmental Physics Laboratory (EPhysLab), at the University of Vigo, Spain. In this Lagrangian approach it is assumed that the specific humidity changes along trajectories are due to physical processes, i.e. evaporation and precipitation (Figure 5).

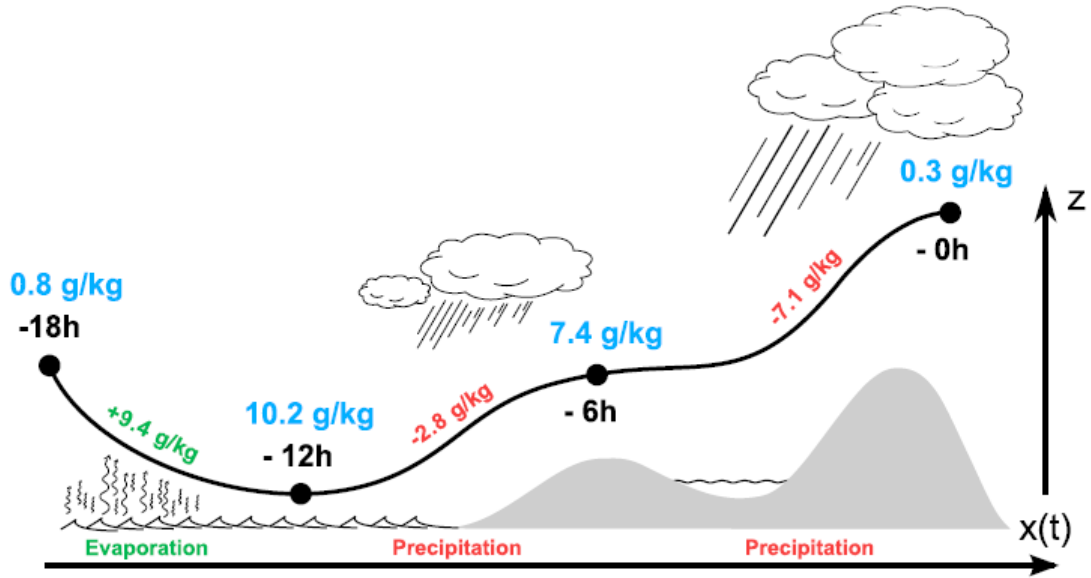


**Figure 5.** Schematic illustration of an air parcel that gains and loses moisture during its spatial and temporal journey (black dots) along with its trajectory (black line). The specific humidity content of the air parcel is given in blue for each time step. An identified evaporation event is illustrated in green and two precipitation events in red. Based on the time between the evaporation event and the final precipitation event (weighted by the effective contribution of the evaporated moisture to the final precipitation), the residence time can be calculated. From Läderach and Sodemann (2016).

Along the trajectories obtained with FLEXPART it is possible to compute the budget of the evaporation minus the precipitation ( $e - p$ ). The backward time analysis allows for the determination of the potential source contributions for given receptors (Stohl et al., 1995). The backward mode is computationally advantageous if the number of receptors is less than the number of sources considered (Seibert and Frank, 2004). The advection of air parcels mainly consists of a “zero acceleration” scheme that solves the trajectory equation (1),

$$dx/dt = v[x(t)] \quad (1)$$

where  $dx$  is the position of the parcel and  $v[x(t)]$  is the spatial and temporally interpolated wind speed. The gain (through evaporation from the environment,  $e$ ) or loss (through convection and precipitation,  $p$ ) of the specific humidity ( $q$ ) by each parcel is calculated following the equation (2). Thus,

$$(e - p) = m \left( \frac{dq}{dt} \right) \quad (2)$$

where  $m$  is the mass of a parcel, and  $dt$  the interval of time set in these experiments as every 6 h. Integrating  $(e - p)$  in the entire atmospheric vertical column for all the resident particles obtains a diagnosis of the surface freshwater flux, represented by  $(E - P)$  (Stohl and James, 2004) in equation (3), where  $K$  is the number of particles in residence over a specific area  $A$ :

$$(E - P) \approx \frac{\sum_{k=1}^k (e-p)}{A} \quad (3)$$

Along the individual trajectories,  $q$  fluctuations can occur for nonphysical reasons (e.g. because of  $q$  interpolation or trajectory errors), a limitation that is partially compensated for by the presence of significant quantities of particles in the atmospheric column over the target area.

In some regions, atmospheric moisture is not precipitated but merely flows through. In other regions, the moisture convergence ensures that precipitation occurs (Pokam et al., 2012). FLEXPART can track parcels backward and/or forward in time. An analysis performed backward in time distinguishes the origin of the atmospheric moisture in the air masses over the basins, enabling us to identify the main oceanic and continental sources of moisture. In the backward experiment, a region is then considered as a **moisture source** when  $(E - P) > 0$ , and the net moisture budget of the tracked particles favours evaporation from the environment to the particles. The opposite occurs in **moisture sink** regions, where  $(E - P) < 0$ , i.e. the associated moisture budget favours moisture loss from the tracked particles to the environment. In the forward experiment, the approach is the same and thus, the moisture losses computed in air masses from a source over a basin is considered to contribute to the precipitation. Both  $(E - P) > 0$  and  $(E - P) < 0$  were computed by integrating the values during 10-day cycles in back and forward mode, respectively. This 10-day length is considered as the mean residence time of water vapour in the atmosphere (Eltahir and Bras, 1996; Numaguti, 1999), but the results could vary if the integration is performed over a different number of days. This

topic is currently controversial as the studies from Läderach and Sodemann (2016) and van der Ent and Tuinenburg (2017) demonstrate. The first study used estimates of about 4–5 days for the global mean residence time, while the second derived a global average residence time of  $8.9 \pm 0.4$  days (that is nearest the assumption in this thesis and the commonly assumed value). Regardless, in this study, for the backward and forward trajectories, the sum of the daily ( $E - P$ ) values of the four daily outputs (00, 06, 12, and 18 h) were calculated daily from the first day of the trajectory to the last along the  $n^{\text{th}}$  day ( $n=1, 2, \dots, 10$ ), and the ( $E - P$ ) value for each day was entitled as ( $E - P$ ) $n$ -day. For further clarity, the spatial pattern ( $E - P$ ) $3$  indicates where the air masses uptake or lose moisture in the third day of the trajectory. The ( $E - P$ ) integrated for the 10-day period is named throughout as: ( $E - P$ ) $i10$ .

### **3.1.2 Methods for diagnosing the atmospheric branch of the hydrological cycle: FLEXPART advantages**

The three principal methods available for the identification of source and sink regions of atmospheric moisture are analytical or box models, physical water vapour tracers (isotopes), and numerical water vapour tracers (see Gimeno et al., 2012). Diagnoses of the atmospheric water budget through **analytical or box models** in a defined region were initially conducted by bulk methods, based on wind and station data utilising the vertically integrated balance of water vapour equation in one or two dimensions (Eq. 4) (e.g. Budyko 1974; Brubaker et al., 1993; Savenije, 1995a,b; Eltahir and Bras, 1996; Trenberth 1997). This method has been extensively applied to compute the local recycling ratio.

$$\frac{\partial(w)}{\partial(t)} + \frac{\partial(wu)}{\partial(x)} + \frac{\partial(wv)}{\partial(y)} = (E - P) \quad (4)$$

**Stable water isotopes** can be used as a tracer to detect water vapour sources and support the understanding of atmospheric moisture transport mechanisms on the scale from months to years. The isotopic composition of water vapour and precipitation ( $\delta^{18}\text{O}$  and  $\delta\text{D}$ , respectively) measurements are based on in-situ locations and implementation

dates (Dansgaard, 1964). The isotopic compositions of precipitation (and hence in the climate archive) are a result of fractionation processes along the air mass trajectory. This integrated signal is correlated with local parameters (e.g. local temperature) only as long as the trajectories are roughly similar throughout the study period (Sturm et al., 2010). This is usually accompanied by the analysis of the atmospheric circulation and dynamic conditions. On shorter time scales, however, the isotopic composition of precipitation can be influenced by a multitude of factors, and it is often difficult to interpret the data unequivocally (Gedzelman et al., 1989, 2003). Although some limitations remain in terms of spatial and temporal coverage, resolution, precision, and accuracy, the resulting maps have improved the general understanding of the distribution of isotopes and the physical processes that trigger the isotopic distributions (Gimeno et al., 2012).

**Eulerian and Lagrangian atmospheric numerical transport models** are widely utilised for several purposes. The two approaches principally differ with respect to the perspective of atmospheric motion. Eulerian models define specific reference points in a gridded system that monitors atmospheric properties including temperature, pressure, and the chemical concentration of tracers over time. Unlike Eulerian models, Lagrangian models take the perspective of a finite element or so-called ‘air parcel’. Over time, both the position and properties of this air parcel are calculated according to the mean wind field data. The path along which the air parcel travels is called its trajectory.

Eulerian treatments are generally plagued with instabilities, unrealistic negative constituent values, diffusion, and dispersion errors. A higher-order Eulerian model improves one error at significant cost but results in the magnification of another error. The cost of semi-Lagrangian models is often too high for many applications. Furthermore, traditional trajectory “Lagrangian” models do not solve both the dynamic and tracer equations simultaneously in the Lagrangian frame (Alam and Lin, 2008). Nevertheless, Alam and Lin, (2008) pointed out the strong value of constructing an atmospheric model based on a fully Lagrangian approach. Advanced equations for the trajectory contain two components; mean winds and random turbulence. The main advantage of such a Lagrangian moisture diagnostic is that it can parallel the information gained from Eulerian tagging methods, and hence be comparable to the results from these other approaches. However, they are limited with respect to the definite demarcation of the

moisture sources (Sodemann, 2006). Table 1 summarises the main strengths and weaknesses of the Numerical Eulerian and Lagrangian Water Vapour Tracer methods.

**Table 1.** Summary of the main strengths and weaknesses of the Numerical Eulerian and Lagrangian Water Vapour Tracer methods. Adapted from Gimeno et al., (2012).

<b>Numerical Water Vapour Tracers</b>	<b>Strength</b>	<b>Weakness</b>	<b>References (Non-exhaustive)</b>
Eulerian	Detailed atmospheric processes; realistic moisture circulation.	Dependent on the model bias; global forcing is required; poor representation of short-timescale hydrological cycle parameters; does not include the remote sources of water for a region.	Benton and Estoque (1954) Starr and Peixoto (1958) Peixoto and Oort (1982) Joussaume et al., (1984) Koster et al., (1986) Bosilovich and Schubert (2002)
Lagrangian	High spatial resolution moisture source diagnostics; quantitative interpretation of the moisture origin allowed; not limited by a specific RCM domain and spin-up; establishment of source-receptor relationship can be easily assessed as budgets can be traced along suitably defined trajectory ensembles; net freshwater flux can be tracked from a region both forward and backward in time; realistic	Sensitivity of moisture flux computations leads to increases in data noise for shorter time periods or smaller regions; simple method does not provide a diagnostic of the surface moisture fluxes; surface fluxes under (over) estimation if dry (cold) air masses tracking as the budget is not closed; evaporation rates are based on calculations rather than observations in some methods; evaporation and precipitation are not clearly separable (in some methods); movement and extraction of water does not depend on the physical tendencies included in the reanalysis data.	D'Abreton and Tyson (1995) Wernli (1997) Massacand et al., (1998) Dirmeyer and Brubaker (1999) Brubaker et al., (2001) Dirmeyer and Brubaker (2006) Stohl and James (2004, 2005)

	tracking of air parcels; computationally efficient compared to performing multi-year GCM simulations or reanalyses; more information provided than a purely Eulerian description of the velocity fields; parallel use of information from Eulerian tagging methods allowed.		
--	--	--	--

### 3.2 Identification of the onset and demise of the rainy season

The onset and end of the rainy season in monsoonal basins can be considered as the beginning and end of the longest period during which the rainfall exceeds its annual climatology (Liebmann et al., 2007). To determine the dates associated with the onset/demise, an objective was applied that was previously implemented for the Amazon River Basin by Liebmann and Marengo (2001), for South America by Liebmann et al., (2007), and for the Indian Summer Monsoon region by Noska and Misra (2016). This method is based on the daily cumulative precipitation anomalies ( $C'm$ ) from each basin throughout the year calculated as:

$$C'm(i) = \sum_{n=1}^i [Dm(n) - C] \quad (5)$$

$$C = \frac{1}{MN} \sum_{m=1}^M \sum_{n=1}^N D(m, n) \quad (6)$$

where  $D(m, n)$  is the daily average precipitation over each basin for day  $n$  of year  $m$ , and  $C$  is the climatology of the annual mean precipitation over  $N$  (365 or 366) days for  $M$  years. Therefore, starting in January, the onset date is defined as the day after  $C'm$  reaches

its absolute minimum value. After this date, a positive slope indicates the rainy season until  $C'm$  reaches its absolute maximum value, considered as the demise because it is the point when the precipitation starts to decrease.

### **3.3 Identification of dry and wet conditions**

Many indices have been developed and used by meteorologists and climatologists around the world ranging from simple indices such as the percentage of normal precipitation and precipitation percentiles to more complicated examples (WMO, 2012). Normal drought Indices are quantitative measurements that characterise drought levels by assimilating data from one or several variables (indicators) such as precipitation and/or evapotranspiration into a single numerical value (Zargar et al., 2011). However, these indices are also capable of diagnosing wet conditions. A numerical standard is needed for comparing drought measurements from one region to another, as well as for comparing past drought events. However, the considerable disagreement that exists regarding the definition of a drought makes it impossible to devise a universal drought index (Heim, 2002). Thus, no single indicator or index can be used to determine appropriate actions for all types of droughts given the number and variety of sectors affected. The preferred approach is to use different thresholds with different combinations of inputs. Ideally, this would involve prior studies to determine which indicators/indices are best suited to the timing, area, and type of climate and drought [WMO & Global Water Partnership (GWP), 2016]. Here, it is important clarify that ‘Indicators’ are variables or parameters used to describe the drought conditions (e.g. precipitation, temperature, streamflow) while ‘Indices’ are typically computed numerical representations of the drought severity, assessed using climatic or hydrometeorological inputs including the indicators listed above. Regardless, indices are technically also indicators.

#### **3.3.1 Meteorological drought Indices**

The use of meteorological drought indices varies according to drought type, ranging from those used for meteorological droughts, agricultural droughts, hydrological droughts, and socio-economical droughts. The latter three types of drought result as a consequence of a prolonged meteorological drought and they are defined according to

their impacts on society (Lake, 2011). Table 2 presents three of the most common drought indices along with their strengths and weakness.

**Table 2.** Strengths and weaknesses of the three most popular meteorological drought indices. Adapted from Zargar et al., (2011) and from WMO & GWP (2016).

Index	Strengths	Weaknesses
SPI (McKee et al., 1993)	<ul style="list-style-type: none"> <li>• Simplicity; SPI relies only on precipitation data</li> <li>• As SPI is adaptable for the analysis at variable time scales it can be used for monitoring agricultural and hydrological events.</li> <li>• Possibility to compare precipitation changes from nominal conditions for various regions with highly different climates.</li> <li>• Equally represents both wet and dry climates and hence can be used for monitoring wet periods.</li> </ul>	<ul style="list-style-type: none"> <li>• Uses only precipitation data, loosely connected to ground conditions. PET is a valuable additional indicator (Hu and Will Willson 2000; Tsakiris and Vangelis 2005; Vicente-Serrano et al., 2010).</li> <li>• Limitations of the precipitation data including accuracy of the measurements, number of gauging stations, and length of the record.</li> <li>• Lacks the ability to identify regions with greater droughts tendencies; requires knowledge of the local climatology.</li> </ul>
SPEI (Vicente-Serrano et al., 2010)	<ul style="list-style-type: none"> <li>• Combines multi-timescale aspects of the Standardized Precipitation Index (SPI) with information about evapotranspiration, making it more useful for climate change studies.</li> <li>• Statistically based index that requires only climatological information without assumptions about the characteristics of the underlying system.</li> </ul>	<ul style="list-style-type: none"> <li>• More data requirements than the precipitation SPI.</li> <li>• Sensitive to the method that calculates the potential evapotranspiration (PET).</li> <li>• As with other drought indices, a long base period (30-50+ years) that samples the natural variability should be used.</li> </ul>
PDSI (Palmer 1965; Alley, W.M., 1984)	<ul style="list-style-type: none"> <li>• More comprehensive than precipitation only indices; evapotranspiration and soil moisture are also considered.</li> <li>• Can use basic data for calculation: precipitation and air temperature with records that exist further in the past.</li> <li>• Most effective where impacts are sensitive to soil moisture.</li> <li>• Factors in antecedent conditions.</li> </ul>	<ul style="list-style-type: none"> <li>• Arbitrary selection of start and end intensity values and less algorithm transparency because of the more sophisticated computation.</li> <li>• Calibrated for US Great Plains' conditions; limited applicability in locations with climatic extremes, mountainous terrain, or snow-pack unless calibrated.</li> <li>• Variable performance across regions and time periods.</li> </ul>

- 
- Applicability to regions with extreme climate (e.g., highly variable rainfall, runoff, and mountainous areas).
  - Handling of snow and soil freeze.
  - Neglects the lag between rainfall and runoff.
- 

### **3.3.1.1 The Standardized Precipitation-Evapotranspiration Index (SPEI)**

Among the indices previously explained, the Standardized Precipitation-Evapotranspiration Index (SPEI) was chosen to identify dry and/or wet conditions in the basins analysed in this study. Proposed by Vicente-Serrano et al., (2010), the SPEI is based on precipitation and potential evapotranspiration (PET) data, and has the advantage of combining multi-scalar character data with the capacity to include the effects of temperature variability on drought assessments. The PET is considered to be a reliable approximation of the atmospheric evaporative demand (AED) information. Positive SPEI values indicate above-average moisture conditions (wet), while negative values reveal below-normal (dry) conditions (Table 3). Dry episodes begin when the SPEI falls below zero, reaching a value of -1 or less, and end when the SPEI returns to positive values. To identify the dry episodes, the criterion of Mckee et al., (1993) was applied to each basin. They identified seasons and/or years affected by severe and extremely dry and/or wet conditions according to the SPEI threshold of  $\pm 1.5$ , and the onset and demise of the dry episodes. Several indicators were calculated for such episodes, including the duration (number of months between the start and the end month that were included in the selected period), and the severity computed as the absolute value of the sum of all the SPEI values during the episode (Spinoni et al., 2014, 2018; Tan et al., 2015).

### **3.3.1.2 Computation of the SPEI**

The SPEI computation was based on the original SPI (Mckee et al., 1993) calculation procedure. Here was utilised the monthly precipitation and potential evapotranspiration input data. The SPEI is primarily obtained by the difference between the  $P$  and the  $PET$ .  $PET$  values can be obtained through several methods, namely, the Thornthwaite equation, the Penman-Monteith equation, the Hargreaves equation, and

others. The *PET* values in this study were obtained from the Climate Research Unit (CRU). To obtain *PET* values, Harris et al., (2014) utilised a variant of the Penman–Monteith method using data reference crop evapotranspiration [ $\text{mm d}^{-1}$ ], net radiation at crop surface [ $\text{MJm}^{-2} \text{d}^{-1}$ ], soil heat flux [ $\text{MJm}^{-2} \text{d}^{-1}$ ], average temperature at 2 m height [ $^{\circ}\text{C}$ ], windspeed measured (or estimated from  $U_{10}$ ) at 2 m height [ $\text{ms}^{-1}$ ];  $U_{10}$ , windspeed measured at 10 m height [ $\text{m s}^{-1}$ ], vapour pressure deficit for measurement at 2 m height [ $\text{kPa}$ ], slope of the vapour pressure curve [ $\text{kPa } ^{\circ}\text{C}^{-1}$ ], psychrometric constant [ $\text{kPa } ^{\circ}\text{C}^{-1}$ ], coefficient for the reference crop [ $\text{kJ}^{-1} \text{kgK d}^{-1}$ ], Allen et al., (1994); 0.34: wind coefficient for the reference crop [ $\text{sm}^{-1}$ ] (Allen et al., 1994).

$P$  minus *PET* represents a simple climatic water balance that can be calculated at different time scales, according to equation 6:

$$Di = Pi - PETi \quad (7)$$

The calculated  $Di$  values were aggregated at different time scales ( $i$ ), following the same procedure as the SPI. According to Vicente-Serrano et al., (2010), the selection of the most suitable statistical distribution to model the  $D$  series is difficult given the similarity among the four distributions (Pearson III, lognormal, log-logistic, and General Extreme Value (GEV)). These authors argued that the log-logistic distribution showed a gradual decrease in the curve for low values, and coherent probabilities were obtained for very low values of  $D$ , corresponding to 1 occurrence in 200–500 years.

The log-logistic distribution provided better results than other distributions for obtaining the SPEI series in standardized  $z$  units (mean=0, SD=1) (Vicente-Serrano et al., 2010). The probability distribution function of a variable  $D$  according to a log-logistic distribution is given by:

$$F(D) = \left[ 1 + \left( \frac{\alpha}{D-\gamma} \right)^{\beta} \right]^{-1} \quad (8)$$

where  $\alpha$ ,  $\beta$ , and  $\gamma$  represent the scale, shape, and location parameters that are estimated from the sample  $D$ . The SPEI can easily be obtained as the standardized values of  $F(D)$ . For example, following the classical approximation of Abramowitz and Stegun (1965):

$$SPEI = W - \frac{C_0 + C_1W + C_2W^2}{1 + d_1W + d_2W^2 + d_3W^3} \quad (9)$$

where  $W = -2\ln(P)$  and  $C_0 = 2.515517$ ,  $C_1 = 0.802853$ ,  $C_2 = 0.010328$ ,  $d_1 = 1.432788$ ,  $d_2 = 0.189269$ , and  $d_3 = 0.001308$  are constants. For calculating the SPEI, the R package SPEI v1.7 of 7 June 2017 was implemented and is available at: <http://cran.r-project.org/web/packages/SPEI> (Beguería et al., 2014).

**Table 3.** Drought classification based on the SPEI according to the initial definition of Mckee et al., (1993) for the SPI.

<b>Conditions</b>	<b>Category</b>
Extremely wet	$SPEI > 2.0$
Severely wet	$1.5 < SPEI \leq 2.0$
Moderate wet	$1.0 < SPEI \leq 1.5$
Mild wet	$0 < SPEI \leq 1.0$
Mild drought	$-1.0 < SPEI < 0$
Moderate drought	$-1.5 < SPEI \leq -1.0$
Severe drought	$-2.0 < SPEI \leq -1.5$
Extreme drought	$SPEI \leq -2.0$

### 3.3.2 Hydrological Drought Indices

Standardised indices for the characterisation of hydrological drought use different hydrological variables (from observed or simulated data) as inputs. Most common is a focus on streamflow, because streamflow is frequently measured, easily simulated, and of significant interest to water resources management (Van Loon, 2015). Other variables used in hydrological drought indices include groundwater levels and lake levels. In Table 4, some of the hydrological drought indices usually utilised are presented. However, in the absence of hydrological records, the meteorological drought indices, like the SPI and SPEI calculated at different time scales are useful for identifying and assessing hydrological droughts (Zhu et al., 2016).

**Table 4.** Strengths and weaknesses of popular hydrological drought indices. Adapted from WMO & GWP (2016).

Index	Strengths	Weaknesses
Palmer Hydrological Drought Index (PHDI) (Palmer, 1965)	<ul style="list-style-type: none"> <li>Based on the original PDSI and modified to take into account longer-term dryness that can affect water storage, streamflow, and groundwater; allows the total water system to be considered.</li> </ul>	<ul style="list-style-type: none"> <li>Frequencies will vary by region and time of year, where extreme drought may not be a rare event during some months of the year.</li> <li>The impact of human influences, such as management decisions and irrigation, are not considered in the calculations.</li> </ul>
Standardized Streamflow Index (SSI) (Vicente-Serrano et al., 2012)	<ul style="list-style-type: none"> <li>Possibility to utilise two different approaches: distribution of the best monthly fit (BMF) and the minimum orthogonal distance (MD), ensuring a robust index that guarantees the spatial and temporal comparability of drought conditions.</li> </ul>	<ul style="list-style-type: none"> <li>A single input (streamflow) does not take into account management decisions, and periods of no flow can skew the results.</li> </ul>
Streamflow Drought Index (SDI) (Nalbantis and Tsakiris, 2009)	<ul style="list-style-type: none"> <li>The program is widely available and easy to use. Missing data are allowed, and the longer the streamflow record, the more accurate the results. As with SPI, various timescales can be examined.</li> </ul>	<ul style="list-style-type: none"> <li>A single input (streamflow) does not take into account management decisions, and periods of no flow can skew the results.</li> </ul>
Standardized Reservoir Supply Index (SRSI) (Gusyev et al., 2015)	<ul style="list-style-type: none"> <li>Easy to compute, as it mimics SPI calculations using a standard gamma distribution of the probability distribution function.</li> </ul>	<ul style="list-style-type: none"> <li>Does not take into account changes due to the management of the reservoir and losses due to evaporation.</li> </ul>

### 3.3.2.1 The Standardised Streamflow Index (SSI)

In this study, the Standardised Streamflow Index (SSI) (Vicente-Serrano et al., 2012) was used to diagnose the hydrological conditions of major tropical river streams. The SSI is measured in the same units that are currently used for other climate drought indexes, particularly the SPI and SPEI. Thus, considering both the SPEI and SSI it is

possible to assess when precipitation deficits propagate through the hydrological cycle through different accumulation periods.

### **3.3.2.2 Computation of the Standardised Streamflow Index (SSI)**

The SSI uses the same principle as the SPI. To compute the SSI, six parameter distributions (lognormal, Pearson Type III, log-logistic, general extreme value, generalized Pareto, and Weibull) can be used and along with two different approaches to select the most suitable distribution, the best monthly fit (BMF), and the minimum orthogonal distance (MD). In previous studies some authors (e.g. Zaidman et al., 2002; López-Moreno et al., 2009; Nalbanltis and Tsakiris, 2009; Lorenzo-Lacruz et al., 2010) implemented the SSI using a unique probability distribution and did not obtain a reliable index because of the large variability in the statistical properties of the monthly series (Vicente-Serrano et al., 2012). The standardised anomalies of monthly river discharge datasets were calculated to obtain accurate SSI values. Of the six probability distributions, the log-logistic seemed the most appropriate to obtain the SSI on the basis of the BMF and the MD approaches.

## **3.4 Tropical River Basins analysed in this Study**

Localized between the latitudinal band of 30° N-30° S, seven tropical river basins were chosen for this study. The basins include the Congo and Niger River Basins in Africa, the Indus, Ganges and Brahmaputra River Basins in Southeast Asia, and the Negro and Madeira River Basins in the Amazon region in South America. The catchment areas of each river studied are plotted in Figure 6. The Congo, Niger, Negro and Madeira River Basins were defined using geo-referenced watershed boundaries on a 30 arcsec resolution map (a HydroBASIN product of HydroSHEDS, or Hydrological data and maps based on SHuttle Elevation Derivatives at multiple Scales; Lehner and Grill, 2013). The geographic location and boundaries of the Indus, Ganges, and Brahmaputra River Basins were freely provided by Hasson et al., (2013).

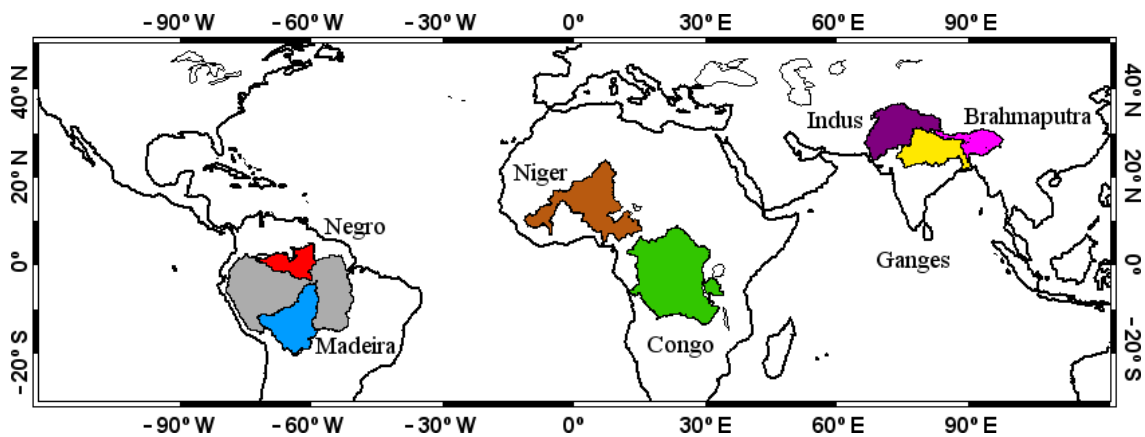


**Figure 6.** Geographical location and extension of the Negro (red), Madeira (blue) within the Amazon (in grey), Congo (light green), Niger (orange), Indus (purple), Ganges (yellow), and Brahmaputra (pink) River Basins.

### 3.5 Datasets

#### 3.5.1 FLEXPART inputs

The data used in this study was collected for a 37-year period from 1980–2016. The Lagrangian data used in this work were obtained from a FLEXPART v9.0 experiment that was executed on a global domain, in which the atmosphere was divided into approximately 2 million uniformly distributed particles. FLEXPART uses ERA-Interim global data (Dee et al., 2011) at 6 h intervals (00:00, 06:00, 12:00, and 18:00 UTC) with a longitude and latitude resolution of 1° at 61 vertical levels from 0.1–1000 hPa. The model requires five three-dimensional fields including the horizontal and vertical wind components, temperature, and specific humidity in the ECMWF vertical hybrid coordinate system. The model also requires the two-dimensional fields for surface pressure, total cloud cover, 10 m horizontal wind components, 2 m temperature and dew point temperature, large-scale and convective precipitation, sensible heat flux, east/west and north/south surface stress, topography, land-sea-mask, and sub-grid standard topography deviation. It also considers approximately 14 model levels below 1500 m and 23 below 5000 m. This configuration is important because the transport of water vapour

mainly occurs in the lower troposphere that is clearly affected by the Earth's topography (Peixoto and Oort, 1992).

### **3.5.2 SPEI inputs**

Drought usually affects large areas, but hydrological analyses are often interested in resolving the smaller-scale diversity of the headwater contributions, for example, the contributions to large river basins during droughts. For this task, it is often impossible to obtain high-resolution meteorological data sets that are consistently produced and it may be more convenient to use global data sets (Hellwig et al., 2018). As such, the following was used:

- Monthly data of precipitation (P) and potential evapotranspiration (PET) from the Climate Research Unit (CRU) CRU 3.23, 3.2401, and 3.4. Freely available from <http://www.cru.uea.ac.uk/data>.

For the calculation of the SPEI, the R package SPEI v1.7 of 7 June 2017 was implemented (<http://cran.r-project.org/web/packages/SPEI>) (Beguería et al., 2014).

### **3.5.3 Other datasets**

A complementary set of datasets were used in each area according to the specific objective requirements.

- The vertical integral of the eastward and northward water vapour flux from ERA-Interim available at: <https://www.ecmwf.int/en/forecasts/datasets/archive-datasets/reanalysis-datasets/era-interim> was utilised to calculate the Vertical Integrated Moisture Flux (VIMF) and its divergence.
- Daily precipitation from the Climate Hazards Group InfraRed Precipitation with Station data (CHIRPS) (Chris et al., 2015) that has the advantage of incorporating 0.05° resolution satellite imagery with in-situ station data. Determination of the onset/demise dates and the length of the rainy season in the Amazon region and South America were obtained from <http://chg.geog.ucsb.edu/data/chirps/>.

- Monthly ocean evaporation data were obtained from the Objectively Analyzed air-sea Fluxes (OAFflux) for the Global Oceans project (Yu et al., 2008). Available at: <http://oaflux.whoi.edu/>.
- Monthly land evaporation was assessed from the Global Land Evaporation Amsterdam Model (GLEAM) v2 data (Miralles et al., 2011), available from a previous request at <https://www.gleam.eu/>.
- Monthly runoff data in the Congo River Basin were obtained from the ERA-Interim available at <https://www.ecmwf.int/en/forecasts/datasets/archive-datasets/reanalysis-datasets/era-interim>.
- To calculate the SSI, the corrected monthly mean discharge of the Congo River as recorded at the gauging station of Kinshasa (4.0° S, 15.3° E) was freely provided by the Global Runoff Data Centre (GRDC) and accessible at [https://www.bafg.de/GRDC/EN/Home/homepage\\_node.html](https://www.bafg.de/GRDC/EN/Home/homepage_node.html).
- Data to calculate the water level (WL) anomalies of the Negro and Madeira Rivers were downloaded from the Observatory of Research for the Environment: The Observation Service (formerly Environmental Research Observatory). Available online at <http://www.ore-hybam.org/>.
- Daily data of the Interpolated Outgoing Longwave Radiation (OLR) (Liebmann and Smith, 1996) available at [https://www.esrl.noaa.gov/psd/data/gridded/data.interp\\_OLR.html](https://www.esrl.noaa.gov/psd/data/gridded/data.interp_OLR.html), was used to investigate the response of the convection associated with the  $|(E - P)/10 < 0|$  anomalies over the basins.

**Table 5.** Collection of datasets, sources, period and spatial resolution.

<b>Datasets</b>	<b>Source</b>	<b>Period</b>	<b>Spatial resolution (longitude x latitude)</b>
Precipitation	CRU 3.23; 3.2401, 3.4	1980-2016	0.5° x 0.5°
Potential Evapotranspiration	CRU 3.23; 3.2401, 3.4	1980-2016	0.5° x 0.5°
Vertical integral of eastward and northward water vapour flux	ERA-Interim	1980 – 2016	1° x 1°
Precipitation	CHIRPS	1981 – 2016	0.25° x 0.25°

Ocean evaporation	OAFIux	1980–2010	0.5° x 0.5°
Land evaporation	GLEAM	1980–2010	0.5° x 0.5°
Monthly discharge of the Congo River	GRDC	1980–2010	
OLR	NOAA	1980–2016	1° x 1°
Water Level	HYBAM	1980–2016	

# 4

## Set of publications

Seven large tropical river basins characterised by humid climatic conditions were investigated individually. Five publications have been used to construct this final document. Table 5 shows the title, authors, year of publication, and the journal where the articles have been published. In the table, the articles are not listed in order of publication. As discussed in the objectives, the identification of the moisture sources of each basin was addressed individually for each basin as well as the dry and/or wet conditions and the role of the sources providing humidity during the extremes events. The periods of analysis for each study varied according to the beginning of each study and the availability and progressively updated datasets utilised. In Table 6, a description of each journal and certain characteristics such as the Quartile, the Scientific Impact Factor, and the ISSN are listed for the publications.

The first article in Table 6 is entitled: ‘*A Lagrangian perspective of the hydrological cycle in the Congo River basin*’. In this article, the main continental and oceanic regions were identified that provide moisture to the Congo River Basin along with an assessment of their temporal and spatial contribution to precipitation over the basin and their effectivity across the year. Additionally, the role of the sources during years affected by severe and extremely dry and wet conditions was assessed. In this article, the possible temporal impact of water balance conditions on hydrological conditions was also assessed.

The second article documented in Table 6 is: ‘*The atmospheric branch of the hydrological cycle over the Indus, Ganges, and Brahmaputra river basins*’. In this

article, the principal continental and oceanic sources of moisture for the Indus, Ganges, and Brahmaputra River Basins are identified. The study focused on the westerly precipitation regime (WPR) (November–April) and the monsoonal precipitation regime (MPR) (May–October). The roles of the sources in the moisture contribution to precipitation during severe and extremely dry and wet conditions in the basins were assessed through WPR and MPR composites.

The third article: ‘*The Atmospheric Branch of the Hydrological Cycle over the Negro and Madeira River Basins in the Amazon Region*’, was performed for the Negro and Madeira River Basins, located within the Amazon River Basin, in the north and southwest respectively. The source-sink relationships of atmospheric moisture were investigated to reveal the most important sources of moisture of both sub-basins and their role on the rainy season onset/demise. Dry and wet conditions affecting each basin were computed and for the driest episodes, the role of the sources was assessed. In this article, a section was dedicated to determining the average role of the moisture contribution from the sources during the warm (El Niño) and cold (La Niña) events of the El Niño Southern Oscillation (ENSO) phenomenon.

For the Niger River Basin, two articles were published separately with different aims. The first one: ‘*The Niger River Basin Moisture Sources: A Lagrangian Analysis*’, had as its fundamental objective the identification of the main sources of humidity in the basin. In the second article: ‘*Dry conditions in the Niger River Basin and the link with atmospheric moisture transport from the South Atlantic Ocean*’, dry and wet conditions were identified during the last years and the role of the oceanic source located in the South Atlantic Ocean was evaluated during the dry and rainy seasons affected by severe and extremely dry conditions.

**Table 6.** List of articles

<b>Title</b>	<b>Authors</b>	<b>Year</b>	<b>Journal</b>
“A Lagrangian perspective of the hydrological cycle in the Congo River basin”	Rogert Sorí, Raquel Nieto, Sergio M. Vicente-Serrano, Anita Drumond, and Luis Gimeno	2017	<i>Earth System Dynamic (ESD)</i>
“The atmospheric branch of the hydrological cycle over the Indus, Ganges, and Brahmaputra river basins”	Rogert Sorí, Raquel Nieto, Anita Drumond, Sergio M. Vicente-Serrano, and Luis Gimeno	2017	<i>Hydrology and Earth System Sciences (HESS)</i>
“The Atmospheric Branch of the Hydrological Cycle over the Negro and Madeira River Basins in the Amazon Region”	Rogert Sorí, José A. Marengo, Raquel Nieto, Anita Drumond, and Luis Gimeno	2018	<i>Water</i>
“The Niger River Basin Moisture Sources: A Lagrangian Analysis”	Rogert Sorí, Raquel Nieto, Anita Drumond, and Luis Gimeno	2017	<i>Atmosphere</i>
“Dry conditions in the Niger River Basin and the link with atmospheric moisture transport from the South Atlantic Ocean”	Rogert Sorí, Raquel Nieto, Anita Drumond, and Luis Gimeno	Expected in 2018	<i>Water</i>

**Table 7.** Summary of the impact and quality of the Journals

<b>Journal</b>	<b>Description</b>	<b>Journal characteristics</b>
<i>Earth System Dynamic (ESD)</i>	Earth System Dynamics (ESD) is an international scientific journal dedicated to the publication and public discussion of studies that take an interdisciplinary perspective of the functioning of the whole Earth system and global change.	<ul style="list-style-type: none"> <li>- Current Impact Factor: 3.769</li> <li>- 5-year Impact Factor: 4.522</li> <li>- JCR category rank: 25/188 (Q1) in “<i>Geosciences, Multidisciplinary</i>”</li> <li>- ISSN: 2190-4979</li> </ul>

<p><i>Hydrology and Earth System Sciences (HESS)</i></p>	<p>Hydrology and Earth System Sciences (HESS) is an international two-stage open-access journal for the publication of original research in hydrology.</p>	<ul style="list-style-type: none"> <li>- Current Impact Factor: 4.256</li> <li>- 5-year Impact Factor: 4.819</li> <li>- JCR category rank: 3/88 (Q1) in ‘<i>Water Resources</i>’</li> <li>- ISSN: 1027-5606</li> </ul>
<p><i>Atmosphere</i></p>	<p>Atmosphere is an international peer-reviewed open access journal of scientific studies related to the atmosphere published monthly online by MDPI.</p>	<ul style="list-style-type: none"> <li>- Current Impact Factor: 1.704</li> <li>- 5-year Impact Factor: 1.775</li> <li>- JCR category rank: 57/86 (Q3) in ‘<i>Meteorology &amp; Atmospheric Sciences</i>’</li> <li>- ISSN: 2073-4433</li> </ul>
<p><i>Water</i></p>	<p>Water is a peer-reviewed open access journal on water science and technology, including the ecology and management of water resources, and is published monthly online by MDPI.</p>	<ul style="list-style-type: none"> <li>- Current Impact Factor: 2.069</li> <li>- 5-year Impact Factor: 2.250</li> <li>- JCR category rank: 34/90 (Q2) in ‘<i>Water Resources</i>’</li> <li>- ISSN: 2073-4441</li> </ul>



# A Lagrangian perspective of the hydrological cycle in the Congo River basin

Rogert Sorí<sup>1</sup>, Raquel Nieto<sup>1,2</sup>, Sergio M. Vicente-Serrano<sup>3</sup>, Anita Drumond<sup>1</sup>, and Luis Gimeno<sup>1</sup>

<sup>1</sup>Environmental Physics Laboratory (EphysLab), Universidade de Vigo, Ourense, 32004, Spain

<sup>2</sup>Department of Atmospheric Sciences, Institute of Astronomy, Geophysics and Atmospheric Sciences, University of São Paulo, São Paulo, 05508-090, Brazil

<sup>3</sup>Instituto Pirenaico de Ecología, Consejo Superior de Investigaciones Científicas (IPE-CSIC), Zaragoza, 50059, Spain

*Correspondence to:* Rogert Sorí (rogert.sori@uvigo.es)

Received: 3 March 2017 – Discussion started: 9 March 2017

Revised: 26 May 2017 – Accepted: 16 June 2017 – Published: 4 August 2017

**Abstract.** The Lagrangian model FLEXPART is used to identify the moisture sources of the Congo River basin (CRB) and investigate their role in the hydrological cycle. This model allows us to track atmospheric parcels while calculating changes in the specific humidity through the budget of evaporation minus precipitation. This method permits the annual-scale identification of five continental and four oceanic principal regions that provide moisture to the CRB from both hemispheres over the course of the year. The most important is the CRB, which provides more than 50 % of the total atmospheric moisture contribution to precipitation over itself. Additionally, both the land that extends to the east of the CRB and the eastern equatorial South Atlantic Ocean are very important sources, while the Red Sea source is merely important in the ( $E - P$ ) budget over the CRB despite its high evaporation rate. The moisture-sink patterns over the CRB in air masses that were tracked forward in time from all the sources follow the latitudinal rainfall migration and are mostly highly correlated with the pattern of the precipitation rate, ensuring a link between them. In wet (dry) years, the contribution of moisture to precipitation from the CRB over itself increases (decreases). Despite the enhanced evaporative conditions over the basin during dry years, the vertically integrated moisture flux (VIMF) divergence inhibits precipitation and suggests the transport of moisture from the CRB to remote regions.

## 1 Introduction

The water that falls on a given area as precipitation may be supplied by local evaporation and/or transpiration. Alternatively, this water may have been advected from a remote terrestrial source or originated as evaporation from the oceans (Dirmeyer and Brubaker, 1999). In recent years, a great number of studies have focused on deepening our understanding of these issues, particularly the mechanisms of water vapour transport in the atmosphere and the identification of moisture sources. These issues are considered to be some of the major challenges in the atmospheric sciences (Gimeno, 2013). Several techniques and methods have been implemented to address these matters; a summary of the main strengths and

weaknesses of each method was provided by Gimeno et al. (2012).

Some authors have investigated the sources of moisture for the entire continent of Africa (van der Ent et al., 2010; Gimeno et al., 2010, 2012) and specific regions such as the Sahel (Nieto et al., 2006; Salih et al., 2015; Keys et al., 2012, 2014), Ethiopia (Viste and Sorteberg, 2013), and the wider region of West Africa (Savenije, 1995; Eltahir and Gong, 1996; Druyan and Koster, 1989). Nevertheless, the Congo River basin (CRB) in the highly convective region of Central Equatorial Africa (CEA) is one of the least studied of the major global river basins (Alsdorf et al., 2016). Stohl and James (2005), who focused on several world river catchments such as the Congo, used the Lagrangian model FLEXPART

over a period of 4 years (December 1999–November 2003) to diagnose the net ( $E - P$ ) budget, in which ( $E$ ) denotes evaporation and ( $P$ ) precipitation. However, the short timescale in this study was not sufficient to properly investigate the variability and other aspects of the hydrological cycle over the CRB. Gimeno et al. (2010) argued that the evaporation rate in tropical South Africa during the austral winter is so high that this region provides moisture for most of the precipitation over the Congo. According to van der Ent et al. (2010), the moisture that evaporates in East Africa is the main source of rainfall in the CRB.

More accurate results on the evaporative moisture sources for the CRB, together with their seasonal variations and mean contributions over a period of 25 years, are available online from the Center for Ocean–Land–Atmosphere Studies (COLA, 2017). These data were calculated by using a quasi-isentropic method, a Eulerian approach that was implemented in Dirmeyer et al. (2009), and the results highlighted that the main evaporative sources for precipitation lie within the basin itself, in addition to the land to the east of the basin along the Oriental African coasts, and the Atlantic and Indian oceans. However, the role of the CRB's moisture sources in other stages of the hydrological cycle and during extreme events in the basin remains unclear. Most studies that were based on instrumental records in Africa indicated that droughts have become more frequent, intense, and widespread over the last 50 years (Dai, 2013; Masih et al., 2014). The occurrence of drought is especially important in regions where economic activities greatly depend on water resources (such as the CRB) and particularly African nations that heavily rely on agriculture (Lobell et al., 2011a, b).

The objectives of this study are (i) to identify the main continental and oceanic moisture sources for the CRB from a Lagrangian perspective and determine their role, including that of the basin itself, in the total moisture contribution to precipitation over itself and (ii) to investigate drought and wet conditions in the CRB and their relationship to the atmospheric moisture supply.

### Study region

The CRB is located in central-equatorial Africa, an important region of the continent that contains major rivers and dense forest (Fig. 1). With an approximate area of 3 687 000 km<sup>2</sup> (Alsdorf et al., 2016), the basin includes several African countries: the Democratic Republic of the Congo (DRC), the People's Republic of the Congo, the Central African Republic, and portions of Zambia, Angola, Cameroon, and Tanzania (Chishugi, 2008). The Congo River (previously known as the Zaire) is over 4375 km long and is considered to be the fifth longest river in the world and the second longest in Africa after the Nile River (IBP, 2015). Its discharge shows a composite variability because of the sum of its tributaries (Laraque et al., 2001). With an annual discharge of 5000 m<sup>3</sup> s<sup>-1</sup> at its mouth, the Oubangui River is the sec-

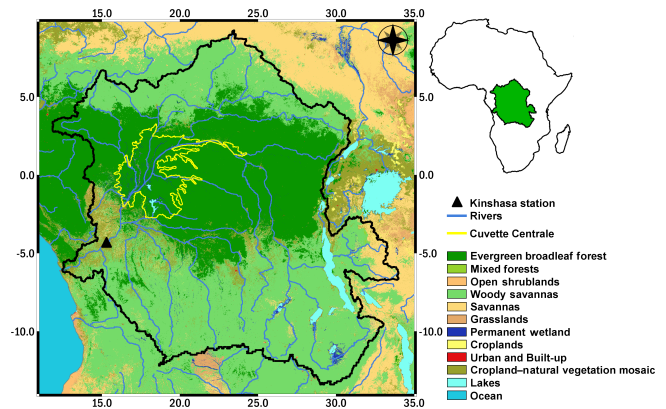


**Figure 1.** Geographic location of the Congo River basin, which shows the Kinshasa gauging station, the fluvial system, and the land use based on 10 years (2001–2010) (source: Broxton et al., 2014). The boundaries of the Cuvette Centrale are contoured in yellow (adapted from Betbeder et al., 2014).

ond most important tributary to the Congo River (mean flow 41 000 m<sup>3</sup> s<sup>-1</sup>) after the Kasai River (8000 m<sup>3</sup> s<sup>-1</sup>) (Briquet, 1995).

The CRB comprises the second largest continuous rainforest in the world, covering an area of approximately 1.8 million km<sup>2</sup>. The high evaporation rate is comparable to that of the oceans and is one of the main features of the forests, which are extremely important for storing carbon, affecting the continental and global climate system, mainly through the water cycle (Haensler et al., 2013; Marquant et al., 2015; Wasseige et al., 2015). The basin basically consists of a central area that contains an immense forest swamp that is known as Cuvette Centrale, an immense depression at the centre of the basin where sediment accumulation has occurred since the Quaternary; alluvial deposits rest on thick sediments of continental origin, which principally consist of sands and sandstones (Kadima et al., 2011; Gana and Herbert, 2014) (Fig. 1). Here, the spatial distribution of forested wetland is controlled by the topography and the time and intensity of submersion, making this area the most extensive peatland complex in the tropics (Dargie et al., 2017). From a rainfall perspective, the Congolese central basin largely functions as a closed system of precipitation, on-site evaporation, and precipitation because of the topographic barrier around the Cuvette Centrale (Robert, 1946; Sorre, 1948). An immense elliptical body of water (3 m deep with a surface of 23 km<sup>2</sup> and maximum water storage of 55 × 10<sup>6</sup> m<sup>3</sup>) called Lake Télé is located in the heart of the dense Congolese equatorial forest, where hydrological exchanges are almost exclusively vertical with very little lateral contribution from the surrounding swamp (Laraque et al., 1998). Furthermore, the basin contains several large, permanent open-water lakes, including Lake Tanganyika, the largest of the African rift lakes and the world's second largest by volume and depth (Coulter, 1991; Cohen et al., 1993).

The central basin contains a dense humid evergreen forest, while mosaics of mixed forest, woody savannas, and savannas are present to the north and south (Marquant et al., 2015). The current distribution of different forest types strongly correlates with the annual rainfall and particularly with the length and severity of dry seasons (CARPE, 2005). The CRB's moist forests are the continent's main forest resource, containing extraordinary biodiversity (Ilumbe, 2006; SCBD-CAFC, 2009) that brings important economic benefits to approximately 60 million people in local communities (Nlom, 2011; Marquant et al., 2015). Unfortunately, the deforestation rate in the CRB varies between countries. Overall, the basin had a net deforestation rate of 0.09 % between 1990 and 2000 compared to 0.17 % between 2000 and 2005 (Tchatchou et al., 2015). In fact, satellite data showed a widespread decline in greenness in the northern Congolese forest over the past decade, which is generally consistent with decreases in rainfall, terrestrial water storage, and other related aspects (Potapov et al., 2012; Zhou et al., 2014; Hua et al., 2016) such as hydrological regimes (Laraque et al., 2001, 2013; Wesselink et al., 1996).

The air masses that originate from three permanent anticyclones to the northwest (Azores), southwest (St. Helena), and southeast (Mascarene) of the CRB converge along the Intertropical Convergence Zone (ITCZ), which separates the southerly low-level winds from the northerly winds, and the Inter-Oceanic Confluence Zone (IOCZ), which separates the westerly from the easterly winds in southern Africa (Samba and Nganga, 2012). Generally, two modes of circulation, namely, the Hadley circulation and the Walker circulation, control the movement of air masses and the climate in Central Africa, leading to non-uniform moisture convergence in the atmospheric column (Tsalefac et al., 2015; Pokam et al., 2012). Areas that are positively correlated with Congo convection are areas of the ascending arm of the Hadley cell (Matari, 2002), while the east–west oscillation of the Walker circulation cell modulates moisture advection from the Atlantic Ocean and the upward motion over the CRB (Matari, 2002; Lau and Yang, 2002). The rainfall-generation mechanisms are controlled by a zone of shallow depression systems in the CRB (Samba and Nganga, 2012), north–south ITCZ migration (Samba and Nganga, 2012; Alsdorf et al., 2016), mesoscale convective systems (MCSs) (Jackson et al., 2009), the African easterly jet, and the typical circulation of the Hadley cell (Nicholson, 2009; Pokam et al., 2012; Haensler et al., 2013).

## 2 Data and methodology

The drainage area of the CRB (Fig. 1) was defined by using geo-referenced watershed boundaries on a 30 arcsec resolution map (a HydroBASIN product of HydroSHEDS, or Hydrological data and maps based on Shuttle Elevation Derivatives at multiple Scales; Lehner and Grill, 2013). This map

was used to obtain the spatial mask of the basin, which was later implemented in the computations.

The methodology in this study was based on the Lagrangian model FLEXPART, which was developed by Stohl and James (2004, 2005). This model enabled us to track air parcels backward and forward; thus, the model outputs were used to compute the gain and loss of humidity along trajectories of air particles that leave from and arrive in the CRB. The backward analysis was utilised to identify the moisture sources for the CRB, and the forward analysis was performed to obtain their climatological moisture supply and the relationship with the precipitation over the basin. This approach has been widely and successfully applied to study the atmospheric branch of the hydrological cycle (e.g. Stohl and James, 2004, 2005; Nieto et al., 2008; Gimeno et al., 2010, 2012; Chen et al., 2012; Viste and Sorteberg, 2013; Drumond et al., 2014).

In this method, the atmosphere is divided into  $N$  evenly distributed particles or parcels, whose advection is described by Eq. (1):

$$dx/dt = v[x(t)], \quad (1)$$

in which  $x$  is the position of the parcel and  $v[x(t)]$  is the interpolated wind speed in space and time. The gain (through evaporation from the environment  $e$ ) or loss (through precipitation  $p$ ) of specific humidity ( $q$ ) by each parcel is calculated following Eq. (2). Along with individual trajectories,  $q$  fluctuations can occur for nonphysical reasons (e.g. because of  $q$  interpolation or trajectory errors), a limitation that is partially compensated for by the presence of so many particles in an atmospheric column over the target area. Thus,

$$(e - p) = m(dq/dt), \quad (2)$$

in which  $m$  is the mass of a particle. Integrating over an area of interest produces the net effect of the moisture changes in all the particles in the atmospheric column and thus determines the surface freshwater flux, hereafter represented by  $(E - P)$  (Stohl and James, 2004). In some regions, atmospheric moisture is not precipitated but merely flows through; in other regions, the convergence of moisture ensures that precipitation occurs (Pokam et al., 2012). A region is then considered a moisture source when  $(E - P) > 0$ , and the net moisture budget of the tracked particles favours evaporation from the environment to the particles. The opposite occurs in moisture sink regions, i.e. the associated moisture budget favours moisture loss from the tracked particles to the environment. An analysis that is performed backward in time distinguishes the origin of the atmospheric moisture in the air masses over the CRB, enabling us to identify the main oceanic and continental sources of moisture. This analysis was applied for 10 days, which is the average residence time of water vapour in the atmosphere (hereafter, we use  $(E - P)_i$ ; Eltahir and Bras, 1996; Numaguti, 1999).

The Lagrangian data that were used in this work were obtained from a FLEXPART v9.0 experiment that was executed

on a global domain, in which the atmosphere was divided into approximately 2 million uniformly distributed particles. FLEXPART uses ERA-Interim reanalysis data (Dee et al., 2011), which are available at 6 = h intervals (00:00, 06:00, 12:00, and 18:00 UTC) at a resolution of 1° at 61 vertical levels from 0.1 to 1000 hPa, with approximately 14 model levels below 1500 m and 23 below 5000 m. This configuration is important because the transport of water vapour mainly occurs in the lower troposphere, which is clearly affected by the Earth's topography (Peixoto and Oort, 1992).

A threshold was used to ensure the selection of the most important annual moisture source regions for the CRB, which was defined by the value of the 90th percentile as calculated from the annual  $(E - P) > 0$  values after integration over the 10 days of transport. This value acted as a boundary to delimit regions where air masses gained more humidity during their journey to the CRB, representing the 10% of grid points with the highest positive  $(E - P)$  values on the map. This criterion was applied for similar purposes by Drumond et al. (2014, 2016a, b). The CRB itself is considered a source of moisture; thus, we could evaluate its role in the local  $(E - P)$  budget. Tracking the air parcels forward from each of the delimited moisture sources enabled us to compare their moisture contributions to precipitation ( $(E - P) < 0$ ) over the CRB.

Precipitation data were obtained from the CRU TS v3.23 database (Harris et al., 2014) with a spatial resolution of 0.5°. The runoff and the vertically integrated moisture flux (northward and eastward) (VIMF) formed a portion of the ERA-Interim reanalysis project (Dee et al., 2011), with a resolution of 1° × 1° in latitude and longitude. The role of general circulation in the hydrological cycle can be clearly shown through maps of vertically integrated atmospheric moisture flow (Peixoto and Oort, 1992). The VIMF also enables readers to compare moisture transport under a Eulerian perspective (Drumond et al., 2014); consequently, these maps should support explanations of moisture budgets that are calculated by using FLEXPART.

The corrected monthly mean discharge of the Congo River as recorded at the gauging station of Kinshasa (4.0° S, 15.3° E) was provided by the Global Runoff Data Centre (GRDC). We used two state-of-the-art base datasets, namely, OAFflux and Global Land Evaporation Amsterdam Model (GLEAM) (Miralles et al., 2011), to estimate the actual evaporation over the moisture sources. The monthly ocean evaporation data were obtained from the OAFflux project, which uses surface meteorological fields from satellite remote sensing and reanalysis outputs from the NCEP and ECMWF models (Yu et al., 2008). The monthly evaporation from the land was estimated from GLEAM v2 data, which consider a set of algorithms, including transpiration, bare-soil evaporation, interception loss, open-water evaporation, and sublimation (Miralles et al., 2011), all of which are important because of the dense forests in the CRB.

Global datasets were selected because of documented gaps in the hydrological information for the CRB (Tshimanga, 2012). However, observational data series are available on the SIEREM website (Boyer et al., 2006), mainly to the north of the basin. In this work, the analysis covered the period 1980–2010 because of the availability of ERA-Interim since 1980 and the available river discharge data from the Kinshasa gauge station until 2010.

The methodology to quantify drought or wet conditions in the CRB was based on the Standardised Precipitation Evapotranspiration Index (SPEI), which is a multi-scalar drought index that considers the effects of both precipitation and atmospheric evaporative demand (AED) (Vicente-Serrano et al., 2010). The SPEI for the CRB was calculated on timescales from 1 to 24 months by using precipitation and reference evapotranspiration (ET<sub>o</sub>) data from the CRU TS v3.23 dataset. The criterion of McKee et al. (1993) was used to identify years of severe and extreme drought and wet conditions (according to the SPEI threshold of ±1.5). The hydrological drought conditions were quantified at the gauging station of Kinshasa by using the Standardised Streamflow Index (SSI) (Vicente-Serrano et al., 2012).

### 3 Results and discussion

#### 3.1 Climatology: rainfall and runoff over the basin and the Congo River's discharge

The annual cycle of precipitation over the CRB is depicted in Fig. 2. The most notable feature of the monthly patterns is the latitudinal migration of the maximum precipitation throughout the year, which leads to different seasonal patterns over the territory (Bultot, 1971; Chishugi, 2008). Based on previous results, Mahe (1993) defined four great climatic zones over the Congo Basin: the North (Oubangui River basin), where the influence of the North African continental air mass is prominent; the South (Kasai River basin), which is influenced by South African air masses; the eastern and south-eastern areas of the basin (Lualaba River upper basin), which are influenced by the humid Indian Ocean air masses; and the Centre-West, where the climate is controlled by the Atlantic Ocean. In fact, the effect of rainfall on various sectors and its distribution throughout the annual cycle may be as important as the total annual rainfall (Owiti and Zhu, 2012). During January, February, and March, the southern half receives more precipitation, while April is a transitional month with maximum rainfall in the western-central and northeastern areas of the basin. From May to August, the rainfall pattern appears homogeneous, and the majority of the average precipitation occurs in the northern area, which coincides with the northward excursion of the ITCZ between February and August (Nicholson and Grist, 2003; Suzuki, 2011). From May to October, the northeastern CRB receives the highest rainfall, which favours the Oubangui catchment, a right-bank tributary of the Congo River that drains an area of 488 500 km<sup>2</sup>

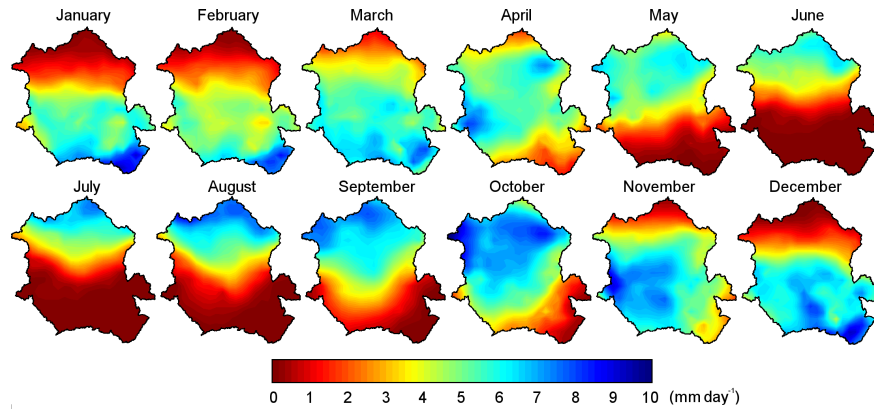


**Figure 2.** Monthly mean precipitation over the CRB for 1980–2010. The data are from CRU TS v3.23.

at the Bangui gauge station (Runge and Nguimalet, 2005). In September, the rainfall increases to the south and affects the centre of the basin, with the greatest extension in October. In November, the central and southwestern areas of the CRB receive more rainfall; December also exhibits an extension to the southeast (Fig. 2). The precipitation regime over the CRB is clearly differentiated by a latitudinal oscillation of maximum accumulated values, in accordance with several studies as reviewed by Alsdorf et al. (2016), and an inter-annual variability that is higher to the north and south than in the central units of the basin (Mahe, 1993).

The monthly average precipitation for the entire basin shows an annual cycle with two maximum peaks during March–April and October–December, with values above  $4.5 \text{ mm day}^{-1}$  and each comprising 21 and 32.6 % of the mean annual rainfall in the CRB, respectively (Fig. 3). During June and July, the average rainfall reaches its lowest level of around  $2 \text{ mm day}^{-1}$ . This cycle is similar to what was described by Washington et al. (2013), who compared the Congo’s rainfall climatology through several datasets from reanalysis and ensemble models. However, these authors argued that the maximum rainfall in the basin occurs from March to May and from September to November, while the minimum occurs in June–August. These differences in monthly average precipitation may be caused by the areas that were used; these authors used a box region over equatorial West Africa, while we used the CRB’s boundaries.

The mean annual cycle of runoff in the CRB (Fig. 3) follows the same annual cycle as rainfall, although the former is always lower, varying between maximum values of  $3.0$  and  $3.5 \text{ mm day}^{-1}$  during November–March and minimum values below  $1.5 \text{ mm day}^{-1}$  during July and August. The long-term distribution of precipitation and runoff over the African continent is almost the same (Siam et al., 2013), but the highest runoff values are concentrated in the heart of the equatorial forest along the middle Congo River branch (Alemaw, 2012), with these wetlands receiving the majority of their waters from upland runoff (Lee et al., 2011) and

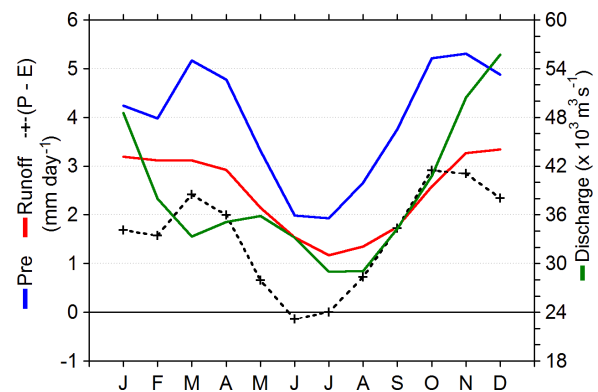


**Figure 3.** Annual cycle of precipitation, runoff, and  $(P - E)$  in the CRB (left axis) and the Congo River’s discharge (right axis). The data are from CRU, ERA-Interim, GLEAM, and the Global Runoff Data Center, respectively.

several large rivers that drain into the Congo in this middle section; the largest of these rivers is the Oubangui to the north of the Congo Basin (Harrison et al., 2016). The calculated inter-annual correlation between the two series (precipitation and runoff) over the CRB is high:  $r = 0.73$  (significant at  $p < 0.05$ ) and  $r = 0.72$  with a 1-month lag. Figure 3 shows that the runoff from March onward exhibits a 1-month lag compared to the precipitation. Generally, under steady-state conditions, the precipitation exceeds the evaporation (or evapotranspiration) over the land and the residual water runs off, resulting in the continental freshwater discharge into the oceans (Dai and Trenberth, 2002). This process also occurs in the CRB, where the monthly precipitation minus the actual evaporation seems to follow the same annual cycle as the precipitation (Fig. 3). June  $(P - E)$  has a negative value, which means that the average evaporation exceeds the precipitation in the basin (as in Dai and Trenberth, 2002, and Siam et al., 2013).

The mean annual discharge of the Congo River is  $38\,617.4 \text{ m}^3 \text{ s}^{-1}$ , which was calculated from the GRDC

monthly discharge values at the Kinshasa gauging station in the period 1980–2010. According to the secular chronic of the hydro-pluviometric data (1903–2010) that were recorded at the Brazzaville gauge station close to Kinshasa, which was analysed by Laraque et al. (2013), the average flow of the Congo River from 1982 to 1994 was below the annual mean, followed by a period of stability from 1995 to 2010. The long-term results of Mahe et al. (2013) suggested that the Congo River's runoff time series (at the Brazzaville station) followed no long-term trend (here, these authors referred to the runoff as the discharge) and that the minimum showed less inter-annual variability than the average or maximum.

The annual cycle of discharge (which is very similar to the precipitation and runoff) shows climatological maxima during November–December (Fig. 3), with values above  $48\,000\text{ m}^3\text{ s}^{-1}$ , while the minimum in July and August is less than  $30\,000\text{ m}^3\text{ s}^{-1}$ . However, one difference is seen during March, when high precipitation and runoff occur but the discharge is low. During the next few months, the precipitation and runoff decrease while the discharge increases, reaching a maximum in May. This lag should reflect both the required time for the surface runoff to reach the river mouth and the groundwater contribution (Dai and Trenberth, 2002; Dai et al., 2008; Marengo, 2005; Rwetabula et al., 2007; Sear et al., 1999), as documented by Matera et al. (2012), who used data that were recorded at the Brazzaville station approximately 400 km upstream of the river mouth. The direct relationship between the precipitation over the basin and the discharge has a correlation of 0.52, which increases to 0.66 for a 1-month lag (both statistically significant at  $p < 0.05$ ), confirming the aforementioned lagged response. Bricquet (1993) noted that a translation of the stability of this hydrological regime is shown by a high (low) frequency of floods on similar dates in each year. Future climate projections (21st century), although uncertain, show a basin-wide average increase in both rainfall and evaporation, but the total increase in rainfall tends to be higher than the increase in evaporation; the result in most scenarios is increasing runoff (Beyene et al., 2013). Nevertheless, Tshimanga and Hughes (2012) downscaled scenarios for the northern sub-basins of the Oubangui and Sangha rivers, in which more than a 10 % decrease in the total runoff occurs because of the relatively little increase in rainfall and a consistent increase in potential evapotranspiration.

### 3.2 Identification of the moisture sources

In December, January, and February over the CRB, areas where  $(E - P)i_{10} > 0$  (moisture sources) are represented by reddish colours and are located over the northern half of the basin and over the river mouth (Fig. 4). Negative values  $(E - P)i_{10} < 0$  (sinks), which are portrayed in blueish colours, cover the southern CRB. Outside the boundaries of the basin,  $(E - P)i_{10} > 0$  values can be seen spread over the northeast of the continent, the Mediterranean Sea, the Red

Sea, the Arabian Sea, and the tropical eastern South Atlantic Ocean. Negative values are observed in the southeast of the basin, the tropical western Indian Ocean, and the equatorial Atlantic Ocean around the Equator. For these 3 months, the moisture convergence over central-equatorial Africa is between  $0$  and  $20^\circ\text{ S}$ , and a divergence belt of  $0^\circ$  occurs to the north. The atmospheric divergence and convergence patterns are associated with high-pressure systems and low pressures at the Equator and in the ITCZ. The deep convection of the ITCZ depends on the contribution of water vapour from the surface moisture flux, which is supplied as surface latent heat flux, and the horizontal moisture flux in the lower free atmosphere (Suzuki, 2011). The VIMF identifies moisture that reaches the CRB from divergence zones over the Sahel and the Arabian Sea. Assessing the VIMF is extremely important because the seasonal variability in the spatial gradient of precipitation recycling in equatorial Central Africa is regulated by both the direction and strength of the moisture flux (Pokam et al., 2012).

In March, the  $(E - P)$  pattern changes over the basin, with the establishment of intense moisture sinks to the centre-west. March seems to be a transitional month; in April, the  $(E - P)$  pattern undergoes a more obvious change that is characterised by moisture loss over the northern half of the basin, a region that acts as a source in preceding months. However, the VIMF flows from east to west over the basin in both months, and the convergence and divergence fields of moisture flux are not that different from those in previous months, instead highlighting a decrease in the divergence over the Arabian Sea (Fig. 4).

Similar to in April, the  $(E - P)$  budget over the basin from May to September is characterised by negative values in the northern half, which match the maximum precipitation rates for these months (see Fig. 2). From June to August (the driest months), these values are confined to the northern area of the basin, while an evaporative regime prevails over the rest of the CRB, which demonstrates the ability of FLEXPART to simulate moisture losses in the basin that are associated with convective precipitation and rainfall migration. Beyond the CRB, the source areas  $(E - P)i_{10} > 0$  over the Arabian Sea diminish and the VIMF changes from its previously southward direction from May to September, which means that moisture transport from this region to Africa is no longer favoured. The  $(E - P)i_{10}$  patterns are very similar to those of previous months for the other regions. During these months, the moisture sinks in the equatorial Indian Ocean are less intense than in previous months. At the same time, a latitudinal displacement of moisture convergence and divergence zones occurs over central-equatorial Africa; a joint analysis of the maximum precipitation and convergence of the VIMF provides a rough estimate of the position of the ITCZ (Žagar et al., 2011).

Locations where values of  $(E - P)i_{10} > 0$  are generally accompanied by moisture flux divergence. However, the Arabian Sea acts as moisture sink from May to October (blueish

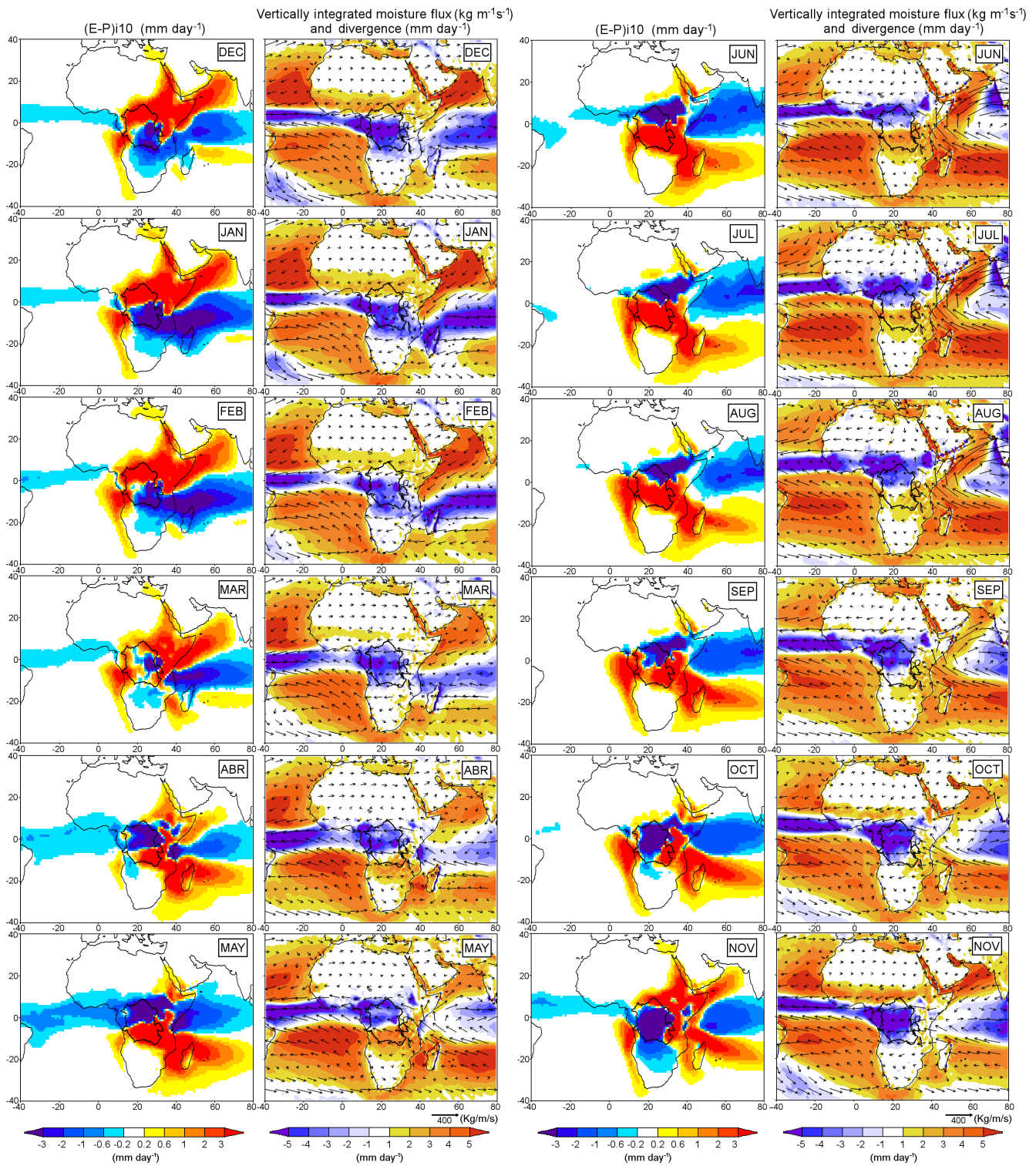


**Figure 4.** Monthly climatological  $(E - P)$  values integrated backward over 10 days ( $\text{mm day}^{-1}$ ) alongside the vertically integrated moisture flux ( $\text{kg m}^{-1} \text{s}^{-1}$ ) and divergence–convergence (reddish-blueish colours) ( $\text{mm day}^{-1}$ ). Period: 1980–2010.

colour in the left-hand panels); specifically, the VIMF shows an anticyclonic circulation over the Indian Ocean during June–September, which induces intense northeastward flow from the Arabian Sea to the Indian Peninsula and acts as an important moisture source for Indian monsoon rainfall (Levine and Turner, 2012).

The sink regions cover almost the entire CRB in October and November, when the southeastern Atlantic Ocean, the continental regions to the east and north of the basin, and the southwestern Indian Ocean all act as moisture sources. A transition in the scheme of the moisture source regions occurs in November, when  $(E - P)i_{10} > 0$  values appear once again over the Arabian Sea (Fig. 4). This result coincides with the beginning of the summer in the Southern Hemisphere and the decay of the Indian monsoon. The VIMF illustrates the moisture transport from the source regions to an area to the south of  $0^\circ$  in central-equatorial Africa, which enhances the precipitation over the CRB in accordance with the southward movement of the ITCZ over Africa.

The climatological annual backward average of 10-day integrated  $(E - P)$  from the CRB is presented in Fig. 5. This figure summarises the most important moisture sources for the CRB throughout the year. As discussed earlier, the boundaries of the moisture source regions were delimited by imposing the 90th percentile ( $p_{90}$ ) threshold of the annual  $(E - P)i_{10} > 0$  values. This result equates  $0.43 \text{ mm day}^{-1}$ , which is denoted in Fig. 5 by the dashed lines. Five continental (C) and four oceanic (O) moisture sources were defined (Fig. 6). The five continental regions are as follows: central and northeastern Africa (C1), the equatorial-western section of the continent on both sides of the Equator and at the river mouth (C2 to the north and C3 to the south), the eastern CRB along the coast of Africa from the north of Somalia and Ethiopia to approximately  $20^\circ \text{ S}$  (C4), and the CRB itself. The four oceanic sources are in the Red Sea (O1), the Arabian Sea (O2), the eastern tropical equatorial South Atlantic Ocean along the coast of Africa (O3), and the tropical western Indian Ocean (O4). Such moisture source regions are not stationary, varying in intensity from year to year, and are expected to change in the future (Gimeno et al., 2013). In addition, their role may change given the high decadal- and century-scale variability in the African climate (Masih et al., 2014). Nevertheless, these source regions provide insight into the mechanisms by which atmospheric moisture transport occurs toward central equatorial Africa. A combination of factors may influence the role of each source in the moisture influx into the CRB, such as the amount of evaporated water, the distance between each source and its target area, the atmospheric circulation, and the residence time of water vapour in the atmosphere.

A comparison with the evaporative moisture sources for the CRB from the quasi-isentropic method and online data (<http://cola.gmu.edu/wcr/river/basins.html>) confirms the importance of recycling in the CRB, which matches our results in terms of the CRB retaining humidity from itself

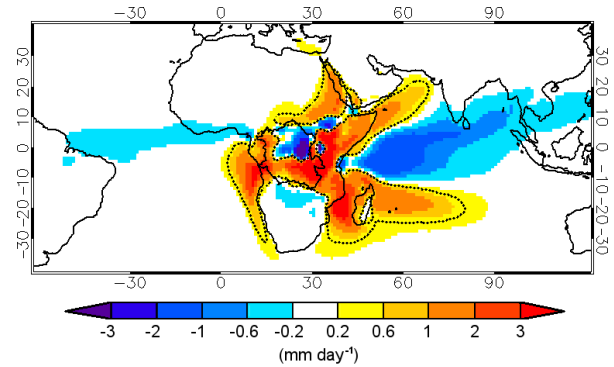


**Figure 5.** Annual mean  $(E - P)i_{10}$  values backward-integrated over 10 days for the period 1980–2010. The dashed lines represent the boundaries of the moisture sources, which are defined as  $p_{90} = 0.4 \text{ mm day}^{-1}$ .

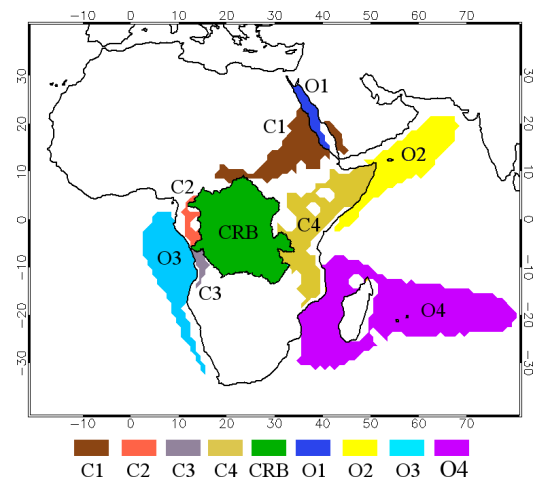


**Figure 6.** Continental moisture sources for the CRB: C1, C2, C3, C4, and the CRB itself; oceanic moisture sources: O1, O2, O3, and O4.

(Figs. 4, 5). Nevertheless, some differences exist on the annual scale: sections of the northern half of the basin act as moisture sinks (Fig. 5), while the aforementioned quasi-isentropic climatology considers the entire basin to be an evaporative source. Another clear difference is the Indian Ocean: our results more clearly reflect the seasonal latitudinal migration of the evaporative regions over the year.

### 3.3 Freshwater evaporation in the sources

An analysis of the evaporation rate over the moisture sources may support our understanding of their role in the moisture uptake for the CRB over the year. Although the mean evaporation over a region that is considered to be a moisture source, quantified here by using GLEAM and OAFflux, can be high, its contribution to precipitation over the CRB might not be as high because this source could also be providing moisture for precipitation into other target regions. The geographical lo-

**Table 1.** Mean annual evaporation rate over the sources. The data for the continent were obtained from GLEAM and those for the ocean from OAFlux.

Sources →	Evaporation rate (mm day <sup>-1</sup> )								
	C1	C2	C3	C4	CRB	O1	O2	O3	O4
	1.0	2.5	1.6	1.5	2.4	4.6	1.1	0.71	4.7

cation of the basin enables this area to receive moisture from the Atlantic and Indian oceans and from land regions around the basin, as Fig. 6 shows. Oceanic evaporation is very important if we consider that evaporation from the ocean surface equates roughly 86 % of the total amount of water that is evaporated from the planet (Schmitt, 1995) and that the role of the oceans is decisive in continental precipitation (Gimeno et al., 2010). The mean annual evaporation from the sources is given in Table 1 by using data from OAFlux and GLEAM for the ocean and continental regions, respectively. On average, O4 and O1 are the most evaporative sources while O3 is the least evaporative. Among the continental sources, the most evaporative are C2, CRB, and C3.

These sources are located in two different hemispheres and thus should have different annual evaporation cycles (Fig. 7). According to the FLEXPART backward experiment from the CRB, monthly positive ( $E - P$ ) values were calculated over each source (hereafter E-FLEX) to compare them with the yearly average evaporation at the sources. ( $E - P$ ) > 0 can be discounted after ( $E - P$ ) has been integrated without altering the general patterns of net precipitation by using a monthly or longer timescale (Castillo et al., 2014). Figure 7 displays both series for comparison alongside E-GLEAM (evaporation data over continental sources) or E-OAF (for oceanic ones) and E-FLEX. On the African continent, E-GLEAM is higher than E-FLEX in C1 from May to October (boreal summer), while the opposite occurs in the other months, indicating when this source becomes more efficient in providing moisture to the CRB (grey shaded areas in Fig. 7, C1). The next continental source is C2, which shows a higher land annual evaporative value (Table 1). In this source, the annual cycles of E-GLEAM and E-FLEX differ from those of C1. Over this region, the E-FLEX values are greater than the calculated local evaporation when using the GLEAM dataset during February and from June to October (grey shaded areas in Fig. 7, C2). Despite this local evaporation, E-GLEAM does not show any great variations over the year, varying from 2 to 3 mm day<sup>-1</sup>. E-FLEX shows a bimodal cycle with a minimum in May ( $\sim 0.3$  mm day<sup>-1</sup>), when major local evaporation occurs, and a maximum in August ( $\sim 4.2$  mm day<sup>-1</sup>), when local evaporation is at its lowest. This behaviour illustrates that moisture can be available in the atmosphere (higher E-GLEAM values) but less humidity is taken up by air masses and then carried toward our target region (lower E-FLEX values). In this mechanism, the atmospheric circulation and the rainfall over the

region must play a key role; E-FLEX could be lower than E-GLEAM because of high  $P$  values over the region. The grey shaded areas in Fig. 7 indicate months when the transport of moisture is favoured from the source to the CRB. Over the course of several days, an air parcel may undergo multiple cycles of evaporation and precipitation (Sodemann et al., 2008). After we integrated monthly data over 10 days, the E-FLEX values could be greater than the local evaporation. Nevertheless, C2 is a land region, where the recycling concept is most useful because moisture for evaporation is limited by precipitation, whereas the surface of oceans is clearly wet with or without rain (Trenberth, 1999). The C3 source, which is separated from C2 by the Congo River mouth, follows a similar annual evaporation cycle to C2 but with lower values ( $< 1$  mm day<sup>-1</sup>) during June–October (Fig. 7, C3). In addition, the E-FLEX values are higher than E-GLEAM in February and July–September. In the months of March–May and November, C3 becomes less efficient at providing moisture to the CRB. For the continental source C4, the annual cycle of local evaporation (E-GLEAM) is similar to those of C2 and C3, but the moisture uptake by air masses that are tracked backward from the CRB (E-FLEX) over C4 is always greater than E-GLEAM (unless in February); thus, this source is very efficient in terms of moisture uptake for the CRB, which matches the results of van der Ent et al. (2014). For the CRB, the annual cycle of E-GLEAM is characterised by maximum values during December and March–May and minimum values in July–August (Fig. 7, CRB). In January–February, April–October, and December, E-FLEX is higher than E-GLEAM, which matches the decreasing precipitation over the basin (Fig. 3). This pattern is understandable because the moisture uptake (E-FLEX) over the basin itself must be favoured when the precipitation over the area decreases. Comparing the annual precipitation cycle in the CRB (Fig. 3) with E-GLEAM (Fig. 7) indicates the same annual cycle, but both sets of results show opposite behaviour from E-FLEX (Fig. 7, CRB). This relationship describes a scheme in which the precipitation and evaporation are strongly linearly related; in fact, evaporation as a source for precipitation over land depends on the availability of surface moisture, which in turn depends on the disposition of precipitation once it hits the ground (Trenberth, 1999). However, the moisture uptake is the opposite, determining when the source is more effective in providing moisture for itself, which is favoured when precipitation decreases. This relationship is not strictly interdependent because it could be

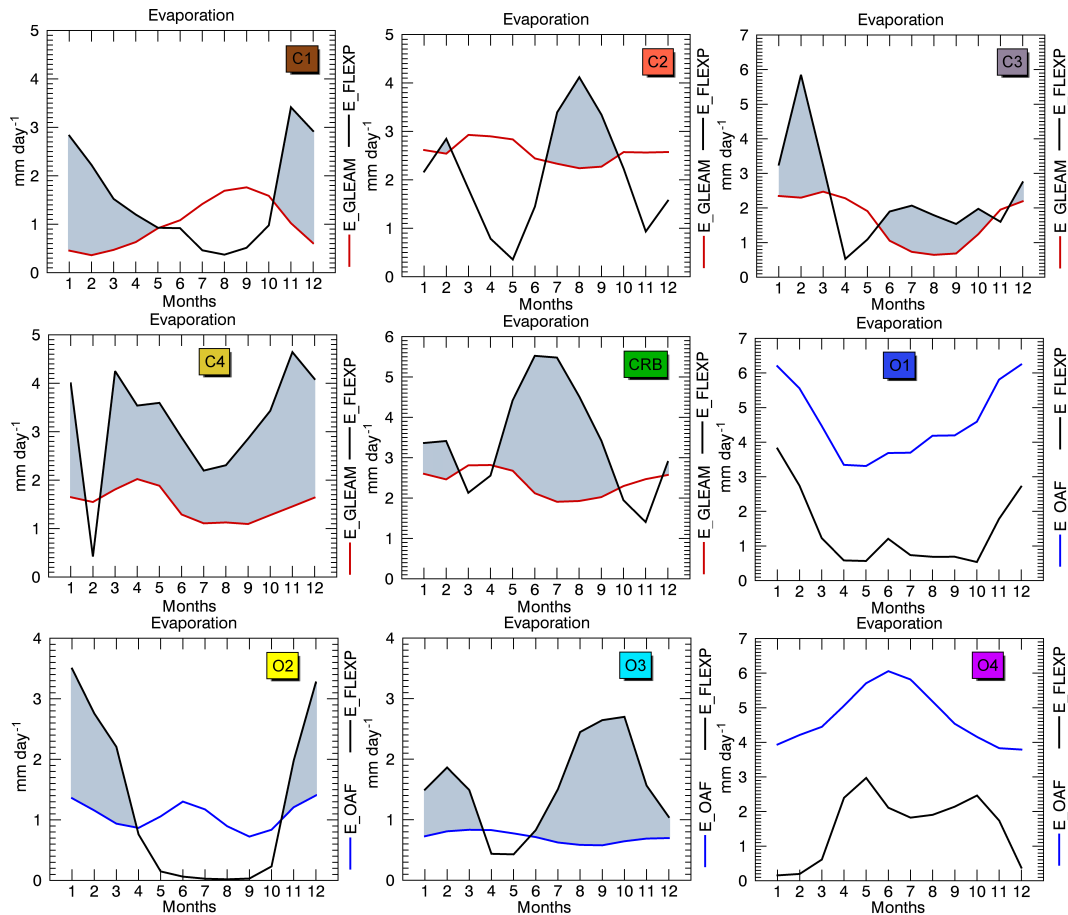


**Figure 7.** Monthly mean evaporation ( $\text{mm day}^{-1}$ ) in the continental (C) and oceanic (O) sources. The data are from GLEAM (red lines) and OAF flux (blue lines). E-FLEX: evaporation values over the sources from FLEXPART (black lines). The areas that are shaded in grey mark where E-FLEX > evaporation. Data period: 1980–2010.

modulated by moisture income from other sources or transported outside the boundaries of the target region (the basin).

In source O1, the mean annual E-OAF is  $4.60 \text{ mm day}^{-1}$  (Table 1). This source is located in the Red Sea, where the oceanic evaporation rate is the highest in the world according to Abdulaziz (2012). After reviewing many studies, Sofianos et al. (2002) confirmed several differences in the mean annual evaporation rate for the Red Sea, but this value was estimated at around  $2.06 \text{ m year}^{-1}$  ( $\sim 5.6 \text{ mm day}^{-1}$ ). Figure 7 shows the annual evaporation cycle (E-OAF) in this source, which is characterised by higher values during the boreal winter months and minimum values in summer, which matches Bower and Farrar (2015). The monthly E-FLEX values over this source follow the same annual cycle as E-OAF but with lower values. Despite being a high evaporative source, the moisture uptake from O1 to the air masses in transit to the CRB is less than what it must provide itself to the atmosphere, converting this area into a region that is not efficient in terms of the moisture supply to the CRB. In contrast, this area seems to be an important moisture source during December–February over continental areas to its north-

east and during June–August to the remote area of the Indian Peninsula (Gimeno et al., 2010). The O2 source in the Arabian Sea shows two evaporation peaks during December–January and June and two minima in April and September (Fig. 7). This cycle was also noted by Pokhrel et al. (2012) and Sadhuram and Kumar (1987), who showed that the maxima are related to strong winds and the minima are a result of low wind speeds and weak vapour pressure across the Arabian Sea. The moisture uptake over this source between April and October is almost insignificant, but the evaporation from OAF flux is greater; thus, this source is not efficient in delivering moisture to the CRB because this region contributes to the Indian monsoon during these months (Levine and Turner, 2012). The source in the Atlantic (O3) has the smallest monthly average evaporation rate among all the oceanic sources throughout the year ( $< 1 \text{ mm day}^{-1}$ ) (Table 1), showing a negligible annual cycle. Matera et al. (2012) determined that the evaporation rate from the ocean surface is lower because a portion of this oceanic region is affected by the huge freshwater discharge of the Congo River, decreasing the sea surface salinity (SSS) and sea surface temperature

(SST). However, E-FLEX is greater than E-OAF except during April and May, when the moisture uptake over this source is less than  $1 \text{ mm day}^{-1}$ . The moisture uptake has two peaks: one in February and the other in September–October. The last oceanic source is O4, which is the most evaporative and is characterised by a maximum average E-OAF in May–July ( $> 5.5 \text{ mm day}^{-1}$ ) and a minimum at the beginning and end of the year (Fig. 7, O4). This behaviour matches the results of Yu (2007), who argued that evaporation in the Northern (Southern) Hemisphere intensifies during the boreal (austral) wintertime. The positive E-FLEX values over this source (O4) are lower and quite different from the mean E-OAF during all months. On average, this source is not very efficient in supplying moisture to the CRB. The efficiency of a region that provides moisture for precipitation to a target area depends on the amount of evaporated water that reaches it and not just the initial evaporation rate. In this mechanism, we must highlight the importance of the atmospheric circulation patterns in determining the water vapour transport, the water vapour's residence time in the atmosphere, and moisture uptake from each source that is completely different from the evaporation.

### 3.4 Moisture contribution from the sources: forward analysis

Having identified the moisture source regions and their efficiency in providing moisture to air masses in transit to the CRB, we determined the quantities and locations of the moisture loss over the CRB from those particles that leave each source by using forward tracking. For this purpose, a forward experiment with FLEXPART was used to integrate particles forward over 10 days. FLEXPART was used to compute the changes in  $(E - P)$  by tracking air parcels with or without rain; in this case, we only computed the result for those particles that arrive in the CRB that lost humidity  $(E - P)_{i10} < 0$ , hereafter called the moisture contribution.

The annual cycle of the percentage moisture contribution to precipitation from each source with respect to the total moisture contribution to the basin appears in Fig. 8 alongside the monthly mean precipitation over the CRB from CRU TS v3.23 data (Harris et al., 2014). The basin itself is the most important moisture source throughout the year, contributing more than 50 % each month (green line) to the total moisture supply from all the sources to the basin. The contribution from each of the remaining continental and oceanic sources does not exceed 20 % of the total. This result suggests the importance of moisture recycling over the basin, which differs from the result of van der Ent et al. (2010), who argued that the main source of rainfall in the Congo is moisture that evaporates over East Africa, particularly over the Great Lakes region. This result is probably a consequence of the methods that were used; their approach considered how much of the evaporated water returns as precipitation to the same region

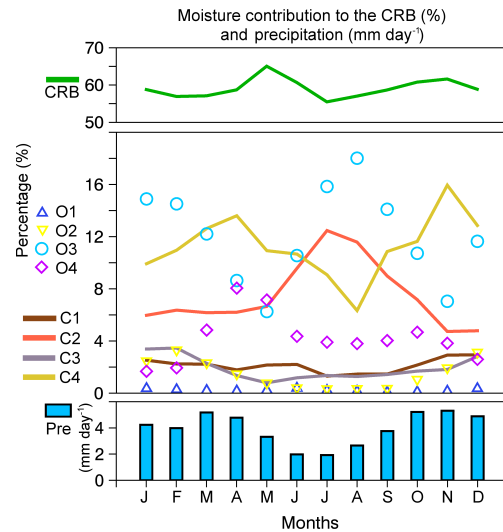


**Figure 8.** Monthly percent of moisture loss, which is calculated as  $|(E - P)_{i10} < 0|$  forward-integrated from each source over the CRB over 10 days of transport, and the monthly mean precipitation from the CRU datasets for the period 1980–2010.

(regional evaporation recycling) and how much of this water is advected out of the region.

The percentage of the moisture contribution to precipitation over the CRB is quite similar for the C1 and C3 sources, less than 4 %. C2 and C4 are the most important continental sources (after the CRB itself) that supply moisture to the CRB across the year; these sources are located to the east and west of the basin, respectively, and play opposite roles throughout the year. The moisture supply that was calculated for C4 from FLEXPART,  $|(E - P)_{i10} < 0|$ , follows the annual precipitation cycle in the basin particularly well. The moisture contributions to the basin from O1 and O2 with respect to the total are less important than those from O3 and O4. The contribution from O3 increases and is thus important when the contribution decreases from the CRB itself, confirming the importance of moisture transport from the Atlantic Ocean. The contribution of moisture from O3 reaches a maximum in January–February and July–August ( $> 14 \%$ ) when the precipitation rate decreases over the CRB (Fig. 3). The maximum monthly contribution from O4 in the Indian Ocean occurs in April–May ( $\sim 8 \%$ ).

We analysed the percentage of moisture that is supplied from land-based and oceanic sources to the total moisture inflow to the CRB for the period 1980–2010. The results confirm that close to or more than 80 % of the total moisture contribution to precipitation over the basin during the year originates from land sources, with more than 50 % of the total originating from the CRB itself (Fig. 9). Evaporation as a source for precipitation over land depends on the availability of surface moisture, which in turn depends on the disposition of precipitation once it hits the ground (Trenberth, 1999). According to Eltahir (1998), the soil mois-

ture conditions over any large region should be associated with relatively large moist static energy in the boundary layer, which favours the occurrence of more rainfall. This hypothesis was also confirmed for West African monsoons by Zheng and Eltahir (1998). In this vein, van der Ent and Savenije (2011) quantified the spatial and temporal scale of moisture recycling independent of the size and shape of the region and found that approximately 70 % of the precipitation in the centre of the South American continent is of terrestrial origin, as in many regions of Africa but specifically in the CRB, where strong moisture feedback occurs. Pokam et al. (2012) and Trenberth (1999) reported a higher recycling ratio (the fraction of rainfall from evapotranspiration and not from moisture that is advected to the target region) for CEA than what was obtained for the Amazon in Eltahir and Bras (1994) and Burde et al. (2006). As previously mentioned, the role of forests in the CRB is also fundamental because these areas sustain atmospheric moisture through evapotranspiration, which is of utmost importance for the region's water resources, particularly in the evergreen forest region (Matsuyama et al., 1994; van der Ent and Savenije, 2011). The key role of continental moisture sources has also been documented for monsoonal regions such as western Mexico (Bosilovich et al., 2003; Domínguez et al., 2008), South America (Drumond et al., 2014; Keys et al., 2014), and the Indian region (Misra et al., 2012; Pathak et al., 2015).

The annual role of the moisture sources that contribute to precipitation in the CRB is shown in Table 2 as the percentage of the total annual  $|(E - P)|_{10 < 0}$  amounts over the CRB. The CRB itself is responsible for 59.3 % and is the most effective source, followed by C4 with 12 % and O3 with 11.5 %. These three sources comprise 82.8 % of the total moisture supply to the CRB throughout the climatological year. The remaining sources contribute 17.2 % of the total precipitable moisture. The O1 source in the Red Sea is responsible for only 0.2 %.

To analyse the linear relationship, Table 3 shows the significant correlation values among the monthly series of evaporation, precipitation, runoff in the CRB, river discharge at Kinshasa gauge station,  $|(E - P)|_{10 < 0}$  from each source over the CRB, and the total  $|(E - P)|_{10 < 0}$  from all the sources ( $T$ ). All the correlation coefficients are positive and statistically significant at 95 %, with the exception of those among  $|(E - P)|_{10 < 0}$  over the CRB from C2, the evaporation in the basin, and the Congo River discharge at the Kinshasa gauge station. As expected, the correlation is greater with precipitation than evaporation because  $|(E - P)|_{10 < 0}$  may be associated with rainfall over the CRB. In most of the cases, the initial correlation values with the evaporation and those from the rest of the variables decreased because of the lagged response of the hydrological system. This behaviour is best exhibited by the correlation with  $|(E - P)|_{10 < 0}$  over the CRB in the air masses that were tracked forward in time from the CRB itself and for the total contribution. According to the correlation values in Table 3,  $|(E - P)|_{10 < 0}$  is bet-

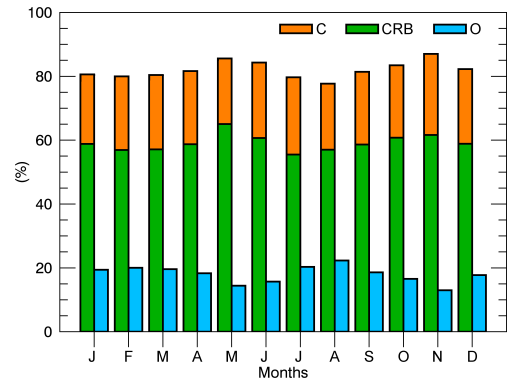


**Figure 9.** Monthly percentage moisture contributions to the CRB from continental sources (orange bars), the CRB itself (green bars), and oceanic sources (blue bars). The data are from FLEXPART for the period 1980–2010.

ter correlated with the discharge than the evaporation in the basin, except for the  $|(E - P)|_{10 < 0}$  values in the air masses from O4.

Figure 10 shows the spatial relationship between the moisture supply from the sources and the precipitation over the CRB. The mean seasonal  $|(E - P)|_{10 < 0}$  values over the CRB are plotted for December–February (DJF), March–May (MAM), June–August (JJA), and September–November (SON). Each map shows the correlation (bottom right) of these patterns with the respective climatological precipitation patterns over the basin (not shown).

The moisture sinks for the air masses from C1 to the CRB during DJF are more intense ( $\sim 1.5 \text{ mm day}^{-1}$ ) along a belt in the central-northern section of the basin that extends beyond this area to the south (Fig. 10). In MAM, the maximum moisture loss moves northward and almost disappears altogether in JJA, while the moisture loss in SON covers the entire CRB with major sinks in the northern half, which matches the high observed rainfall during these months (see Fig. 2). For SON, the best correlations were those between the  $|(E - P)|_{10 < 0}$  patterns from C1 and the precipitation over the CRB ( $r = 0.50$ ). From C2, whose sources are located to the west of the CRB, the greatest moisture contribution occurs over the west of the basin. In MAM and JJA, the  $|(E - P)|_{10 < 0}$  patterns are observed over the northern half, and the best correlation was obtained for JJA ( $r = 0.63$ ). Contrary to what occurs with moisture loss over the basin from C2, the greatest moisture sinks over the CRB for air masses that were tracked forward from C3 are mostly positioned to the southwest (best observed for SON and DJF). In MAM and JJA, the sinks are mainly located in the northern half of the basin. For C4 (located to the east of the CRB), the sinks over the CRB decrease in intensity from east to west (the eastern areas show the most intense sinks,  $> 6 \text{ mm day}^{-1}$ ). In southern equatorial Africa and specifically in the CRB region, the precipitation pattern provides a mech-

**Table 2.** Moisture contribution from the sources to the CRB (%).

Sources →	$(E - P)i10 < 0$ in %									
	C1	C2	C3	C4	CRB	O1	O2	O3	O4	
	2.3	6.8	2.0	12.0	59.3	0.2	1.8	11.5	4.1	

**Table 3.** Significant monthly correlation ( $p < 0.05$ ) between the precipitation from the CRU, runoff from ERA-Interim, river discharge from the GRDC and evaporation from GLEAM or OAFflux, and forward-integrated  $|(E - P)i10 < 0|$  series with FLEXPART from the sources over the CRB, with the total  $|(E - P)i10 < 0|$  amount ( $T$ ). Period used: 1980–2010.

	C1	C2	C3	C4	CRB	O1	O2	O3	O4	$T$
Evaporation	0.35		0.35	0.36	0.37	0.35	0.43	0.14	0.35	0.36
Precipitation	0.60	0.53	0.65	0.77	0.80	0.36	0.58	0.60	0.58	0.83
Runoff	0.66	0.43	0.72	0.69	0.75	0.59	0.73	0.59	0.43	0.75
Discharge	0.49		0.59	0.53	0.54	0.47	0.55	0.33	0.12	0.53

anism of atmospheric communication between Africa's eastern and western coasts; these two equatorial regions are generally treated as climatically separate units (Dezfuli et al., 2015). As expected, the  $|(E - P)i10 < 0|$  pattern is more intense during SON and DJF (the rainiest months). The correlations vary between 0.36 and 0.43, all of which are significant at  $p < 0.05$ . Throughout the year, the CRB is the most important moisture source for itself (Fig. 9), which is confirmed by the intensity of the values in the  $|(E - P)i10 < 0|$  patterns (Fig. 10). In DJF and SON, the greatest moisture sinks ( $> 12 \text{ mm day}^{-1}$ ) cover the majority of the centre and south of the basin. In MAM and JJA, these sinks are similar to the other sources. The correlation of these patterns with the spatial precipitation was the highest ( $r > 0.63$ ).

We previously discussed how the oceanic source O1, despite being an important evaporative region, is not an effective moisture source for precipitation over the CRB. This fact can also be seen in the  $|(E - P)i10 < 0|$  pattern over the CRB in Fig. 10, in which the values are low and oscillate around 0 to  $0.5 \text{ mm day}^{-1}$ . The pattern also reflects the north–south variability in the precipitation over the year. The greatest moisture contribution from the O2 source in the Arabian Sea occurs in the eastern and northeastern areas of the basin, except in JJA, when the pattern is confined to the northwest and the moisture loss is lower. The O3 source in the eastern tropical Atlantic Ocean is the most important oceanic source for the CRB, as shown in Table 2. In DJF, the major moisture sinks are over the southwest of the basin. In MAM and JJA, the moisture loss is mainly over the central and north of the basin. In SON, this loss is to the east. These patterns show a good correlation with the rainfall's spatial distribution ( $r > 0.43$ ). The greatest moisture contribution from O4 in the western Indian Ocean during DJF occurs over the south and along a longitudinal belt in the centre of the basin in MAM; in JJA, the largest contribution can be detected over the northern area of the basin. During SON, when the moisture loss

from O4 covers practically the entire territory, with the highest loss over the east, the correlation with the precipitation pattern is negative ( $r = -0.18$ ). The highest precipitation for these months shows maxima over the northern and western areas (Fig. 2), which explains the negative correlation.

A common characteristic of the  $|(E - P)i10 < 0|$  patterns is that the most intense values are generally located near the moisture sources, as is clear for the contributions from C2, C3, O3, O4, and the CRB itself. The geographic location of the continental sources around the CRB and the dominant atmospheric circulation are the key factors that make this result possible.

### 3.5 Role of moisture sources during severe dry and wet periods in the CRB

We now consider the characteristics of the extreme hydrological conditions in the CRB. CEA has experienced a long-term drying trend over the past 2 decades (Diem et al., 2014; Zhou et al., 2014). The rainfall trend from 1951 to 1989 toward central Africa is initially much less clear near the Atlantic Ocean and then becomes more intense toward the interior of the continent (Olivry et al., 1993). This pattern was also noted by Hua et al. (2016) for CEA, who obtained a trend of  $0.21 \text{ mm day}^{-1}$  per decade ( $p < 0.01$ ) for the period 1979–2014 by utilising precipitation data from the Global Precipitation Climatology Project (GPCP).

The temporal evolution of the 1- and 12-month SPEI series for the CRB shows dry conditions during the periods 1980–1985, 1992–1998, and 2004–2006 (Fig. 11a, b). The prevalence of wet conditions can be seen from 1985 to 1991 and from 2007 to 2010. Hua et al. (2016) have documented consistently strong negative anomalies since the 1990s for CEA from April to June, and these were primarily related to SST variations over the Indo-Pacific seas from the enhanced and westward-extending tropical Walker circulation. These

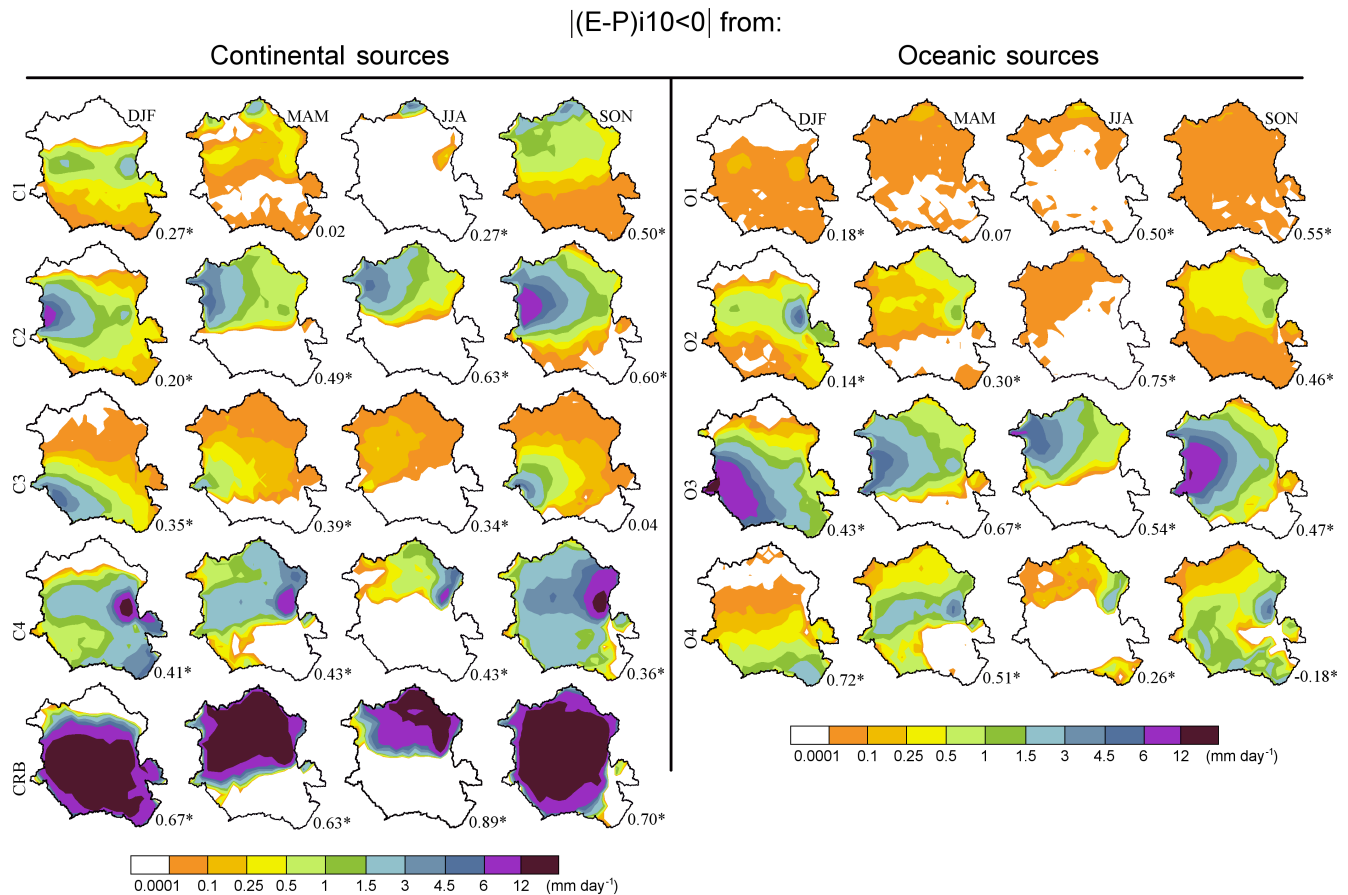


**Figure 10.** Seasonal mean  $|(E - P)_{i10 < 0}|$  (mm day<sup>-1</sup>) integrated forward from the moisture sources over the CRB for December–February (DJF), March–May (MAM), June–August (JJA), and September–November (SON). The number in the bottom-right corner of each plot indicates the correlation with the mean precipitation pattern (asterisks indicate significant values at  $p < 0.05$ ). Period: 1980–2010.

anomalies are also consistent with the weakened ascent over central Africa from the reduced low-level moisture transport. The hydrological drought conditions for the Congo River according to the Kinshasa gauge station records show temporal consistency with climate drought conditions in the basin (Fig. 11c).

We calculated the monthly correlations in the total moisture contribution to the basin  $|(E - P)_{i10 < 0}|$  (summed from all the sources), runoff, and SSI for the 1- to 24-month SPEI timescales (Fig. 12) to investigate any possible temporal relationships. The significance of the correlation threshold was set at  $p < 0.05$ . The correlations between the monthly values of  $|(E - P)_{i10 < 0}|$  and SPEI show significant and high values for all months (Fig. 12a) for short SPEI timescales. The relationship is positive and statistically significant from January to March within the 24 SPEI timescales. During low-rainfall climatological months in the basin, especially in June, July, and August, the correlations are the lowest and even negative after the SPEI4 and SPEI5 timescales and generally remain so until the end. This result indicates negative feedback that may reflect the increased evapotranspiration

that modulates the SPEI. As the months advance and the period of less rain ends, the correlations increase and become positive and significant from October to December from the first SPEI temporal scales until SPEI12. In these months, the correlations are the lowest and become negative for the major SPEI temporal scales, as shown in Fig. 12a. However, these correlations change for January and February, which exhibit positive correlations for all SPEI timescales and show a lag of approximately 1 month for the SPEI to reflect the recovery of wet conditions in the CRB.

In Fig. 12b, the surface runoff seems to strongly depend on SPEI for both shorter and longer temporal scales from January to April. Afterward (May–July), negative correlations appear after SPEI6 (Fig. 12b). The correlations also increase when the rainfall increases over the basin from July onward (Fig. 3). Here, we observe the same relationship between  $|(E - P)_{i10 < 0}|$  and SPEI, but higher correlations were obtained. Correlations between SSI from the Kinshasa gauge station's discharge and SPEI (1–24 months) show that the evolution of the hydrological conditions is consistent with the meteorological rainfall deficit (excess) state over the

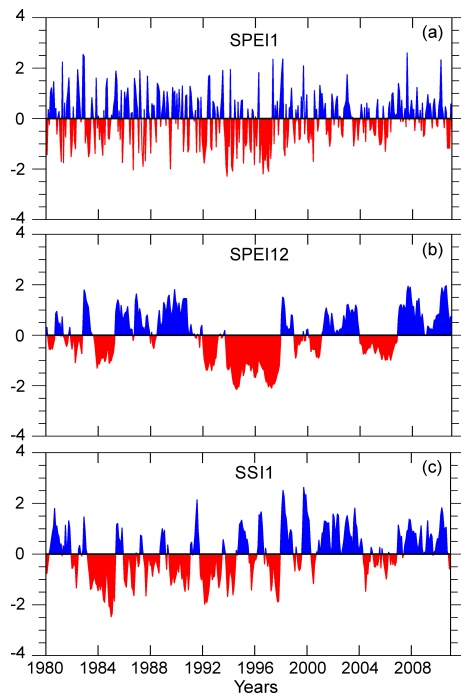


**Figure 11.** Time evolution of the SPEI in the Congo River basin after 1 (a) and 12 months (b) and the Standardised Streamflow Index (SSI) (c) that was computed for the Congo River's discharge. Period: 1980–2010.

basin (Fig. 12c). In particular, the strongest and most significant correlations were found from SPEI5 to SPEI7 from January to May, with a maximum in April; this result suggests the most appropriate timescales when identifying hydrological droughts (according to the Congo River's discharge at the Kinshasa gauge station) in terms of its relationship with the computed SPEI values for the entire CRB. The correlations from May to July, when the precipitation and discharge are the smallest (Fig. 3), are negative for the initial SPEI temporal scales, which suggest a time response of 2 or 3 months to reflect SPEI changes in river discharge.

We selected a few years affected by severe and extreme conditions to investigate the role of the moisture sources during drought and wet conditions in the CRB. For this purpose, SPEI values at the 12-month timescale for December were used to diagnose the status of the water balance throughout each year. Moreover, long drought timescales are generally used to assess streamflow droughts (Svoboda et al., 2012). On this timescale, we should represent the water balance in a region where the precipitation climatology is dictated by latitudinal migration across the Equator over the year, such as what occurs in the CRB.

During the period 1980–2010, the years 1995 and 1996 were characterised by severe (SPEI12\_December =  $-1.69$ ) and extreme (SPEI12\_December =  $-2.06$ ) drought conditions, respectively, while 1982 was characterised as severely wet (SPEI12\_December =  $1.68$ ). Figure 13 shows the mean

annual contribution (average over the number of grid points of the basin) from all sources and the  $|(E - P)i10 < 0|$  anomaly for each event. In 1982 (Fig. 13a), the most important moisture contributions are from the basin itself ( $\sim 12.0 \text{ mm day}^{-1}$ ), O3 ( $\sim 2.8 \text{ mm day}^{-1}$ ), and C4 ( $\sim 2.7 \text{ mm day}^{-1}$ ). The  $|(E - P)i10 < 0|$  anomalies from all the sources are positive but are particularly high for the basin itself ( $1.8 \text{ mm day}^{-1}$ ). In 1995 and 1996 (Fig. 13b and c), the greatest moisture loss continues to be that from the air masses from the CRB itself, the oceanic source O3, and the continental source C4. However, when the anomalies were analysed, all the sources showed negative values; thus, the moisture support was less than the average conditions for the entire period. In 1995, the deficit in the contribution from the CRB and O4 is highlighted. Hua et al. (2016) described how an increase in subsidence across the western edge of the Indian Ocean (O4) and a decrease in convection over the CRB led to a reduction in moisture transport and rainfall across CEA. In 1996, a year that was characterised by extreme drought conditions, the negative anomaly in the moisture contribution to precipitation from all the sources remains, but the value that was computed for the basin was higher than in 1995. These results explain a mechanism in which the CRB is more (less) efficient in providing moisture for precipitation over itself during wet (dry) periods.

To clarify these results, we calculated the  $|(E - P)i10 < 0|$  (moisture contribution) and  $(E - P)i10 > 0$  (moisture uptake) anomalies in air masses that were tracked forward and backward in time, respectively, from the CRB for the 3 years under study. We utilised FLEXPART and obtained the  $(E - P)$  budget but not the exact recycling, which computes the amount of precipitation that evaporates and falls again within the same region. Additionally, we calculated the anomaly of the VIMF to check the dynamical conditions that were favourable to the convergence–divergence of moisture flux.

In 1982, which was a severely wet year, higher positive  $|(E - P)i10 < 0|$  anomalies were observed in the northern half of the CRB, but mostly negative values were observed in the southern half (Fig. 14a). This pattern is clearly opposite to that for the same year in the  $(E - P)i10 > 0$  anomalies for the backward experiment (Fig. 14d), which explains the strengthening role of the southern half of the basin as a moisture source and mainly favours moisture loss over the northern CRB's evergreen forests. The VIMF anomalies support this result: negative values that identify convergence are observed over the northern half of the CRB, while positive anomalies that indicate divergence are observed in the southern half (Fig. 15a). Recycling supposedly decreases during wet periods, but Pathak et al. (2014) described how monsoons enhance the soil moisture and vegetation cover in the Indian region, increasing evapotranspiration and recycled precipitation. Additionally, a positive feedback was previously described by Bosilovich et al. (2003) and Domínguez et al. (2008) for the North American Monsoon region. Ad-

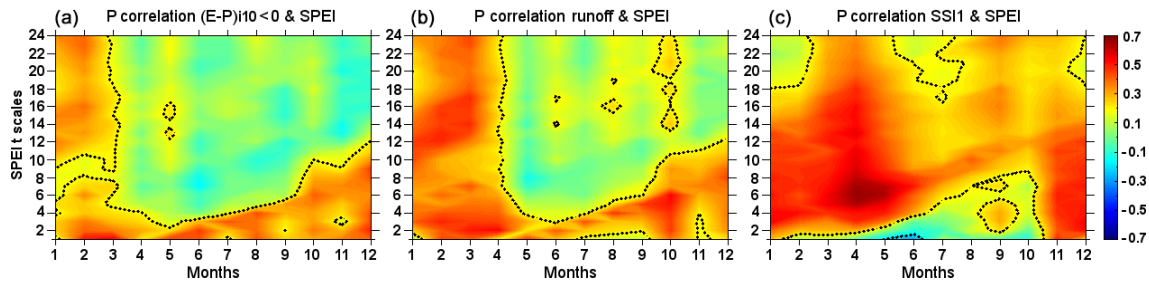


**Figure 12.** Monthly correlations among  $|(E - P)i_{10} < 0|$  (a), runoff (b), and SSI (c) from SPEI1 to SPEI24 in the Congo River basin. The dotted lines represent significant correlations at  $p < 0.05$

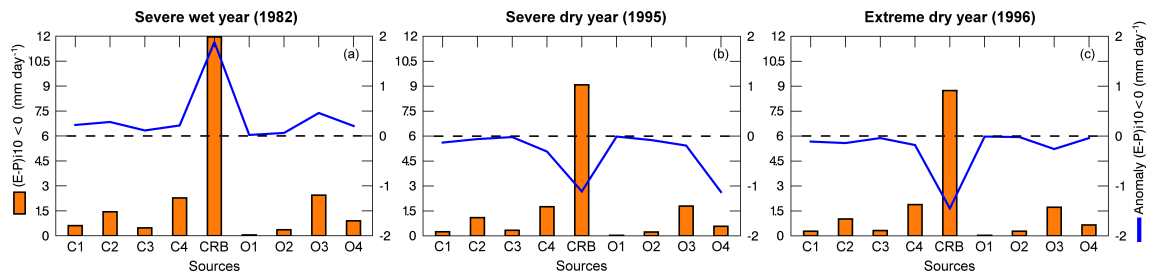


**Figure 13.** Mean annual moisture contribution from the sources to the CRB (orange bars) in 1982 (severe wet conditions, (a) 1995 (severe dry conditions, (b) and 1996 (extreme dry conditions, (c) alongside the corresponding anomaly (blue line).

ditionally, when the tropical rainbelt shifts northward during boreal summer months, the evergreen forest in the CRB rapidly becomes active because of the onset of the rainy season, increasing the evapotranspiration (Matsuyama et al., 1994). In 1982, both the evaporation and precipitation may have increased in the northern half of the CRB, with the latter increasing to a much greater degree, thus affecting the  $(E - P)$  budget.

The Oubangui Basin in the northeastern CRB should have benefited in 1982 because of positive  $|(E - P)i_{10} < 0|$  anomalies, which favour precipitation in the northern CRB. A decrease in runoff throughout the Oubangui Basin coincides with a decrease in rainfall with a time lag of 3 years, which can be explained by the sponge-like functioning of the drainage basin, where inter-annual variability is less important for runoff than for the rainfall series (Orange et al., 1997). An important finding of these authors was that the maxima and minima of the annual rainfall did not completely coincide with extreme flow events; the year 1982 was a severely wet year with positive  $|(E - P)i_{10} < 0|$  anomalies over the northern half of the basin, including the Oubangui Basin. According to the results of Orange et al. (1997) and Laraque et al. (2013), the Oubangui Basin remained in a drought phase from 1982 to 2010 as the Congo returned to a phase of stability.

In 1995, which was a severely dry year, negative  $|(E - P)i_{10} < 0|$  anomalies covered the majority of the basin (Fig. 14b) and were more intense over the western and northern regions. In the backward analysis, these areas exhib-

ited positive  $(E - P)i_{10} > 0$  anomalies (Fig. 14e) and positive VIMF anomalies, indicating the prevalence of divergence (Fig. 15b). In 1996, which was an extremely dry year, the mechanism was the same as in 1995, but negative  $|(E - P)i_{10} < 0|$  anomalies occurred in almost the entire basin alongside the positive  $(E - P)i_{10} > 0$  anomalies. Trenberth and Guillemot (1996) discussed the importance of land-surface feedbacks in the 1988 drought and 1993 flood in the United States, while Dirmeyer and Brubaker (1999), Bosilovich and Schubert (2001), and Domínguez et al. (2006) agreed that 1988 had a higher recycling ratio than 1993. The CRB exhibited positive  $(E - P)i_{10} > 0$  anomalies during the dry years of 1995 and 1996, indicating moisture uptake by the atmosphere, which surely occurred because the evapotranspiration was enhanced and precipitation decreased. However, the prevalent divergence of the VIMF (Fig. 15b and c) did not favour moisture loss over the basin, which must have been transported outside, suggesting the role of the CRB itself as a moisture source for remote regions. A more detailed analysis should be performed in future works to determine the role of forests during drought conditions in the CRB. Figure 11c indicates that the lowest SSI values for the Kinshasa gauge station's discharge data occurred after 1995 and 1996 because of the lag period for precipitation, runoff, and underground water to feed rivers.

An important feature for 1982, 1995, and 1996 is that anomalies of moisture uptake and moisture contribution in air masses that were tracked backward and forward in time

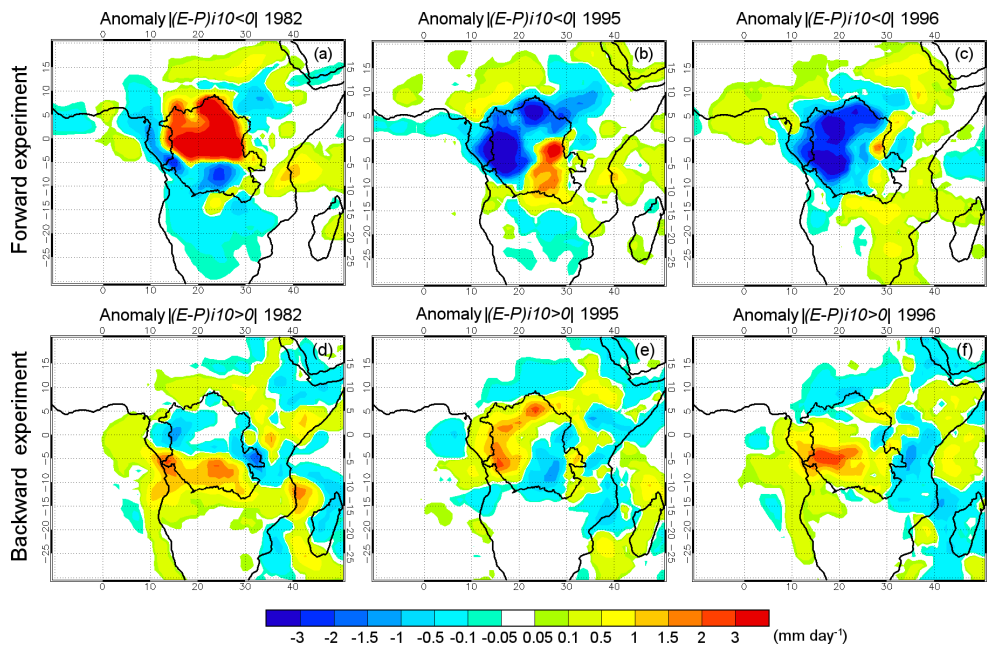


**Figure 14.** Anomaly of the  $|(E - P)i_{10} < 0|$  ( $\text{mm day}^{-1}$ ) integrated forward from the Congo River basin in 1982 (severe wet year, **a**), 1995 (severe dry year, **b**), and 1996 (extreme dry year, **c**). Anomaly of the  $|(E - P)i_{10} > 0|$  ( $\text{mm day}^{-1}$ ) integrated backward from the Congo River basin in 1982 (severe wet year, **d**), 1995 (severe dry year, **e**), and 1996 (extreme dry year, **f**).

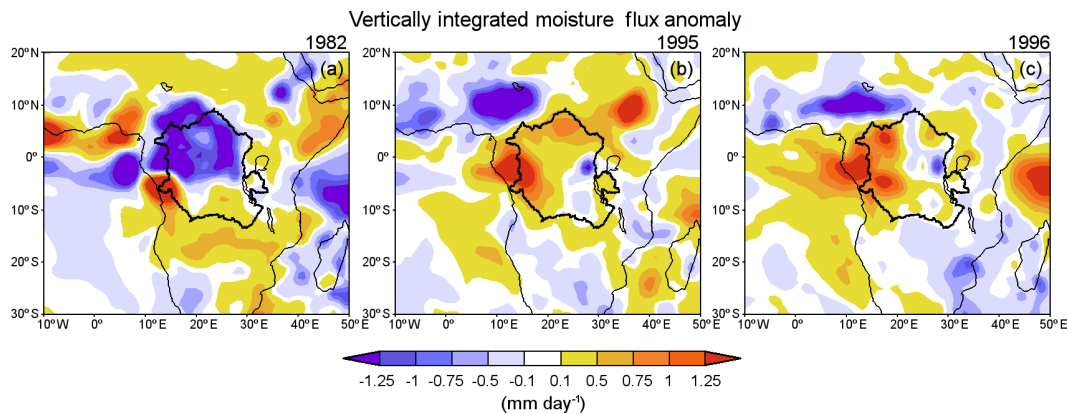


**Figure 15.** Anomaly of the vertically integrated moisture flux (VIMF) in 1982 (severe wet year, **a**), 1995 (severe dry year, **b**), and 1996 (extreme dry year, **c**).

from the CRB, respectively, are not homogenous over the CRB itself. In fact, 1982 and 1995 exhibit a relocation of regional sources and sinks of moisture in the basin. This result confirms that research on the hydrological cycle should not be developed for the entire basin, which matches Matsuyama et al. (1994). These authors argued that seasonal changes in the water budget throughout the CRB can be recognised as a combination of those in the evergreen forest and southern deciduous forest regions, but the regional characteristics of the water budget in the basin cannot be explained by studying the entire basin.

#### 4 Conclusions

The most important climatological moisture sources for the Congo River basin were identified by using the Lagrangian model FLEXPART for a 31-year dataset (1980–2010). The precipitation, runoff, and river discharge at the Kinshasa gauging station were assessed. The mean annual precipitation pattern in the CRB confirmed a north–south dipole that is associated with the annual migration of the ITCZ. On average, the maximum rainfall occurs between October and April, while minima are observed in June and July, which are always in good correlation with the runoff and Congo River discharge; in particular, the monthly discharge values

have the best correlation ( $r = 0.66$ ) with the precipitation, exhibiting a lag of 1 month, which is the time required to pass before the runoff can be considered freshwater in the Congo River. The backward tracking of air masses revealed that the CRB receives humidity from both hemispheres. Four annual-scale oceanic moisture sources were identified in the Atlantic Ocean, the Indian Ocean, and the Red Sea, while the continent contains four sources that surround the CRB alongside the basin itself, which acts as its own moisture source. The importance of each source in the contribution from moisture to precipitation over the CRB confirms the main role of the CRB in the negative ( $E - P$ ) budgets over the basin itself, which represent more than 50 % of the total moisture loss over the basin from all sources. Hence, local recycling processes are very important, as noted by other authors. Other important sources that provide moisture to the CRB are the tropical Atlantic Ocean (O3) and the continental region to the east of the target area (C4). At the same time, the source O1 in the Red Sea, despite its high evaporation rate, is considered the least efficient source for providing humidity to the basin. The efficiency of the sources that provide moisture to the CRB depends on the evaporation rate and influences the amount of water vapour that is transported to the basin, making the sources more or less effective in terms of precipitation over the CRB. Indeed, the spatial variability in the  $(E - P)_{i10} < 0$  patterns over the CRB after tracking the air masses forward from all the sources confirmed the link between the geographical location of the sources and the location of the greatest moisture sinks over the basin, which are associated with atmospheric circulation. These patterns showed a good spatial correlation with the precipitation distribution over the basin and demonstrated the ability of FLEXPART to reproduce the temporal and spatial variability in the precipitation over the CRB.

The roles of the sources that provide moisture during years with extreme and severe conditions confirmed the key role of the CRB in modulating the water balance within itself. During wet (dry) years, the contribution of moisture ( $(E - P)_{i10} < 0$ ) from the CRB to precipitation over itself increased (decreased). On average, the water balance in the atmosphere over the CRB was not homogenous in these years, indicating a distinct role within itself. This result confirmed that research on the hydrological cycle should not be developed for the entire basin as a whole. The vertically integrated moisture flux divergence inhibited the precipitation during dry years, when moisture uptake ( $(E - P)_{i10} > 0$ ) was enhanced, which suggests moisture contribution from the CRB to remote regions, an issue to be investigated in future works. The moisture source roles for the sub-basins of the CRB should be determined to better understand the complex nature of the hydrological feedback mechanisms in the Congo River basin.

These results will support further studies to address the role of the CRB's moisture sources during climate extremes such as flooding, droughts, and extreme river discharge in

this basin. One important aspect for consideration in future research is related to the possible influence of modes of climate variability (such as the El Niño–Southern Oscillation or the Madden–Julian Oscillation) on the modulation of moisture transport from these sources to the CRB.

**Data availability.** The ERA-Interim datasets are freely available at <https://www.ecmwf.int/>. The precipitation and potential evapotranspiration data from CRU TS v3.23 (Harris et al., 2014) can be downloaded at <http://www.cru.uea.ac.uk/data>. The land evaporation data from GLEAM model (Miralles et al., 2011) are available from <http://www.gleam.eu> upon request, while the ocean evaporation from OAFUX (Yu et al., 2008) can be downloaded at <http://oafux.whoi.edu>. The river discharge datasets must be requested from the Global Runoff Data Centre ([http://www.bafg.de/GRDC/EN/01\\_GRDC/grdc\\_node.html](http://www.bafg.de/GRDC/EN/01_GRDC/grdc_node.html)). The model FLEXPART (Stohl and James, 2004, 2005) can be freely downloaded (<https://www.flexpart.eu/>) and utilized. For FLEXPART results, please contact Raquel Nieto ([rnieto@uvigo.es](mailto:rnieto@uvigo.es)).

**Competing interests.** The authors declare that they have no conflict of interest.

**Special issue statement.** The 8th EGU Leonardo Conference: From evaporation to precipitation: the atmospheric moisture transport SI statement: This article is part of the special issue “The 8th EGU Leonardo Conference: From evaporation to precipitation: the atmospheric moisture transport”. It is a result of the 8th EGU Leonardo Conference, Ourense, Spain, 25–27 October 2016.

**Acknowledgements.** This work was developed at EPhysLab (UVIGO-CSIC Associated Unit). Thanks for the funding by the Spanish government and FEDER via the SETH (CGL2014-60849-JIN) project. Rogert Sorí would like to acknowledge the grant from the Xunta of Galicia, Spain, in support of his doctoral research work. Raquel Nieto also acknowledges the support that was provided by CNPq grant 314734/2014-7 from the Brazilian government. We also thank the IMDROFLOOD project financed by the Water Works 2014 co-funded call of the European Commission.

Edited by: Ricardo Trigo

Reviewed by: two anonymous referees

## References

- Abdulaziz, S.: Annual and Seasonal Mean Net Evaporation Rates of the Red Sea Water during Jan 1958–Dec 2007, MSc thesis, University of Bergen, 2012.
- Alemaw, B. F.: Hydrological Modeling of Large Drainage Basins Using a GIS-Based Hybrid Atmospheric and Terrestrial Water Balance (HATWAB) Model, *Journal of Water Resource and Protection*, 4, 516–522, 2012.

- Alsdorf, D., Beighley, E., Laraque, A., Lee, H., Tshimanga, R., O'Loughlin, F., Mahé, G., Dinga, B., Moukandi, G., and Spencer, R. G. M.: Opportunities for hydrologic research in the Congo Basin, *Rev. Geophys.*, 54, 378–409, <https://doi.org/10.1002/2016RG000517>, 2016.
- Betbeder, J., Gond, V., Frappart, F., Baghdadi, N. N., Briant, G., and Bartholomé, E.: Mapping of Central Africa Forested Wetlands Using Remote Sensing, *IEEE J. Sel. Top. Appl.*, 7, 531–542, 2014.
- Beyene, T., Ludwig, F., and Franssen, W.: The potential consequences of climate change in the hydrology regime of the Congo River Basin, in: *Climate Change Scenarios for the Congo Basin*, edited by: Haensler, A., Jacob, D., Kabat, P., and Ludwig, F., Climate Service Centre Report No. 11, Hamburg, Germany, 2013.
- Bosilovich, M. G. and Schubert, S. D.: Precipitation recycling over the central United States diagnosed from the GEOS-1 data assimilation system, *J. Hydrometeorol.*, 2, 26–35, 2001.
- Bosilovich, M. G., Sud, Y. C., Schubert, S. D., and Walker, G. K.: Numerical simulation of the large-scale North American monsoon water sources, *J. Geophys. Res.*, 108, 8614, <https://doi.org/10.1029/2002JD003095>, 2003.
- Bower, A. S. and Farrar, J. T.: Air-Sea Interaction and Horizontal Circulation in the Red Sea, in: *The Red Sea*, edited by: Rasul, N. M. A. and Stewart, I. C. F., Springer Berlin Heidelberg, 329–342, 2015.
- Boyer, J. F., Dieulin, C., Rouche, N., Cres, A., Servat, E., Paturel, J. E., and Mahé, G.: SIEREM: an environmental information system for water resources, *Climate Variability and Change – Hydrological Impacts*, Proceedings of the Fifth FRIEND World Conference held at Havana, Cuba, 27 November–1 December 2006, IAHS Publ. 308, 2006.
- Broxton, P. D., Zeng, X., Sulla-Menashe, D., and Troch, P. A.: A Global Land Cover Climatology Using MODIS Data, *J. Appl. Meteor. Climatol.*, 53, 1593–1605, 2014.
- Bultot, F.: Atlas climatique du bassin congolais. Deuxième partie: les composantes du bilan d'eau; Institut National pour l'Etude Agronomique du Congo (INEAC), Hors série, 150 pp., 1971.
- Burde, G. I., Gandush, C., and Bayarjargal, Y.: Bulk recycling models with incomplete vertical mixing, Part II: precipitation recycling in the Amazon Basin, *J. Climate*, 19, 1473–1489, 2006.
- Bricquet, J. P.: Les écoulements du Congo a Brazzaville et la spatialisation des apports, *Grands bassins fluviaux*, Paris, 22–24 Novembre, 27–38, 1993.
- Bricquet, J. P.: Les écoulements du Congo à Brazzaville et la spatialisation des apports, *Grands Bassins Fluviaux Périatlantiques: Congo, Niger, Amazone*, Actes du colloque PEGI-INSU-CNRS-ORSTOM du 22 au 24 Novembre 1993, Orstom, Paris, 27–38, 1995.
- Camberlin, P., Janicot, S., and Pocard, I.: Seasonality and atmospheric dynamics of the teleconnection between african rainfall and tropical sea-surface temperature: Atlantic vs. Enso, *Int. J. Climatol.*, 21, 973–1005, <https://doi.org/10.1002/joc.673>, 2001.
- CARPE: The Forests of the Congo Basin: A Preliminary Assessment, Central African Regional Program for the Environment, 34 pp., available at: [http://carpe.umd.edu/Documents/2005/focb\\_aprelimassess\\_en.pdf](http://carpe.umd.edu/Documents/2005/focb_aprelimassess_en.pdf), 2005.
- Castillo, R., Nieto, R., Drumond, A., and Gimeno, L.: Estimating the Temporal Domain when the Discount of the Net Evaporation Term Affects the Resulting Net Precipitation Pattern in the Moisture Budget Using a 3-D Lagrangian Approach, *PLoS ONE*, 9, e99046, <https://doi.org/10.1371/journal.pone.0099046>, 2014.
- Chen, B., Xu, X. D., Yang, S., and Zhang, W.: On the origin and destination of atmospheric moisture and air mass over the Tibetan Plateau, *Theor. Appl. Climatol.*, 110, 423–435, <https://doi.org/10.1007/s00704-012-0641-y>, 2012.
- Chishugi, J. B.: Hydrological modelling of the Congo River basin: a soil-water balance approach, MSc thesis, University of Botswana, 2008.
- Cohen, A. S., Soreghan, M. J., and Scholz, C. A.: Estimating the age of formation of lakes: an example from Lake Tanganyika, East African Rift system, *Geology*, 21, 511–514, 1993.
- COLA: The Center for Ocean-Land-Atmosphere Studies, available at: <http://cola.gmu.edu/wcr/river/basins.html>, last access: 2 February 2017.
- Coulter, G. W.: *Lake Tanganyika and Its Life*, Oxford Univ. Press, New York, 1991.
- Dai, A.: Increasing drought under global warming in observations and models, *Nature Climate Change*, 3, 52–58, 2013.
- Dai, A. and Trenberth, K. E.: Estimates of Freshwater Discharge from Continents: Latitudinal and Seasonal Variations, *J. Hydrometeorology*, 3, 660–687, 2002.
- Dai, A., Qian, T., and Trenberth, K. E.: Changes in Continental Freshwater Discharge from 1948–2004, *J. Climate*, 22, 2773–2792, <https://doi.org/10.1175/2008JCLI2592.1>, 2008.
- Dargie, G. C., Lewis, S. L., Lawson, I. T., Mitchard, E. T. A., Page, S. E., Bocko, Y. E., and Ifo, S. A.: Age, extent and carbon storage of the central Congo Basin peatland complex, *Nature*, 542, 86–90, 2017.
- Dee, D. P. et al.: The ERA-Interim reanalysis: Configuration and performance of the data assimilation system, *Q. J. Roy. Meteor. Soc.*, 137, 553–597, <https://doi.org/10.1002/qj.828>, 2011.
- Dezfuli, A. K., Zaitchik, B. F., and Gnanadesikan, A.: Regional Atmospheric Circulation and Rainfall Variability in South Equatorial Africa, *J. Climate*, 28, 809–818, <https://doi.org/10.1175/JCLI-D-14-00333.1>, 2015.
- Diem, J. E., Ryan, S. J., Hartter, J., and Palace, M. W.: Satellite-based rainfall data reveal a recent drying trend in central equatorial Africa, *Climatic Change*, 126, 263–272, 2014.
- Dirmeyer, P. A. and Brubaker, K. L.: Contrasting evaporative moisture sources during the drought of 1988 and the flood of 1993, *J. Geophys. Res.*, 104, 19383–19397, <https://doi.org/10.1029/1999JD900222>, 1999.
- Dirmeyer, P. A., Brubaker, K. L., and DelSole, T.: Import and export of atmospheric water vapor between nations, *J. Hydrol.*, 365, 11–22, <https://doi.org/10.1016/j.jhydrol.2008.11.016>, 2009.
- Dominguez, F., Kumar, P., Liang, X., and Ting, M.: Impact of atmospheric moisture storage on precipitation recycling, *J. Climate*, 19, 1513–1530, 2006.
- Domínguez, F. and Kumar, P.: Precipitation Recycling Variability and Ecoclimatological Stability-A Study Using NARR Data. Part II: North American Monsoon Region, *J. Climate*, 21, 5187–5203, 2008.
- Domínguez, F., Kumar, P., and Vivoni, E. R.: Precipitation Recycling Variability and Ecoclimatological Stability – A Study Using 25 NARR Data. Part II: North American Monsoon Region, *J. Climate*, 21, 5187–5203, <https://doi.org/10.1175/2008JCLI1760.1>, 2008.

- Drumond, A., Marengo, J., Ambrizzi, T., Nieto, R., Moreira, L., and Gimeno, L.: The role of the Amazon Basin moisture in the atmospheric branch of the hydrological cycle: a Lagrangian analysis, *Hydrol. Earth Syst. Sci.*, 18, 2577–2598, <https://doi.org/10.5194/hess-18-2577-2014>, 2014.
- Drumond, A., Nieto, R., and Gimeno, L.: A Lagrangian approach for investigating anomalies in the moisture transport during drought episodes, *Cuadernos de Investigación Geográfica*, 42, 113–125, <https://doi.org/10.18172/cig.2925>, 2016a.
- Drumond, A., Taboada, E., Nieto, R., Gimeno, L., Vicente-Serrano, S. M., and López-Moreno, J. I.: A Lagrangian analysis of the present-day sources of moisture for major ice-core sites, *Earth Syst. Dynam.*, 7, 549–558, <https://doi.org/10.5194/esd-7-549-2016>, 2016b.
- Druyan, L. M. and Koster, R. D.: Sources of Sahel Precipitation for Simulated Drought and Rainy Seasons, *J. Climate*, 2, 1438–1446, 1989.
- Eltahir, E. A. B.: A Soil Moisture-Rainfall Feedback Mechanism: 1. Theory and observations, *Water Resour. Res.*, 34, 765–776, <https://doi.org/10.1029/97WR03499>, 1998.
- Eltahir, E. A. B. and Bras, R. L.: Precipitation recycling in the Amazon basin, *Q. J. Roy. Meteor. Soc.*, 120, 861–880, <https://doi.org/10.1002/qj.49712051806>, 1994.
- Eltahir, E. A. B. and Bras, R. L.: Precipitation recycling, *Rev. Geophys.*, 34, 367–378, <https://doi.org/10.1029/96RG01927>, 1996.
- Eltahir, E. A. B. and Gong, C.: Dynamics of Wet and Dry years in West Africa, *J. Climate*, 9, 1030–1042, [https://doi.org/10.1175/1520-0442\(1996\)009<1030:DOWADY>2.0.CO;2](https://doi.org/10.1175/1520-0442(1996)009<1030:DOWADY>2.0.CO;2), 1996.
- Gana, M. B. and Herbert, B.: Spatial analysis from remotely sensed observations of Congo basin of east african high land to drain water using gravity for sustainable management of low laying chad basin of central Africa, *The International Archives of the Photogrammetry, Remote Sensing and Spatial Information Sciences*, Volume XL-1, 2014, ISPRS Technical Commission I Symposium, 17–20 November, Denver, Colorado, USA, 2014.
- Gimeno, L.: Grand challenges in atmospheric science, *Front. Earth Sci.*, 1, 1–5, <https://doi.org/10.3389/feart.2013.00001>, 2013.
- Gimeno, L., Drumond, A., Nieto, R., Trigo, R. M., and Stohl, A.: On the origin of continental precipitation, *Geophys. Res. Lett.*, 37, L13804, <https://doi.org/10.1029/2010GL043712>, 2010.
- Gimeno, L., Stohl, A., Trigo, R. M., Dominguez, F., Yoshimura, K., Yu, L., Drumond, A., Durán-Quesada, A. M., and Nieto, R.: Oceanic and terrestrial sources of continental precipitation, *Rev. Geophys.*, 50, RG4003, <https://doi.org/10.1029/2012RG000389>, 2012.
- Gimeno, L., Nieto, R., Drumond, A., Castillo, R., and Trigo, R.: Influence of the intensification of the major oceanic moisture sources on continental precipitation, *Geophys. Res. Lett.*, 40, 1443–1450, <https://doi.org/10.1002/grl.50338>, 2013.
- Haensler, A., Saeed, F., and Jacob, D.: Assessment of projected climate change signals over central Africa based on a multitude of global and regional climate projections, in: *Climate Change Scenarios for the Congo Basin*, edited by: Haensler, A., Jacob, D., Kabat, P., and Ludwig, F., Climate Service Centre Report No. 11, Hamburg, Germany, 2013.
- Harris, I., Jones, P. D., Osborn, T. J., and Lister, D. H.: Updated high-resolution grids of monthly climatic observations – the CRU TS3.10 Dataset, *Int. J. Climatol.*, 34, 623–642, <https://doi.org/10.1002/joc.3711>, 2014.
- Harrison, I. J., Brummett, R., and Stiassny M. L. J.: Congo River Basin, in: *The Wetland Book*, edited by: Finlayson, C. M., Milton, G. R., Prentice, R. C., and Davidson, N. C., Springer Science+Business Media Dordrecht, [https://doi.org/10.1007/978-94-007-6173-5\\_92-1](https://doi.org/10.1007/978-94-007-6173-5_92-1), 2016.
- Hua, W., Zhou, L., Chen, H., Nicholson, S. E., Raghavendra, A., and Jiang, Y.: Possible causes of the Central Equatorial African long-term drought, *Environ. Res. Lett.*, 11, 1–13, 2016.
- Ilumbe Bayeli Is'ompona, G.: *Rapport des Inventaires Multi-ressources a Bobangi*, Kinshasa, USAID, Innovative Resources Management, 2006.
- IBP (International Bussines Publications): *Congo, Land Ownership and Agricultural Laws Handbook*, Volume 1, Strategic Information and Regulation, Edition Updated Reprint International Business Publications, Washington, USA, 2015.
- Jackson, B., Nicholson, S. E., and Klotter, D.: Mesoscale convective systems over western equatorial Africa and their relationship to largescale circulation, *Mon. Weather Rev.*, 137, 1272–1294, <https://doi.org/10.1175/2008MWR2525.1>, 2009.
- Kadima, E., Delvaux, D., Sebagenzi, S. N., Tack, L., and Kabeya, S. M.: Structure and geological history of the Congo Basin: an integrated interpretation of gravity, magnetic and reflection seismic data, *Basin Res.*, 23, 499–527, 2011.
- Keys, P. W., van der Ent, R. J., Gordon, L. J., Hoff, H., Nikoli, R., and Savenije, H. H. G.: Analyzing precipitationsheds to understand the vulnerability of rainfall dependent regions, *Biogeosciences*, 9, 733–746, <https://doi.org/10.5194/bg-9-733-2012>, 2012.
- Keys, P. W., Barnes, E. A., van der Ent, R. J., and Gordon, L. J.: Variability of moisture recycling using a precipitationshed framework, *Hydrol. Earth Syst. Sci.*, 18, 3937–3950, <https://doi.org/10.5194/hess-18-3937-2014>, 2014.
- Laraque, A., Pouyaud, B., Rocchia, R., Robin, R., Chaffaut, I., Moutsambote, J. M., Maziezoula, B., Censier, C., Albouy, Y., Elenga, H., Etcheber, H., Delaune, M., Sondag, F., and Gasse, F.: Origin and function of a closed depression in equatorial humid zones: the lake Telé in the north Congo, *J. Hydrol.*, 207, 236–253, 1998.
- Laraque, A., Mahé, G., Orange, D., and Mariou, B.: Spatiotemporal variations in hydrological regimes within Central Africa during the XX century, *J. Hydrol.*, 245, 104–117, 2001.
- Laraque, A., Bellanger, M., Adele, G., Guebanda, S., Gulemvuga, G., Pandi, A., Paturel, J. E., Robert, A., Tathy, J. P., and Yambélé, A.: Recent evolution of Congo, Oubangui and Sangha rivers flows/Evolutions récentes des débits du Congo, de l'Oubangui et de la Sangha, *Geo-Eco Trop*, 37, 93–100, 2013.
- Lau, K. M. and Yang, S.: Walker Circulation, in: *Encyclopedia of Atmospheric Sciences*, edited by: Pyle, J., Curry, J. A., and Holton, J. R., Academic Press, New York, USA, 6 pp., 2002.
- Lee, H., Edward, R. B., Alsdorf, D., Jung, H. C., Shum, C. K., Duan, J., Guo, J., Yamazaki, D., and Andreadis, K.: Characterization of terrestrial water dynamics in the Congo Basin using GRACE and satellite radar altimetry, *Remote Sens. Environ.*, 115, 3530–3538, <https://doi.org/10.1016/j.rse.2011.08.015>, 2011.
- Lehner, B. and Grill, G.: Global river hydrography and network routing: baseline data and new approaches to study the world's large river systems, *Hydrol. Process.*, 27, 2171–2186, 2013.

- Levine, R. C. and Turner, A. G.: Dependence of Indian monsoon rainfall on moisture fluxes across the Arabian Sea and the impact of coupled model sea surface temperature biases, *Clim. Dynam.*, 38, 2167–2190, 2012.
- Lobell, D. B., Bänziger, M., Magorokosho, C., and Vivek, B.: Non-linear heat effects on African maize as evidenced by historical yield trials, *Nature Climate Change*, 1, 42–45, 2011a.
- Lobell, D. B., Schlenker, W., and Costa-Roberts, J.: Climate trends and global crop production since 1980, *Science*, 333, 616–620, 2011b.
- Mahe, G.: Modulation annuelle et fluctuations interannuelles des précipitations sur le bassin versant du Congo, Coll. PEGI/INSU/ORSTOM, Paris, 22–24, 13–26, Novembre 1993.
- Mahe, G., Lienou, G., Descroix, L., Bamba, F., Paturol, J. E., Laraqe, A., Meddi, M., Moukolo, N., Hbaieb, H., Adeaga, O., Dieulin, C., Kotti, F., and Khomsi, K.: The rivers of Africa: witness of climate change and human impact on the environnement, *Hydrol. Process.*, 27, 2105–2114, 2013.
- Marengo, J. A.: The characteristics and variability of the atmospheric water balance in the Amazon basin: Spatial and temporal variability, *Clim. Dynam.*, 24, 11–22, 2005.
- Marquant, B., Mosnier, A., Bodin, B., Dessard, H., Feintrenie, L., Molto, Q., Gond, V., and Bayol, N.: Importance des forêts d’Afrique centrale, in: *Les forêts du bassin du Congo – Forêts et changements climatiques*, edited by: de Wasseige, C., Taddoum, M., Eba’a Atyi, R., et Doumenge, C., Weyrich, Belgique, 128 pp., Chapter 1, 17–36, 2015.
- Masih, I., Maskey, S., Mussá, F. E. F., and Trambauer, P.: A review of droughts on the African continent: a geospatial and long-term perspective, *Hydrol. Earth Syst. Sci.*, 18, 3635–3649, <https://doi.org/10.5194/hess-18-3635-2014>, 2014.
- Matari, E. E.: Impacts of Congo convection on tropical Africa’s circulation, rainfall and resources, MSc Thesis, University of Zululand, South Africa, 165 pp., 2002.
- Materia, S., Gualdi, S., Navarra, A., and Terray, L.: The effect of Congo River freshwater discharge on Eastern Equatorial Atlantic climate variability, *Clim. Dynam.*, 39, 2109–2125, <https://doi.org/10.1007/s00382-012-1514-x>, 2012.
- Matsuyama, H., Oki, T., Shinoda, M., and Masuda, K.: The seasonal change of the water budget in the Congo River Basin, *J. Meteorol. Soc. Jpn.*, 72, 281–299, 1994.
- McKee, T., Doesken, N., and Kleist, J.: The relationship of drought frequency and duration to time scales, Eighth Conference on Applied Climatology, 17–22 January, Anaheim, California, 1993.
- Misra, V., Pantina, P., Chan, S. C., and DiNapoli, S.: A comparative study of the Indian summer monsoon hydroclimate and its variations in three reanalyses, *Clim. Dynam.*, 39, 1149–1168, <https://doi.org/10.1007/s00382-012-1319-y>, 2012.
- Miralles, D. G., Holmes, T. R. H., De Jeu, R. A. M., Gash, J. H., Meesters, A. G. C. A., and Dolman, A. J.: Global land-surface evaporation estimated from satellite-based observations, *Hydrol. Earth Syst. Sci.*, 15, 453–469, <https://doi.org/10.5194/hess-15-453-2011>, 2011.
- Nicholson, S. E.: On the factors modulating the intensity of the tropical rainbelt over West Africa, *Int. J. Climatol.*, 29, 673–689, <https://doi.org/10.1002/joc.1702>, 2009.
- Nicholson, S. E. and Grist, J. P.: The seasonal evolution of the atmospheric circulation over West Africa and Equatorial Africa, *J. Climate*, 16, 1013–1030, 2003.
- Nieto, R., Gimeno, L., and Trigo, R. M.: A Lagrangian identification of major sources of Sahel moisture, *Geophys. Res. Lett.*, 33, L18707, <https://doi.org/10.1029/2006GL027232>, 2006.
- Nieto, R., Gallego, D., Trigo, R. M., Ribera, P., and Gimeno, L.: Dynamic identification of moisture sources in the Orinoco basin in equatorial South America, *Hydrol. Sci. J.*, 53, 602–617, 2008.
- Nlom, J. H.: The Economic Value of Congo Basin Protected Areas Goods and Services, *J. Sustainable Development*, 4, 130–142, 2011.
- Numaguti, A.: Origin and recycling processes of precipitating water over the Eurasian continent: Experiments using an atmospheric general circulation model, *J. Geophys. Res.*, 104, 1957–1972, 1999.
- Olivry, J. C., Bricquet, J. P., and Mahé, G.: Vers un appauvrissement durable des ressources en eau de l’Afrique humide?, in: *Hydrology of Warm Humid Regions*, edited by: Gladwell, J. S., Proc. Symp. Yokohama, Japon, July 1993, 67–78, IAHS Publ. 216, IAHS Press, Wallingford, UK, 1993.
- Orange, D., Wesselink, A., Mahé, G., and Feizouré, C. T.: The effects of climate changes on river baseflow and aquifer storage in Central Africa, in: *Sustainability of Water Resources Under Increasing Uncertainty*, edited by: Rosbjerg, D., Boutayeb, N.-E., Gustard, A., Kundzewicz, Z. W., and Rasmussen, P. F., IAHS Publ., 240, 113–123, 1997.
- Owiti, Z. and Zhu, W.: Spatial distribution of rainfall seasonality over East Africa, *J. Geography and Regional Planning*, 5, 409–421, <https://doi.org/10.5897/JGRP12.027>, 2012.
- Pathak, A., Ghosh, S., and Kumar, P.: Precipitation recycling in the Indian subcontinent during summer monsoon, *J. Hydrometeorol.*, 15, 2050–2066, <https://doi.org/10.1175/JHM-D-13-0172.1>, 2014.
- Pathak, A., Ghosh, S., Martínez, J. A., Domínguez, F., and Kumar, P.: Role of Oceanic and Land Moisture Sources and Transport in the Seasonal and Interannual Variability of Summer Monsoon in India, *J. Climate*, 30, 1839–1859, <https://doi.org/10.1175/JCLI-D-16-0156.1>, 2017.
- Peixoto, J. P. and Oort, A. H.: *Physics of Climate*, AIP-Press, New York, NY, Springer Verlag, New York Press, 1992.
- Pokhrel, S., Rahaman, H., Parekh, A., Saha, S. K., Dhakate, A., Chaudhari, H. S., and Gairola, R. M.: Evaporation-precipitation variability over Indian Ocean and its assessment in NCEP Climate Forecast System (CFSv2), *Clim. Dynam.*, 39, 2585–2608, 2012.
- Pokam, W. M., Djiotang, L. A. T., and Mkankam, F. K.: Atmospheric water vapor transport and recycling in Equatorial Central Africa through NCEP/NCAR reanalysis data, *Clim. Dynam.*, 38, 1715–1729, <https://doi.org/10.1007/s00382-011-1242-7>, 2012.
- Potapov, P. V., Turubanova, S. A., Hansen, M. C., Adusei, B., Broich, M., Altstatt, A., Mane, L., and Justice, C. O.: Quantifying forest cover loss in Democratic Republic of the Congo, 2000–2010, with Landsat ETM+ data, *Remote Sens. Environ.*, 122, 106–116, 2012.
- Robert, M.: *Le Congo physique*, ed. 3, Vaillant-Carmanne, Liège, 449 pp., 1946.
- Runge, J. and Nguimalet C.-R.: Physiogeographic features of the Oubangui catchment and environmental trends reflected in discharge and floods at Bangui 1911–1999 Central African Republic, *Geomorphology*, 70, 311–324, 2005.

- Rwetabula, J., De Smedt, F., and Rebhun, M.: Prediction of runoff and discharge in the Simiyu River (tributary of Lake Victoria, Tanzania) using the WetSpa model, *Hydrol. Earth Syst. Sci. Discuss.*, 4, 881–908, <https://doi.org/10.5194/hessd-4-881-2007>, 2007.
- Salih, A. A. M., Zhang, Q., and Tjernström, M.: Lagrangian tracing of Sahelian Sudan moisture sources, *J. Geophys. Res.-Atmos.*, 120, 6793–6808, <https://doi.org/10.1002/2015JD023238>, 2015.
- Samba, G. and Nganga, D.: Rainfall variability in Congo-Brazzaville: 1932–2007, *Int. J. Climatol.*, 32, 854–873, <https://doi.org/10.1002/joc.2311>, 2012.
- Sadhuram, Y. and Kumar, M. R. R.: Does evaporation over the Arabian Sea play a crucial role in moisture transport across the west coast of India during an active monsoon period?, *Mon. Weather Rev.*, 116, 307–312, [https://doi.org/10.1175/1520-0493\(1988\)116<0307:DEOTAS>2.0.CO;2](https://doi.org/10.1175/1520-0493(1988)116<0307:DEOTAS>2.0.CO;2), 1988.
- Savenije, H. H. G.: New definitions for moisture recycling and the relationship with land-use changes in the Sahel, *J. Hydrol.*, 167, 57–78, 1995.
- SCBD-CAFC (Secretariat of the Convention on Biological Diversity and Central African Forests Commission): Biodiversity and Forest Management in the Congo Basin, Montreal, 2009.
- Schmitt, R. W.: The ocean component of the global water cycle, *Rev. Geophys.*, 33, 1395–1409, <https://doi.org/10.1029/95RG00184>, 1995.
- Sear, D. A., Armitage, P. D., and Dawson, F. H.: Groundwater dominated rivers, *Hydrol. Process.*, 13, 255–276, 1999.
- Siam, M. S., Marie-Estelle, D., and Elfatih A. B. E.: Hydrological Cycles over the Congo and Upper Blue Nile Basins: Evaluation of General Circulation Model Simulations and Reanalysis Products, *J. Climate*, 26, 8881–8894, 2013.
- Sodemann, H., Schwierz, C., and Wernli, H.: Interannual variability of Greenland winter precipitation sources: Lagrangian moisture diagnostic and North Atlantic Oscillation influence, *J. Geophys. Res.*, 113, D03107, <https://doi.org/10.1029/2007JD008503>, 2008.
- Sofianos, S. S., Johns, W. E., and Murray, S. P.: Heat and freshwater budgets in the Red Sea from direct observations at Bab el Mandeb, Deep Sea Research Part II: Topical Studies in Oceanography, 49, 1323–1340, 2002.
- Sorre, M.: Le climat écologique de la cuvette centrale congolaise [D'après Mr Etienne Bernard], in: *Annales de Géographie*, 57, 73–75, <https://doi.org/10.3406/geo.1948.12165>, 1948.
- Stohl, A. and James, P.: A Lagrangian analysis of the atmospheric branch of the global water cycle. Part I: Method description, validation, and demonstration for the August 2002 flooding in central Europe, *J. Hydrometeorol.*, 5, 656–678, [https://doi.org/10.1175/1525-7541\(2004\)005<0656:ALAOTA>2.0.CO;2](https://doi.org/10.1175/1525-7541(2004)005<0656:ALAOTA>2.0.CO;2), 2004.
- Stohl, A. and James, P.: A Lagrangian analysis of the atmospheric branch of the global water cycle. Part II: Moisture transports between the Earth's ocean basins and river catchments, *J. Hydrometeorol.*, 6, 961–984, <https://doi.org/10.1175/JHM470.1>, 2005.
- Suzuki, T.: Seasonal variation of the ITCZ and its characteristics over central Africa, *Theor. Appl. Climatol.*, 103, 39–60, <https://doi.org/10.1007/s00704-010-0276-9>, 2011.
- Svoboda, M., Hayes, M., and Wood, D.: Standardized Precipitation Index User Guide, World Meteorological Organization, Geneva, WMO Rp., 1090, 24 pp., 2012.
- Tshimanga, R. M. and Hughes, D. A.: Climate change and impacts on the hydrology of the Congo Basin: the case of the northern sub-basins of the Oubangui and Sangha Rivers, *Phys. Chem. Earth*, 50–52, 72–83, 2012.
- Tchatchou, B., Sonwa, D. J., Ifo, S., and Tiani, A. M.: Déforestation et dégradation des forêts dans le Bassin du Congo: État des lieux, causes actuelles et perspectives, *Papier occasionnel 120*, Bogor, Indonésie, CIFOR, ISBN-13: 978-602-1504-69-7, 2015.
- Trenberth, K. E.: Atmospheric Moisture Recycling: Role of Advection and Local Evaporation, *J. Climate*, 12, 1368–1380, 1999.
- Trenberth, K. E. and Guillemot, C. J.: Physical processes involved in the 1988 drought and 1993 floods in North America, *J. Climate*, 9, 1288–1298, 1996.
- Tsalefac, M., Hiol, F. H., Mahé, G., Laraque, A., Sonwa, D., Scholte, P., Pokam, W., Haensler, A., Beyene, T., Ludwig, F., Mkankam, F. K., Djoufack, V. M., Ndjatsana, M., and Doumenge, C.: Climat de l'Afrique centrale: passé, présent et future, edited by: de Wasseige, C., Tadoum, M., Eba'a Atyi, R., and Doumenge, C., Weyrich, Belgique, 128 pp., Chapter 2, 37–52, 2015.
- Tshimanga, R. M.: Hydrological uncertainty analysis and scenario based streamflow modelling for the Congo River Basin, PhD Thesis, Rhodes University repository, South Africa, 2012.
- van der Ent, R. J. and Savenije, H. H. G.: Length and time scales of atmospheric moisture recycling, *Atmos. Chem. Phys.*, 11, 1853–1863, <https://doi.org/10.5194/acp-11-1853-2011>, 2011.
- van der Ent, R. J., Savenije, H. H. G., Schaeffli, B., and Steele-Dunne, S. C.: Origin and fate of atmospheric moisture over continents, *Water Resour. Res.*, 46, 1–12, <https://doi.org/10.1029/2010WR009127>, 2010.
- van der Ent, R. J., Wang-Erlandsson, L., Keys, P. W., and Savenije, H. H. G.: Contrasting roles of interception and transpiration in the hydrological cycle – Part 2: Moisture recycling, *Earth Syst. Dynam.*, 5, 471–489, <https://doi.org/10.5194/esd-5-471-2014>, 2014.
- Vicente-Serrano, S. M., Beguería, S., and López-Moreno, J. I.: A Multiscalar Drought Index Sensitive to Global Warming: The Standardized Precipitation Evapotranspiration Index, *J. Climate*, 23, 1696–1718, <https://doi.org/10.1175/2009JCLI2909.1>, 2010.
- Vicente-Serrano, S. M., López-Moreno, J. I., Santiago, B., Lorenzo-Lacruz, J., Azorin-Molina, C., and Morán-Tejada, E.: Accurate computation of a streamflow drought index., *J. Hydrol. Eng.*, 17, 318–332, 2012.
- Viste, E. and Sorteberg, A.: The effect of moisture transport variability on Ethiopian summer precipitation, *Int. J. Climatol.*, 33, 3106–3123, <https://doi.org/10.1002/joc.3566>, 2013.
- Washington, R., James, R., Pearce, H., Pokam, W. M., and Moufouma-Okia, W.: Congo Basin rainfall climatology: can we believe the climate models?, *Phil. Trans. R. Soc. B.*, 368, <https://doi.org/10.1098/rstb.2012.0296>, 2013.
- Wasseige, C., Marshall, M., Mahé, G., and Laraque, A.: Interactions between climate characteristics and forest, in: *Les forêts du bassin du Congo – Forêts et changements climatiques*, edited by: de Wasseige, C., Tadoum, M., Eba'a Atyi, R., et Doumenge, C., Weyrich, Belgique, 128 pp., Chapter 3, 53–64, 2015.
- Wesselink, A. J., Orange, D., Feizouré, C. T., and Randriamiarisoa: Les régimes hydroclimatiques et hydrologiques d'un bassin versant de type tropical humide: l'Oubangui (République Centrafricaine), in: *L'Hydrologie Tropicale: géoscience et outil pour*

- le Développement, edited by: Chevallier, P. and Pouyaud, B., Walingford, Oxfordshire, UK, IAHS Publ., 238, 179–194, 1996.
- Yu, L.: Global Variations in Oceanic Evaporation (1958–2005): The Role of the Changing Wind Speed, *J. Climate*, 20, 5376–5390, <https://doi.org/10.1175/2007JCLI1714.1>, 2007.
- Yu, L., Jin, X., and Weller, R. A.: Multidecade Global Flux Datasets from the Objectively Analyzed Air-sea Fluxes (OAFlux) Project: Latent and sensible heat fluxes, ocean evaporation, and related surface meteorological variables, Woods Hole Oceanographic Institution, OAFlux Project Technical Report, OA-2008-01, 64 pp., Woods Hole, Massachusetts, 2008.
- Žagar, N., Skok, G., and Tribbia, J.: Climatology of the ITCZ derived from ERA Interim reanalyses, *J. Geophys. Res.*, 116, D15103, <https://doi.org/10.1029/2011JD015695>, 2011.
- Zheng, X. and Eltahir, E. A. B.: A Soil Moisture-Rainfall Feedback Mechanism: 2. Numerical experiments, *Water Resour. Res.*, 34, 777–785, <https://doi.org/10.1029/97WR03497>, 1998.
- Zhou, L., Tian, Y., Myneni, R. B., Ciais, P., Saatchi, S., Liu, Y. Y., Piao, S., Chen, H., Vermote, E. F., Song, C., and Hwang, T.: Widespread decline of Congo rainforest greenness in the past decade, *Nature*, 509, 86–90, <https://doi.org/10.1038/nature13265>, 2014.



# The atmospheric branch of the hydrological cycle over the Indus, Ganges, and Brahmaputra river basins

Rogert Sorí<sup>1</sup>, Raquel Nieto<sup>1,2</sup>, Anita Drumond<sup>1</sup>, Sergio M. Vicente-Serrano<sup>3</sup>, and Luis Gimeno<sup>1</sup>

<sup>1</sup>Environmental Physics Laboratory (EphysLab), Universidade de Vigo, Ourense, 32004, Spain

<sup>2</sup>Department of Atmospheric Sciences, Institute of Astronomy, Geophysics and Atmospheric Sciences, University of São Paulo, São Paulo, 05508-090, Brazil

<sup>3</sup>Instituto Pirenaico de Ecología, Consejo Superior de Investigaciones Científicas (IPE-CSIC), Zaragoza, 50059, Spain

**Correspondence:** Rogert Sorí (rogert.sori@uvigo.es)

Received: 29 June 2017 – Discussion started: 24 July 2017

Revised: 10 October 2017 – Accepted: 26 October 2017 – Published: 15 December 2017

**Abstract.** The atmospheric branch of the hydrological cycle over the Indus, Ganges, and Brahmaputra river basins (IRB, GRB, and BRB respectively) in the South Asian region was investigated. The 3-dimensional model FLEXPART v9.0 was utilized. An important advantage of this model is that it permits the computation of the freshwater budget on air parcel trajectories both backward and forward in time from 0.1 to 1000 hPa in the atmospheric vertical column. The analysis was conducted for the westerly precipitation regime (WPR) (November–April) and the monsoonal precipitation regime (MPR) (May–October) in the period from 1981 to 2015. The main terrestrial and oceanic climatological moisture sources for the IRB, GRB, and BRB and their contribution to precipitation over the basins were identified. For the three basins, the most important moisture sources for precipitation are (i) in the continental regions, the land masses to the west of the basins (in this case called western Asia), the Indian region (IR), and the basin itself, and (ii) from the ocean, the utmost sources being the Indian Ocean (IO) and the Bay of Bengal (BB), and it is remarkable that despite the amount of moisture reaching the Indus and Ganges basins from land sources, the moisture supply from the IO seems to be first associated with the rapid increase or decrease in precipitation over the sources in the MPR. The technique of the composites was used to analyse how the moisture uptake values spatially vary from the sources (the budget of evaporation minus precipitation ( $E - P$ ) was computed in a backward experiment from the basins) but during the pre-onset and pre-demise dates of the monsoonal rainfall over each basin; this confirmed that

over the last days of the monsoon at the basins, the moisture uptake areas decrease in the IO. The Indian region, the Indian Ocean, the Bay of Bengal, and the basins themselves are the main sources of moisture responsible for negative (positive) anomalies of moisture contribution to the basins during composites of driest (wettest) WPR and MPR.

## 1 Introduction

Research on the hydrological cycle in the Asian region has been extensive, which is mainly because of the strong influence of the Asian summer monsoon (ASM), which develops a crucial role in moisture transport and the supply of precipitation in this region (Webster, 2006). The ASM system has three different but inter-related components: South Asian monsoon (SAM), South East Asian monsoon (SEAM), and east Asian monsoon (EAM) (Janowiak and Xie, 2003). The Indian summer monsoon (ISM) is one of the most studied phenomena and is part of the SAM. It develops in response to the large thermal gradients between the warm Asian continent to the north and the cooler Indian Ocean to the south (Slingo, 1999). Solar heating is considered a fundamental driver of all of the monsoon systems. Heating of the Tibetan Plateau leads to increased ISM rainfall via enhancement of the cross-equatorial circulation and a concurrent strengthening of both the Somali jet and westerly winds that bring moisture to southern India (Rajagopalan and Molnar, 2013). Surface heating over the plateau plays a role in producing cy-

clonic vorticity in the shallow lower layer but negative vorticity in the deep upper layers through atmospheric thermal adaptation (Yanai and Wu, 2006; Song et al., 2010). The satellite and conventional observations support an alternative hypothesis, which considers the monsoon as a manifestation of seasonal migration of the inter-tropical convergence zone (ITCZ) (Gadgil, 2003). Understanding and predicting the variability of the Indian monsoon is extremely important for the well-being of over 1 billion people and the diverse flora and fauna inhabiting the region (Gadgil, 2003).

The monsoonal regimes in India, tropical Africa, and North America are provided with moisture from a large number of regions (Gimeno et al., 2012). According to Misra et al. (2012), instead of rainfall, evaporative sources (of the ISM) may be a more appropriate metric to observe the relationship between the seasonal monsoon strength and intra-seasonal activity. It is worth mentioning that the precipitation over any area of land comes from the moisture already available in the local atmosphere, the convergence of the moisture advected into the region by the winds, and the supply by evaporation from within the same region (Gong and Eltahir, 1996; Trenberth, 1999). The atmospheric branch of the hydrological cycle consists of the atmospheric transport of water, which is mainly in the vapour phase (Peixoto and Oort, 1992), and plays a crucial role in understanding the bridge between evaporation in the sources and precipitation over remote regions. Indeed, the identification of moisture sources for precipitation constitutes an important feature to understand the further mechanisms associated with rainfall variability (Gimeno et al., 2012), and it has become a major research tool in the analysis of extreme events (e.g. floods and droughts) (Gimeno, 2014).

Numerous studies (e.g. Drumond et al., 2011; Misra and DiNapoli, 2014; Ordoñez et al., 2012; Pathak et al., 2017) have determined the origin of moisture that contributes to precipitation in Asia. Ordoñez et al. (2012) confirmed the key action of the Somali low-level jet bringing moisture from the Arabian Sea and the Indian Ocean during the boreal summer and documented the importance of recycling as the main water vapour source in the winter for this region. Chen et al. (2012) identified and quantified the origin (destination) of moisture and air mass transported to (from) the Tibetan Plateau from June to August, and Pathak et al. (2017) made an extensive study of the role of oceanic and land moisture sources during the summer monsoon in India to confirm the strong land–ocean–atmosphere interactions. To determine the evaporative sources of the SEAM region, Misra and DiNapoli (2014) found that the largest evaporative source for the rainy season in the SEAM region came from the local land-based evaporation and the seas in the immediate vicinity. Tuinenberg et al. (2012) applied a water trajectory model to investigate the moisture recycling rates over the Ganges River basin (GRB) and confirmed that a large influx of moisture from the Indian Ocean dominates precipitation. The recycling of precipitation helps in defining the

role of land–atmosphere interactions in the regional climate (Bisselink and Dolman, 2008). The Indus River basin (IRB) is located in the north-west of India. Utilizing stable isotope measurements, Karim and Veizer (2002) determined that the predominant moisture sources for the IRB were located in a closed basin such as the Mediterranean or other inland seas. Together, the IRB, the Ganges River basin (GRB), and the Brahmaputra River basin (BRB) are the largest Asian river basins and occupy a large part of the Indo-Gangetic plain. In these basins, the importance of the basin itself in providing moisture has been previously proven (COLA, 2017).

Nevertheless, due to the complex hydrological cycle over the Indo-Gangetic plain, this region is quite unique compared to the rest of the world and the ASM plays a crucial role. In this region, the moisture source identification and evaluating their role in the moisture contribution for a target region are fundamental for understanding the nature of the precipitation in it. For these reasons, the aim of this work was to investigate the atmospheric branch of the hydrological cycle over the Indus, Ganges, and Brahmaputra river basins. This was done first by identifying the main seasonal oceanic and terrestrial moisture sources for each basin and later quantifying their contribution to precipitation over the basins. This analysis will allow determination of the role of the sources during different precipitation regimes, specifically for the rainfall associated with the monsoon onset and demise and for dry and wet conditions over the basins. Different criteria have been used in the past to define the onset and retreat over different monsoon regions and even over different parts of the same monsoon (Zeng and Lu, 2004). Taniguchi and Koike (2006) argue that the rapid enhancement of the wind speed related well with the abrupt beginning of the rainy season, and it represents a clear transition in atmospheric conditions or the beginning of ISM.

## 1.1 Study area

The study was performed for the Indus, Ganges, and Brahmaputra river basins, which are located in South and South East Asia (Fig. 1). The Ganges is the largest river basin in the Indian sub-continent followed by the IRB and the BRB; all of these river basins are densely populated and represent a complete range of landscapes and ecosystems on which the major agricultural activities rely (Davis, 2003; Hossen, 2015; Tare et al., 2015; Mahanta et al., 2014; Laghari et al., 2012).

Two main climate systems drive the annual precipitation over the basins, the ASM in summer and the western disturbances (WDs) during the winter months (Hasson et al., 2014). It provides some feature of a bimodal precipitation regime: the monsoonal precipitation regime (MPR) for May–October and the westerly precipitation regime (WPR) for November–April (Hasson et al., 2016, 2014). In the MPR, the summer monsoon has a key role in the hydro-climatology of Asia. Even the sub-seasonal river discharge is found to be

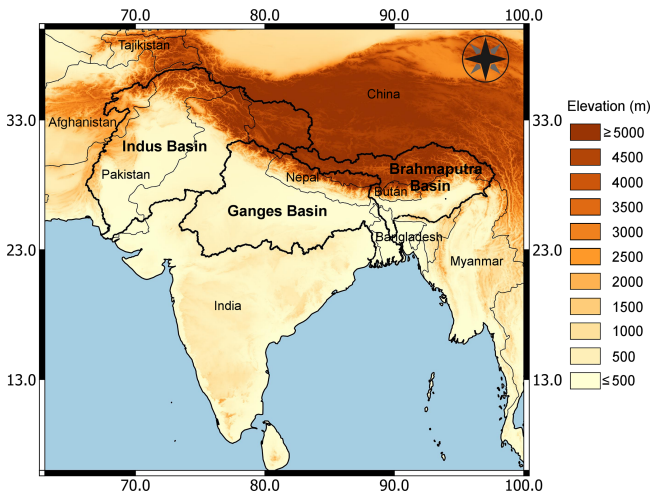


**Figure 1.** The geographic location and boundaries of the Indus, Ganges, and Brahmaputra river basins from Hasson et al. (2013), and the elevation from the Hydrosheds project (Lehner et al., 2008).

strongly tied to the monsoon intraseasonal cycle, which results in a near-in-phase timing of the Ganges and Brahmaputra discharge (Jian et al., 2009), whereas the WDs during the WPR are important synoptic weather systems responsible for almost one-third of the annual precipitation over the northern Indian region and most of the cold season precipitation (Dimri et al., 2015). During the boreal winter, the meltwater is extremely important in the Indus basin and is also important for the Brahmaputra basin, but plays only a modest role for the Ganges (Immerzeel et al., 2010). Indeed, the IRB irrigation system (IBIS) is the largest irrigation system in the world (Qureshi, 2011; Laghari et al., 2012). From a geographic and climatologic perspective, the IRB is at a transition between the monsoon system in the east and the Mediterranean system in the west (Karin and Veizer, 2002).

## 2 Materials and methods

### 2.1 Study period

The study was conducted for the period from 1981 to 2015 and took into account the criterion of Hasson et al. (2016). These authors considered two hydro-climatological periods of the year: May–October, which was named as “monsoonal precipitation regime” and hereafter MPR, and November–April, the “westerly precipitation regime”, which is hereafter referred to as WPR, to study the seasonal cycle of the water balance over the Indus, Ganges, and Brahmaputra River basin. The annual cycle of the precipitation ( $P$ ), evaporation ( $E$ ) and potential evapotranspiration (PET) over the basins are assessed. Monthly data of  $P$  and  $E$  belong to CRU 3.24.01 (Harris et al., 2014) and from monthly means of daily forecast accumulations from ERA-Interim (ERA-I) reanalysis (Dee et al., 2011).

### 2.2 The Lagrangian approach

The 3-d Lagrangian model FLEXPART v9.0, which was developed by Stohl and James (2004, 2005), was utilized to identify the moisture sources for the IRB, GRB, and BRB and investigate their role in the atmospheric water balance over the basins. The model was executed considering the atmosphere is homogeneously divided into approximately 2.0 million uniformly distributed parcels. The parcels were advected backward and forward in time using the 3-dimensional winds field from the ERA-I reanalysis (Dee et al., 2011), which is a mechanism described by Eq. (1):

$$dx/dt = v[x(t)], \quad (1)$$

where  $x$  is the position of the parcel and  $v[x(t)]$  is the wind speed interpolated in space and time. For each parcel, a constant mass ( $m$ ) was considered. By interpolating  $q$  to  $x(t)$ , the net rate of change of the water vapour content of a particle is computed by Eq. (2), where  $e$  represents the moisture gain (through evaporation from the environment) and  $p$  the moisture loss (e.g. through precipitation).

$$(e - p) = m(dq/dt) \quad (2)$$

Integrating  $(e - p)$  in all of the atmospheric vertical column, we obtain a diagnosis of the surface freshwater flux, which is represented by  $(E - P)$  (Stohl and James, 2004) in Eq. (3), where  $K$  is the number of particles residing over an area  $A$ .

$$E - P \approx \frac{\sum_{k=1}^K (e - p)}{A} \quad (3)$$

To calculate the freshwater flux, the average time residence of the water vapour in the atmosphere was considered, and it was set to 10 days according to Eltahir and Bras (1996) and Numaguti (1999). The calculus conducted in the air masses, tracked backward in time from over each basin, permitted identification of those regions where air masses gained and lost humidity before arriving at the basins and thus enabled the identification of the moisture sources of the regions. This indicates that those regions where  $(E - P) > 0$  are considered moisture sources, whereas the opposite  $(E - P) < 0$  are moisture sinks. FLEXPART needs the following 3-dimensional fields: horizontal and vertical wind components, temperature, and specific humidity in the ECMWF vertical hybrid coordinate system. The model also needs the two-dimensional fields: surface pressure, total cloud cover, 10 m horizontal wind components, 2 m temperature and dew point temperature, large-scale and convective precipitation, sensible heat flux, east–west and north–south surface stress, topography, land–sea mask, and sub-grid standard deviation of the topography. To run FLEXPART, it utilized the ERA-I reanalysis dataset (Dee et al., 2011) at 6 h intervals (00:00, 06:00, 12:00, and 18:00 UTC) and at a resolution of  $1^\circ$  in latitude and longitude considering 61 vertical levels from 0.1 to 1000 hPa.

The use in ERA-I of 4D-Var data assimilation contributed to better time consistency than the 3D-Var used in ERA-40. However, the agreement between the global tendencies of mass and total column water vapour (TCWV) and  $(E - P)$  is not very good in ERA-I, but it is still much better than for ERA-40 (Berrisford et al., 2011).

Sebastian et al. (2016) found a huge uncertainty in the estimates of  $(P - E)$  over South Asia, when computed from different reanalyses, but recommend using atmospheric budget for computation of water availability in terms of  $(P - E)$  rather than based on individual values of  $P$  and  $E$ . We also consider that in the state-of-the-science discussion on three reanalyses (ERA-I, MERRA, and CFRS), Lorenz and Kunstmann (2012) found that the ERA-I shows both a comparatively reasonable closure of the terrestrial and atmospheric water balance and a reasonable agreement with the observation datasets. These findings support the use of ERA-I datasets for running FLEXPART in order to reduce the uncertainty in this study. In the same way, the vertically integrated northward and eastward moisture flux data to calculate the vertically integrated moisture flux (VIMF) and its divergence belong to the ERA-I reanalysis with a resolution of  $1^\circ \times 1^\circ$ . Computing the  $(P - E)$  directly from atmospheric budget with divergence of moisture flux for different reanalyses improved correlation with observed values of  $(P - E)$  according to Sebastian et al. (2016) results, and we will take that into consideration for future studies.

Detailed information regarding FLEXPART functionalities can be found in Stohl and James (2004, 2005). Concerning the limitations of the method, Eq. (3) can diagnose  $(E - P)$  but not  $E$  or  $P$  individually according to Stohl and James (2004). These authors also argue that along with individual trajectories,  $q$  fluctuations can occur for nonphysical reasons (e.g. because of  $q$  interpolation or trajectory errors), which is a limitation that is partly compensated for among the many particles in an atmospheric column over the target area. This approach has been used in numerous studies with the main purpose of characterizing the atmospheric branch of the hydrological cycle in different regions, e.g. in western and southern India (Ordoñez et al., 2012), the Sahel (Nieto et al., 2006), China (Drumond et al., 2011; Huang and Cui, 2015), the Mississippi River basin (Stohl and James, 2005), the Amazon River basin (Drumond et al., 2014), and Central America (Durán-Quesada et al., 2010). On a global scale, FLEXPART has been implemented to identify the main oceanic and continental moisture sources for precipitation (Gimeno et al., 2012) as well as a catalogue of moisture sources for two sets of continental climatic regions (Castillo et al., 2014). The main advantage of FLEXPART is that it permits the tracking of air masses backward and forward in time and calculates along the trajectories the water balance in the atmospheric column.

For delimiting the most evaporative regions in the moisture sources, some authors (e.g. Drumond et al., 2014, 2016) have used a threshold (a percentile value) to define the bound-

aries. In this work, we apply the same technique; the value of the 90th percentile in the  $(E - P) > 0$  values integrated over 10 days of transport was considered to delimit the sources. An exception in this work was that each river basin was considered a source region; which permitted the study of the role of each one and the balance of  $(E - P)$  on them.

Once the moisture sources were delimited, a forward-in-time analysis was implemented to determine the contribution of each source to the precipitation over the basins (when  $(E - P)_{i10} < 0$ ). This analysis allowed us to later perform a seasonal correlation analysis between the data of  $(E - P)_{i10} < 0$  with  $P$  and PET to determine the best linear relationships.

### 2.3 Selection of pre-onset and pre-demise monsoonal dates over the basins

Here, we address the spatial variability of the moisture uptake for the basins during composites of dates associated with the pre-onset and demise of the Indian monsoon over the basins. To determine the day on which the increase in rainfall indicates the beginning of the monsoon involvement for each basin, we utilized the method proposed by Noska and Misra (2016). This method is based on daily cumulative anomalies ( $C'm$ ) of the average precipitation for each basin along the year and according to Eqs. (4) and (5).

$$C'm(i) = \sum_{n=1}^i [Dm(n) - C], \quad (4)$$

$$C = \frac{1}{MN} \sum_{m=1}^M \sum_{n=1}^N D(m, n), \quad (5)$$

where  $D(m, n)$  is the daily basin rainfall for day  $n$  of year  $m$ , and  $C$  is the climatology of the annual mean of the precipitation at each basin over  $N$  ( $= 365$  or  $366$ ) days for  $M$  years. The onset is then defined as the day after  $C'm$  reaches its absolute minimum value, but from May onward when the MPR is defined. When applied, this criterion avoids the selection of a false date that could arise and be associated with the previous winter precipitation. Similarly, the demise is considered the day when  $C'm$  reaches the maximum value after the onset. For this analysis, it was necessary to use a series of precipitation on a daily basis over an extended period of the study, 1981–2015. For our goal, we preferred to utilize the observational precipitation datasets from the Climate Hazards Group InfraRed Precipitation with Station data (CHIRPS; Chris et al., 2015) which has the advantage of being based on a combination of satellite and rain gauge data. At least, an analysis on a monthly scale for June–August by Ceglar et al. (2017) revealed that out of the four reanalyses (ERA-I, ERA-I/Land, AgMERRA (an agricultural version of MERRA), and JRA-55), all of them show more uniformly distributed monthly precipitations over monsoon Asia

when compared to CHIRPS than APHRODITE (Yatagai et al., 2009).

Different criteria have been used in the past to define onset and retreat over different monsoon regions and even over different parts of the same monsoon (Zeng and Lu, 2004). Taniguchi and Koike (2006) argue that the rapid enhancement of the wind speed related well with the abrupt beginning of the rainy season and it represents a clear transition in atmospheric conditions or the beginning of ISM. To determine the onset and demise dates, we applied an objective index to the basins from Noska and Misra (2016), which was previously adapted for the Asian monsoon region in Misra and DiNapoli (2014) and builds upon the index proposed by Liebmann et al. (2007). The analysis is based on the cumulative anomalies of daily rainfall averaged (see Eqs. 4 and 5) over the basins and is permitted to identify the date associated with rainfall increase because of the monsoon onset (the day after the minimum accumulated rainfall anomalies) and demise (the day of the maximum accumulated rainfall). According to Noska and Misra (2016), this index is capable of representing the annual rainfall variability across the region and thus must be adequate for our target regions.

## 2.4 Identification of dry and wet conditions

To identify dry and wet conditions in the basins, the Standardised Precipitation–Evapotranspiration Index (SPEI) (Vicente-Serrano et al., 2010) was used. SPEI is based on a standardization of the climatic water balance (Precipitation –  $P$  – minus atmospheric evaporative demand – AED), which is computed on different timescales. The data of  $P$  and AED were obtained from CRU TS v.3.24.01 (Harris et al., 2014). The concept of the PET has proven to be inappropriate because the evaporation climatic demand is not only linked to the climate but also to the type of the evaporative surface, and some authors have adopted a more suitable term: evaporative atmospheric demand (Katerji and Rana, 2011; McVicar et al., 2012). However, we will keep the term “PET” throughout the text as the original data are named by the source. We calculated the 6-month SPEI to assess drought severity conditions on the three basins since this timescale adapts to the time period of the two main hydro-climatological seasons over the basins (WPR and MPR). Thus, the 6-month SPEI at the end of April (October) characterized the water balance for the WPR (MPR). According to the criterion of McKee et al. (1993), we used an SPEI threshold of  $\pm 1.5$  to identify severe and extreme dry ( $-1.99$  to  $-1.5$ ;  $\leq -2.0$  respectively) and wet ( $1.5$  to  $1.99$ ;  $\geq 2.0$  respectively) conditions.

It is important to emphasize that we have used precipitation data from different sources, which is not consistent with the FLEXPART input data from ERA-I reanalysis. Nevertheless, it makes it possible to avoid the any possible co-linearity when analysing different hydro-meteorological process.

## 3 Results and discussion

### 3.1 The precipitation and evaporation over the basins

The mean annual cycle of the  $P$ ,  $E$ , and PET over the Indus, Ganges, and Brahmaputra basins appears in Fig. 2. For the three basins, the maximum  $P$  occurs during the summer months. It can be observed that monthly  $P$  values from ERA-I tend to be slightly greater than those computed from CRU, but the annual cycle is the same. These differences are best appreciated in the annual cycle of  $P$  over the BRB. In the IRB, the  $P$  annual cycle is characterized by two maximum peaks in February–March and July–August (Fig. 2a). The  $E$  approximately follows this cycle but with lower values. In this basin, the PET remains higher than the  $P$  and  $E$  across the year; in fact, Cheema (2012) argue that the major part of this basin is dry and located in arid to semiarid climatic zones. Laghari et al. (2012) also found for the climatology from 1950 to 2000 that PET exceeds  $P$  at the IRB across the year. PET is enhanced after maximum precipitation; maximum values occur in May–June. Over the GRB maximum  $P$  occurs between May and October and is greater than over the IRB. The PET and  $E$  annual cycles over this basin differ, and as expected,  $PET > E$ . The PET annual cycle is mainly like for the IRB. Indeed, both variables reflect close but different information. The  $E$  annual cycle agrees with that obtained by Hasson et al. (2014) for the three river basins. Over the BRB, the monthly average precipitation both from CRU and ERA-I increases abruptly from March until a maximum ( $> 11.0 \text{ mm day}^{-1}$ ) in July and later falls until a minimum is reached in December (Fig. 2c). The PET and  $E$  are very close and do not surpass  $4 \text{ mm day}^{-1}$  in the annual climatology. In particular, the PET annual cycle is notable for being lower than what was obtained for the IRB and GRB. The annual cycles of  $P$  (from CRU and ERA-I) and  $E$  for the IRB, GRB, and BRB follow the same annual cycle as those obtained by Hasson et al. (2014). These authors analysed the seasonality of the hydrological cycle over the same basins for the 20th century climate (1961–2000 period), utilizing PCMDI/CMIP3 general circulation models (GCMs) and observed precipitation data.

Tropical cyclones and weak disturbances contribute to monsoon rainfall. Among these systems, the most efficient rain-producing system (responsible for about half of the Indian summer monsoon rainfall) is known as the Indian monsoon depression (MD) which generally forms around Bay of Bengal and propagates westward or north-westward with a typical life span of 3 to 6 days (Ramage, 1971; Yoon and Huang, 2012). The change in the large-scale circulation, especially the converging atmospheric water vapour flux, is responsible for the MD modulation by the 30–60-day monsoon mode (Yoon and Huang, 2012). Over the Brahmaputra basin, the rainiest, heavy rainstorms are due to the shifting of the eastern end of the seasonal monsoon trough to the foothills of Himalayas in the north and the “break” monsoon situa-

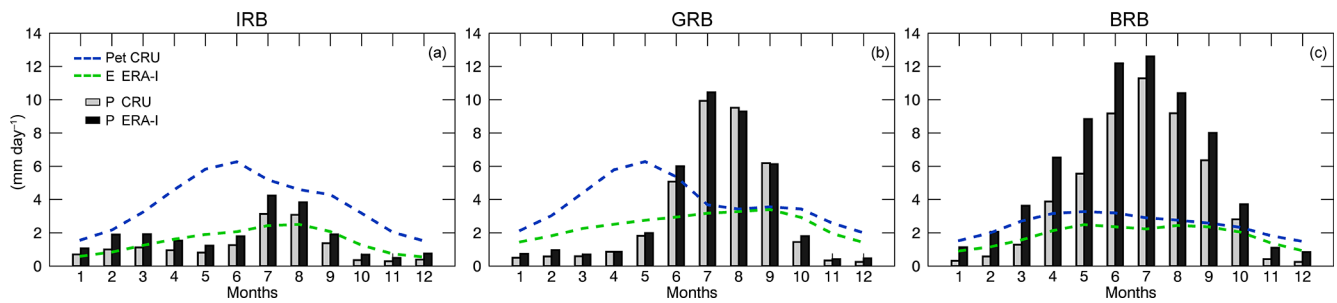


**Figure 2.** The 1981–2015 annual cycle of precipitation (gray, black bars from CRU and ERA-I,  $\text{mm day}^{-1}$ ) and potential evapotranspiration (blue line from CRU,  $\text{mm day}^{-1}$ ) and evaporation (green line from ERA-I,  $\text{mm day}^{-1}$ ) over the Indus (a), Ganges (b), and Brahmaputra (c) river basins from CRU 3.24.01.

tions during the monsoon season (Dhar and Nandargi, 2000). Summarizing, the BRB is wetter than the western GRB and IRB; this is because the monsoon rainfall dominates in the summer months in the eastern region and gets weaker on the western side with a time delay of a period of weeks (Hasson et al., 2014).

### 3.2 Identification of moisture sources

The climatological budget of  $(E - P)i10$  obtained in the backward track experiment of air masses residing over the three basins and the VIMF and its divergence appears in Fig. 3. The analysis was conducted for the WPR and MPR periods. In the first one, the most intense positive values (delimited by p90) in the pattern of  $(E - P)i10$  obtained for the IRB, are over the basin itself and they extend south-west until the Indian Ocean (IO) and East Africa (EA). High  $(E - P)i10 > 0$  values are also confined by the p90 (green line) to the west of the basin (hereafter western Asia; WA), the Persian Gulf (PG), the Red Sea (RS) and to the south-east occupying a major part of the Indian region (IR) and part of the Bay of Bengal (BB). In this season, the field of  $(E - P)i10$  obtained in the backward experiment from the GRB is very similar to the one obtained for the IRB, but the p90 is now extended to the east and even confines part of the East China Sea and South China Sea (CHS). Over the GRB itself, the highest values of  $(E - P)i10 > 0$  are observed. For the BRB in the pattern of  $(E - P)i10$ , the line of p90 is longitudinally extended from East Africa until the CHS and seems less intense than those previously obtained for the IRB and GRB. In this season, the prevalence of the divergence of the VIMF can be distinguished in almost all of the Indian regions except the northern parts of the IRB and the GRB and the western parts of the BRB, where they are overcome by the convergence of the VIMF. In the northern part of the basins, the VIMF is mainly to the east but over the Indian region is mainly to the south-west and is more intense over the Arabian Sea, which is a feature that is known to be linked to excessive latent heat fluxes and is related to both the anomalous meridional temperature gradient originated between the

lands to the north of the Arabian Sea (and elsewhere) and the sea surface temperature (SST) at the Arabian Sea (Levine and Turner, 2012; Marathayil et al., 2013).

In the MPR, the pattern of  $(E - P)i10$  is more extended and intense than in the WPR (Fig. 3). In the backward experiment for the three basins it is commonly distinguished that the p90 line comprises a huge area in the western Indian Ocean and to the west of each basin. The moisture transport from the Indian Ocean crossing the Arabian Sea and penetrating into the continent is revealed by the VIMF; observational analysis shows strong monsoons depend on moisture fluxes across the Arabian Sea (Levine and Turner, 2012). According to Qiao et al. (2013), the inter-annual variation of the moisture source over the western-central south Indian Ocean is determined by the variation of both local precipitation and evaporation. Thus, the use of FLEXPART to assess the role of this region in moisture supply to the target regions could be an advantage. Previous regions that provided moisture for the basins in the East Asian region and the CHS are moisture sinks in this season in accordance with the VIMF convergence. To the east of the IRB, over the east of the GRB and over all of the BRB are moisture sinks. In these areas, the air masses lose humidity before they arrive at each basin, which is apparently because of the intense precipitation over this region associated with the Indian Monsoon.

To determine the different roles within the continental and oceanic moisture sources and taking into account the region where they are located, we made a separation for the WPR and MPR. The selected sources are shown through a schematic representation in Fig. 4. The regions shaded in colour represent the location and spatial extension of the most important moisture sources previously delimited using the p90 values and independently calculated for the  $(E - P)i10 > 0$  values for every basin and period (Fig. 3). The sources clearly divide the continental and oceanic zones where the budget of  $(E - P)i10$  was calculated earlier. The criterion adopted here permits the investigation of the role of continental and oceanic moisture sources according to their location.

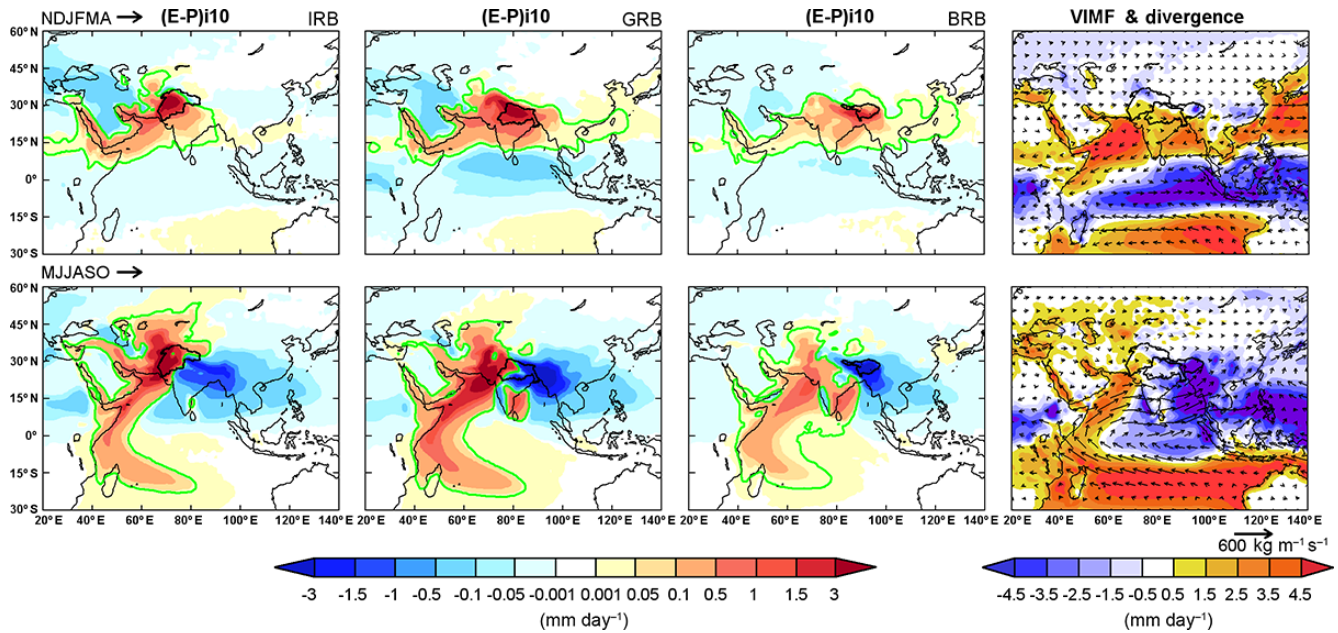


**Figure 3.** November–April (top) and May–October (bottom)  $(E - P)i10$  ( $\text{mm day}^{-1}$ ) backward integrated from the Indus, Ganges, and Brahmaputra river basins (contoured by a black line) (from FLEXPART) and vertically integrated moisture flux (VIMF) (arrows,  $\text{kg m}^{-1} \text{s}^{-1}$ ) and divergence of the VIMF (shaded,  $\text{mm day}^{-1}$ ). The 90th percentile is represented by a green line. Period 1981–2015.

For the IRB in the WPR, the continental moisture sources were divided into East Africa (EA; also extending to the west over the Sahel), the Arabian Peninsula (AP) mainly around the coast, in Asia to the west of this basin (western Asia, WA), and the Indian region (IR) (Fig. 4a). The oceanic moisture sources are easily divided and cover a small part of the western Mediterranean Sea (MS), the whole Red Sea (RS), the Persian Gulf (PG), the Indian Ocean (IO; mostly in the Arabian Sea region), the Bay of Bengal (BB), and finally part of the Caspian Sea (CS). For the IRB in the WPR and MRP, the moisture sources almost remain in the same regions but change spatially because they are more extended in the MPR period with the exception of the IR and the BB, which are almost imperceptible (Fig. 4b). In the MPR the IO, which is extended to the south and south-east, is highlighted. With respect to the rest of the continental sources, the EA is confined to the east of the African continent but the WA increased its spatial extent to the east and north. Because of the relative similar location of the sources for the GRB (Fig. 4c and d) and BRB (Fig. 4e and f), we kept the names already utilized for classification of the IRB moisture sources. However, some new region may appear such as the CHS and central-east Asia (CEA) during WPR, and a small moisture source to the north of the GRB and BRB, named central Asia (CA), in the MPR. In the same period, to the west of the BRB, we approximately divided the areas as previously classified for other basins as WA and IR. Ordoñez et al. (2012) also divided the evaporative regions obtained in a backward analysis from western and southern India, taking into account the

well-known geographical regions. Pathak et al. (2017) also calculated the moisture contribution from oceanic and terrestrial sources for the ISM rainfall. However, in their method, the terrestrial sources were approximately selected based on the uniform climate sub-type of Köppen and the percentage of forest cover in the year 2000, while the oceanic sources were according to the VIMF. They considered divergent areas as the potential sources, whereas regions with high convergence were considered potential sink regions. Nevertheless, in our approach, moisture sources are considered those regions from where air masses uptake humidity before arrive to the basins.

### 3.3 Role of continental and oceanic moisture sources

#### 3.3.1 Budget of $(E - P)$

The budget of  $(E - P)$ , over the 10-day cycles backward in time from each basin for the WPR and MPR and over the continental and oceanic regions and each basin separately, was quantified (Fig. 5). In the WPR, the  $(E - P)i10$  over the IRB itself is positive and greater than that obtained over the remaining continental and oceanic moisture sources (Fig. 5a). As seen in Fig. 2, the PET is greater than  $P$  over the IRB in these periods, which indicates the prevalence of evaporative conditions in this basin. As the IRB is also a land-based source, the budget of  $(E - P)i10$  over the basin, together with the budget over the rest of the continental areas, reveals the importance of the continental moisture sources for the water supply to the IRB and is probably because of

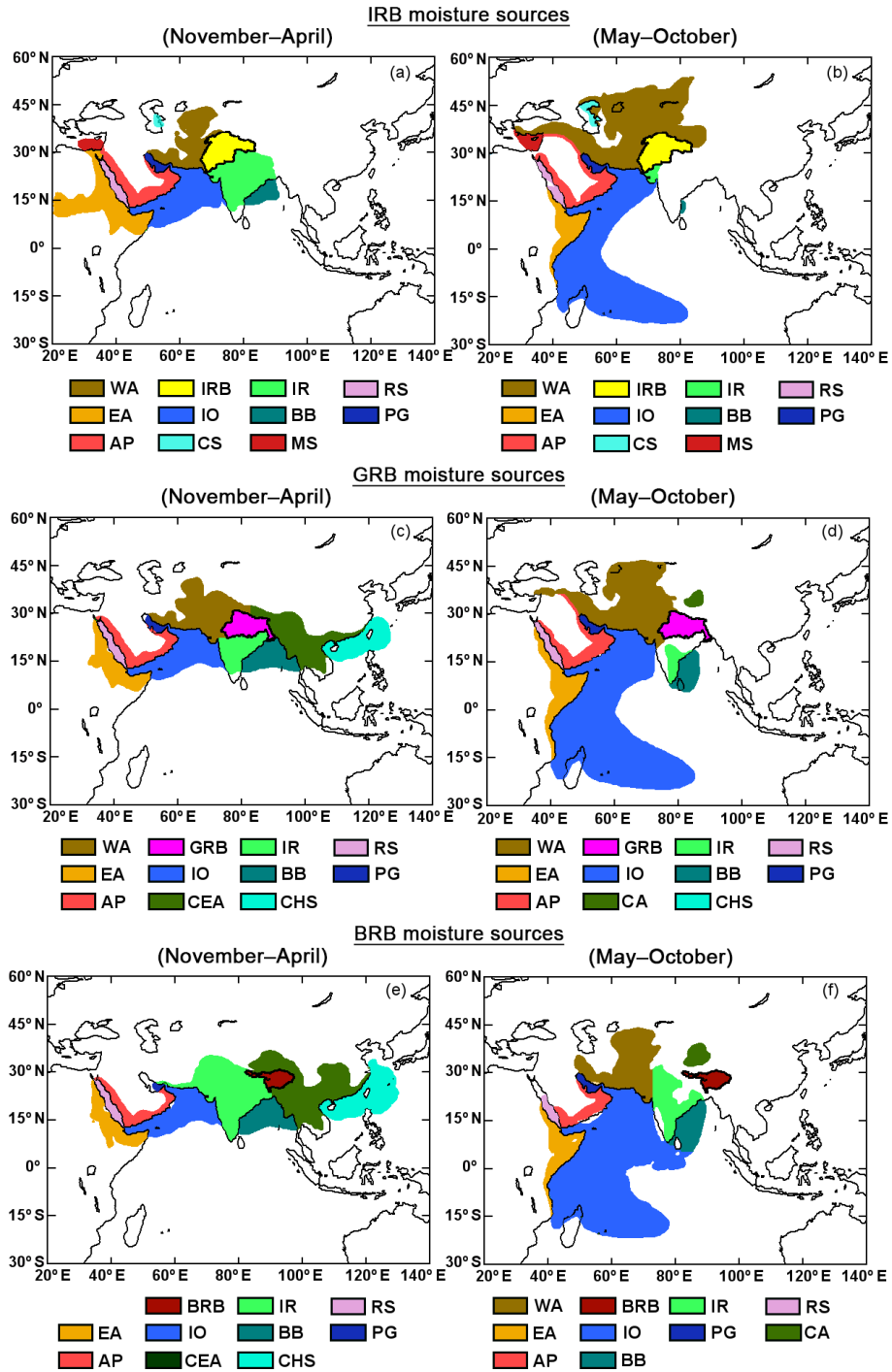


**Figure 4.** Schematic representation of the IRB (a and b), GRB (c and d), and BRB (e and f) moisture sources delimited by the p90 value shown in Fig. 3 for the WPR (left column) and MPR (right column). The acronyms identifying the moisture sources are defined in the text.

the recycled moisture. Because the GRB and BRB occur in both the continental and oceanic sources, the budget of the  $(E - P)i_{10}$  remains positive (Fig. 5a). For the GRB, the positive  $(E - P)i_{10}$  over the continental sources is greater than previously obtained for the IRB and the BRB, but less than that obtained over the oceanic moisture sources of the IRB.

Finally, the  $(E - P)i_{10}$  over the BRB and its continental and oceanic sources are positive but less than previously computed over the moisture source regions of IRB and GRB. During the WPR in the GRB and the BRB, as occurred in the IRB, the PET is greater than  $P$  and coincides with evaporative conditions in the atmospheric column over them.

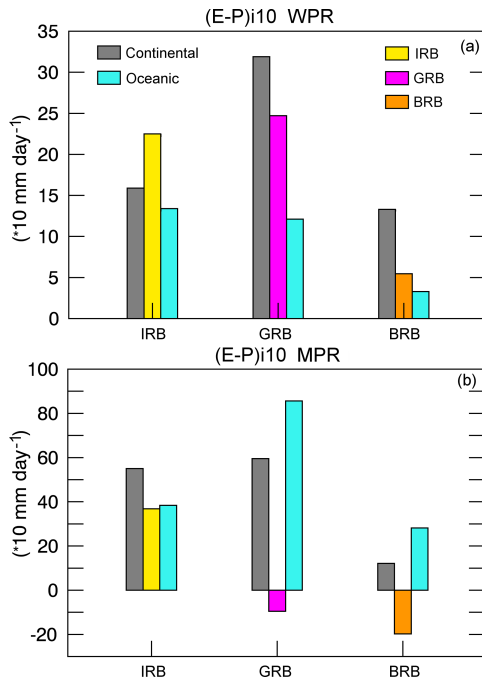


**Figure 5.** Total budget of  $(E - P)$  integrated over 10 days in air masses tracked backward in time from the basins, over continental sources, oceanic sources, and the basins themselves. For the WPR (November–April) and the MPR (May–October) in the period 1981–2015.

The budget of  $(E - P)i10$  was also obtained from the moisture sources delimited by  $p90$  for the MPR (Fig. 5b). In this period, as was previously discussed, the moisture sources are mostly larger, like those that occur in the Indian Ocean or western Asia (Fig. 3), and this could be reflected in the budget of  $(E - P)i10$ . Like in the WPR, the atmospheric moisture budget is positive but greater over continental than oceanic sources and the IRB itself, which confirms the results of Fig. 2 which shows that PET is greater than  $P$  over this basin in the entire year. These results indicate the increase of freshwater inputs to the basins due to continental evaporation (or recycling of moisture advected to the continents from remote regions). According to van der Ent et al. (2010), the continental evaporation recycling ratio is overall very high in Eurasia, which confirms that almost all of the continental evaporation returns to the continent, which can be seen from 50 to 100 %, especially over China, which depends on its water resources almost entirely from terrestrial evaporation from the Eurasian continent. These findings confirm our results. The  $(E - P)i10$  values in the air masses, tracked backward in time from the GRB and BRB, reveal a negative budget over GRB and BRB themselves (greatest for the BRB), which reflects that they act as an average moisture sink for humidity on air masses residing over them. In our approach, the resulting positive (negative) values of the moisture budget indicate moisture uptake,  $E > P$  (for sinks,

$E < P$ ); however, as we do the interpretation of the water balance and not the single evaporation or precipitation values, it could increase both  $E$  and  $P$  but one more than the other. Indeed, in this season, the  $P$  exceeds the PET in both the GRB and BRB (Fig. 2b and c). In contrast, over the other terrestrial and oceanic sources of these basins, the budget is positive, which highlights the major amount of moisture uptake over the oceanic sources. Applying the water accounting model described by van der Ent et al. (2010) and van der Ent and Savenije (2011), Nikoli et al. (2012) also found that among the nine global river basins studied on an annual scale, the Indus River basin shows the highest increase in evaporation, but due to the land-use change, the Ganges–Brahmaputra shows the highest precipitation increase (of continental origin).

### 3.3.2 Moisture contribution to precipitation $((E - P) < 0)$

The moisture contribution  $((E - P) < 0)$  from the sources to precipitation over the basins was obtained in a forward analysis over 10 days with FLEXPART. The percentage of moisture contribution from the IRB moisture sources (defined in Fig. 5) and the IRB itself appears in Fig. 6a. In both periods the WPR and the MPR, the IRB itself, the IO, and WA are the most important sources of moisture. The IR is also an important source for this basin in the WPR. In Fig. 6a it can be seen that the percentage of moisture supplied from continental sources represents a major percentage in both periods under study, although, in the MPR, the IO (38 %) is the second most important source after the IRB itself (42 %). To summarize these results, we calculated the seasonal average of  $|(E - P)i10 < 0|$  from all of the continental and oceanic sources. To understand these averages it must be noted that basin’s areas are not spatially of the same size; they were calculated at  $1^\circ$  in longitude and latitude.

The results confirm that terrestrial sources and overall the IRB itself can be responsible for the largest average moisture input to this basin (Fig. 6b). This result may seem erroneous because of the very well-known role of the Indian Ocean as a source of moisture for the Indian monsoon. However, it must be understood that the moisture transported from the Indian Ocean contributes to precipitation processes throughout Asia, and once it precipitates, it can evaporate and precipitate over the region and become the recycling that is fundamental to understanding this process. Karim and Veizer (2002) revealed that evapotranspiration is the major route for the loss of water from the IRB. As well as this, as river discharges fall short of reaching the sea during certain periods of the year, it is considered a closed basin (Molle et al., 2010). Thus, this increases the important role of evapotranspiration of natural vegetation and crops across the basin.

The same analysis performed in the air masses tracked forward in time from the GRB reveals that continental sources are the most important during the WPR for this basin, and

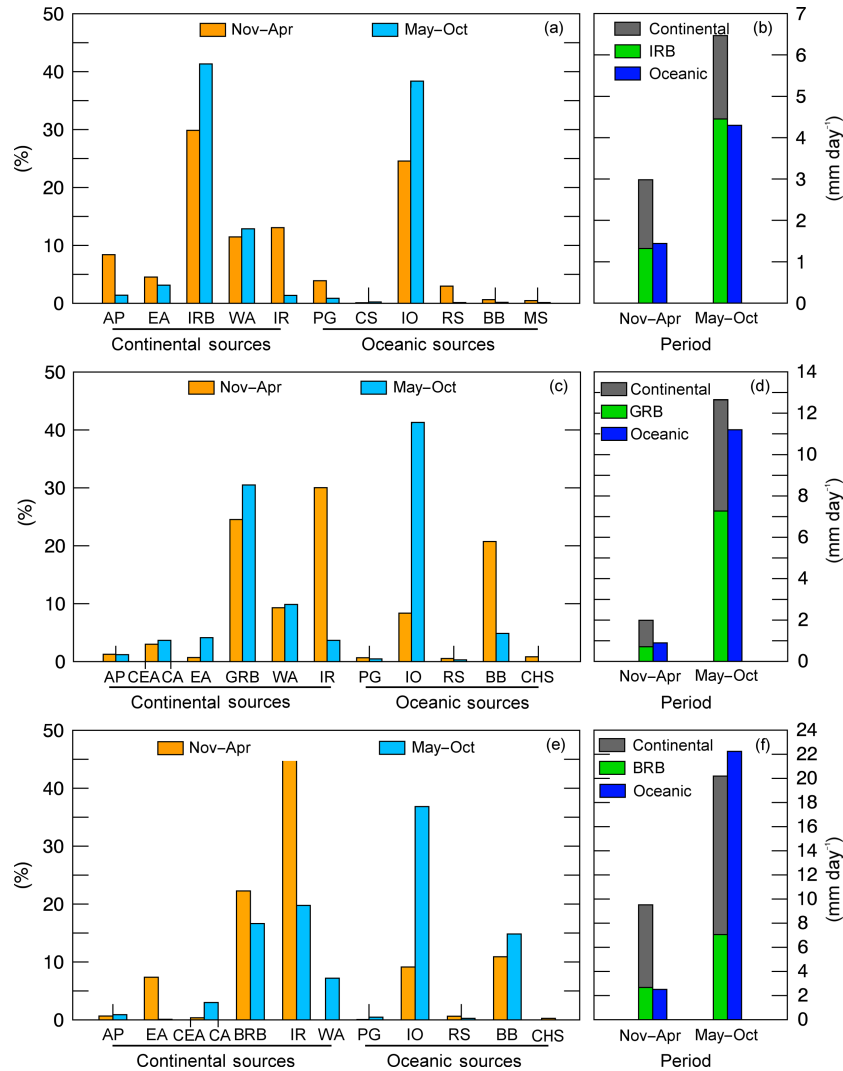


**Figure 6.** (Left panels) The percentage of moisture contributions ( $|(E - P)_{i10} < 0|$ ) from the moisture sources to the IRB (a), GRB (c), and BRB (e) during November–April (WPR) (orange bars) and May–October (MPR) (blue bars) (right panels). The average moisture contribution from continental sources (grey bars), the IRB (b), GRB (d), BRB (f) (green bars), and oceanic sources (dark blue bars).

among these, the most important are the IR, GRB, and the WA (Fig. 6c). Among the oceanic sources, the most important in this season are the BB and IO. In the MPR, the IO provides more than the 40 % of the total atmospheric moisture influx to the GRB, which is followed by the GRB itself (32 %). The average moisture loss (contributing to precipitation) over the GRB in the WPR from continental sources is greater than oceanic (Fig. 6d) sources and the MPR; however, in both periods, the moisture contribution from the oceanic sources is greater than those occurring over the GRB in air masses residing over itself. Indeed, the GRB is responsible for less than  $1 \text{ mm day}^{-1}$  of moisture loss over itself in the WPR. In the MPR, the average contribution from all of the continental sources (including the GRB) is  $12.8 \text{ mm day}^{-1}$ , whereas from the oceanic sources, the contributions are less at approximately  $11 \text{ mm day}^{-1}$ . As the monsoon progresses

through India, enhanced soil moisture and vegetation cover lead to increased evapotranspiration and recycled precipitation, which makes it possible for north-eastern India to have the highest recycling ratio (approximately 25 %) (Pathak et al., 2014). Specifically, within the Ganges basin, the fraction of evaporation that ends up as precipitation is approximately 50–60 % according to Tuinenburg et al. (2012).

For the Brahmaputra basin, the most important moisture sources in the WPR are the IR and the BRB itself, BB and IO. In this period, the moisture supply from the IR to the BRB represents the 48 % of the total moisture loss and this indicates that local moisture recycling must be favoured in this period (Fig. 6e). Indeed, it is shown in Fig. 6e that continental sources are responsible for a major percentage of the moisture loss over the BRB in the WPR. Overall, for the MPR, the IO is the most important moisture source and is responsible

for approximately 37% of the total moisture loss over BRB. The BB is the second most important oceanic source while the rest of the oceanic sources are minimally important (even the CHS, which only appears in this season). The IR, BRB, and WA are among the continental moisture sources that are the most important in this period. An average of the total moisture loss over the BRB, calculated as the contribution from oceanic and land-based moisture sources and including the BRB, appears in Fig. 6f. In the WPR, the major role of the continental regions as moisture sources for the BRB is clear, but in May–October, the average  $|(E - P)_{10 < 0}|$  is greater in air masses arriving at the basin from the oceanic sources ( $\sim 22 \text{ mm day}^{-1}$ ). Nevertheless, there is not much difference from that computed in air masses with the continental origin.

Gimeno et al. (2010) observed that the Red Sea source provides vast amounts of moisture that precipitate between the Gulf of Guinea and the region of China and India in June–August. As well as this, Pathack et al. (2017) noted that a significant fraction of atmospheric moisture to the ISM rainfall comes from five main moisture sources: the western Indian Ocean, central Indian Ocean, upper Indian Ocean, Ganges basin, and Red Sea and its neighbouring gulf. In agreement with the previous findings, we obtained that the Red Sea and the Persian Gulf act as sources of moisture for the Indus, Ganges, and Brahmaputra river basins. Nevertheless, in our analysis we considered them separated (unlike Pathack et al., 2017), obtaining a negligible role from each one to the total moisture contribution mainly for the GRB and BRB in both the WPR and MPR.

It may be confusing that the total contribution to precipitation from continental sources is a little greater than from ocean sources for the IRB and GRB in the MPR (Fig. 6b, d), contrary to the results of Pathack et al. (2017) for the Indian region (which mostly comprises the GRB). Differences may arise because the method is used to calculate the moisture contribution, even when both are based on a Lagrangian approach. In particular, Pathack et al. (2017) implemented an extension of the Dynamic Recycling Model (DRM) developed by Domínguez et al. (2006) and modified by Martínez and Domínguez (2014). Their method permit quantification of the relative contributions from different sources to the atmospheric moisture over a given sink region, by calculating the fraction of atmospheric moisture collected by an air column along its trajectory between times considering the evaporation and the precipitable water, respectively, along the two-dimensional trajectory. With the aim of clarifying this, we calculated the climatological daily accumulated anomalies of moisture contribution from the sources (from FLEXPART) and the precipitation over them (from CHIRPS) along with the MPR, which is of utmost importance because of the monsoon influence. This analysis on a daily scale permits an understanding of the temporal relationship variability between the contribution of moisture from the sources to the precipitation (rapid increase & decrease) over the basins within the MPR.

For the IRB, the minimum rainfall-accumulated anomalies occur on 23 June (Fig. 7a), and from this date onwards the rainfall-accumulated anomalies are increased until 9 September. At the beginning of June, the moisture supply to this basin was enhanced first by IO and later by WA and the IRB itself. The accumulated anomalies on the contribution by the rest of the continental and oceanic sources occur after the abrupt rainfall increase over the basin and do not represent great changes to the amount of humidity according to low anomalies (Fig. 7a and b). Before the maximum accumulated anomaly of precipitation (on 9 September), it is possible to observe a decay of accumulated anomalies of  $|(E - P)_{10 < 0}|$  values from the basin itself after the second half of August. A decrease of anomalies in the WA's contribution starts less abruptly and a few days before the decay of the rainfall anomalies. From the beginning of the second half of August, the accumulated anomalies of moisture supply from the IO to the IRB starts to decrease; however, an abrupt decay is not clearly seen after it occurs for the precipitation.

Accumulated anomalies on the moisture contribution from the IO to the GRB during the first days of June reach the minimum value and then immediately increase rapidly (before the contribution from the rest of the sources); later, on June 15, the minimum value of rainfall-accumulated anomalies occurs over the basin (Fig. 7c). In fact, from the rest of oceanic sources, these values are mostly positive during all of the MPR and do not surpass  $50 \text{ mm day}^{-1}$ . At the beginning of the second half of August, the accumulated anomalies from the IO reach almost  $500 \text{ mm day}^{-1}$ , which confirms the huge amount of moisture transported from this source to the GRB. A day later, as previously commented, the precipitation anomaly falls and reflects a time response between moisture input to the basin from the IO and a rainfall decrease over it. These results show that the most significant amount of moisture to the GRB first comes from the IO, and the results of Fig. 6d must be explained by the moisture recycling process over the continental sources of the GRB and/or a minor residence time of the water vapour over the continent, which influences the budget of  $(E - P)$ . Among the continental sources, the accumulated anomalies of the contribution of moisture from the basin itself at the beginning showed a similar cycle to the precipitation-accumulated anomalies, but later reach maximum values in the middle of August, days before 16 September, when the rainfall actually reaches this point. From the rest of the continental sources, the annual cycle of accumulated anomalies reflects less similarity than the rainfall. These results confirm that although the total moisture input to the GRB during the MPR is greater from continental sources than from oceanic (Fig. 6d), the IO plays a crucial primary role in the hydrological cycle for the monsoonal precipitation onset over this basin, in agreement with Pathack et al. (2014, 2017), who highlight the key role of the IO on the ISM and the role of land surface processes in the generation of precipitation within the Indian sub-continent.

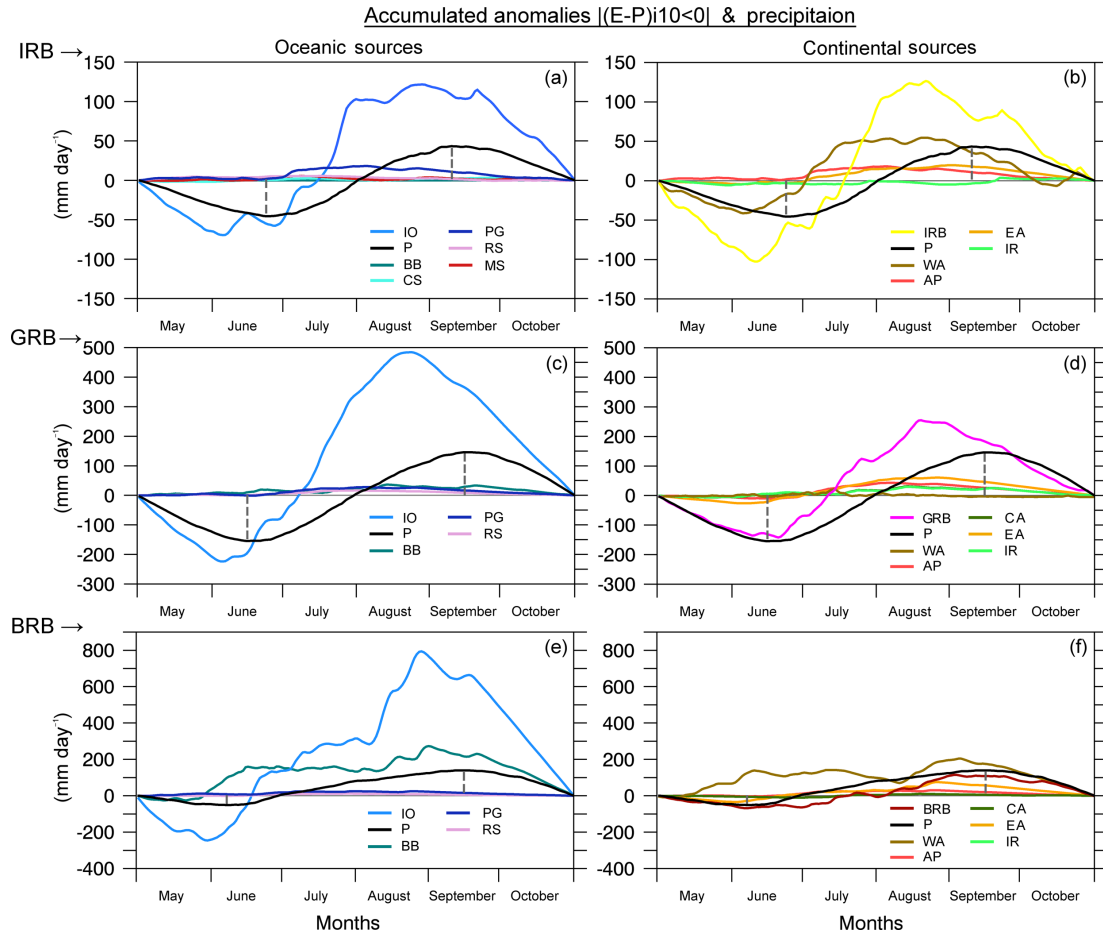


**Figure 7.** Daily accumulated anomalies of  $|(E - P)i_{10} < 0|$  values computed over each basin on air masses forward in time and tracked from the oceanic sources (left panels), continental sources (right panels) (the colour of the lines are in accordance with the name of the sources in Fig. 5), and precipitation (red line) from CHIRPS.

Over the BRB, the seasonal accumulated anomaly of rainfall reaches a minimum on 7 June (Fig. 7e). However, before this date and around mid-May minimum values also occur in the accumulated anomalies of the moisture contribution from the BB and later at the end of May from the IO. After this, the moisture supply starts to increase from these. Before the rainfall decay on 13 September (1 day after maximum rainfall-accumulated anomalies), the moisture contribution decreases first from the IO and later from the BB towards the end of August. Both sources (as was discussed) are the main oceanic moisture sources for the BRB. From the continental sources of accumulated anomalies, the majority follow the accumulated anomaly of precipitation except for the moisture input from WA, which is positive after the first days of May. Nevertheless, this region is not the most important continental source of moisture for the BRB.

Correlations were calculated between the total  $|(E - P)i_{10} < 0|$  values computed from all of the sources and separately for the  $P$  and PET in the basins for the WPR and MPR. Significant  $r$  values only appear in Fig. 8. As expected, con-

sidering the annual cycle of the  $P$  and PET at the basins, we obtained positive correlations between  $|(E - P)i_{10} < 0|$  and  $P$  and negative correlations for  $|(E - P)i_{10} < 0|$  and PET. For the IRB in the WPR, the best positive correlations ( $r > 0.60$ ) are for the moisture input to the basin from the IO with precipitation, followed by significant  $r$  values also obtained with the contribution from the RS, PG, AP, and the IRB itself. The moisture loss over the IRB is oppositely correlated with PET in this basin, and only the moisture supply from the BB is not significantly correlated with the PET. In the MPR, the only positive significant correlations were obtained for the precipitation and the moisture influx from EA, IRB itself, IR, and IO. For the monsoon season, no correlation was significant between PET and  $|(E - P)i_{10} < 0|$ , which indicates that there is not a statistically direct relationship during the MPR.

The correlations for the WPR and MPR in the GRB were expressed like that for the IRB and showed positive (negative) and statistically significant correlations for  $P$  and  $|(E - P)i_{10} < 0|$  (PET and  $|(E - P)i_{10} < 0|$ ). In the WPR,

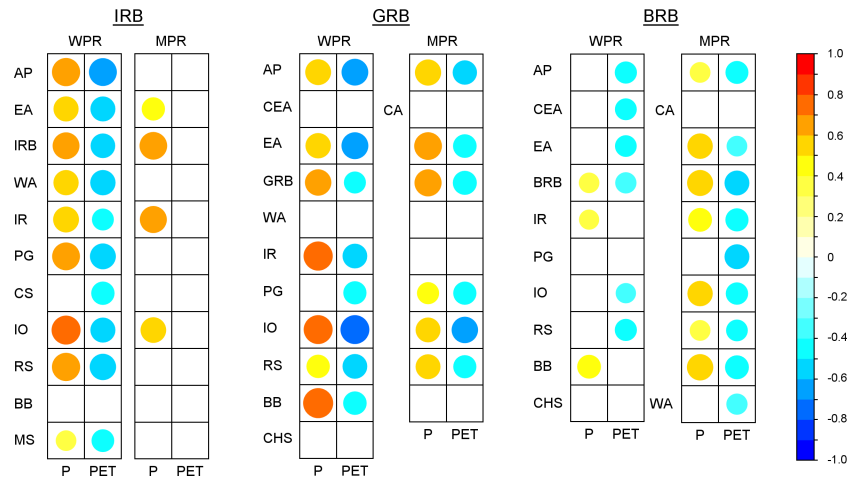


**Figure 8.** Monthly correlations (statistically significant at  $p < 0.05$ ) for the WPR (November–April) and MPR (May–October) periods between precipitation and potential evapotranspiration ( $P$ ,  $PET$ ; from CRU) with total (summed average contributions from all the sources)  $|(E - P)i10 < 0|$  over each basin (from FLEXPART).

the positive feedback occurred for the series from the IO, BB, and IR with  $P$ , while the greatest negative correlations are for the IO, EA, and AP with  $PET$ . Some correlations are not significant: for example, for the moisture contribution from the CHS, WA, and CEA in WPR and from BB, IR, WA, and CA in the MPR. For the BRB, the analysis showed a contrast from the previous findings and few low and significant correlations for the moisture contribution from the BB, IR, and the basin itself with the precipitation over this basin in the WPR. The  $PET$  and  $|(E - P)i10 < 0|$  correlations were negative for most of the cases in this period. In the monsoonal period, as seen in Fig. 8, the  $r$  values indicate the best correlation of both  $P$  and  $PET$  with  $|(E - P)i10 < 0|$  from the basin itself and from the BB and IO, which are the two most important oceanic sources for the BRB.

A climatological analysis of the North American monsoon system (NAMS) precipitation recycling reveals a positive feedback mechanism between monsoon precipitation and a subsequent increase in the precipitation of a recycled origin (Domínguez et al., 2008). For the wettest NAMS monsoons, Bosilovich et al. (2003) documented that the evaporation and soil wetness time series tends to track similarly to the precipitation. In the Gangetic Plain and north-eastern India, a significant amount of precipitation also comes from precipitation recycling (Pathak et al., 2014). For example, for the GRB and at the initial phase of the monsoon, the Indian Ocean is a strong moisture source and the subsequent recharge of soil moisture makes the evapotranspiration over the Ganges basin become active after the onset of the monsoon (Pathak et al., 2017). Despite these results, we found negative correlations between the moisture contribution to the basins and the  $PET$  on them, which suggests the need for a monthly analysis to determine whether or not it occurs on a minor or major temporal scale.

### 3.4 Variability of $(E - P)$ during the SAM onset and the demise over the basins

We calculated the budget of  $(E - P)i10$  in air masses tracked backward in time from each basin at days  $-1$ ,  $-4$ ,  $-7$ , and  $-10$  before the rainfall increase (decrease) associated with the SAM onset (demise) over the IRB, GRB, and BRB. To determine the onset and demise dates, we applied an objective index from Noska and Misra (2016) for the basins, which is based on the cumulative anomalies of averaged daily rainfall (see Eqs. 4 and 5). To illustrate the method, Fig. 9 shows the daily average precipitation from CHIRPS (Chris et al., 2015) over the GRB in 2010 and the cumulative anomalies. The cumulative anomalies reached the minimum value on 15 June and the maximum on 22 September. For this year, the rainfall associated with the monsoon onset occurred on 16 June and ends on 22 September over the GRB. Observation indicates that the daily precipitation rate changes occur abruptly for the onset and demise, which agrees with similar findings for different regions across the Indian region and South East Asia (e.g. Ananthakrishnan and Soman, 1988; Soman and Kumar, 1993; Cook and Buckley, 2009).

By applying Eqs. (4) and (5), it was possible to obtain the onset and demise dates of precipitation associated with the monsoonal influence for every year. These dates are represented in Fig. 10 and it is possible to observe that rainfall associated with the SAM onset starts first at the BRB (commonly in May), later the GRB (commonly in June), and finally at the IRB (commonly in June, and some cases in July) (Fig. 10a). In contrast, the precipitation decline because of the SAM demise occurs first over the IRB, followed by the GRB and the BRB (Fig. 10b), which indicates that the length of the monsoonal rainy season at the IRB is shorter than over the GRB and both were shorter than over the BRB. This re-

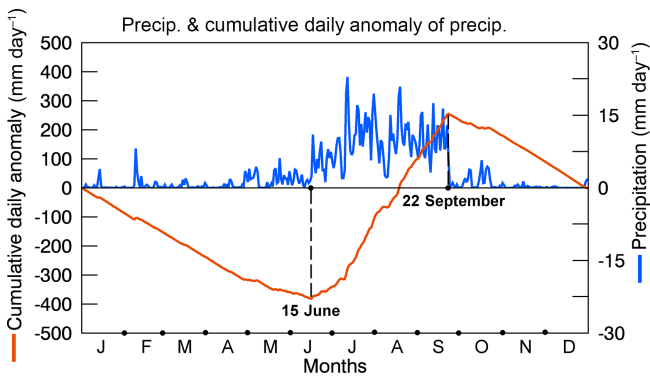


**Figure 9.** Daily precipitation (blue line) and the cumulative daily anomaly of the precipitation (orange line) (from CHIRPS) over the GRB during 2010. 15 June (22 September) represents the minimum (maximum) cumulative daily anomaly of the precipitation.

veals that from the east to the west the onset of monsoon rainfall takes longer to occur. A climatology of the length of the summer monsoon season (in days) obtained by Misra and DiNapoli (2014) also reflects that over the region of the BRB the number of days between the onset and demise is greater than in regions to the west (where the GRB and IRB are located) and where the length decreases longitudinally. Similar onset and retreat dates were obtained by Hasson et al. (2016) but utilizing a distinct method on a CMIP5 climate model's data for observational and future periods.

A composite of the days for the monsoonal rainfall onset and demise over each basin was performed. Utilizing each composite, the budget of  $(E - P)$  for days  $-1$ ,  $-4$ ,  $-7$ , and  $-10$  was calculated before the onset and demise; this way, it was possible to determine the spatial changes of moisture uptake by air masses in travel to the basins. One day backward in time from the onset at the IRB, air masses uptake humidity over the basin itself and the surrounding regions (Fig. 11). At day  $-4$ , air masses arriving at the IRB uptake humidity from the western Indian Ocean, the Arabian Sea, the Persian Gulf, the continental regions to the west of the basin and the basin itself. Over the north-eastern Arabian Sea, a remarkable change from conditions of pre-monsoon onset days was also described by Howland and Sikdar (1983) when the specific humidity increased as much as  $5 \text{ g kg}^{-1}$  from pre-monsoon to monsoon onset. At days  $-7$  and  $-10$ , the pattern of  $(E - P)$  is more extended with positive values (moisture uptake) mainly to the west of the basin, part of the Arabian Sea and the western Indian Ocean. Particles arrive at the IRB losing humidity from over the south and South East Asia and the Bay of Bengal.

Analysing the  $(E - P)$  pattern for the pre-demise, at day  $-1$  it is very similar to the same day before the onset; however, in the centre and north-east of the basin appear  $(E - P) < 0$  areas, which indicates the prevalence of moisture loss. At day  $-4$ , areas with  $(E - P) > 0$  seem to occupy less than on day  $-4$  of the pre-onset, whereas more parcels arrive

at the basin after losing humidity (according to the greater spatial extension of areas of  $(E - P) < 0$ ). At days  $-7$  and  $-10$  of the pre-demise, the main differences on the  $(E - P)$  pattern (with respect to the same days for the pre-onset) are over the basin, and greater  $(E - P) > 0$  values are apparent over the Arabian Sea at day  $-10$  where moisture uptake is major for the pre-demise. This is because days before the demise there should be major precipitation and consequently greater moisture uptake for the basin.

One day backward in time from the monsoonal rainfall onset over the GRB, the air masses over this basin gain humidity almost over the entire basin itself, but to the east is a moisture sink, which in contrast covers practically the entire basin at day  $-1$  from the rainfall demise of this basin. At day  $-4$  from the onset and on the budget of  $(E - P)$ , the positive values are very intense for mainly those over the basin itself, to the west of the basin, over India, the Arabian Sea, and part of the Bay of Bengal. For the days before the onset, the positive values in the field of  $(E - P)$  are more restricted in the northern part of the Arabian Sea, which suggests this region plays a key role in the monsoonal rainfall onset but also the demise over the GRB. The negative values (moisture sink) are more intense to the east of the GRB before the demise (as expected). For the pattern of  $(E - P)$  at days  $-7$  and  $-10$  from the onset, the WA and IO play as crucial role in providing humidity to this basin, and their sources contribute for the same dates before the demise; however, the eastern part of the basin (on average) behaves as a moisture sink and  $(E - P) > 0$  values are more restricted to the north of the budget pattern.

For the GRB, the results of the backward experiment highlight that at day  $-1$  from the onset this basin acts as a moisture sink for the region as a whole. On this day, the  $(E - P)$  reveals that air parcels arrive at the basin and gain humidity just from a small region to the south-west of the basin. The pattern is very similar at day  $-1$  from the demise but  $(E - P) > 0$  values are not located to the north-east of the basin. These results are not surprising since, from the Fig. 2 results, we understand that for the MPR the water balance over the BRB suggests that  $P$  exceeds  $E$  in the budget. At day  $-4$  of the onset, the basin uptake humidity from the west, the Indian region, and the western part of the Bay of Bengal is visually noticeable. However, the  $(E - P)$  pattern completely changed for the day  $-4$  from the demise, which shows that air masses arrive at the BRB and gain and transport moisture from the west and north of the basin and from the small regions in the north-eastern Arabian Sea and the Bay of Bengal. Furthermore, moisture loss prevails in air masses travelling to the BRB from the south and when remaining over itself. At days  $-7$  and  $-10$ , the spatial pattern of  $(E - P)$  is quite similar for the pre-onset and pre-demise with the most remarkable difference over the south-east of Asia, the Bay of Bengal, and the BRB itself due to the moisture loss prevalence.

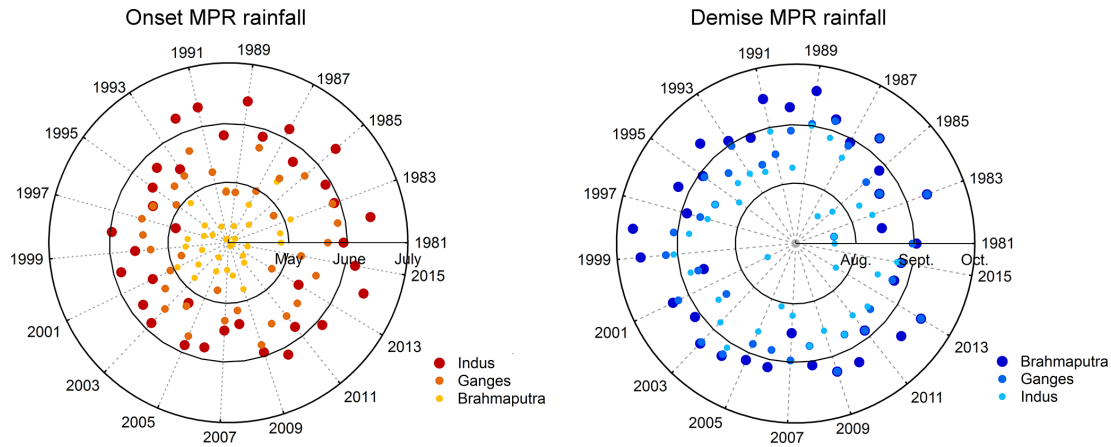


**Figure 10.** Onset and demise of the monsoonal rainfall for the Indus, Ganges, and Brahmaputra river basins.

### 3.5 Moisture contribution during the dry and wet conditions in the basins

The SPEI was utilized to identify dry and wet conditions at the IRB, GRB, and BRB. The temporal evolution of this index on the temporal scale of 6 months is shown in Fig. 12. We identify dry conditions at the IRB from 1998 to 2002 and increasing wet conditions from 2011 to 2015. A drought-intensive period in Pakistan was identified by Xie et al. (2013) for the late 1990s to early 2000s, in agreement with our results. Pakistan is mostly located within the IRB, and hence, the hydrological condition of the basin regulated those of the country. In the GRB during the 2000–2010 decade, dry conditions were very frequent, whereas in the BRB dry conditions mainly occurred in 1981–1986, 2003–2010, and 2012–2015 (Fig. 12). Kumar et al. (2013) documented that short-term drought (SPEI6) over the Indian region is characterized by strong periodicity on quasi-biennial (2–4 years) and decadal (12–16 year) timescales.

We use the 6-month SPEI at the end of October (April) to diagnose dry and wet conditions at the basins over the MPR (WPR) season. We selected those seasons under severe and extremely dry and wet conditions according to SPEI6 values (Tables 1 and 2), and the anomalies on the moisture contribution ( $| (E - P) i 10 < 0 |$ ) from each moisture source to the basins were calculated by creating composites of the WPR and MPR affected by severe and extremely dry and wet conditions. The SPEI6 was also utilized for the same purposes by Drumond et al. (2016) to investigate drought episodes in the climatological sinks of the Mediterranean moisture source.

Common dry WPR occurred at the IRB and BRB in 2001 and at the GRB and the BRB in 1999. According to SPEI > 1.5 values, severe and extreme wet WPR seasons occurred at the IRB in 2015 and 1983 (Table 1). In 2015, it was also severely wet in the GRB (as well as in 1982) and extremely so in 1998, whereas at the BRB, just two seasons were classified as severely wet (2007 and 2010). In the period from

**Table 1.** WPR under severe and extremely dry and wet conditions at the Indus, Ganges, and Brahmaputra river basins during the period from 1981 to 2015.

Dry		IRB		GRB		BRB	
Date	SPEI-6	Date	SPEI-6	Date	SPEI-6	Date	SPEI-6
April 2001	-1.64	April 1999	-1.55	April 2001	-1.72		
		April 2009	-2.25	April 2014	-1.88		
				April 1999	-1.88		
Wet							
April 2015	1.51	April 1982	1.78	April 2007	1.69		
April 1983	2.0	April 2015	1.89	April 2010	1.92		
		April 1998	2.0				

1981 to 2015, there were three severely dry MPR periods at the IRB and also three for the GRB, but one of them was extremely dry (2014) (Table 2). For the BRB, despite being the wettest basin, four MPR are characterized under severely dry conditions and of these, the WPR of 2005 accounted for both the GRB and the BRB. During the wettest MPR periods (Table 2), the greatest number of cases occurred at the GRB as well, and all were severely wet (like the two periods in the BRB), whereas at the IRB, of the two wet periods only one was extremely wet in 2010.

The moisture contribution negative anomalies for the WPR dry composites at the IRB are evidence of the major deficit in the moisture supply from the IR, the IRB itself, and the IO (Fig. 13a, orange bars); the same sources are responsible for greatest positive moisture loss anomalies for the wettest WPR (Fig. 13a, green bars). For the MPR, the anomalies in the moisture input to the IRB during dry periods occur mainly from two sources, the IO and the own IRB. This indicates that during the monsoonal season under dry conditions, as it rains less over the basin it will not favour the precipitation over itself but could for remote regions. For the wettest MPR, the opposite occurs.

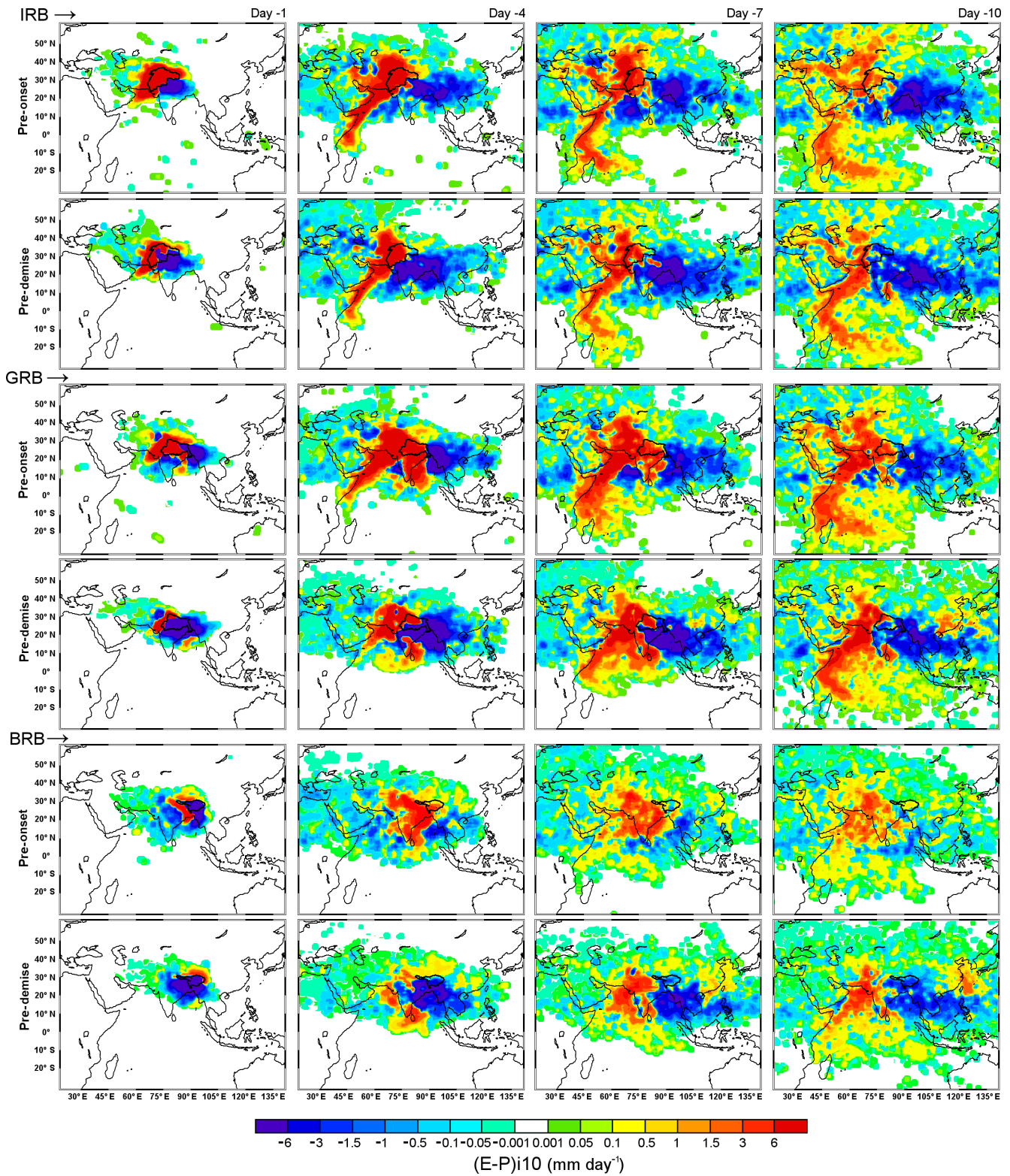


**Figure 11.** Composite of  $(E - P)$  in a backward experiment from the IRB for a composite of days  $-1$ ,  $-4$ ,  $-7$ , and  $-10$  from the onset and demise of the monsoon.

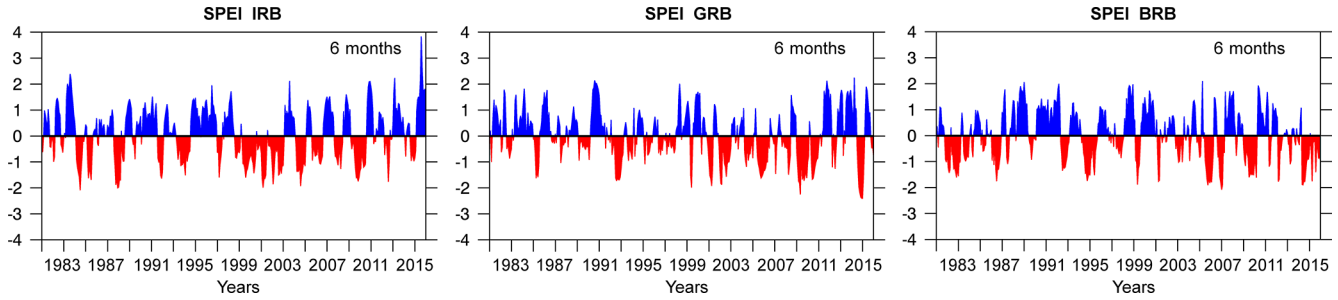


**Figure 12.** Monthly SPEI for a timescale of 6 months averaged for the Indus, the Ganges, and Brahmaputra river basins in the period from 1981 to 2015.

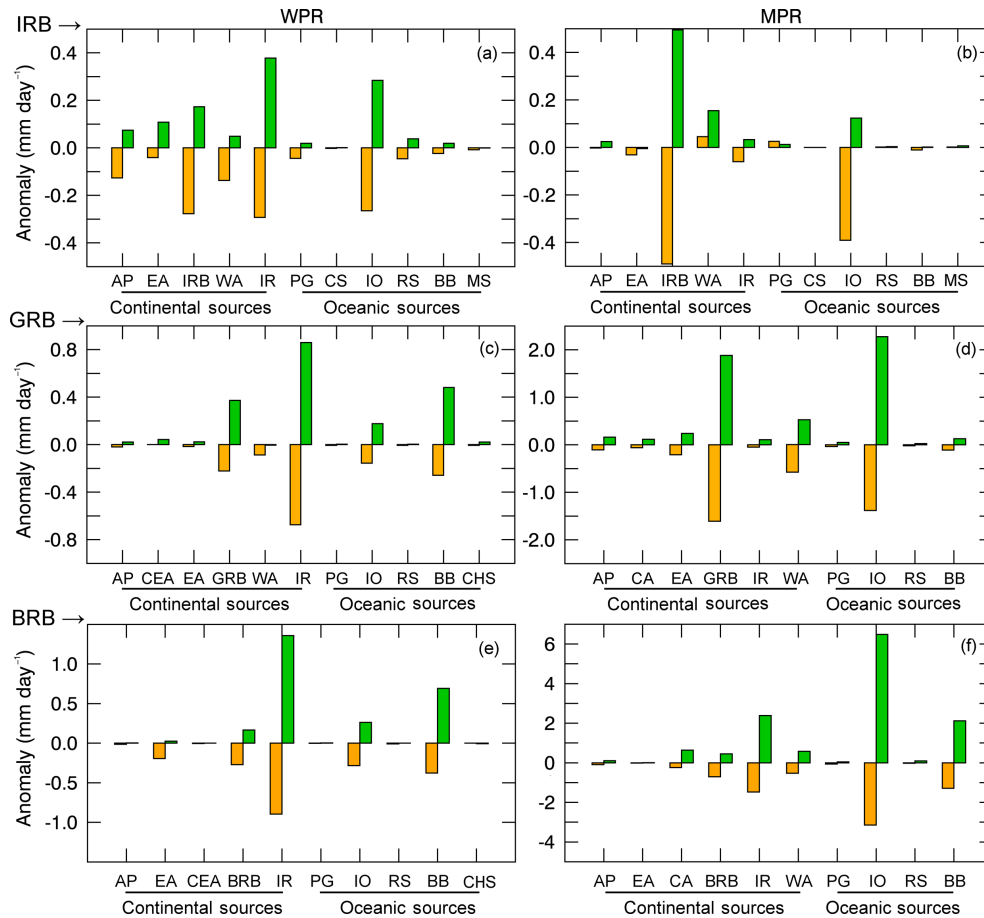


**Figure 13.** Anomalies of the moisture contribution ( $|(E - P)_{i10} < 0|$ ) from each source to the IRB, GRB, and BRB during severe and extremely dry and wet condition at the basins (orange and green bars, respectively) from the period of 1981–2015.

In the GRB, the driest WPRs are associated with negative anomalies of moisture supply mainly from two continental moisture sources, IR and the basin itself, and two oceanic sources, BB and IO (Fig. 13c, orange bars). The same sources are responsible for positive anomalies during the wettest WPRs (green bars). This means that during the WPR months, severely and extremely dry and wet conditions are regulated in the GRB by anomalies of the moisture supply from the surrounding land regions (mainly to the south

over India), the Bay of Bengal and less from the IO and the GRB itself. For MPR, the greatest negative anomalies of the  $|(E - P)_{i10} < 0|$  values over the GRB in the composite of the dry conditions occur in air masses arriving at the basin from itself, the IO, and WA, whereas for wettest periods the highest positive anomalies are on the moisture inputs to the GRB from the same sources: the IO, followed by the GRB itself and WA. These anomalies allow confirmation that the wettest periods in the GRB are related to an increase of the moisture

**Table 2.** MPR under severe and extremely dry and wet conditions at the Indus, Ganges, and Brahmaputra river basins during the period from 1981 to 2015.

Dry		IRB		GRB		BRB	
Date	SPEI-6	Date	SPEI-6	Date	SPEI-6	Date	SPEI-6
October 1991	-1.51	October 2005	-1.56	October 1994	-1.58		
October 1987	-1.62	October 1992	-1.68	October 2006	-1.60		
October 2009	-1.74	October 2014	-2.35	October 2005	-1.60		
				October 1982	-1.61		
Wet							
October 2015	1.75	October 1999	1.62	October 1998	1.56		
October 2010	2.08	October 2013	1.65	October 1988	1.72		
		October 2011	1.83				
		October 1990	1.92				

supply from the IO, and the local contribution is surely enhanced because of moisture recycling, which is a mechanism well explained for the GRB by Tuinenburg et al. (2012).

In the BRB during the WPR as well as for the GRB, the IR, BB, IO, and the basin itself are the regions from where a reduction of moisture supply to the BRB drastically occurs during the driest November–April periods (Fig. 13e, orange bars) and the moisture supply increases during the wettest periods (green bars). In the MPR, the IO becomes the source from which the atmospheric transport that contributes to precipitation over the BRB experiment shows the highest reduction during the driest periods ( $< 3 \text{ mm day}^{-1}$ ) (Fig. 13f, orange bar) and the maximum increase for the wettest periods ( $> 6 \text{ mm day}^{-1}$ ) (Fig. 13f, green bar). The BB is the second most important oceanic source in terms of the anomalies, whereas the IR is the most important among the terrestrial sources. For almost all of the cases when dry (wet) conditions occur at the basins, negative (positive) anomalies occur for the moisture contribution to precipitation, which is generally from all of the sources over the basins. As precipitation depends on the amount of water vapour in the atmosphere, the most important anomalies in the contribution from these sources highlight the main aspects responsible for drought and intense precipitation over the basins.

#### 4 Conclusions

The 3-dimensional model FLEXPART was used to track backward in time the air masses residing over the IRB, GRB, and BRB. The model permitted the calculation of the budget of evaporation minus precipitation ( $E - P$ ) along backward and forward trajectories integrated over 10 days and allowed the identification of the climatological moisture sources of each basin for the westerly precipitation regime (November–April) and monsoonal precipitation regime (May–October) over 35 years (1981–2015). The results indicate that moisture sources are positioned in continental and oceanic regions as well as the basins themselves. Their spatial extension increases during the MPR (when the rainfall is highest

over the basins) and principally in the Indian Ocean. Along each trajectory, the budget of ( $E - P$ ) over most evaporative continental and oceanic sources was calculated, which revealed the importance of moisture uptake for the basins over continental regions during the WPR. A forward analysis performed from the sources revealed the important role of continental regions on the average moisture contribution to precipitation over the IRB and GRB during the MPR and during which the oceanic sources are the most important for the BRB. However, during the MPR, the greatest moisture contribution to precipitation over the basins occurs from the IO, except for the IRB, where local moisture losses in ( $E - P$ ) play a dominant role. Additionally, the IO seems to be responsible for first providing moisture to the basins in the MPR period and is linked to the rapid rainfall increase or decrease. Generally, the most important moisture sources for the IRB, GRB, and BRB are the western Asia extension, the Indian region, the Indian Ocean, the Bay of Bengal and the basins themselves. A spatial analysis of the resulting ( $E - P$ ) pattern in the pre-onset and pre-demise of the monsoonal precipitation over each basin exposed the spatial differences mainly on the moisture uptake variability and confirmed the spatial reduction mainly of the evaporative source in the IO days before the demise.

As expected, the average moisture (summed ( $E - P$ )  $< 0$  from all the sources) loss over the basins' values integrated over 10 days is positively correlated with the precipitation and negatively correlated with the potential evapotranspiration even during the MPR, when some studies suggest that both variables increase. The roles of the sources in the moisture contribution to precipitation during severe and extremely dry and wet conditions at the basins were assessed through WPR and MPR composites, and confirmed the crucial role of those most important moisture sources (eg. IR, IO, BB, and the basins themselves) in providing less (more) humidity during dry (wet) conditions in both periods WPR and MPR. Even though the hydrological cycle over the Asian region has been widely investigated, the results obtained here will also support further climate research, but specifically over the IRB, GRB, and BRB. Future research would be an important contribution to investigating the influence of the modes of climate variability, principally ENSO, on the modulation of moisture transport from the sources of moisture to the basins.

*Data availability.* The ERA-Interim datasets are freely available at <https://www.ecmwf.int/> (Dee et al., 2011). The precipitation and potential evapotranspiration data from CRU TS v3.24.01 (Harris et al., 2014) can be downloaded at <http://www.cru.uea.ac.uk/data>. The daily precipitation data from CHIRPS are available from <http://chg.geog.ucsb.edu/data/chirps/> (Chris et al., 2015). The model FLEXPART (Stohl and James, 2004, 2005) can be freely downloaded (<https://www.flexpart.eu/>) and utilized. For FLEXPART results, please contact Raquel Nieto ([rnieto@uvigo.es](mailto:rnieto@uvigo.es)).

*Competing interests.* The authors declare that they have no conflict of interest.

*Special issue statement.* This article is part of the special issue “The changing water cycle of the Indo-Gangetic Plain”. It is not associated with a conference.

*Acknowledgements.* This work was supported by EPhysLab (UVIGO-CSIC associated unit). Rogert Sorí would like to acknowledge the grant received by the Xunta of Galicia, Spain, in support of his doctoral research work. Raquel Nieto acknowledges the support provided by CNPq grant 314734/2014-7 from the Brazilian government. Anita Drumond acknowledges the support of the Spanish Government and FEDER via the SETH (CGL2014-60849-JIN) project. The authors thank the Water Works 2014 co-funded call of the European Commission, which financed the IMDROFLOOD project. This research was partially supported by Xunta de Galicia under project ED413C 2017/64 “Programa de Consolidación y Estructuración de Unidades de Investigación Competitivas (Grupos de Referencia Competitiva)” co-funded by European Regional Development Fund (FEDER).

Edited by: Pradeep P. Mujumdar

Reviewed by: Vasu Misra and one anonymous referee

## References

- Ananthakrishnan, R. and Soman, M. K.: The onset of the southwest monsoon over Kerala: 1901–1980, *J. Climatol.*, 8, 283–296, 1988.
- Berrisford, P., Källberg, P., Kobayashi, S., Dee, D., Uppala, S., Simmons, A. J., Poli, P., and Sato, H.: Atmospheric conservation properties in ERA-Interim, *Q. J. Roy. Meteor. Soc.*, 137, 1381–1399, <https://doi.org/10.1002/qj.864>, 2011.
- Bisselink, B. and Dolman, A. J.: Precipitation Recycling: Moisture Sources over Europe using ERA-40 Data, *J. Hydrometeorol.*, 9, 1073–1083, <https://doi.org/10.1175/2008JHM962.1>, 2008.
- Bosilovich, M. G., Sud, Y. C., Schubert, S. D., and Walker, G. K.: Numerical simulation of the large-scale North American monsoon water sources, *J. Geophys. Res.*, 108, 8614, <https://doi.org/10.1029/2002JD003095>, 2003.
- Castillo, R., Nieto, R., Drumond, A., and Gimeno, L.: Estimating the Temporal Domain when the Discount of the Net Evaporation Term Affects the Resulting Net Precipitation Pattern in the Moisture Budget Using a 3-D Lagrangian Approach, *PLoS ONE*, 9, e99046, <https://doi.org/10.1371/journal.pone.0099046>, 2014.
- Ceglar, A., Toreti, A., Balsamo, G., and Kobayashi, S.: Precipitation over Monsoon Asia: A Comparison of Reanalyses and Observations, *J. Climate*, 17, 465–476, 2017.
- Cheema, M. J. M.: Understanding water resources conditions in data scarce river basins using intelligent pixel information, Case: Transboundary Indus Basin, PhD thesis, TU Delft, University Delft, the Netherlands, 209 pp., 2012.
- Chen, B., Xu, X.-D., Yang, S., and Zhang, W.: On the origin and destination of atmospheric moisture and air mass over the Tibetan Plateau, *Theor. Appl. Climatol.*, 110, 423–435, <https://doi.org/10.1007/s00704-012-0641-y>, 2012.
- Chris, F., Peterson, P., Landsfeld, M., Pedreros, D., Verdin, J., Shukla, S., Husak, G., Rowland, J., Harrison, L., Hoell, A., and Michaelsen, J.: The climate hazards infrared precipitation with stations – a new environmental record for monitoring extremes, *Scientific Data* 2, 150066, <https://doi.org/10.1038/sdata.2015.66>, 2015 (data available at: <http://chg.geog.ucsb.edu/data/chirps>, last access: 1 May 2017).
- COLA: The Center for Ocean-Land-Atmosphere Studies, available at: <http://cola.gmu.edu/wcr/river/basins.html>, last access: 2 February 2017.
- Cook, B. I. and Buckley, B. M.: Objective determination of monsoon season onset, withdrawal, and length, *J. Geophys. Res.*, 114, D23109, <https://doi.org/10.1029/2009JD012795>, 2009.
- Davis, T.: Agricultural water use and river basin conservation, A World Wide Fund For Nature (WWF) Summary Report, 2003.
- Dee, D. P., et al.: The ERA-Interim reanalysis: Configuration and performance of the data assimilation system, *Q. J. Roy. Meteor. Soc.*, 137, 553–597, <https://doi.org/10.1002/qj.828>, 2011 (data available at: <https://www.ecmwf.int/>, last access: 1 May 2017).
- Dhar, O. N. and Nandargi, S.: A study of floods in the Brahmaputra basin in India, *Int. J. Climatol.*, 20, 771–781, 2000.
- Dimri, A. P., Niyogi, D., Barros, A. P., Ridley, J., Mohanty, U. C., Yasunari, T., and Sikka, D. R.: Western Disturbances: A review, *Rev. Geophys.*, 53, 225–246, <https://doi.org/10.1002/2014RG000460>, 2015.
- Domínguez, F., Kumar, P., Liang, X.-Z., and Ting, M.: Impact of atmospheric moisture storage on precipitation recycling, *J. Climate*, 19, 1513–1530, <https://doi.org/10.1175/JCLI3691.1>, 2006.
- Domínguez, F., Kumar, P., and Vivoni, E. R.: Precipitation Recycling Variability and Ecoclimatological Stability – A Study Using NARR Data. Part II: North American Monsoon Region, *J. Climate*, 5187–5203, <https://doi.org/10.1175/2008JCLI1760.1>, 2008.
- Drumond, A., Nieto, R., and Gimeno, L.: Sources of moisture for China and their variations during drier and wetter conditions in 2000–2004: a Lagrangian approach, *Clim. Res.*, 50, 215–225, <https://doi.org/10.3354/cr01043>, 2011.
- Drumond, A., Marengo, J., Ambrizzi, T., Nieto, R., Moreira, L., and Gimeno, L.: The role of the Amazon Basin moisture in the atmospheric branch of the hydrological cycle: a Lagrangian analysis, *Hydrol. Earth Syst. Sci.*, 18, 2577–2598, <https://doi.org/10.5194/hess-18-2577-2014>, 2014.
- Drumond, A., Gimeno, L., Nieto, R., Trigo, R. M., and Vicente-Serrano, S. M.: Drought episodes in the climatological sinks of the Mediterranean moisture source: The role of moisture transport, *Global Planet. Change*, 151, 4–14, <https://doi.org/10.1016/j.gloplacha.2016.12.004>, 2016.
- Durán-Quesada, A. M., Gimeno, L., Amador, J. A., and Nieto, R.: Moisture sources for Central America: Identification of moisture sources using a Lagrangian analysis technique, *J. Geophys. Res.*, 115, D05103, <https://doi.org/10.1029/2009JD012455>, 2010.
- Eltahir, E. A. B. and Bras, R. L.: Precipitation recycling, *Rev. Geophys.*, 34, 367–378, <https://doi.org/10.1029/96RG01927>, 1996.
- Gadgil, S.: The Indian Monsoon and its variability, *Annu. Rev. Earth Planet. Sci.*, 31, 429–467, <https://doi.org/10.1146/annurev.earth.31.100901.141251>, 2003.

- Gimeno, L.: Grand challenges in atmospheric science, *Front. Earth Sci.*, 1, 1–5, <https://doi.org/10.3389/feart.2013.00001>, 2014.
- Gimeno, L., Drumond, A., Nieto, R., Trigo, R. M., and Stohl, A.: On the origin of continental precipitation, *Geophys. Res. Lett.*, 37, L13804, <https://doi.org/10.1029/2010GL043712>, 2010.
- Gimeno, L., Stohl, A., Trigo, R. M., Dominguez, F., Yoshimura, K., Yu, L., Drumond, A., Durán-Quesada, A. M., and Nieto, R.: Oceanic and terrestrial sources of continental precipitation, *Rev. Geophys.*, 50, RG4003, <https://doi.org/10.1029/2012RG000389>, 2012.
- Gong, C. and Eltahir, E. A. B.: Sources of Moisture for Rainfall in West Africa, *Water Resour. Res.*, 32, 3115–3121, 1996.
- Harris, I., Jones, P. D., Osborn, T. J., and Lister, D. H.: Updated high-resolution grids of monthly climatic observations – the CRU TS3.10 Dataset, *Int. J. Climatol.*, 34, 623–642, <https://doi.org/10.1002/joc.3711>, 2014 (data available at: <http://www.cru.uea.ac.uk/data>, last access: 1 May 2017).
- Hasson, S., Lucarini, V., and Pascale, S.: Hydrological cycle over South and Southeast Asian river basins as simulated by PCMDI/CMIP3 experiments, *Earth Syst. Dynam.*, 4, 199–217, <https://doi.org/10.5194/esd-4-199-2013>, 2013.
- Hasson, S., Lucarini, V., Pascale, S., and Böhner, J.: Seasonality of the hydrological cycle in major South and Southeast Asian river basins as simulated by PCMDI/CMIP3 experiments, *Earth Syst. Dynam.*, 5, 67–87, <https://doi.org/10.5194/esd-5-67-2014>, 2014.
- Hasson, S., Pascale, S., Lucarini, V., and Böhner, J.: Seasonal cycle of Precipitation over Major River Basins in South and Southeast Asia: A Review of the CMIP5 climate models data for present climate and future climate projections, *Atmos. Res.*, 180, 42–63, 2016.
- Hossen, M. A.: The Ganges Basin management and community empowerment, Bandung: *Journal of the Global South*, 2, 14, <https://doi.org/10.1186/s40728-014-0005-3>, 2015.
- Howland, M. R. and Sikdar, D. N.: The moisture budget over the Northeastern Arabian Sea during Premonsoon and Monsoon onset, 1979, *Mon. Weather Rev.*, 11, 2255–2268, 1983.
- Huang, Y. and Cui, X.: Moisture sources of an extreme precipitation event in Sichuan, China, based on the Lagrangian method, *Atmos. Sci. Lett.*, 16, 177–183, <https://doi.org/10.1002/asl2.562>, 2015.
- Immerzeel, W. W. and Bierkens, M. F. P.: Seasonal prediction of monsoon rainfall in three Asian river basins: the importance of snow cover on the Tibetan Plateau, *Int. J. Climatol.*, 30, 1835–1842, 2010.
- Janowiak, J. E. and Xie, P.: A Global-Scale Examination of Monsoon-Related Precipitation, *J. Climate*, 16, 4121–4133, 2003.
- Jian, J., Webster, P. J., and Hoyos, C. D.: Large-scale controls on Ganges and Brahmaputra river discharge on intraseasonal and seasonal time-scales, *Q. J. Roy. Meteor. Soc.*, 135, 353–370, <https://doi.org/10.1002/qj.384>, 2009.
- Karim, A. and Veizer, J.: Water balance of the Indus River Basin and moisture source in the Karakoram and western Himalayas: Implications from hydrogen and oxygen isotopes in river water, *J. Geophys. Res.*, 107, 4362, <https://doi.org/10.1029/2000JD000253>, 2002.
- Katerji, N. and Rana, G.: Crop Reference Evapotranspiration: A Discussion of the Concept, Analysis of the Process and Validation, *Water Resour. Manag.*, 25, 1581–1600, 2011.
- Kumar, K. N., Rajeevan, M., Pai, D. S., Srivastava, A. K., and Preethi, B.: On the observed variability of monsoon droughts over India, *Weather and Climate Extremes*, 1, 42–50, 2013.
- Laghari, A. N., Vanham, D., and Rauch, W.: The Indus basin in the framework of current and future water resources management, *Hydrol. Earth Syst. Sci.*, 16, 1063–1083, <https://doi.org/10.5194/hess-16-1063-2012>, 2012.
- Lehner, B., Verdin, K., and Jarvis, A.: New global hydrography derived from spaceborne elevation data, *Eos, Transactions, AGU*, 89, 93–94, 2008.
- Levine, R. C. and Turner, A. G.: Dependence of Indian monsoon rainfall on moisture fluxes across the Arabian Sea and the impact of coupled model sea surface temperature biases, *Clim. Dynam.*, 38, 2167–2190, <https://doi.org/10.1007/s00382-011-1096-z>, 2012.
- Liebmann, B., Carmargo, S. J., Seth, A., Marengo, J. A., Carvalho, L. M. V., Allured, D., Fu, R., and Vera, C. S.: Onset and end of the rainy season in South America in observations and the ECHAM 4.5 atmospheric general circulation model, *J. Climate*, 20, 2037–2050, 2007.
- Lorenz, C. and Kunstmann, H.: The hydrological cycle in three state-of-the-art reanalyses: Intercomparison and performance analysis, *J. Hydrometeorol.*, 13, 1397–1420, 2012.
- Mahanta, C., Zaman, A. M., Newaz, S. M. S., Rahman, S. M. M., Mazumdar, T. K., Choudhury, R., Borah, P. J., and Saikia, L.: Physical Assessment of the Brahmaputra River, International Union for Conservation of Nature (IUCN), Dhaka, Bangladesh, ISBN-13: 978-984-91041-8-6, 2014.
- Marathayil, D., Turner, A. G., Shaffrey, L. C., and Levine, R. C.: Systematic wintersea-surface temperature biases in the northern Arabian Sea in HiGEM and the CMIP3 models, *Environ. Res. Lett.*, 8, 014028, <https://doi.org/10.1088/1748-9326/8/1/014028>, 2013.
- Martinez, J. A. and Dominguez, F.: Sources of atmospheric moisture for the La Plata River basin, *J. Climate*, 27, 6737–6753, <https://doi.org/10.1175/JCLI-D-14-00022.1>, 2014.
- McKee, T. B., Doesken, N. J., and Kliest, J.: The relationship of drought frequency and duration to time scales, *Proceedings of the 8th Conference on Applied Climatology*, 17–22 January, Anaheim, CA, American Meteorological Society, Boston, MA, 179–184, 1993.
- McVicar, T. R., Michael, L. R., Donohue, R. J., Li, L. T., Van Niel, T. G., Thomas, A., Grieser, J., Jhajharia, D., Himri, Y., Mahowald, N. M., Mescherskayai, A. V., Krugerj, A. C., Rehman, S., and Dinpashoh, Y.: Global review and synthesis of trends in observed terrestrial near-surface wind speeds: Implications for evaporation, *J. Hydrol.*, 416–417, 182–205, 2012.
- Misra, V. and DiNapoli, S.: The variability of the South-east Asian summer monsoon, *Int. J. Climatol.*, 34, 893–901, <https://doi.org/10.1002/joc.3735>, 2014.
- Misra, V., Pantina, P., Chan, S. C., and DiNapoli, S.: A comparative study of the Indian summer monsoon hydroclimate and its variations in three reanalyses, *Clim. Dynam.*, 39, 1149, <https://doi.org/10.1007/s00382-012-1319-y>, 2012.
- Molle, F., Wester, P., and Hirsch, P.: River basin closure: Processes, implications and responses, *Agr. Water Manage.*, 97, 569–577, <https://doi.org/10.1016/j.agwat.2009.01.004>, 2010.

- Nieto, R., Gimeno, L., and Trigo, R. M.: A Lagrangian identification of major sources of Sahel moisture, *Geophys. Res. Lett.*, 33, 1–6, 2006.
- Nikoli, R., van der Ent, R. J., Savenije, H. H. G., Hoff, H., and Waha, K.: Moisture recycling and the effect of land-use change, Master Thesis, TU Delft University, the Netherlands, 2012.
- Noska, R. and Misra, V.: Characterizing the onset and demise of the Indian summer monsoon, *Geophys. Res. Lett.*, 43, 4547–4554, <https://doi.org/10.1002/2016GL068409>, 2016.
- Numaguti, A.: Origin and recycling processes of precipitating water over the Eurasian continent: Experiments using an atmospheric general circulation model, *J. Geophys. Res.*, 104, 1957–1972, 1999.
- Ordoñez, P., Ribera, P., Gallego, D., and Peña-Ortiz, C.: Major moisture sources for Western and Southern India and their role on synoptic-scale rainfall events, *Hydrol. Process.*, 26, 3886–3895, <https://doi.org/10.1002/hyp.8455>, 2012.
- Pathak, A., Ghosh, S., and Kumar, P.: Precipitation recycling in the Indian subcontinent during summer monsoon, *J. Hydrometeorol.*, 15, 2050–2066, <https://doi.org/10.1175/JHM-D-13-0172.1>, 2014.
- Pathak, A., Ghosh, S., Martínez, J. A., Domínguez, F., and Kumar, P.: Role of Oceanic and Land Moisture Sources and Transport in the Seasonal and Interannual Variability of Summer Monsoon in India, *J. Climate*, 30, 1839–1859, <https://doi.org/10.1175/JCLI-D-16-0156.1>, 2017.
- Peixoto, J. P. and Oort, A. H.: *Physics of Climate*, New York, Springer-Verlag New York Press, United States, 1992.
- Qiao, Y., Wu, R., Huang, W., and Jian, M.: Interannual variability of moisture source over southern Indian Ocean during boreal summer and its relationship with local SST, *Int. J. Climatol.*, 33, 556–567, <https://doi.org/10.1002/joc.3445>, 2013.
- Qureshi, M. T.: Water Management in the Indus Basin in Pakistan: Challenges and Opportunities, *Mt. Res. Dev.*, 31, 252–260, 2011.
- Rajagopalan, B. and Molnar, P.: Signatures of Tibetan Plateau heating on Indian summer monsoon rainfall variability, *J. Geophys. Res.-Atmos.*, 118, 1170–1178, <https://doi.org/10.1002/jgrd.50124>, 2013.
- Ramage, C. S.: *Monsoon Meteorology*. Academic Press, New York and London, 296 pp., 1971.
- Rasul, G.: Water for growth and development in the Ganges, Brahmaputra, and Meghna basins: an economic perspective, *International Journal of River Basin Management*, 13, 387–400, <https://doi.org/10.1080/15715124.2015.1012518>, 2015.
- Sebastian, D. E., Pathak, A., and Ghosh, S.: Use of Atmospheric Budget to Reduce Uncertainty in Estimated Water Availability over South Asia from Different Reanalyses, *Sci. Rep.*, 6, 29664, <https://doi.org/10.1038/srep29664>, 2016.
- Slingo, J.: The Indian summer monsoon and its variability, in: *Beyond El Niño: Decadal Variability in the Climate System*, edited by: Navarra, A., Springer-Verlag, 103–118, 1999.
- Soman M. K. and Kumar, M. K.: Space-time evolution of Meteorological Features-associated with the onset of Indian summer monsoon, *Mon. Weather Rev.*, 121, 1177–1194, 1993.
- Song, J.-H., Kang, H.-S., Byun, Y.-H., and Hong, S.-Y.: Effects of the Tibetan Plateau on the Asian summer monsoon: a numerical case study using a regional climate model, *Int. J. Climatol.*, 30, 743–759, <https://doi.org/10.1002/joc.1906>, 2010.
- Stohl, A. and James, P.: A Lagrangian analysis of the atmospheric branch of the global water cycle. Part I: Method description, validation, and demonstration for the August 2002 flooding in central Europe, *J. Hydrometeorol.*, 5, 656–678, [https://doi.org/10.1175/1525-7541\(2004\)005<0656:ALAOA>2.0.CO;2](https://doi.org/10.1175/1525-7541(2004)005<0656:ALAOA>2.0.CO;2), 2004.
- Stohl, A. and James, P.: A Lagrangian analysis of the atmospheric branch of the global water cycle. Part II: Moisture transports between the Earth's ocean basins and river catchments, *J. Hydrometeorol.*, 6, 961–984, <https://doi.org/10.1175/JHM470.1>, 2005.
- Taniguchi, K. and Koike, T.: Comparison of definitions of Indian summer monsoon onset: Better representation of rapid transitions of atmospheric conditions, *Geophys. Res. Lett.*, 33, L02709, <https://doi.org/10.1029/2005GL024526>, 2006.
- Tare, V., Roy, G., and Bose, P.: *Ganga River Basin Management Plan*. Main document, Indian Institutes of Technology of Bombay, Delhi, Guwahati, Kanpur, Kharagpur, Madras, Roorkee, 2015.
- Trenberth, K. E.: Atmospheric Moisture Recycling: Role of Advection and Local Evaporation, *J. Climate*, 12, 1368–1380, 1999.
- Tuinenburg, O. A., Hutjes, R. W. A., and Kabat, P.: The fate of evaporated water from the Ganges basin, *J. Geophys. Res.*, 117, D01107, <https://doi.org/10.1029/2011JD016221>, 2012.
- van der Ent, R. J. and Savenije, H. H. G.: Length and time scales of atmospheric moisture recycling, *Atmos. Chem. Phys.*, 11, 1853–1863, <https://doi.org/10.5194/acp-11-1853-2011>, 2011.
- van der Ent, R. J., Savenije, H. H. G., Schaeffli, B., and Steele-Dunne, S. C.: Origin and fate of atmospheric moisture over continents, *Water Resour. Res.*, 46, 1–12, <https://doi.org/10.1029/2010WR009127>, 2010.
- Vicente-Serrano, S. M., Berguería, S., and López-Moreno, J. I.: A Multiscalar Drought Index Sensitive to Global Warming: The Standardized Precipitation Evapotranspiration Index, *J. Climate*, 23, 1696–1718, <https://doi.org/10.1175/2009JCLI2909.1>, 2010.
- Webster, P. J.: The coupled monsoon system, in: *The Asian Monsoon*, edited by: Mason, J., Springer-Verlag Berlin Heidelberg, New York, USA, 3–66, [https://doi.org/10.1007/3-540-37722-0\\_1](https://doi.org/10.1007/3-540-37722-0_1), 2006.
- Xie, H., Ringler, C., Zhu, T., and Waqas, A.: Droughts in Pakistan: a spatiotemporal variability analysis using the Standardized Precipitation Index, *Water Int.*, 38, 620–631, <https://doi.org/10.1080/02508060.2013.827889>, 2013.
- Yanai, M. and Wu, G.: Effects of the Tibetan plateau, in: *The Asian Monsoon*, edited by: Wang, B., Springer Berlin Heidelberg, 514–549, 2006.
- Yatagai, A., Arakawa, O., Kamiguchi, K., Kawamoto, H., Nodzu, M. I., and Hamada, A.: A 44-year daily precipitation dataset for Asia based on dense network of rain gauges, *SOLA*, 5, 137–140, <https://doi.org/10.2151/sola.2009-035>, 2009.
- Yoon, J.-H. and Huang, W.-R.: Indian Monsoon Depression: Climatology and Variability, in: *Modern Climatology*, edited by: Wang, S.-Y., InTech, 45–73, 2012.
- Zeng, X. and Lu, E.: Globally Unified Monsoon Onset and Retreat Indexes, *J. Climate*, 17, 2241–2248, 2004.

Article

# The Atmospheric Branch of the Hydrological Cycle over the Negro and Madeira River Basins in the Amazon Region

Rogert Sorí <sup>1,\*</sup>, José A. Marengo <sup>2</sup> , Raquel Nieto <sup>1</sup> , Anita Drumond <sup>1</sup>  and Luis Gimeno <sup>1</sup>

<sup>1</sup> Environmental Physics Laboratory (EPhysLab), Facultad de Ciencias, Universidade de Vigo, 32004 Ourense, Spain; rnieto@uvigo.es (R.N.); anitadru@uvigo.es (A.D.); l.gimeno@uvigo.es (L.G.)

<sup>2</sup> National Center for Monitoring and Early Warning of Natural Disasters (CEMADEN), São José dos Campos, São Paulo 12247-016, Brazil; jose.marengo@cemaden.gov.br

\* Correspondence: rogert.sori@uvigo.es; Tel.: +34-988-387-208

Received: 6 May 2018; Accepted: 2 June 2018; Published: 5 June 2018



**Abstract:** The Amazon region, in South America, contains the largest rainforest and biodiversity in the world, and plays an important role in the regional and global hydrological cycle. In the present study, we identified the main sources of moisture of two subbasins of the Amazon River Basin, the Negro and Madeira River Basins respectively. The source-sink relationships of atmospheric moisture are investigated. The analysis is performed for the period from 1980–2016. The results confirm two main oceanic moisture sources for both basins, i.e., oceanic regions in the Tropical North and South Atlantic oceans. On the continents are, the Negro River Basin itself, and nearby regions to the northeast. For the Madeira River Basin, the most important continental sources are itself, and surrounding regions of the South American continent. Forward-trajectory analysis of air masses over the source regions is used to compute the moisture contribution to precipitation over basins. Oceanic (continental) sources play the most important role in the Negro River Basin (Madeira River Basin). The moisture contribution from the Tropical North Atlantic region modulates the onset and demise of the rainy season in the Negro River Basin; while the moisture contribution from the rest of the Amazon River Basin, the Madeira Basin itself, and Tropical South America leads to the onset of the rainy season in the Madeira River Basin. These regions also played the most important role in decreasing the moisture supply during most severe dry episodes in both basins. During “El Niño”, generally occurs a reduction (increase) of the moisture contribution to the Negro River Basin (Madeira River Basin; mainly from April to August) from almost all the sources, causing a decrease in the precipitation. Generally, the contrary occurs during “La Niña”.

**Keywords:** hydrological cycle; sources of moisture; moisture transport; precipitation; water level; dry episodes; Negro River Basin; Madeira River Basin

## 1. Introduction

The Amazon River Basin (ARB) (Figure 1) hosts the world’s largest tropical rainforest and drainage basin on the planet. It is an important source of natural resources for human economic development and is characterised by large biodiversity. Its drainage area includes more than one-third of the South American continent and the discharge of the Amazon River (AR) accounts for almost one-fifth of the total discharge of all rivers of the world [1]. The ARB contains several subbasins. The most important subbasins are the Negro and Madeira River basins (NRB, MRB; Figure 1) in the north and southwest, respectively. The Negro and Madeira Rivers (NR and MR respectively) are the most important Amazonas tributaries, contributing more than one-third of the total water discharge [1]. Consequently, the ARB plays an important role in the local and regional hydrological cycle [2–4].

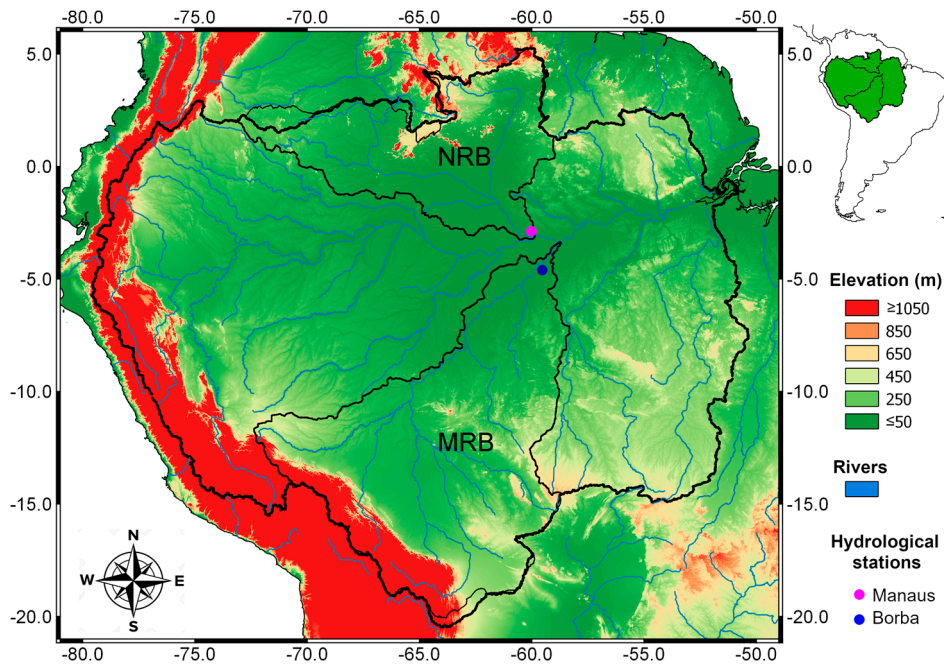


**Figure 1.** The black contour lines delimit the geographical locations of the Amazon River basin (ARB) and two subbasins, that is, the Negro River Basin (NRB) and Madeira River Basin (MRB) in the north and southwest of the ARB, respectively. Green and reddish colours indicate the ground elevation (m), while the blue lines represent the rivers. The pink (dark blue) circle indicates the location of the hydrological station of Manaus (Borba).

The basic principle of the hydrological cycle is that evaporation in one region contributes to precipitation in that region or in another region through atmospheric moisture transport. Several authors have investigated the origin of the Amazon's rainfall using different methods to finally highlight the important role of the Tropical North and South Atlantic regions (TNA and TSA, respectively), as sources of moisture [3,5–10]. The role of the ARB providing humidity for itself and surrounded regions has been also documented. The continental moisture recycling, the process by which evapotranspiration from the continent returns as precipitation to the continent [11–14], is particularly important for the South American hydrological cycle. Between 25% and 35% of the moisture is regionally recycled in the ARB [15]. However, in northern Amazon regions, the continental evaporation recycling efficiencies are higher than in the south [16,17]. The moisture from the ARB is transported out of the basin via the South American low-level jet (SALLJ) along the Andes during the austral wet season, and contributes to precipitation over the La Plata Basin [3,4,14,18–23]. In fact, the moisture transport in and out of the ARB has been studied since the 1990s using different methods, that is, a variety of upper-air and global reanalysis datasets, observations, and climate model simulations [2]. In the present climate, the ARB behaves as a moisture sink, which receives moisture from sources, such as the tropical rainforest, by intense recycling from vegetation [2,15,24] and by moisture advection over the tropical North and South Atlantic oceans [2,3,25–29]. Based on van der Ent et al. [13], 70% of the water resources of the Río de la Plata Basin depend on evaporation over the Amazon forest. They also indicated that the decrease of evaporation in areas in which continental evaporation recycling is high (e.g., by land use change for agriculture and urbanization) would enhance droughts in downwind areas with overall low precipitation amounts. This might result in the reduction of the regional moisture supply and have important consequences for the stability of the Amazon rainforest [30–33]. Therefore, the acceleration of human-driven climate change raises serious questions and poses challenges for conservation strategies in the Amazonian forest of the ARB [34]. Deforestation and land use change within the ARB are major challenges [35].

Business-as-usual deforestation (based on deforestation rates prior to 2004) would lead to an  $8.1\% \pm 1.4\%$  reduction in the annual mean ARB rainfall by 2050, which is greater than the natural variability [36]. Future scenarios of complete deforestation in the region indicate a restrained water cycle [37,38]; the total deforestation of the Amazon would result in a 10%–20% decrease of the annual rainfall in the entire ARB [37].

The annual cycle of the water balance within the ARB is characterised by differences between the northern and southern sections [6,18,39]. The evaporation–precipitation budget ( $E - P$ ) of the entire region shows that the precipitation generally exceeds evaporation and the basin acts as a moisture sink ( $P > E$ ) [18,40]. However, the basin can act as a moisture source ( $P < E$ ) under extreme conditions, such as those related to deficient rainfall during the strong El Niño of 1983 in northern Amazonia [18]. Usually, negative precipitation anomalies over Amazonia occur during intense El Niño events and anomalously cold (warm) sea surface temperatures (SST) in the tropical South Atlantic, coupled with anomalously warm (cold) SST in the tropical North Atlantic [5,6,8,41–43]. The identification of moisture sources has become a major research tool for the analysis of extreme events (e.g., floods and droughts) and a basic tool used for regional and global climate assessment [44]. Recent studies confirmed the occurrence of several extreme hydrological events in the ARB, such as droughts (e.g., 2005, 2010, 2016), floods (2009, 2012, 2014), and notable terrestrial water storage variability [45–49].

The climate of Amazonia is principally affected by seasonal changes of the position of the Intertropical Convergence Zone (ITCZ), which is the main rainfall-producing system in the eastern ARB during the rainy season [50–52]. The South Atlantic Convergence Zone (SACZ), which enhances the convection during the austral summer, is important for rainfall in the southern ARB [53,54]. The life cycle of the South American Monsoon System (SAMS) also plays an important role, featuring strong seasonal variability in the distribution and duration of the rainy season, mainly over southwestern Amazonia and the La Plata Basin [28,55]. The cross-equatorial flux plays an important role for moisture flux changes that ultimately enhance the convection over central–eastern Brazil on intraseasonal timescales, representing an increase in the contribution to the monsoon precipitation from moisture transported from the northern Amazon toward eastern South America [56,57]. An important climatological structure in the upper-tropospheric summertime circulation over South America is the Bolivian High and the accompanying Nordeste trough over the east. The results of a study by Lenters and Cook [58] indicate that these systems are generated in response to precipitation over the ARB, central Andes, and the South Atlantic convergence zone.

A great number of studies have related the rainfall variability over the ARB with the SST changes in the Tropical North and South Atlantic regions (e.g., Marengo [5,6], Marengo et al. [7], Yoon and Zeng [8], Andreoli et al. [59], Espinoza et al. [60], Yoon [61]). Nevertheless, few studies have quantified the moisture contribution from these regions (e.g., Drumond et al. [3], COLA [62]). Usually, the ARB is studied as a whole. However, considering the reported differences of the hydrological cycle between the northern and southern ARB, our aim is to identify the main continental and oceanic moisture sources of the NRB and MRB. Furthermore, we attempt to obtain and assess the impact of their moisture contribution on the onset and demise of the rainy season, during dry episodes, and under warm (El Niño) and cold events (La Niña) of El Niño–Southern Oscillation (ENSO). ENSO is the main driver of interannual climate extremes in Amazonia and other tropical regions [63]. Respect previous studies, our point is to establish a source–sink of atmospheric moisture relationship to further understand some steps of the hydrological cycle in both the NRB and MRB.

## 2. Materials and Methods

### 2.1. The Lagrangian Approach

The global atmosphere was homogeneously divided into finite elements of volume, that is, approximately 2.0 million parcels. The Lagrangian particle dispersion model, FLEXPART (FLEXible PARTicle dispersion model) v9.0 [25,64], was applied to track backward-in-time the air masses over

the NRB and MRB, and to calculate the rate of moisture increase (through evaporation from the environment,  $e$ ) or decrease (through condensation or precipitation,  $p$ ) along the trajectories of the parcels. Based on Equation (1), this budget equals the specific humidity ( $q$ ) changes over time ( $t$ ), assuming a constant parcel mass ( $m$ ). Based on Stohl and James [64], the equation contains a small error because the mass of a particle (thus, the mass of the whole atmosphere) is assumed to be constant. Nevertheless, the atmosphere mass slightly changes through the addition and removal of water. The residence time of water vapour in the atmosphere varies in different regions of the planet. In this work, we considered it to be ten days, as stated by Numaguti [65].

$$(e - p) = m(dq/dt) \quad (1)$$

The total surface freshwater flux during ten days, hereafter represented by  $(E - P)i10$ , was obtained from Equation (2) by integrating the  $(e - p)$  values of all parcels in a vertical column from 0.1 to 1000 hPa over an area  $A$ . The area depends on the resolution of the input data and  $K$  is the number of particles over  $A$ . The values of  $(E - P)$ , summed over the period in which clouds formed and evaporated, were not affected, but separating  $E$  and  $P$  led to the identification of extra precipitation and surface evaporation upon cloud formation and evaporation of cloud droplets, respectively. These errors were reasonably accurate only when one of the two terms was known to be much larger than the other, for instance, when  $P > E$  during rain events [25]. Thus, for our purposes, the determination of the freshwater budget was quite enough. The analysis was performed for the period from 1980–2016.

$$E - P \approx \frac{\sum_{k=1}^k (e - p)}{A} \quad (2)$$

The historical backward-in-time analysis allowed the determination of the main moisture sources for the given receptors. Those regions in which  $(E - P)i10 > 0$ , which indicates that air parcels gain humidity rather than lose it during their movement to the target region, were considered moisture sources. On the contrary, regions in which the  $(E - P)i10$  budget was negative and moisture loss prevailed were considered as moisture sinks. To determine the most important regions in which air masses in transient to the basins uptake humidity, a threshold was defined. This threshold represented the 90th percentile and was calculated from the annual budget,  $(E - P)i10 > 0$ . This criterion has previously been utilised with a similar aim by Drumond et al. [66], Ciric et al. [67], and Sorí et al. [68]. The NRB and MRB were considered moisture sources for themselves to evaluate their role. To assess the moisture contribution of sources to the precipitation over the basins, air masses over each source region were tracked forward-in-time to compute the moisture loss,  $(E - P)i10 < 0$ , over the respective basin.

The model FLEXPART has been widely used to investigate the atmospheric branch of the hydrological cycle in several regions worldwide, for example, to investigate the origin of continental precipitation [69], to identify the major moisture sources for East China [70] and the Sudan-Sahel [71], or to understand the causes of extreme sea ice loss over the Arctic [72]. The main advantage of using this model is the possibility of computing the atmospheric water budget along backward and forward trajectories. To run FLEXPART, we utilised datasets from ERA-Interim reanalysis [73] at 6-h intervals (00:00, 06:00, 12:00, and 18:00 UTC) and a resolution of  $1^\circ$  in longitude and latitude along 61 vertical levels from 0.1 to 1000 hPa. We also used the vertical monthly integral of northward and eastward water vapour flux data from ERA-Interim reanalysis [73] at a resolution of  $1^\circ \times 1^\circ$  to calculate vertically integrated moisture flux (VIMF) divergence anomalies. Several factors were considered for the use of ERA-Interim reanalysis datasets. Significant improvements have been made between ERA-Interim and ERA-40 [74] with respect to the global hydrological cycle, that is, in terms of water vapour, clouds, and precipitation, especially over the oceans. The unrealistic interannual drift of precipitation observed in ERA-40 over the ARB has been reduced in ERA-Interim and the annual precipitation was largely unbiased, although the seasonal amplitude of precipitation remained too small [75]. De-Almeida et al. [76] assessed the ability of three global reanalysis products (NCEP-2,

ERA-Interim, and CFSR-1) to reproduce South American Monsoon (SAMS) precipitation. They found that ERA-Interim provided more consistent results regarding the climatology of precipitation and 850 hPa moisture flux divergence monthly means, both averaged over the SAMS region.

### 2.2. Identification of the Onset and Demise of the Rainy Season

The onset and end of the rainy season in the NRB and MRB can be considered as the beginning and end of the longest period during which the rainfall exceeds its annual climatology [77]. To determine the dates associated with the onset/demise, we applied an objective previously implemented for the ARB by Liebmann et al. [78], for South America by Liebmann et al. [77], and for the Indian Summer Monsoon by Noska and Misra [79]. This method was based on daily cumulative precipitation anomalies ( $C'm$ ) of each basin throughout the year:

$$C'm(i) = \sum_{n=1}^i [Dp(n) - C], \quad (3)$$

$$C = \frac{1}{MN} \sum_{m=1}^M \sum_{n=1}^N Dp(m, n), \quad (4)$$

where  $Dp(m, n)$  is the daily average precipitation over each basin for day  $n$  of year  $m$  and  $C$  is the climatology of the annual mean precipitation over  $N$  (365/366) days for  $M$  years. Therefore, starting in January, the onset date was defined as the day after  $C'm$  reached its absolute minimum value. After this date, a positive slope indicated the rainy season until  $C'm$  reached its absolute maximum value, which was considered to be the demise because it was the point at which the precipitation started to decrease. In this analysis, we used the daily precipitation from the Climate Hazards Group InfraRed Precipitation with Station data (CHIRPS) [80], which has the advantage of incorporating  $0.05^\circ$  resolution satellite imagery with in situ station data. The determination of the onset/demise dates and the length of the rainy season in the Amazon region and South America have already been investigated by different methods [7,77,78,81–85]. However, the method used in our study was sufficient for our purpose. Daily data of the Interpolated Outgoing Longwave Radiation (OLR) [86] freely provided by the NOAA/OAR/ESRL PSD, Boulder, Colorado, USA, from their Web site at <https://www.esrl.noaa.gov/psd/> was used to investigate the response of the convection associated with the  $|E - P|10 < 0|$  anomalies over the basins.

### 2.3. Identification of Dry and Wet Conditions

In this study, we used the Standardised Precipitation–Evapotranspiration Index (SPEI) [87] to identify dry and wet conditions in the NRB and MRB. The SPEI is based on the same methodology as the Standardised Precipitation Index (SPI) [88], but computed the probability distribution of the difference between precipitation ( $P$ ) and Atmospheric Evaporative Demand (AED), which were computed on different time scales. Here, we considered the potential evapotranspiration (PET) to be a reliable approximation of the AED. The  $P$  and PET data with a resolution of  $0.5^\circ \times 0.5^\circ$  belonged to the Climatic Research Unit CRU3.25 [89]. The use of the SPEI is of advantage if we considered the dense forest of the region and its effect on evapotranspiration. Positive SPEI values indicate above-average moisture conditions (wet), while negative values reveal below-normal (dry) conditions. To identify dry episodes, the criterion of Mckee et al. [88] was applied to each basin. Dry episodes started when the SPEI fell below zero, reaching a value of  $-1$  or less, and ended when the SPEI returned to positive values. Several indicators were calculated for such episodes, such as the duration [number of months between the beginning (included) and end (last month, not included)] and severity (absolute value of the sum of all SPEI values during the episode) [90–92]. We considered the parameter ‘severity’ to be an indicator of the possible impact. The most severe five dry episodes were selected to investigate the role of the climatological moisture sources of each basin on the moisture contribution

to precipitation over the basins. Stojanovic et al. [93,94] have performed similar assessments for the Euro Mediterranean region. For each dry episode was also calculated the average pattern of the Vertically Integrated Moisture Flux (VIMF) anomalies from the ERA-Interim [73] to assess dynamical atmospheric conditions. The classification of the SPEI values into categories (Table 1; according to Mckee et al. [88] for the SPI) permitted the association of the magnitude of this index with water deficit conditions in the basins. A correlation analysis was performed between the SPEI at 1 to 24 temporal scales and the water level (WL) of the NR and MR recorded in Manaus and Borba, respectively, to investigate possible relationships. The WL data were provided by the Observatory of Research for the Environment [95].

**Table 1.** Drought classification based on the SPEI.

Drought Category	Range
Non-drought	$0 \leq \text{SPEI}$
Mild drought	$-1.0 < \text{SPEI} < 0$
Moderate drought	$-1.5 < \text{SPEI} \leq -1.0$
Severe drought	$-2.0 < \text{SPEI} \leq -1.5$
Extreme drought	$\text{SPEI} \leq -2.0$

#### 2.4. Moisture Transport during El Niño and La Niña Events

Considering that one of the most significant causes of the climate variability in the tropics is the ENSO, we obtained composites of months affected by the warm (El Niño) and cold (La Niña) events. The  $P$  anomalies over each basin and  $|E - P|/10 < 0|$  anomalies of air masses arriving from each source of moisture were calculated for each composite of months. The El Niño/La Niña conditions were obtained from the Bivariate EnSo Timeseries (BEST ENSO index) [96]. The alternative, less stringent definition that uses the top/bottom 33% events or standard deviation (std) =  $\pm 0.96$  of the BEST values was utilised. This index was chosen because it was obtained by combining an atmospheric component of the ENSO phenomenon (the Southern Oscillation Index 'SOI') with an oceanic component (Nino 3.4 Sea Surface Temperature 'SST' that was defined as the SST averaged over the region  $5^\circ \text{N}$ – $5^\circ \text{S}$  and  $170^\circ \text{W}$ – $120^\circ \text{W}$ ).

### 3. Results and Discussion

#### 3.1. Precipitation, Potential Evapotranspiration, and Annual Water Level Cycles

The monthly average  $P$  patterns within the ARB are shown in Figure 2. It shows the spatial variability of the  $P$  between the north and south of the basin, specifically between the NRB and MRB. During the austral summer from December to March, the maximum  $P$  was observed in the central southeast of the ARB. The  $P$  rate over the MRB was greater than over the NRB during these months. April was a transitional month; the maximum precipitation occurred over the northern half of the ARB, but major rainfall was favoured over the NRB in May and June. Espinoza et al. [97] reported that the maximum  $P$  was concentrated in the northwest of the ARB during four months (July–October), which was consistent with our results. In October, the  $P$  increased over the southeast of the ARB; this phenomenon was best observed in November and December. Marengo [18] investigated the December–January and March–May seasonal rainfall in the ARB derived from different gridded data sources. He considered that these two seasons represented the peak of the rainy season in southern and northern Amazonia, respectively. However, Figure 2 shows that the strongest rainfall was concentrated in northern Amazonia from May to September. The March–May (MAM) maximum and September–November (SON) minimum rainfall close to the Amazon Delta were associated with the seasonal migration of the Intertropical Convergence Zone (ITCZ). Overall, the rainfall regimes over the ARB indicated a strong contrast between the northern and southern tropics, which was due to the alternating warming of each hemisphere [97]. The spatial distribution of various precipitation datasets

(GPCP, GPCC, and HYBAM) averaged for the 1989–2008 period showed similar patterns within the ARB with slight differences in the northwestern ARB, where SO HYBAM datasets presented a larger area with higher precipitation rates [82]. The study results of Geritana et al. [98] also showed that evapotranspiration (ET) was greater in the south and west of the ARB in the period from 2000–2008, indicating the principal differences of this variable between the NRB and MRB. Based on Gloor et al. [99], the intensification of the hydrological cycle in the ARB has been concentrated in the wet season since approximately 1990, driving the progressively increasing differences between the peak and minimum flows in the ARB.

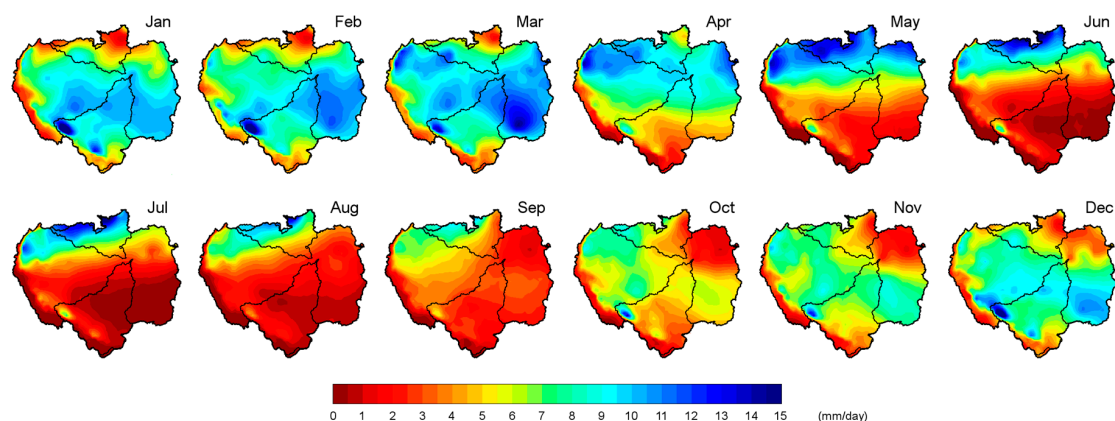


**Figure 2.** Monthly average precipitation (from CRU 3.2401) in the Amazon River basin (ARB). The Negro and Madeira River basin (NRB and MRB, respectively) boundaries are marked by contours. Period: 1980–2016.

The monthly average  $P$  for each subbasin was calculated. The annual cycle of the subbasins differed, as expected from previous analysis (Figure 3). Figure 3 also shows the annual PET cycle of each basin and the annual WL cycle of the Negro and Madeira rivers recorded at hydrological stations located in Manaus and Borba, respectively. The monthly average  $P$  (light grey bars) in the NRB increased from October to May when it reached the average annual maximum rainfall ( $\sim 11.0$  mm/day). The average  $P$  decreased after May, reaching a minimum in October ( $\sim 4.9$  mm/day). Less rainfall occurred in July ( $\sim 0.9$  mm/day) in the MRB (dark grey bars) in the Southern Hemisphere southwest of the ARB. From July onwards, it increased during the austral summer months until it reached a peak in January ( $\sim 8.7$  mm/day) and then decreased. The monthly average  $P$  in the NRB was greater than that in the MRB. Thus, the annual average rainfall in the NRB ( $\sim 7.0$  mm/day) was greater than that in the MRB ( $\sim 4.6$  mm/day). Both annual PET cycles (NRB and MRB) were very similar, although they differed from June to December when the PET in the NRB (red line) was higher than that in the MRB (green line). On the contrary, the PET in the MRB was higher in February and March. The PET in the NRB increased with decreasing  $P$ . However, this was not the case in the MRB, reflecting a lag time. Utilizing several datasets, Marengo [18] described similar annual  $P$  and evaporation ( $E$ ) cycles for northern and southern Amazonia. Nevertheless, the annual ET cycle obtained by Maeda et al. [100] for the NRB slightly differed from the PET in Figure 3. These authors described two maximum ET peaks in April and October. This indicates that the methods adopted to calculate the ET, land cover, soil types, and meteorological forcing used in the models and the study period have a significant impact on ET rates [101].

The WL of both annual cycles lagged in time with respect to the  $P$ . The maximum WL ( $\sim 28$  m) in Manaus occurred in June, one month after the maximum  $P$  in the NRB, while the maximum WL ( $\sim 20.4$  m) in Borba occurred in April, three months after the maximum  $P$  in the MRB. A strong seasonal signal of the Negro River water storage was described by Frappart et al. [101], with minima in October and maxima in June, in accordance with the minimum and maximum climatological WL. Marengo [5]

revealed that the WL in Manaus and rainfall in northern Amazonia vary in unison and had less in common with the rainfall anomalies in southern Amazonia. In this analysis, we must consider that WL fluctuations were generally influenced by hydrological, hydrometeorological, and hydrogeological phenomena, such as groundwater recharge, evapotranspiration, phreatophytic consumption, artificial recharge, groundwater pumping, and return flows from irrigation [102]. Therefore, these phenomena are not analysed in this work because our purpose was to provide a general overview of the hydrological cycles of both basins.

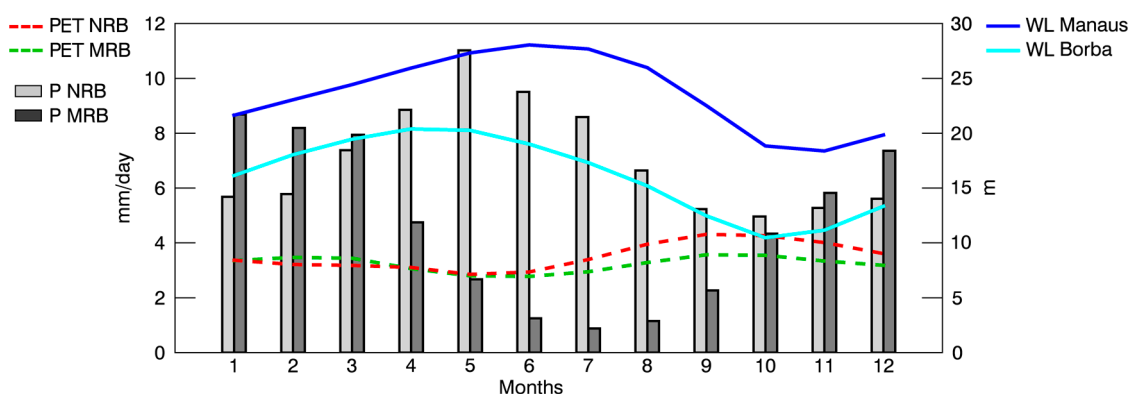


**Figure 3.** Precipitation (P; bars), potential evapotranspiration (PET; dashed lines) annual climatological cycle of the Negro and Madeira river basins (NRB and MRB, respectively). Annual water level cycle in Manaus and Borba (WL; solid lines). Period: 1980–2016.

### 3.2. Moisture Source Identification

The monthly budget  $(E - P)i/10$  obtained with FLEXPART for the NRB and MRB in the air-mass back-trajectory analysis is shown in Figure 4. Positive values represented by reddish colours indicate areas in which the net moisture budget in the vertical column was positive, which means that evaporation exceeded precipitation ( $E > P$ ) and the air masses transient to the basins in these regions gained humidity rather than lost it. These regions act as moisture sources for the basins. In contrast, the bluish colours represent regions in which air parcels moving toward the basins lost humidity ( $E < P$ ), which were considered to be moisture sinks. The spatial pattern of  $(E - P)i/10$  from January to May shows that for the NRB, where was an uptake in humidity from an extended area in the Tropical North Atlantic region (TNA);  $(E - P)i/10 > 0$  was also observed in a visibly smaller area in the Tropical South Atlantic region (TSA) and in the northeast of the NRB. The NRB mainly acted as a water vapour sink from April to July, which was consistent with major precipitation over itself (Figure 2). We must highlight that during the rainiest month in the NRB, that is, May, the moisture uptake was less intense in the TNA than in previous months; however, the extension and intensity of areas with  $(E - P)i/10 > 0$  in the TSA increased. The main oceanic moisture source for the NRB from June to October seemed to be the TSA; the main continental moisture sources were the eastern ARB and NRB itself. The humidity gain was reintensified in the TNA region and this source became more important than the TSA in December (visual analysis of Figure 4). The TNA and TSA regions were commonly associated with restricted areas, delimited by boxes in the North and South Atlantic Ocean. However, we named the sources according to the geographical location in this study. Drumond et al. [3] confirmed the tropical Atlantic regions to be the most important remote moisture sources for the ARB. Other studies have attempted to establish a relationship between the Atlantic and Pacific SST with rainfall over Amazonia. For example, Ronchail et al. [43] argued that the northeastern part of the basin, north of  $5^\circ$  S and east of  $60^\circ$  W, was significantly related to the tropical SST and a rainier wet season was observed when the equatorial Pacific and northern (southern) tropical Atlantic are anomalously cold (warm).

The historical  $(E - P)$  budget of air parcels tracked backward-in-time from MRB and integrated into the vertical column over ten days (Figure 4) showed positive values in the TNA, mainly from

January to March, while at TSA the  $(E - P)i10 > 0$  was less intense during these months. From October to April, the MRB mainly acted as a moisture sink in concordance with the major annual rainfall (Figure 3). The most important continental regions acted as moisture sources during these months based on areas in which  $(E - P)i10 > 0$ , such as the northern half of the ARB, northern South America, northeast of Brazil, and a region to the southeast of this basin. The positive values of the  $(E - P)i10$  budget over the ocean were most intense ( $> 0.2$  mm/day) in the TNA and TSA, except for October and November when the TNA seemed to be not effective in providing moisture to the MRB. In May, the  $(E - P)i10$  budget was positive in most parts of the MRB, mainly in the centre and south; negative values were observed in the north. When the Austral winter commences in June, the  $(E - P)i10$  pattern revealed a dipole. Negative values were observed in the north of the MRB, in the northern half of the ARB, and north of the continent, while positive values (indicating moisture uptake) were detected in the southern half of the ARB, northeast of Brazil, and in the southeast of the MRB. These patterns could be detected until September. As previously commented, areas with  $(E - P)i10 < 0$  values (moisture loss) were observed over parts of the MRB and in the eastern and northern ARB in October. Based on Yoon and Zheng [8], the Atlantic influence on the Amazon rainfall was due to changes in the north–south divergent circulation and the movement of the ITCZ following warm SST. Therefore, it was strongest in the southern part of the ARB during the dry season (July–October). Differences between the  $(E - P)i10$  budget over the NRB and MRB were partly due to the seasonality of the water balance in the ARB and played an important role in the interannual variability of the water balance within the ARB [20]. As well as Durán et al. [9] we found an apparent absence of contributions of moisture from the Pacific Ocean; possibly because the presence of the Andes did not permit moist winds to reach the basins.

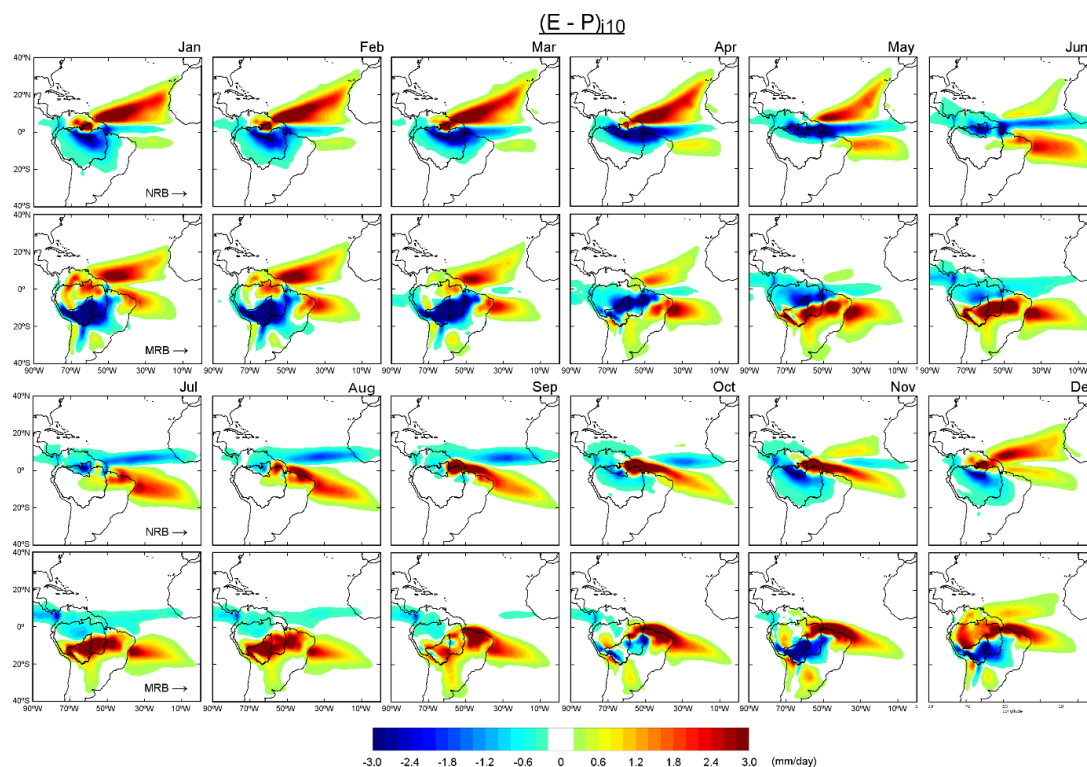


**Figure 4.** Monthly  $(E - P)i10$  patterns for the NRB and MRB based on the backward in time experiment. Period: 1980–2016.

The  $(E - P)i10$  budget was also computed in the backward in time experiment for each basin, at the annual scale (Figure 5a). The positive values within the 90th percentile ( $p90 = 0.26$  mm/day) represent regions in which the most intense moisture uptake occurred. The  $(E - P)i10$  budget was

positive in the historical experiment for the NRB, mainly over two regions in the Atlantic Ocean, that is, the TNA and TSA regions (Figure 5a). On land, it received humidity from the northeast of the basin and parts of the basin itself. The rest of the ARB did not play an important role in providing humidity to the NRB. Annual climatological  $(E - P)_{i10} > 0$  values for the MRB delimited by  $p90 = 0.14$  mm/day were observed in a large area of the continent (Figure 5b). This basin uptakes humidity from the northern half of the ARB, north and northeast of the continent, southeast (from the Plata River Basin), and southwest (from the Andes region). At the annual scale, the NRB and MRB mainly acted as a moisture sink. The ARBp, TNA, and TSA were the most important continental and oceanic moisture sources for the MRB, based on the extension and intensity of the positive values in the  $(E - P)_{i10}$  pattern. Nevertheless, a part or the whole MRB acted as a source of humidity for itself from May to September (Figure 4). Therefore, we considered the whole MRB and NRB as moisture sources for themselves, which allowed the investigation of their roles in the hydrological cycles. A schematic representation of the sources considered in this study is shown in Figure 6. In this figure, we divided the sources into oceanic and continental sources considering the origin of the air masses. To the north of the NRB was a small source we called N, to the northeast of Brazil, NEB; and the TNA and TSA on the Tropical Atlantic. A source region in the north of the ARB called N also appeared for the MRB; also, NEB, and the TNA and TSA sources. The southeastern ARB was not an important moisture source for the MRB at the annual scale; however, it was an important moisture source if we consider the monthly variability of the  $(E - P)_{i10}$  pattern (Figure 4) from May to September. Thus, we consider the rest of the ARB (ARBp) in addition to the MRB, as previously defined. Two important sources named ‘Southeast’ (SE) and Andes region (AND) were in the south of the MRB.

The cross-equatorial flux played an important role in changing the moisture fluxes that ultimately enhance the convection over central–eastern Brazil on intraseasonal timescales. The contribution of moisture transported from northern Amazon towards eastern South America generated the monsoon precipitation [56,57]. Despite this mechanism, our results also showed that the MRB and therefore the southwestern ARB received moisture from the south. Based on a quasi-isentropic calculation of the trajectories of water vapor back-in-time (QIBT) utilised by Dirmeyer and Brubaker [103], a ‘catalogue’ of moisture sources based on river basins was developed, which is available at <http://cola.gmu.edu/wcr/river/basins.html>. Based on this catalogue, the most evaporative moisture sources for the ARB were very similar to those shown in Figure 5 for the NRB and MRB. However, our results indicated that the TSA extended more to the east and SE and AND were more important evaporative regions.

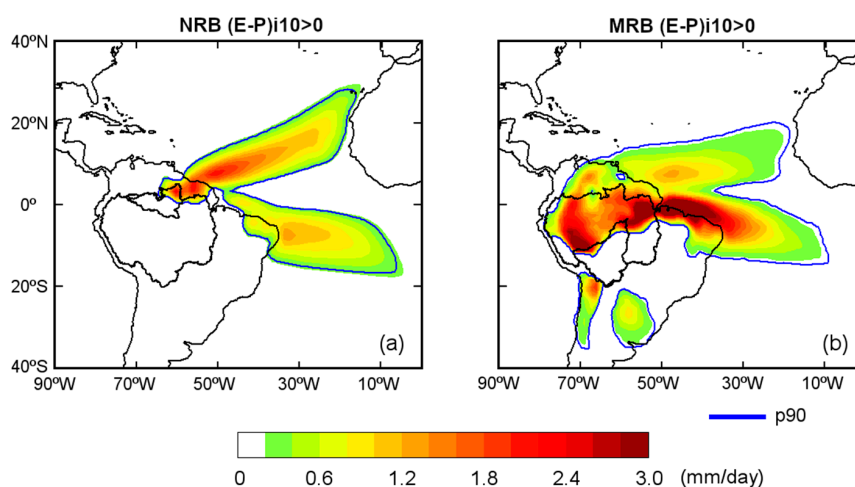


**Figure 5.** Annual  $(E - P)_{i10} > 0$  budget obtained in the backward in time experiment for the NRB (a) and MRB (b). Period: 1980–2016.

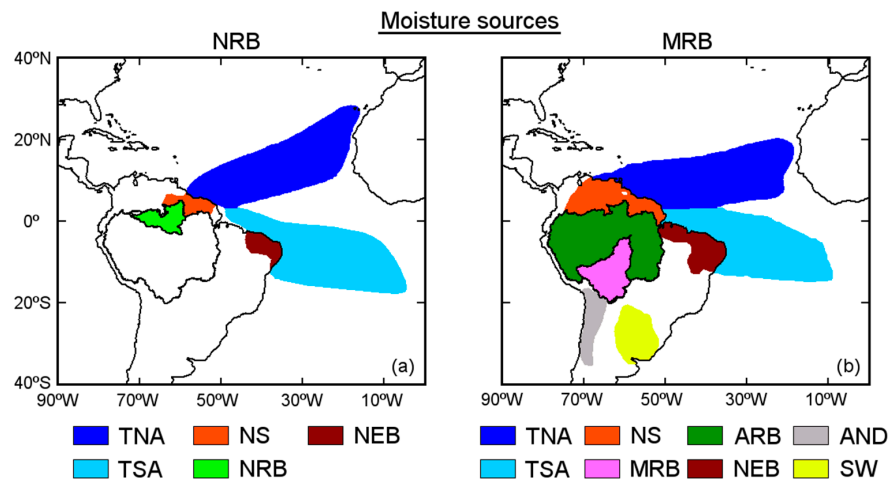


**Figure 6.** Schematic representation of the continental and oceanic moisture sources of the NRB (a) and MRB (b) considered in this study based on the p90 values in Figure 5.

### 3.3. Moisture Contribution from the Sources

The average moisture contribution to the  $P$  of the basins (Figure 7) was computed by tracking forward-in-time, the air masses based on all climatological sources. As the  $P$  increased in the NRB from January onwards, the moisture contribution from all sources increased; the TNA and NRB itself contributed the most (Figure 7a). The maximum moisture loss of air masses from the TNA over the NRB occurred in April, one month before the annual maximum  $P$  was reached. In fact, the correlation between  $|(E - P)_{i10} < 0|$  and  $P$  increased to 0.52 at a lag time of one month (Table 2). The maximum moisture loss over the NRB from itself also occurred in April but the correlation with  $P$  was highest without lag time. From May to October (austral winter), the maximum moisture supply from the TNA decreased and principal moisture input from the TSA and NRB occurred. It is very interesting that the TNA and TSA seemed to provide almost the same amount of moisture to  $P$  over the NRB in May, with the maximum rainfall peak over the NRB. In this month, 61% of the total moisture income to the NRB was due to oceanic sources. Lower atmospheric moisture contribution from the basin itself occurred in the following months; associated with a  $P$  decrease. Both sources, the TNA and TSA, seemed to play opposite roles in providing moisture to the NRB throughout the year. In September and October, with less rainfall over the NRB, continental sources became the most important, possibly because of the increase of recycling. The moisture contribution from N and NEB despite following the  $P$  annual cycle approximately, was less than that from the rest of the sources. Considering  $|(E - P)_{i10} < 0|$  when performing a multiple regression led to 54% of the  $P$  variance explained (Table 2).

We must clarify that the transport of moisture into a region in which it can become entrained into a precipitation weather system depends on the atmospheric dynamics and moisture sources from other parts of the globe (e.g., the rest of the sources) [104]. The moisture contribution from climatological moisture sources in the MRB, especially from ARBp, MRB, N, and TNA, followed the annual  $P$  cycle (Figure 7b). The correlations were positive and higher than 0.5, but decreased at a lag in time of one or two months (Table 3). Every month, the moisture loss over the MRB due to continental sources was greater than that from oceanic sources; particularly from the ARBp and the MRB itself. The  $|(E - P)_{i10} < 0|$  over the MRB from December to March (the rainiest months) from the TNA was greater than that from the TSA, while the moisture supply from the TSA was more important than that from the TNA during the remaining months. However, the moisture income from the TNA correlated best with  $P$  over the MRB. With respect to continental sources, the moisture contribution from AND to  $P$  in the MRB was the lowest. The comparison between the moisture provided by continental and oceanic sources to the MRB revealed the major contribution of moisture of continental regions during all of the year.

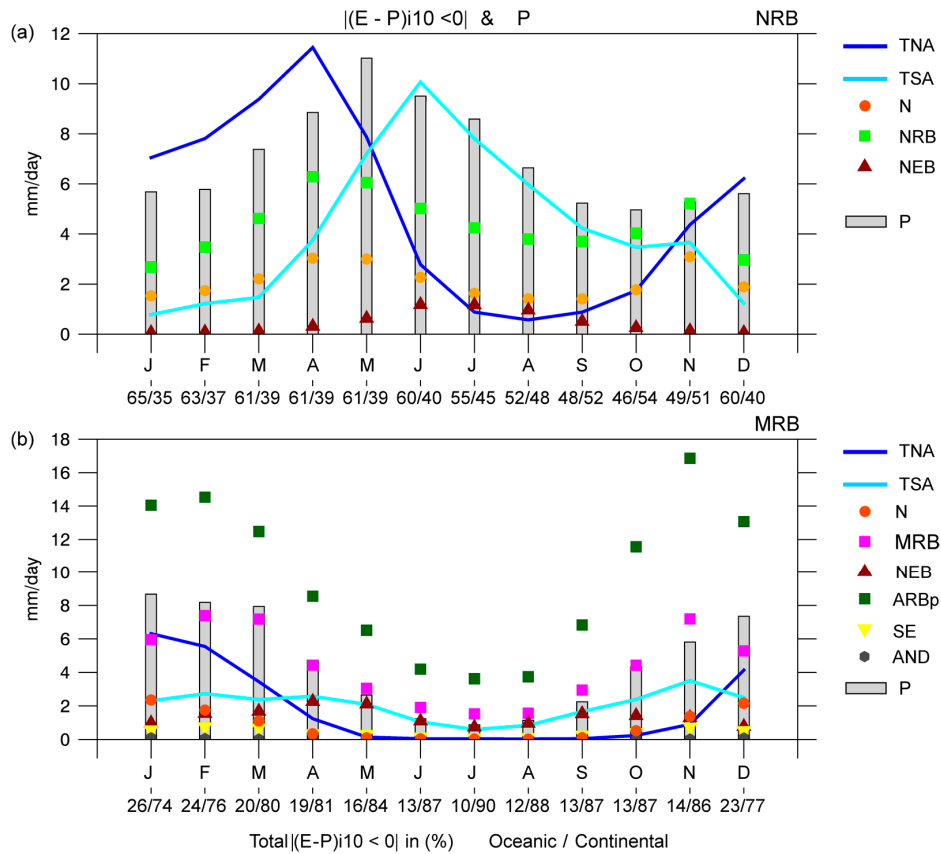


**Figure 7.** Precipitation (grey bars) and moisture contribution to annual precipitation ( $|E - P|/10 < 0$ ) cycles in the NRB (a) and MRB (b). Period: 1980–2016.

**Table 2.** Significant monthly correlations (at  $p < 0.05$ ) between  $|E - P|/10 < 0$  from the sources and  $P$  over the NRB.

	Moisture Sources					$r^2$ (%)
	TNA	TSA	N	NRB	NEB	
$r$	0.29	0.51	0.49	0.58	0.46	54
$r$ (lag 1 month)	0.52	0.16	0.42	0.46	0.10	43
$r$ (lag 2 months)	0.58	-0.21	0.29	0.28	-0.26	42

**Table 3.** Significant monthly correlations (at  $p < 0.05$ ) between  $|E - P|/10 < 0$  from the sources and  $P$  over the MRB.

	Moisture Sources								$r^2$ (%)
	TNA	TSA	N	MRB	NEB	ARB <sub>r</sub>	AND	SE	
$r$	0.79	0.46	0.78	0.74	0.08	0.80	0.45	0.56	80
$r$ (lag 1 month)	0.65	0.42	0.76	0.62	-0.09	0.77	0.39	0.57	58
$r$ (lag 2 months)	0.32	0.29	0.55	0.36	-0.23	0.58	0.25	0.40	36

### 3.4. Role of the Sources during the Onset and Demise of the Rainy Season

Liebman et al. [77] defined the onset and end of the rainy season in the ARB as the beginning and end of the longest period during which the rainfall exceeds its annual climatology, which was consistent with our approach. As previously commented, several studies investigated the onset/demise and length of the rainy season in the Amazon region and South America. Here we aim to determine the role of the moisture contribution from the sources in the climatological onset/demise of the rainy

season over the basins. Figure 8 shows the daily climatological  $P$  and cumulative anomalies of  $P$ ,  $|(E - P)|_{10 < 0|}$ , and OLR over the NRB and MRB obtained by applying Equations (3) and (4). The day after the minimum value of the daily  $P$  cumulative anomalies indicated the rainy season onset, while the day when the anomalies reached the maximum, pointed out the rainy season demise. The cumulative anomalies of the moisture loss ( $|(E - P)|_{10 < 0|}$ ) over the basins allowed us to identify from which source(s) there was an increase (decrease) on the moisture contribution before the rainy season onset (demise). A similar approach was utilised by Sorí et al. [105] to determine the day on which the increase in rainfall indicated the beginning of the monsoon involvement for the Indus, Ganges, and Brahmaputra River Basins.

The minimum cumulative daily anomalies of  $P$  over the NRB occurred on May 23 (Figure 8a). Before this date, the minimum cumulative daily anomalies of  $|(E - P)|_{10 < 0|}$  were due to the moisture supply from the N and NRB itself. Considering the annual climatological cycle of  $P$  and not the calendar year, the minimum value occurred from the TNA in the beginning of December. After these peaks, the cumulative daily anomalies of  $|(E - P)|_{10 < 0|}$ , from the TNA, N, and NRB started to increase and were responsible for the subsequent  $P$  increase over the NRB. In the beginning of June, the cumulative daily anomalies of  $|(E - P)|_{10 < 0|}$  over the NRB from the TNA, N, and NRB reached a maximum and later started to decrease, but the  $P$  decreased abruptly on 1 August. The cumulative daily anomalies of the moisture contribution from the NEB and TSA seemed not to be associated with the rainy season onset/demise at the NRB. To support these results, we also calculated the cumulative daily anomalies of the OLR. Several days after the rainfall increase causes the onset of the rainy season over the NRB, the cumulative daily anomalies of the OLR decreased (due to major cloud cover); reached the minimum value when the accumulated anomalies from TNA was at its maximum, and progressively increased when the rainfall decreased over the NRB. Results of Marengo shows that the onset of the rainy season has been strongly associated with changes in large-scale weather conditions in the region due to the effect of the Madden–Julian Oscillation (MJO).

The cumulative daily anomalies of  $P$  over the MRB reached the annual minimum value on 25 October (Figure 8b) and one day after (26) the onset of the rainy season occurred and subsequently positive anomalies of daily  $P$  occurred. Before the onset of rainy season, the moisture loss of the air masses over the MRB reached the minimum  $|(E - P)|_{10 < 0|}$  anomaly and afterwards started to increase due to the MRB itself, ARBp, and TSA contributions. The contributions from the rest of the sources seemed not to be associated with the onset of the rainy season. Before the rainy season demise on 26 April, a reduction of the moisture loss over the MRB occurred based on the decrease in the daily accumulated anomalies of  $|(E - P)|_{10 < 0|}$  of almost all sources, except from the NEB. The annual cycle of the cumulative daily anomalies of the OLR was opposite to  $|(E - P)|_{10 < 0|}$ , as expected.

According to the observation of the annual cycle and cumulative daily anomalies of  $P$  over both basins, we confirmed that the rainy season started first over the MRB and later over the NRB, which agreed with the results of Liebman et al. [77]. These authors reported that the rainy season progresses northward from the southern ARB rather than from northwest to southeast, as suggested in previous studies. The atmospheric circulation and atmospheric dynamical condition were clearly key factors that modulates the transport of moisture and the  $P$  over the Amazon region. Thus, based on the rapid increase/decrease of the moisture contribution from the sources to the precipitation over NRB and MRB, we tried to explain the climatological onset/demise of the rainy season over the NRB and MRB. Nevertheless, other authors, such as Wright et al. [106], described another mechanism in which the Amazon rainforest transpiration enables the increase of shallow convection that moistens and destabilises the atmosphere during the initial stages of the dry-to-wet season transition and finally leads to the onset of the rainforest-initiated wet season in the southern ARB.

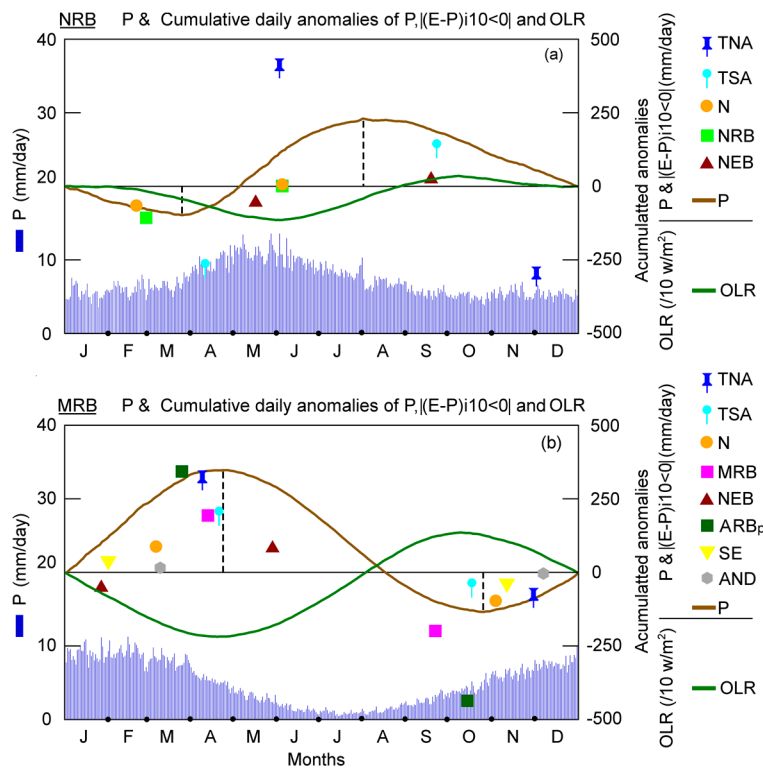


**Figure 8.** Daily  $P$  (blue bars) and cumulative daily anomalies of  $P$ ,  $|E - P|10 < 0|$  and OLR from the CHIRPS datasets, OLR from NOAA and  $|E - P|10 < 0|$  over the NRB (a) and MRB (b) obtained in a forward experiment from the climatological moisture sources using FLEXPART. Period: 1981–2016.

### 3.5. Dry and Wet Conditions in the NRB and MRB

The evolution of the SPEI at temporal scales of 1, 6, and 12 months (SPEI1; 6, 12) from 1980–2016 for the NRB and MRB is shown in Figure 9. Figure 9 also shows the monthly standardised anomalies of the WL of the Niger and Madeira rivers at the hydrological stations of Manaus and Borba, respectively. Dry conditions prevailed in the NRB from 1980–1993 and from 2013–2016. The SPEI reached values below  $-2$  on few occasions, revealing extremely dry conditions. In the MRB, we must highlight the period of 1980–1986 because it was the longest period of wet conditions, which was followed by more frequent dry conditions among which the periods 1995–1996, 1998, 2003–2005, and 2015–2016 stood out because of their magnitude and/or duration. Indeed, dry conditions simultaneously affected both basins from 2015–2016. The 2005 drought in southwestern Amazonia has been documented to be one of the most intense droughts of recent years. However, the index value was not as large when compared with other years mentioned earlier, but the duration of dry conditions was considerable higher in the MRB. Dos Santos et al. [107] found that the drought of 1998 was the most intense drought (average SPEI equal to  $-1.69$ ) that occurred in Amazonia in the period from 1979 to 2014. The MRB experienced an important wet period starting in the end of 2013 and continuing throughout 2014. Espinoza et al. [60] confirmed that the rainfall in the southwestern ARB was  $\sim 100\%$  above normal during the 2014 summer (December–March).

The temporal evolution of WL-standardised anomalies in Manaus and Borba is shown in Figure 9b,e. It mostly matched the temporal evolution of SPEI6 in the NRB and MRB (Figure 9b,e). The widely investigated intense droughts of 2005 and 2010 that affected southwestern Amazonia were represented by negative SPEI values for the MRB and negative WL anomalies in Borba (Figure 9b). According to Marengo et al. [26], the 2005 drought was manifested as weak peak river season from autumn to winter because of a weak summertime season. This drought was not related to El Niño; it experimented a pattern different from the El Niño-related droughts in 1926, 1983, and 1998, but the

anomalously warm tropical North Atlantic, the reduced intensity in northeast trade wind moisture transport into southern Amazonia during the peak summertime season, and the weakened upward motion over this section of Amazonia, resulting in reduced convective development and rainfall [45].

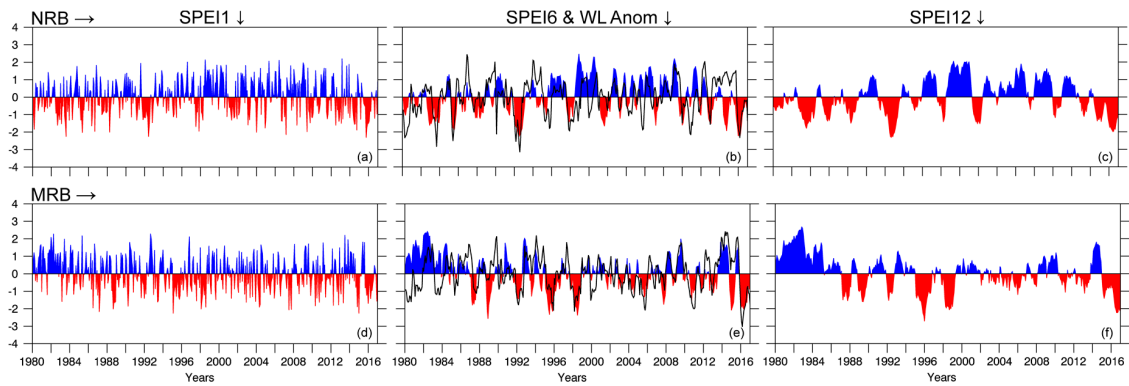


**Figure 9.** SPEI time series at 1-, 6-, and 12-month temporal scales (a–c) for the Negro (top, NRB) and Madeira (d–f) (bottom, MRB) river basins. The blue (red) colour represents wet (dry) conditions. The black line represents the standardised anomalies of the water level (WL) recorded at the fluvial stations in Manaus (b) and Borba (e). Period: 1980–2016.

As each source of moisture contributed to the total precipitation, each one had a role on the water balance conditions. Correlations were calculated between  $|E - P|_{i10} < 0|$  values in the NRB and MRB from all sources with 1- to 24-month SPEI values, respectively (Figure 10). Significant *r*-values were observed for the first temporal scales of the SPEI, especially in the NRB (Figure 10a). All correlations were positive in the NRB, highlighting the correlation between the moisture contribution from N and the NRB itself with the SPEI at first temporal scales. In particular, the correlation between the moisture contribution from NEB and the SPEI, increased after the SPEI12. No significant correlations were obtained between  $|E - P|_{i10} < 0|$  from TSA and the SPEI7–SPEI11. The same analysis was performed for the MRB. The strongest correlations occurred at the first temporal scales of the SPEI (Figure 10b). However, although all the *r*-values were positive at the first temporal scales, the highest occurred for correlations during the three first temporal scales of the SPEI. All correlations became insignificant after SPEI6 and even reached negative values (unless for N). The negative correlations indicated that the water balance conditions (even if accumulated from previous months) were not directly associated with the moisture loss over the basins.

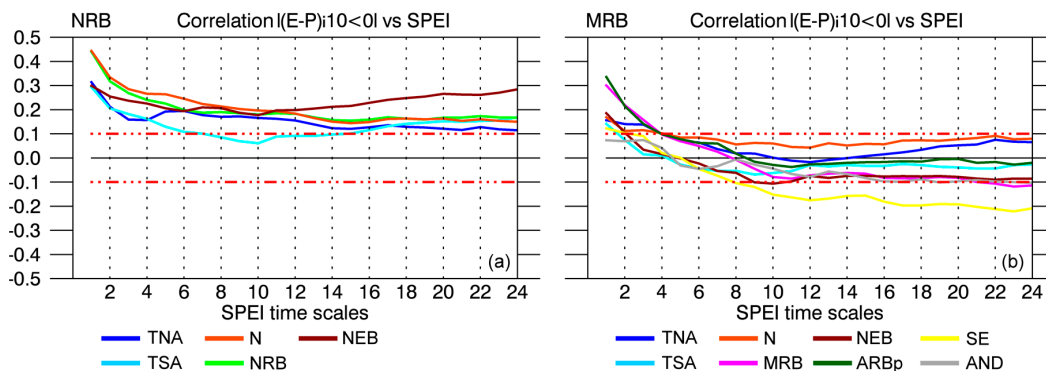


**Figure 10.** Monthly correlation between  $|E - P|_{i10} < 0|$  with SPEI1–24 temporal scales over the NRB (a) and MRB (b). Period: 1980–2016.

To understand the possible impact of water balance conditions in the basins on the WL of the Negro and Madeira rivers, respectively, we calculated the monthly correlations between standardised

WL anomalies and the SPEI1- to SPEI24-month timescales for each basin (Figure 11). The correlations in the NRB were positive at the first SPEI temporal scales from November to July, in accordance with the hydrological year. The  $r$ -values increased after December and become positive in February and March at all SPEI temporal scales. The maximum correlation occurred in March at SPEI4, suggesting that the WL was highly influenced by the water balance conditions of the previous four months. The correlations at the first SPEI temporal scales decreased with respect to previous months from April to July, which was the rainiest period, and they decreased month after month at longer SPEI temporal scales. This revealed a mechanism in which the WL does not instantaneously increase when the rainfall is the highest, but increases in following months when the water balance conditions of previous months are considered. Negative anomalies between the WL standardised anomalies and SPEI prevailed in September and October. The  $P$  was at a minimum over the NRB in October, while in the WL reached the minimum climatological level in November (Figure 2). As previously described, starting in November, when rainfall started to increase, the correlations increased from first to longer SPEI temporal scales as the months went by, highlighting the relationship between the two variables.

The same analysis was performed for the MRB. Positive correlations are observed for almost all months. During the driest months (June–October), the correlations were the lowest at the first SPEI temporal scales (negative at SPEI1 in August). Approximately from SPEI3 onwards, the  $r$ -values were statistically significant. This suggests that the impact of the rainfall deficit/surplus, over the WL (at Borba) may be effective when was calculated for the three previous months and longer temporal scales. However, the correlations were higher in November and December than in the previous months at the first SPEI temporal scales. To understand these correlations, it must be noted that the  $r$ -values increased at all SPEI temporal scales and become statistically significant from September onwards until January, when the rainfall was at its maximum over the MRB. In February, the rainfall started to decrease, the WL was increasing, and the correlations decreased at the longer SPEI temporal scales with respect to previous months. They generally become statistically insignificant and clearly divide the two transitional periods based on the highest (lowest) rainfall over the MRB. Based on the correlations, the WL of the driest months (June to July) were highly influenced by the water balance conditions of several previous months. This was expected for the NRB and MRB because of the lag between the peak rainfall in the early austral summer in the MRB and the peak WL during early austral fall, while the WL in the NRB peaked in late fall–early winter.

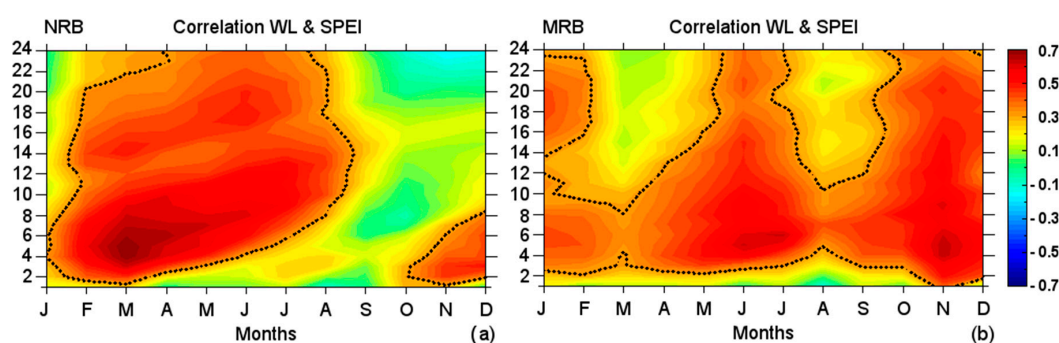


**Figure 11.** Monthly correlations between standardised WL anomalies and SPEI1 to SPEI24 in the NRB (a) and MRB (b). The dotted lines represent significant correlations at  $p < 0.05$ . Period: 1980–2016.

The dry episodes in the NRB and MRB were identified utilizing the SPEI1 for the period 1980–2016. Table S1 in Supplementary Materials shows the date, severity, duration, and peak of the dry episodes for each basin. The five most severe episodes in each basin (Table 4) from 1980–2016 were selected to investigate the role of the sources on the moisture contribution. The episodes of September 1991–July 1992 and May 2015–March 2016 in the NRB were the longest with a duration of 11 months, reaching a peak under  $-2.0$  (extremely dry), and were characterised by major severity. The episodes January–

October 1995 and August 2015–July 2016 were the most severe and longest in the MRB. Figure 9 shows that the dry conditions simultaneously affected both basins after 2014 and hence the time coincidence of the May 2015–March 2016 and August 2015–July 2016 episodes in the NRB and MRB.

**Table 4.** Top five most severe dry episodes occurring in the NRB and MRB according to SPEI1 and their duration and peak. Period: 1980–2016.

NRB				MRB			
Month/Year	Severity	Duration	Peak	Month/Year	Severity	Duration	Peak
September 1991– July 1992	12.8	11	−2.26	January 1995– October 1995	10.8	10	−2.27
May 2015– March 2016	11.3	11	−2.32	August 2015– July 2016	10.6	12	−1.70
December 2000– August 2001	6.9	9	−1.33	June 1988– November 1988	8.7	6	−2.02
May 1982– November 1982	6.7	7	−1.62	January 1998– August 1998	8.5	8	−2.03
January 1985– June 1985	6.4	6	−2.03	August 2014– March 2015	6.3	8	−2.27

Pampuch et al. [108] examined the distributions of anomalies of SST and of the moisture sources in the South Atlantic Ocean during extreme dry events in southeastern Brazil. However, these authors did not quantify the anomalies in the moisture contribution to the target regions. In our approach, we attempt to investigate the drought phenomenon from a close perspective, that is, by computing the moisture anomalies of  $|(E - P)/10 < 0|$  that caused a rainfall decrease over the NRB and MRB during severe dry conditions. Therefore, the monthly anomalies of the moisture contribution to precipitation from each climatological moisture source previously identified were calculated for each episode of Table 4 (Figures 12 and 13). The negative anomalies of  $|(E - P)/10 < 0|$  from all sources prevailed during the most severe dry episode in the NRB (September 1991–July 1992). The  $|(E - P)/10 < 0|$  anomalies over the NRB, calculated in air masses from all the sources, generally followed the same temporal evolution as the SPEI1, as expected. Nevertheless, the major moisture loss anomalies usually occur in the moisture contribution from the TNA, which could be observed in May 1992 when the  $|(E - P)/10 < 0|$  anomaly over the NRB due to the TNA reaching a minimum value (−5.8 mm/day) and the SPEI1 consequently reached the minimum peak (−2.26) of the episode.

A decrease of the moisture loss over the basins may be also associated with dynamic factors. Then, we calculated the VIMF divergence anomalies for each dry episode (Figures 12 and 13). The average VIMF divergence anomalies for the September 1991–July 1992 episode were positive over the NRB, indicating the prevalence of moisture flux divergence, favouring the rainfall decrease. During the second episode (May 2015–March 2016), the SPEI reached the threshold of −1 from September to February, when negative anomalies of  $|(E - P)/10 < 0|$  occurred over the NRB in air masses from almost all the sources. The moisture contribution to the precipitation over the NRB from all sources decreased in September 2015 and consequently, the SPEI1 sharply dropped, reaching the minimum of the episode (−2.32). The greatest decrease in the moisture supply occurred from the TSA (−3.16 mm/day) during this month. From September 2015 to January 2016, the moisture loss anomalies of the air masses arriving from all sources over the NRB were negative. They were positive in the last two months of the episode when the rainfall deficit decreases (according to SPEI1 values). The  $|(E - P)/10 < 0|$  anomalies of the TSA and NRB itself perfectly matched the SPEI1 evolution. Positive anomalies of the VIMF divergence prevailed in the northeast of the ARB and over almost all the NRB. Negative anomalies of the VIMF diverged in the west and northwest of the ARB, which suggested a convergence of the moisture flux that enhanced the conditions necessary for rainfall occurrence. In the third dry episode (December 2000–August 2001), the  $|(E - P)/10 < 0|$  anomalies from all sources and the SPEI1 did not show the same temporal evolution. Nevertheless,

we must consider the temporal lag that may exist between the contribution from the sources and the climatological role of the sources across the year. At the end of the episode, the moisture contribution from the TNA decreased, which was consistent with the SPEI1 decrease. The VIMF divergence anomaly patterns for this episode showed few areas with positive divergence anomalies. In the fourth episode (May 1982–November 1982) almost all  $|E - P|_{i10} < 0$  anomalies were negative, but did not match completely the SPEI1 evolution. During the fifth episode (January 1985–June 1985), the anomalies in the moisture contribution from TNA seemed to be the best associated with SPEI and predominant positive VIMF anomalies over the NRB indicated divergence of the vertically moisture flux.

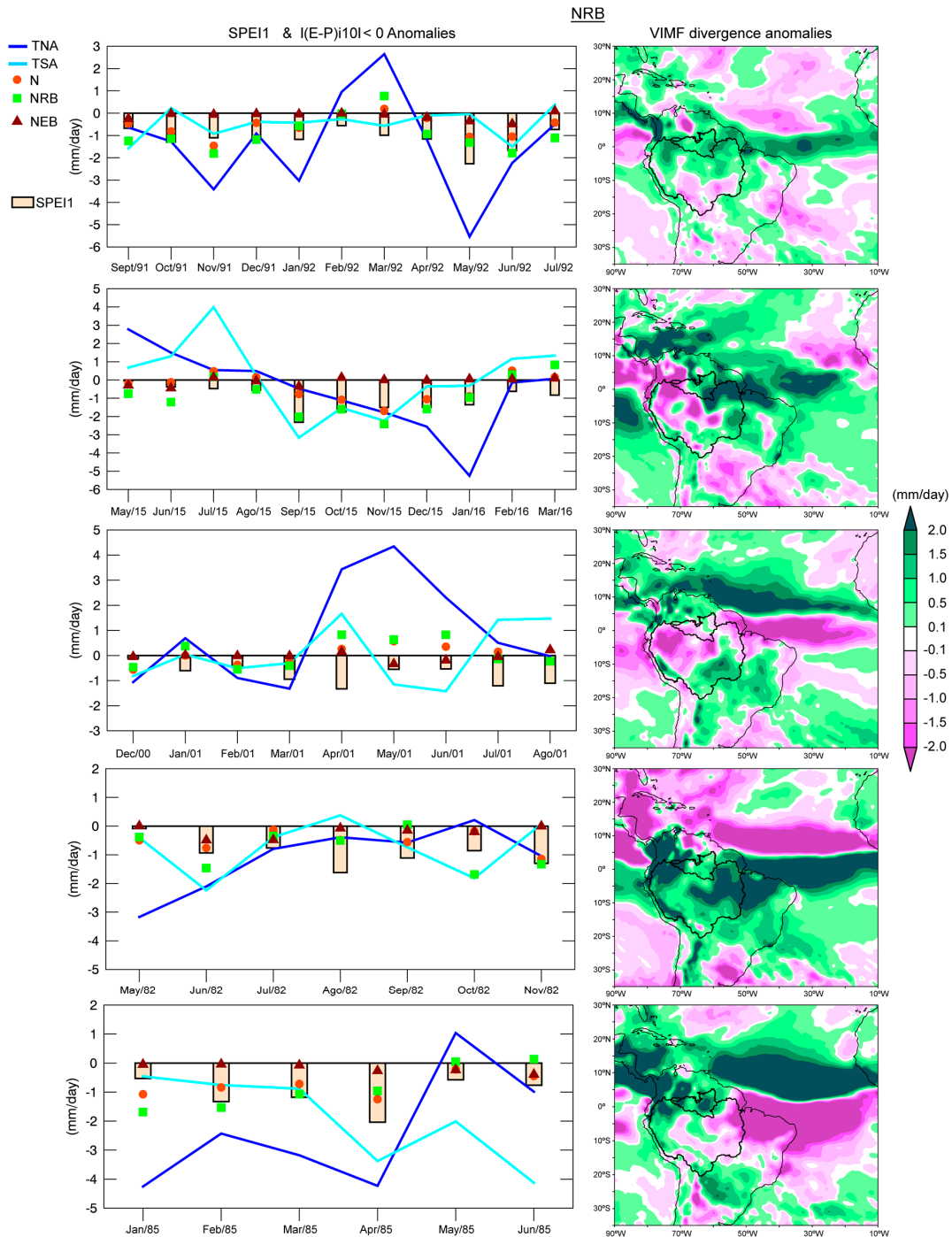


**Figure 12.** The SPEI1 and monthly anomalies of  $|E - P|_{i10} < 0$  during the most severe dry episodes (left panel) in the NRB (ordered as in Table 4) and VIMF divergence anomalies for each episode (right panel).

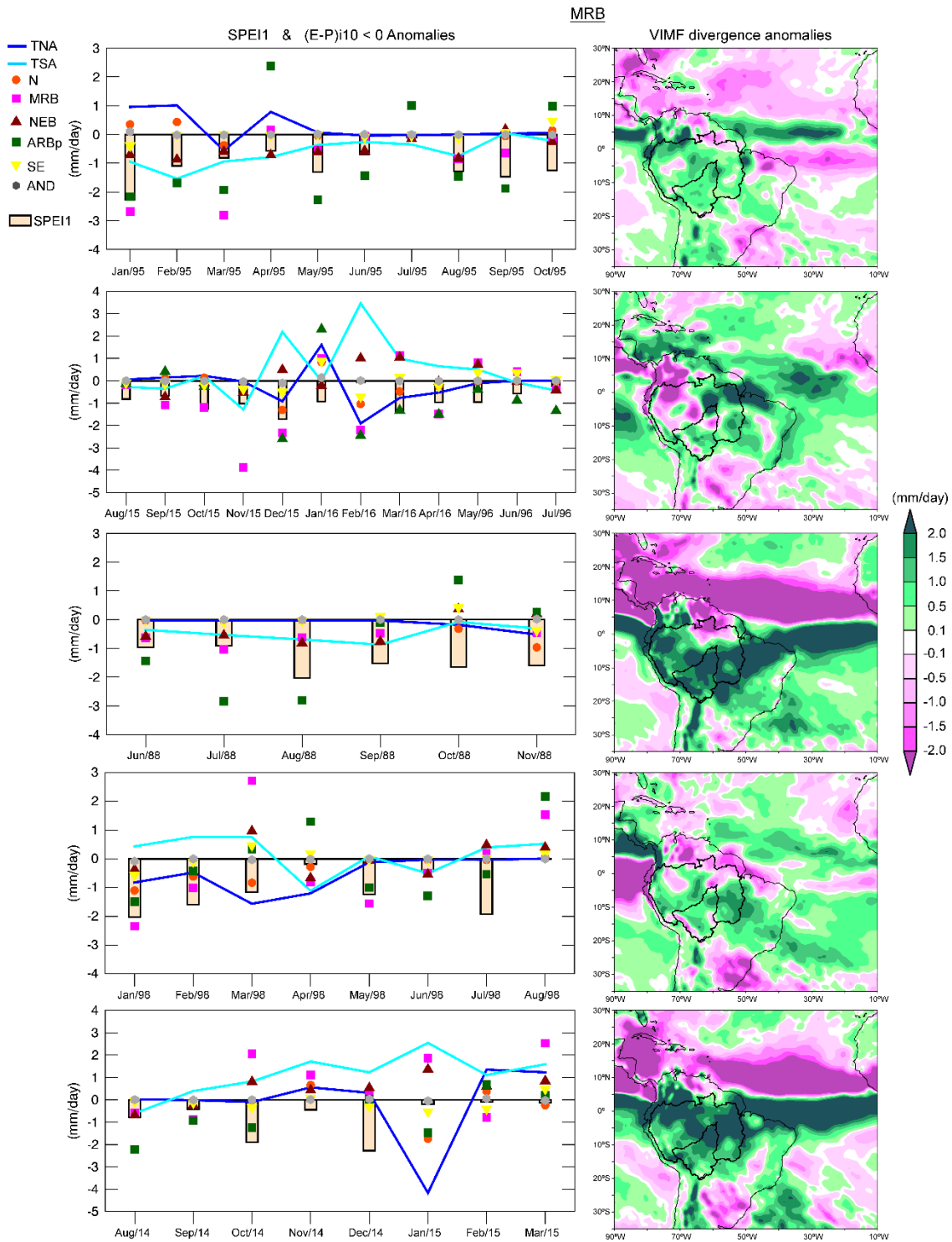


**Figure 13.** The SPEI1 and monthly anomalies of  $|(E - P)i_{10} < 0|$  during the most severe dry episodes (left panel) in the MRB (ordered as in Table 4) and VIMF divergence anomalies for each episode (right panel).

Negative anomalies of the moisture contribution to the basin from all sources predominated during the most severe dry episode (January 1995 to October 1995) in the MRB (Figure 13). The negative anomalies of  $|(E - P)i_{10} < 0|$  from ARBp, MRB, and TSA seemed to be the most related with the dry conditions (according with the SPEI1). The average pattern of the VIMF divergence anomalies

was positive over the MRB and almost all the ARB. In the second episode (August 2015 to July 2016), the anomalies of  $|(E - P)_{i10} < 0|$  from two continental sources, the MRB itself and ARBp, seemed to be the most important considering their magnitude and the SPEI values. With respect to the oceanic sources, the anomalies of the TNA and TSA showed an inverse behaviour. A lag of approximately one month was observed in some cases. The  $|(E - P)_{i10} < 0|$  anomalies from MRB was  $-3.8$  mm/day, respectively, in November 2015. One month later, the SPEI abruptly decreased with respect to the previous months and reached the minimum value of the episode. This phenomenon could also be observed from February to March 2016 for  $|(E - P)_{i10} < 0|$  anomalies from the MRB, ARBp, SE, N, and TNA. However, the SPEI reached the greatest value (near zero) in February 2016, when the greatest amount of moisture contribution from the TSA and NEB could compensate the less supply from the rest of the sources. The dry conditions decreased toward the end of the episode along with the anomalies in the moisture supply, specifically that from the TNA and MRB. Positive and negative anomalies of the VIMF divergence anomalies over the MRB were observed; however, the positive anomalies prevailed.

During all months of the third dry episode (June–November 1988), almost all  $|(E - P)_{i10} < 0|$  anomalies were negative, while intense positive anomalies of the VIMF divergence were observed over the MRB. In the fourth episode (January–August 1998), under El Niño conditions, the moisture contribution from TNA experienced a major reduction than that from the TSA. In August 1998, the last month of the episode, the  $|(E - P)_{i10} < 0|$  anomalies from all sources were positive, which favoured the rainfall occurrences and consequently the SPEI become positive. The VIMF divergence anomalies of this period were mostly positive. In the fifth episode (August 2014 to March 2015) the negative anomalies of  $|(E - P)_{i10} < 0|$  occurred in a major number of months from the ARBp. After October 2014, the relationship between the SPEI and  $|(E - P)_{i10} < 0|$  anomalies remained unclear. The SPEI reached the minimum value ( $-2.3$ ) of the episode during December 2014, indicating extremely dry conditions, but negative anomalies of  $|(E - P)_{i10} < 0|$  were only observed for the SE. Dry conditions diminish in January 2015. In this month, the anomalies on the moisture supply from TNA, N, ARBp, AND, and SE were negative but those from NEB, MRB and TSA were positive. The VIMF divergence anomalies of the episode were mostly positive.

### 3.6. Moisture Contribution during El Niño and La Niña Conditions

The rainfall variability and climate extremes in Amazonia and other tropical regions were strongly linked to the ENSO. El Niño events, such as in 1982/83, 1997/98, and 2015/16, or La Niña events in 1988/89 and 2010 were related to dry conditions [4,27,42,45,63,97,109,110]. However, the dry years of 1963–64 and 2004–05 were related to near normal conditions in the tropical Pacific and to anomalously warm SST in the tropical North Atlantic [45]. Tables 5 and 6 summarises the average  $P$  and  $|(E - P)_{i10} < 0|$  anomalies over the NRB and MRB for composites of months under El Niño/La Niña conditions according to the BEST index. Negative rainfall anomalies prevailed in the NRB under El Niño conditions unless in April and July when were positive. Under La Niña conditions, positive  $P$  anomalies occurred mostly during boreal winter (Table 5). With respect to the composite under El Niño conditions, positive anomalies of  $P$  may be related to the positive  $|(E - P)_{i10} < 0|$  anomalies from TSA and N. With respect to the composite of months under La Niña conditions, the  $P$  anomalies were positive from September to March and in May. The moisture contribution to precipitation from all sources, except for the TSA in March, were favoured during these months. In April, June, July, and August (boreal summer), the  $P$  anomalies were negative. Based on the analysis of the moisture loss anomalies over the NRB, negative anomalies occurred in April were related the contribution from TSA and N, while in June were associated with the TNA source. Negative  $|(E - P)_{i10} < 0|$  anomalies rarely occurred in July; they did occur in August and were associated with the moisture supply from TSA. Here, we confirmed the opposite impact of warm and cold events of the ENSO on the hydroclimatology in the NRB.

**Table 5.** Anomalies of  $P$  and  $|(E - P)/10 < 0|$  in the NRB for the composite of months under El Niño and La Niña conditions. Simultaneous negative (positive) anomalies of  $P$  and  $|(E - P)/10 < 0|$  are shaded in blue (red). Period: 1980–2016.

P/Sources	Months											
	January	February	March	April	May	June	July	August	September	October	November	December
<b>El Niño</b>												
$P$	-2.12	-1.08	-0.43	0.44	-1.19	-1.35	0.04	-0.42	-0.71	-0.19	-0.73	-2.26
TNA	-3.20	-1.80	0.54	-0.99	-2.21	-0.84	-0.20	-0.07	-0.17	-0.01	-0.53	-2.56
TSA	-0.36	-0.15	0.22	0.89	0.99	-0.19	0.86	-0.02	-0.77	-0.95	-0.50	-0.36
N	-0.76	-0.43	0.19	-0.12	-0.44	-0.37	0.07	-0.10	-0.23	-0.23	-0.56	-1.05
NRB	-1.17	-0.61	0.15	-0.54	-0.67	-0.76	-0.36	-0.32	-0.42	-0.57	-0.67	-1.59
NEB	-0.03	-0.02	-0.03	-0.09	-0.02	-0.23	-0.10	-0.08	-0.12	-0.08	-0.01	-0.02
<b>La Niña</b>												
$P$	1.68	1.62	1.47	-0.91	1.63	-1.24	-0.36	-0.50	0.49	0.14	1.18	1.12
TNA	2.08	1.71	0.48	0.49	0.27	-0.96	0.26	0.14	0.12	0.49	0.54	0.89
TSA	0.32	0.11	-0.41	-0.76	1.77	2.62	0.81	-0.60	1.01	1.08	1.35	0.39
N	0.60	0.35	0.33	-0.05	0.51	0.11	0.35	0.24	0.44	0.55	0.68	0.46
NRB	0.93	0.48	0.83	0.15	1.03	0.54	0.78	0.56	0.64	1.00	1.18	0.82
NEB	0.04	0.05	0.00	0.08	0.37	0.56	0.27	0.11	0.22	0.07	0.05	0.04

**Table 6.** Anomalies of  $P$  and  $|(E - P)/10 < 0|$  over the MRB for composited of months under El Niño and La Niña conditions. Simultaneous negative (positive) anomalies of  $P$  and  $|(E - P)/10 < 0|$  are shaded in blue (red). Period 1980–2016.

P/Sources	Months											
	January	February	March	April	May	June	July	August	September	October	November	December
<b>El Niño</b>												
$P$	-1.17	-1.13	-0.43	0.15	0.29	0.07	0.24	0.10	-0.03	-0.25	-0.19	0.05
TNA	0.39	-0.34	-0.83	-0.39	-0.07	0.02	0.02	0.01	0.01	0.09	-0.13	0.23
TSA	-0.04	0.93	0.77	0.13	-0.02	-0.06	0.19	-0.03	-0.08	-0.30	0.49	0.11
N	-0.28	-0.34	-0.42	-0.18	-0.01	0.04	0.02	0.01	0.02	0.09	-0.30	-0.38
MRB	-1.22	-1.40	0.14	-0.43	-0.15	-0.29	0.18	-0.09	-0.21	-0.95	-2.01	-1.52
NEB	-0.33	0.17	0.37	-0.04	-0.09	-0.16	0.17	0.06	-0.18	-0.30	-0.04	-0.14
ARBp	-1.03	-1.55	-1.09	-0.27	0.91	0.57	0.81	-0.10	-0.31	-0.52	-2.43	-1.52
SE	-0.10	-0.36	-0.11	0.00	0.00	-0.05	0.00	-0.05	-0.05	-0.13	-0.32	-0.35
AND	0.01	-0.01	0.01	-0.01	0.00	0.00	0.00	0.00	0.00	-0.01	-0.01	-0.04
<b>La Niña</b>												
$P$	-0.08	0.79	0.03	-0.43	-0.36	-0.41	-0.15	-0.47	-0.31	-0.09	-0.70	0.29
TNA	0.24	0.85	0.21	0.92	-0.06	0.05	-0.01	-0.02	0.00	0.00	-0.77	-0.40
TSA	0.23	0.11	-0.48	0.02	-0.15	-0.75	-0.25	-0.34	-0.13	-0.24	0.61	-0.17
N	0.16	0.44	0.46	0.11	-0.01	-0.01	-0.02	0.00	0.05	-0.01	-0.74	0.16
MRB	1.73	1.10	2.61	1.30	-0.29	-0.27	-0.12	-0.07	0.39	1.11	3.68	1.28
NEB	0.29	0.31	-0.01	0.06	-0.12	-0.58	-0.16	-0.37	0.04	0.26	0.46	0.12
ARBp	1.41	2.00	3.32	1.15	-1.90	-1.36	-0.23	-0.86	0.94	-0.16	1.93	1.14
SE	0.24	0.15	0.40	0.14	-0.02	0.00	-0.03	0.01	0.13	0.41	-0.33	0.45
AND	0.00	0.00	-0.02	0.00	0.01	0.00	0.00	0.00	0.00	-0.01	0.00	-0.01

The same analysis was performed for the MRB and the results are shown in Table 6. During El Niño, positive  $P$  anomalies occurred from April to August (austral winter) and in December. In these months positive  $|(E - P)/10 < 0|$  anomalies occurred from some sources alternatively; but all of them in July. Negative  $P$  anomalies occurred in the rest of months (austral summer). Based on the  $|(E - P)/10 < 0|$  anomalies, the reduction of the contribution was higher from continental sources. For the composite under La Niña conditions, the average  $P$  decreased over the MRB (according to negative  $P$  anomalies) from April to November and in January. A reduction of the moisture contribution from almost all the sources was observed from May to August (winter months). This behavior was very similar to what happened when, in 2010, drought started during an El Niño event in early austral summer and then became more intense during La Niña in the austral winter dry season and the following spring [27]. In December, February, and March, the anomalies indicated that  $P$  was favoured over the basin, which must have been related to the increased moisture contribution from sources. In those three months, there occurred positive anomalies of  $|(E - P)/10 < 0|$  from the ARBp, MRB, N, and SE. Drumond et al. [3] argued that, in comparison to La Niña episodes, it seemed that the contribution from the tropical and subtropical Atlantic to the ARB was weakened during an El Niño cycle. However, our results showed that mainly El Niño (La Niña) reduced the moisture contribution from the sources and the  $P$  over the NRB (MRB).

#### 4. Conclusions

The precipitation regimes of the northern and southern ARB strongly vary. The main moisture sources of the NRB and MRB in the northern and southwestern ARB, respectively, were identified. The results confirmed the main roles of oceanic regions in the TNA, TSA, and surrounding continental areas in providing moisture to the NRB and MRB. In the NRB, the oceanic sources generally provided the major amount of humidity throughout the year, particularly the TNA (TSA) during boreal winter (summer). In contrast, the MRB received the greatest amount of humidity from land sources north and south of the basin. The high amount of moisture loss in air masses tracked forward-in-time from the basins themselves, confirmed that recycling played an important role in Amazonia, as previously reported. Particularly, part of the ARB (ARBp) played an important role in providing humidity to the MRB. We consider that the onset and demise of the rainy season in the NRB depended on moisture contribution from the TNA, while in the MRB mostly depended on the moisture contribution from the basin itself, rest of the ARBp, and TSA. These results may be highly useful to monitor and predict the onset and demise of the rainy season, which progresses northward from the southern ARB.

Dry and wet conditions within the ARB have not usually occurred simultaneously in the period under study. However, the NRB and MRB were simultaneously affected by intense dry conditions in 2015–2016. Through the five most severe episodes in the NRB the anomalies on the contribution from TNA principally, and TSA, seemed to be associated with the SPEI temporal evolution. It also happened in the MRB, where both oceanic and terrestrial sources played an important role. On average, the episodes were associated with a reduction of atmospheric moisture contribution from the sources, and subsidence based on predominantly positive VIMF divergence anomalies over the basins. Concerning the role of ENSO, it affected the moisture supply from the sources and thus the  $P$  over them. The impact varied between the NRB and MRB. In this study, we investigated the source-sink of atmospheric moisture relationship to identify and evaluate the role of the climatological moisture sources of the NRB and MRB on the precipitation and its variability over them. We consider this approach useful to understand better the hydrological cycle, but essentially to diagnose the causes of droughts and floods. However, further research must be done to investigate the influences of other modes of climate variability in the variations in the moisture contribution from the sources, and the role of the basins themselves as sources of moisture for surrounding continental regions.

**Supplementary Materials:** The following are available online at <http://www.mdpi.com/2073-4441/10/6/738/s1>, Table S1: Dry episodes occurring in the NRB and MRB according to SPEI1 and their duration, severity and peak. Sorted according to the date of occurrence. Period: 1980–2016.

**Author Contributions:** R.S., J.A.M., R.N., L.G. designed, proposed and conducted the research; R.S. performed the experiments and R.S., J.A.M., R.N., L.G. analysed the data; all the authors wrote the paper.

**Acknowledgments:** R.S. would like to acknowledge the grant from the Xunta of Galicia, Spain, in support of his doctoral research work and to Campus DoMar of the University of Vigo for the support to carry out a research stay at CEMADEN; R.N. acknowledges support from CNPq grant 314734/2014-7 provided by the Brazilian government, and A.D. acknowledges the support of the Spanish Government and FEDER via the SETH (CGL2014-60849-JIN) project. J.A.M. was supported by the National Institute of Science and Technology for Climate Change Phase Phase 2 under CNPq Grant 465501/2014-1, and FAPESP Grants 2014/50848-9 and 2015/50122-0; the National Coordination for High Level Education and Training (CAPES) Grant 16/2014, and the Deutsche Forschungsgemeinschaft Grant DFG-GRTK 1740/2. This research was partially supported by Xunta de Galicia under project ED413C 2017/64 “Programa de Consolidación e Estructuración de Unidades de Investigación Competitivas (Grupos de Referencia Competitiva)” co-funded by European Regional Development Fund (FEDER). All the authors acknowledge the Water Journal by financing this publication.

**Conflicts of Interest:** The authors declare no conflicts of interest. The founding sponsors had no role in the design of the study; in the collection, analyses, or interpretation of data; in the writing of the manuscript, or in the decision to publish the results.

## References

1. Barthelm, R.B.; Charvet-Almeida, P.; Montag, L.F.A.; Lanna, A.E. *Amazon Basin, GIWA Regional Assessment 40b*; Printed and bound in Sweden by Sunds Tryck Öland AB; UNEP, University of Kalmar: Kalmar, Sweden, 2004.
2. Marengo, J.A. On the Hydrological Cycle of the Amazon Basin: A historical review and current state-of-the-art. *Rev. Bras. Meteorol.* **2006**, *21*, 1–19.
3. Drumond, A.; Marengo, J.; Ambrizzi, T.; Nieto, R.; Moreira, L.; Gimeno, L. The role of the Amazon Basin moisture in the atmospheric branch of the hydrological cycle: A Lagrangian analysis. *Hydrol. Earth Syst. Sci.* **2014**, *18*, 2577–2598. [[CrossRef](#)]
4. Marengo, J.A.; Ezpinoza, J.C. Extreme seasonal droughts and floods in Amazonia: Causes, trends and impacts. *Int. J. Climatol.* **2016**, *36*, 1033–1050. [[CrossRef](#)]
5. Marengo, J.A. Interannual Variability of Surface Climate in the Amazon Basin. *Int. J. Climatol.* **1992**, *12*, 853–863. [[CrossRef](#)]
6. Marengo, J.A. Interdecadal variability and trends of rainfall across the Amazon basin. *Theor. Appl. Climatol.* **2004**, *78*, 79–96. [[CrossRef](#)]
7. Marengo, J.A.; Liebmann, B.; Kousky, V.E.; Filizola, N.P.; Wainer, I.C. Onset and end of the rainy season in the Brazilian Amazon Basin. *J. Clim.* **2001**, *14*, 833–852. [[CrossRef](#)]
8. Yoon, J.-H.; Zeng, N. An Atlantic influence on Amazon rainfall. *Clim. Dyn.* **2010**, *34*, 249–264. [[CrossRef](#)]
9. Durán-Quesada, A.M.; Reboita, M.; Gimeno, L. Precipitation in tropical America and the associated sources of moisture: A short review. *Hydrol. Sci. J.* **2012**, *57*, 612–624. [[CrossRef](#)]
10. Satyamurty, P.; da Costa, C.P.W.; Manzi, A.O. Moisture source for the Amazon Basin: A study of contrasting years. *Theor. Appl. Climatol.* **2013**, *111*, 195–209. [[CrossRef](#)]
11. Salati, E.; Dall'Olio, A.; Matsui, E.; Gat, J.R. Recycling of water in the Amazon basin: An isotopic study. *Water Resour. Res.* **1979**, *15*, 1250–1258. [[CrossRef](#)]
12. Brubaker, K.L.; Entekhabi, D.; Eagleson, P.S. Estimation of continental precipitation recycling. *J. Clim.* **1993**, *6*, 1077–1089. [[CrossRef](#)]
13. Van der Ent, R.J.; Savenije, H.H.G.; Schaeffli, B.; Steele-Dunne, S.C. Origin and fate of atmospheric moisture over continents. *Water Resour. Res.* **2010**, *46*, W09525. [[CrossRef](#)]
14. Zemp, D.C.; Schleussner, C.F.; Barbosa, H.M.J.; van der Ent, R.J.; Donges, J.F.; Heinke, J.; Sampaio, G.; Rammig, A. On the importance of cascading moisture recycling in South America. *Atmos. Chem. Phys.* **2014**, *14*, 13337–13359. [[CrossRef](#)]
15. Eltahir, E.A.B.; Bras, R.L. Precipitation recycling in the Amazon basin. *Q. J. Roy. Meteorol. Soc.* **1994**, *120*, 861–880. [[CrossRef](#)]
16. Van der Ent, R.J.; Savenije, H.H.G. Length and time scales of atmospheric moisture recycling. *Atmos. Chem. Phys.* **2011**, *11*, 1853–1863. [[CrossRef](#)]
17. Van der Ent, R.J.; Wang-Erlandsson, L.; Keys, P.W.; Savenije, H.H.G. Contrasting roles of interception and transpiration in the hydrological cycle—Part 2: Moisture recycling. *Earth Syst. Dyn.* **2014**, *5*, 471–489. [[CrossRef](#)]

18. Marengo, J.A. Characteristics and spatio-temporal variability of the Amazon River Basin Water Budget. *Clim. Dyn.* **2005**, *24*, 11–22. [[CrossRef](#)]
19. Vera, C.; Baez, J.; Douglas, M.; Emmanuel, C.B.; Marengo, J.; Meitin, J.; Nicolini, M.; Nogues-Paegle, J.; Paegle, J.; Penalba, O.; et al. The South American low-level jet experiment. *Bull. Am. Meteorol. Soc.* **2006**, *87*, 63–77. [[CrossRef](#)]
20. Drumond, A.; Nieto, R.; Gimeno, L.; Ambrizzi, T. A Lagrangian identification of major sources of moisture over Central Brazil and La Plata Basin. *J. Geophys. Res.* **2008**, *113*, D14128. [[CrossRef](#)]
21. Arraut, J.M.; Satyamurty, P. Precipitation and water vapor transport in the Southern Hemisphere with emphasis on the South American region. *J. Appl. Meteorol. Climatol.* **2009**, *48*, 1902–1912. [[CrossRef](#)]
22. Arraut, J.M.; Nobre, C.; Barbosa, H.M.; Obregon, G.; Marengo, J. Aerial rivers and lakes: Looking at large-scale moisture transport and its relation to Amazonia and to subtropical rainfall in South America. *J. Clim.* **2012**, *25*, 543–556. [[CrossRef](#)]
23. Martinez, J.A.; Dominguez, F. Sources of Atmospheric Moisture for the La Plata River Basin. *J. Clim.* **2014**, *27*, 6737–6753. [[CrossRef](#)]
24. Bosilovich, M.G.; Chern, J. Simulation of Water Sources and Precipitation Recycling for the MacKenzie, Mississippi, and Amazon River Basins. *J. Hydrometeorol.* **2006**, *7*, 312–329. [[CrossRef](#)]
25. Stohl, A.; James, P. A Lagrangian analysis of the atmospheric branch of the global water cycle. Part II: Moisture transports between the Earth's ocean basins and river catchments. *J. Hydrometeorol.* **2005**, *6*, 961–984. [[CrossRef](#)]
26. Marengo, J.A.; Nobre, C.A.; Tomasella, J.; Cardoso, M.F.; Oyama, M.D. Hydro-climatic and ecological behaviour of the drought of Amazonia in 2005. *Philos. Trans. R. Soc. B* **2008**, *363*, 1773–1778. [[CrossRef](#)] [[PubMed](#)]
27. Marengo, J.A.; Tomasella, J.; Alves, L.M.; Soares, W.; Rodriguez, D.A. The drought of 2010 in the context of historical droughts in the Amazon region. *Geophys. Res. Lett.* **2011**, *38*, 1–5. [[CrossRef](#)]
28. Marengo, J.A.; Liebmann, B.; Grimm, A.M.; Misra, V.; Silva Dias, P.L.; Cavalcanti, I.F.A.; Carvalho, L.M.V.; Berbery, E.H.; Ambrizzi, T.; Vera, C.S.; et al. Review Recent developments on the South American monsoon system. *Int. J. Climatol.* **2012**, *32*, 1–21. [[CrossRef](#)]
29. Enfield, D.B. Relationships of inter-American rainfall to tropical Atlantic and Pacific SST variability. *Geophys Res Lett.* **1996**, *23*, 3305–3308. [[CrossRef](#)]
30. Cox, P.M.; Betts, R.A.; Collins, M.; Harris, P.P.; Huntingford, C.; Jones, C.D. Amazonian forest dieback under climate carbon cycle projections for the 21st century. *Theor. Appl. Climatol.* **2004**, *78*, 137–156. [[CrossRef](#)]
31. Betts, R.; Cox, P.; Collins, M.; Harris, P.; Huntingford, C.; Jones, C. The role of ecosystem-atmosphere interactions in simulated Amazonian precipitation decrease and forest dieback under global climate warming. *Theor. Appl. Climatol.* **2004**, *78*, 157–175. [[CrossRef](#)]
32. Spracklen, D.V.; Arnold, S.R.; Taylor, C.M. Observations of increased tropical rainfall preceded by air passage over forests. *Nature* **2012**, *489*, 282–285. [[CrossRef](#)] [[PubMed](#)]
33. Zemp, D.C.; Schleussner, C.; Barbosa, H.M.J.; Hirota, M.; Montade, V.; Sampaio, G.; Staal, A.; Wang-Erlandsson, L.; Rammig, A. Self-amplified Amazon forest loss due to vegetation–atmosphere feedbacks. *Nat. Commun.* **2017**, *8*, 14681. [[CrossRef](#)] [[PubMed](#)]
34. Ometto, J.P.; Sampaio, G.; Marengo, J.; Assis, T.; Tejada, G.; Aguiar, A.P. *Climate Change and Land Use Change in Amazonia*; Report for Global Canopy Programme and International Center for Tropical Agriculture as Part of the Amazonia Security Agenda Project; Global Canopy Programme: Oxford, UK, 2013.
35. Aragao, L.E.O.C.; Anderson, L.O.; Fonseca, M.G.; Rosan, T.M.; Vedovato, L.B.; Wagner, F.H.; Silva, C.V.J.; Junior, C.H.L.S.; Arai, E.; Aguiar, A.P.; et al. 21st Century drought-related fires counteract the decline of Amazon deforestation carbon emissions. *Nat. Commun.* **2018**, *9*, 536. [[CrossRef](#)] [[PubMed](#)]
36. Spracklen, D.V.; Garcia-Carreras, L. The impact of Amazonian deforestation on Amazon basin rainfall. *Geophys. Res. Lett.* **2015**, *42*, 9546–9552. [[CrossRef](#)]
37. Moore, N.; Arima, E.; Walker, R.; Da Silva, R. Uncertainty and changing hydroclimatology of the Amazon. *Geophys. Res. Lett.* **2007**, *34*, L12707. [[CrossRef](#)]
38. D'Almeida, C.; Vor smarty, C.J.; Hurtt, G.C.; Marengo, J.A.; Dingman, S.L.; Keim, B.D. The effects of deforestation on the hydrological cycle in Amazonia: A review on scale and resolution. *Int. J. Climatol.* **2007**, *27*, 633–647. [[CrossRef](#)]

39. Costa, M.H.; Foley, J.A. Trends in the hydrologic cycle of the Amazon Basin. *J. Geophys. Res.* **1999**, *104*, 14189–14198. [[CrossRef](#)]
40. Do Nascimento, M.G.; Herdies, D.L.; Oliveira de Souza, D. The South American Water Balance: The Influence of Low-Level Jets. *J. Clim.* **2016**, *29*, 1429–1449. [[CrossRef](#)]
41. Uvo, C.B.; Repelli, C.A.; Zebiak, S.E.; Kushnir, Y. The Relationships between Tropical Pacific and Atlantic SST and Northeast Brazil Monthly Precipitation. *J. Clim.* **1998**, *11*, 551–562. [[CrossRef](#)]
42. De Souza, E.B.; Kayano, M.T.; Tota, J.; Pezzi, L.; Fisch, G.; Nobre, C. On the influences of the El Niño, La Niña and Atlantic dipole pattern on the Amazonian rainfall during 1960–1998. *Acta Amazon.* **2000**, *30*, 305–318. [[CrossRef](#)]
43. Ronchail, J.; Cochonneau, G.; Molinier, M.; Guyot, J.; De Miranda Chaves, A.G.; Guimarães, V.; de Oliveira, E. Interannual rainfall variability in the Amazon basin and sea-surface temperatures in the equatorial Pacific and the tropical Atlantic Oceans. *Int. J. Climatol.* **2002**, *22*, 1663–1686. [[CrossRef](#)]
44. Gimeno, L. Grand challenges in atmospheric science. *Front. Earth Sci.* **2013**, *1*, 1–5. [[CrossRef](#)]
45. Marengo, J.; Nobre, C.; Tomasella, J.; Oyama, M.; de Oliveira, G.; de Oliveira, R.; Camargo, H.; Alves, L. The drought in Amazonia in 2005. *J. Clim.* **2008**, *21*, 495–516. [[CrossRef](#)]
46. Marengo, J.A.; Tomasella, J.; Soares, W.R.; Alves, L.M.; Nobre, C.A. Extreme climatic events in the Amazon basin. *Theor. Appl. Climatol.* **2012**, *107*, 73–85. [[CrossRef](#)]
47. Marengo, J.A.; Borma, L.S.; Rodriguez, D.A.; Pinho, P.; Soares, W.R.; Alves, L.M. Recent Extremes of Drought and Flooding in Amazonia: Vulnerabilities and human adaptation. *Am. J. Clim. Chang.* **2013**, *2*, 87–96. [[CrossRef](#)]
48. Espinoza, J.C.; Ronchail, J.; Guyot, J.L.; Junquas, C.; Drapeau, G.; Martinez, J.M.; Santini, W.; Vauchel, P.; Lavado, W.; Ordonez, J.; et al. From drought to flooding: Understanding the abrupt 2010–2011 hydrological annual cycle in the Amazonas River and tributaries. *Environ. Res. Lett.* **2012**, *7*, 024008. [[CrossRef](#)]
49. Dias de Paiva, R.C.; Buarque, D.C.; Collischonn, W.; Bonnet, M.-P.; Frappart, F.; Calmant, S.; Mendes, C.A.B. Large-scale hydrologic and hydrodynamic modeling of the Amazon River basin. *Water Resour. Res.* **2013**, *49*, 1226–1243. [[CrossRef](#)]
50. Furley, P.A. Tropical Forest of the Lowlands. In *The Physical Geography of South America*; Veblen, T.T., Young, K.R., Orme, A.R., Eds.; Oxford University Press: Oxford, UK, 2015; 448p, p. 136.
51. Figueroa, S.N.; Nobre, C.A. Precipitation distribution over central and western tropical South America. *Climanálise* **1990**, *5*, 36–45.
52. Da Silva Ferreira, D.B.; Barreiros de Souza, E.; Cavalcanti de Moraes, B.; Meira Filho, L.G. Spatial and Temporal Variability of Rainfall in Eastern Amazon during the Rainy Season. *Sci. World J.* **2015**, *2015*, 209783. [[CrossRef](#)] [[PubMed](#)]
53. Carvalho, L.M.V.; Jones, C.; Liebmann, B. The South Atlantic Convergence Zone: Intensity, Form, Persistence, and Relationships with Intraseasonal to Interannual Activity and Extreme Rainfall. *J. Clim.* **2004**, *17*, 88–108. [[CrossRef](#)]
54. Vieira, S.D.; Satyamurty, P.; Andreoli, R.V. On the South Atlantic Convergence Zone affecting southern Amazonia in austral summer. *Atmos. Sci. Lett.* **2013**, *14*, 1–6. [[CrossRef](#)]
55. Raia, A.; Cavalcanti, I.F.D.A. The Life Cycle of the South American Monsoon System. *J. Clim.* **2008**, *21*, 6227–6246. [[CrossRef](#)]
56. Wang, H.; Fu, R. Cross-equatorial flow and seasonal cycle of precipitation over South America. *J. Clim.* **2002**, *15*, 1591–1608. [[CrossRef](#)]
57. Carvalho, L.M.V.; Silva, A.E.; Jones, C.; Liebmann, B.; Silva Dias, P.L.; Rocha, H.R. Moisture transport and intraseasonal variability in the South America monsoon system. *Clim. Dyn.* **2011**, *36*, 1865–1880. [[CrossRef](#)]
58. Lenters, J.D.; Cook, K.H. On the Origin of the Bolivian High and Related Circulation Features of the South American Climate. *J. Atmos. Sci.* **1997**, *54*, 656–677. [[CrossRef](#)]
59. Andreoli, R.V.; Ferreira de Souza, R.A.; Kayano, M.T.; Candido, L.A. Seasonal anomalous rainfall in the central and eastern Amazon and associated anomalous oceanic and atmospheric patterns. *Int. J. Climatol.* **2012**, *32*, 1193–1205. [[CrossRef](#)]
60. Espinoza, J.C.; Marengo, J.A.; Ronchail, J.; Molina Carpio, J.; Noriega Flores, L.; Loup Guyot, J. The extreme 2014 flood in south-western Amazon basin: The role of tropical-subtropical South Atlantic SST gradient. *Environ. Res. Lett.* **2014**, *9*, 124007. [[CrossRef](#)]

61. Yoon, J.-H. Multi-model analysis of the Atlantic influence on southern Amazon rainfall. *Atmos. Sci. Lett.* **2016**, *17*, 122–127. [[CrossRef](#)]
62. COLA: The Center for Ocean-Land-Atmosphere Studies. Available online: <http://cola.gmu.edu/wcr/river/Niger.png> (accessed on 2 April 2018).
63. Jiménez-Muñoz, J.C.; Mattar, C.; Barichivich, J.; Santamaria-Artigas, A.; Takahashi, K.; Malhi, Y.; Sobrino, J.A.; Schrier, G.V.D. Record-breaking warming and extreme drought in the Amazon rainforest during the course of El Niño 2015–2016. *Sci. Rep.* **2016**, *6*, 33130. [[CrossRef](#)] [[PubMed](#)]
64. Stohl, A.; James, P. A Lagrangian analysis of the atmospheric branch of the global water cycle. Part I: Method description, validation, and demonstration for the August 2002 flooding in central Europe. *J. Hydrometeorol.* **2004**, *5*, 656–678. [[CrossRef](#)]
65. Numaguti, A. Origin and recycling processes of precipitating water over the Eurasian continent: Experiments using an atmospheric general circulation model. *J. Geophys. Res.* **1999**, *104*, 1957–1972. [[CrossRef](#)]
66. Drumond, A.; Nieto, R.; Gimeno, L. A Lagrangian approach for investigating anomalies in the moisture transport during drought episodes. *Cuad. Investig. Geogr.* **2016**, *42*, 113–125. [[CrossRef](#)]
67. Ciric, D.; Stojanovic, M.; Drumond, A.; Nieto, R.; Gimeno, L. Tracking the Origin of Moisture over the Danube River Basin Using a Lagrangian Approach. *Atmosphere* **2016**, *7*, 162. [[CrossRef](#)]
68. Sorí, R.; Nieto, R.; Vicente-Serrano, S.M.; Drumond, A.; Gimeno, L. A Lagrangian perspective of the hydrological cycle in the Congo River basin. *Earth Syst. Dyn.* **2017**, *8*, 653–675. [[CrossRef](#)]
69. Gimeno, L.; Drumond, A.; Nieto, R.; Trigo, R.M.; Stohl, A. On the origin of continental precipitation. *Geophys. Res. Lett.* **2010**, *37*, L13804. [[CrossRef](#)]
70. Sun, B.; Wang, H. Analysis of the major atmospheric moisture sources affecting three sub-regions of East China. *Int. J. Climatol.* **2015**, *35*, 2243–2257. [[CrossRef](#)]
71. Salih, A.A.M.; Zhang, Q.; Tjernström, M. Lagrangian tracing of Sahelian Sudan moisture sources. *J. Geophys. Res. Atmos.* **2015**, *120*, 6793–6808. [[CrossRef](#)]
72. Vázquez, M.; Nieto, R.; Drumond, A.; Gimeno, L. Extreme Sea Ice Loss over the Arctic: An Analysis Based on Anomalous Moisture Transport. *Atmosphere* **2017**, *8*, 32. [[CrossRef](#)]
73. Dee, D.P.; Uppala, S.M.; Simmons, A.J.; Berrisford, P.; Poli, P.; Kobayashi, S.; Andrae, U.; Balmaseda, M.A.; Balsamo, G.; Bauer, P.; et al. The ERA-Interim reanalysis: Configuration and performance of the data assimilation system. *Q. J. R. Meteorol. Soc.* **2011**, *137*, 553–597. [[CrossRef](#)]
74. Uppala, S.; Dee, D.; Kobayashi, S.; Berrisford, P.; Simmons, A. Towards a climate data assimilation system: Status update of ERA-Interim. *ECMWF Newsletter*. **2008**, *115*, 12–18.
75. Betts, A.K.; Köhler, M.; Zhang, Y. Comparison of river basin hydrometeorology in ERA-Interim and ERA-40 reanalyses with observations. *J. Geophys. Res.* **2009**, *114*, D02101. [[CrossRef](#)]
76. De Almeida, V.A.; Marton, E.; Nunes, A.M.B. Assessing the ability of three global reanalysis products to reproduce South American monsoon precipitation. *Atmósfera* **2018**, *31*, 1–10. [[CrossRef](#)]
77. Liebmann, B.; Camargo, S.J.; Seth, A.; Marengo, J.A.; Carvalho, L.M.; Allured, D.; Fu, R.; Vera, C.S. Onset and End of the Rainy Season in South America in Observations and the ECHAM 4.5 Atmospheric General Circulation Model. *J. Clim.* **2007**, *20*, 2037–2050. [[CrossRef](#)]
78. Liebmann, B.; Marengo, J. Interannual Variability of the Rainy Season and Rainfall in the Brazilian Amazon Basin. *J. Clim.* **2001**, *14*, 4308–4318. [[CrossRef](#)]
79. Noska, R.; Misra, V. Characterizing the onset and demise of the Indian summer monsoon. *Geophys. Res. Lett.* **2016**, *43*, 4547–4554. [[CrossRef](#)]
80. Chris, F.; Peterson, P.; Landsfeld, M.; Pedreros, D.; Verdin, J.; Shukla, S.; Husak, G.; Rowland, J.; Harrison, L.; Hoell, A.; et al. The climate hazards infrared precipitation with stations—A new environmental record for monitoring extremes. *Sci. Data* **2015**, *2*, 150066. [[CrossRef](#)]
81. Kousky, V.E. Pentad outgoing longwave radiation climatology for the South American sector. *Rev. Bras. Meteorol.* **1988**, *3*, 217–231.
82. González, M.; Vera, C.S.; Liebmann, B.; Marengo, J.A.; Kousky, V.; Allured, D. The nature of the rainfall onset over central South America. *Atmósfera* **2007**, *20*, 377–394.
83. Garcia, S.R.; Kayano, M.T. Determination of the onset dates of the rainy season in central Amazon with equatorially antisymmetric outgoing longwave radiation. *Theor. Appl. Climatol.* **2009**, *97*, 361–372. [[CrossRef](#)]

84. Garcia, S.R.; Kayano, M.T. Some considerations on onset dates of the rainy season in Western-Central Brazil with antisymmetric outgoing longwave radiation relative to the equator. *Int. J. Climatol.* **2013**, *33*, 188–198. [[CrossRef](#)]
85. Dos Santos, L.F.; Garcia, S.R. Início e Fim da Estação Chuvosa no Estado de Minas Gerais: Comparação de Duas Metodologias Diferentes. *Rev. Bras. Meteorol.* **2016**, *31*, 92–104. [[CrossRef](#)]
86. Liebmann, B.; Smith, C.A. Description of a Complete (Interpolated) Outgoing Longwave Radiation Dataset. *Bull. Am. Meteorol. Soc.* **1996**, *77*, 1275–1277.
87. Vicente-Serrano, S.M.; Beguería, S.; López-Moreno, J.I. A Multiscalar Drought Index Sensitive to Global Warming: The Standardized Precipitation Evapotranspiration Index. *J. Clim.* **2010**, *23*, 1696–1718. [[CrossRef](#)]
88. McKee, T.B.; Doesken, N.J.; Kleist, J. The relationship of drought frequency and duration to time scales. In Proceedings of the Eighth Conference on Applied Climatology, Anaheim, CA, USA, 17–22 January 1993; pp. 179–184.
89. Harris, I.; Jones, P.D.; Osborn, T.J.; Lister, D.H. Updated high-resolution grids of monthly climatic observations—The CRU TS3.10 Dataset. *Int. J. Climatol.* **2014**, *34*, 623–642. [[CrossRef](#)]
90. Spinoni, J.; Naumann, G.; Carrao, H.; Barbosa, P.; Vogt, J. World drought frequency, duration, and severity for 1951–2010. *Int. J. Climatol.* **2014**, *34*, 2792–2804. [[CrossRef](#)]
91. Spinoni, J.; Vogt, J.V.; Naumann, G.; Barbosa, P.; Dosio, A. Will drought events become more frequent and severe in Europe? *Int. J. Climatol.* **2018**, *38*, 1718–1736. [[CrossRef](#)]
92. Tan, C.; Yang, J.; Li, M. Temporal-Spatial Variation of Drought Indicated by SPI and SPEI in Ningxia Hui Autonomous Region, China. *Atmosphere* **2015**, *6*, 1399–1421. [[CrossRef](#)]
93. Stojanovic, M.; Drumond, A.; Nieto, R.; Gimeno, L. Moisture Transport Anomalies over the Danube River Basin during Two Drought Events: A Lagrangian Analysis. *Atmosphere* **2017**, *8*, 193. [[CrossRef](#)]
94. Stojanovic, M.; Drumond, A.; Nieto, R.; Gimeno, L. Anomalies in Moisture Supply during the 2003 Drought Event in Europe: A Lagrangian Analysis. *Water* **2018**, *10*, 467. [[CrossRef](#)]
95. SO HYBAM. The Observation Service (formerly Environmental Research Observatory). Available online: <http://www.ore-hybam.org/> (accessed on 10 December 2017).
96. Smith, C.A.; Sardeshmukh, P. The Effect of ENSO on the Intraseasonal Variance of Surface Temperature in Winter. *Int. J. Climatol.* **2000**, *20*, 1543–1557. [[CrossRef](#)]
97. Espinoza, J.C.; Ronchail, J.; Guyot, J.L.; Cochonneau, G.; Naziano, F.; Lavado, W.; de Oliveira, E.; Pombosa, R.; Vauchel, P. Spatio-temporal rainfall variability in the Amazon Basin countries (Brazil, Peru, Bolivia, Colombia and Ecuador). *Int. J. Climatol.* **2009**, *29*, 1574–1594. [[CrossRef](#)]
98. Getirana, A.C.; Dutra, E.; Guimberteau, M.; Kam, J.; Li, H.; Decharme, B.; Zhang, Z.; Ducharne, A.; Boone, A.; Balsamo, G.; et al. Water Balance in the Amazon Basin from a Land Surface Model Ensemble. *J. Hydrometeorol.* **2014**, *15*, 2586–2614. [[CrossRef](#)]
99. Gloor, M.; Brienen, R.J.W.; Galbraith, D.; Feldpausch, T.R.; Schöngart, J.; Guyot, J.-L.; Espinoza, J.C.; Lloyd, J.; Phillips, O.L. Intensification of the Amazon hydrological cycle over the last two decades. *Geophys. Res. Lett.* **2013**, *40*, 1729–1733. [[CrossRef](#)]
100. Maeda, E.E.; Ma, X.; Wagner, F.H.; Kim, H.; Oki, T.; Eamus, D.; Huete, A. Evapotranspiration seasonality across the Amazon Basin. *Earth Syst. Dyn.* **2017**, *8*, 439–454. [[CrossRef](#)]
101. Frappart, F.F.P.; Famiglietti, J.S.; Prigent, C.; Rossow, W.B.; Seyler, F. Interannual variations of river water storage from a multiple satellite approach: A case study for the Rio Negro River basin. *J. Geophys. Res.* **2008**, *113*, D21104. [[CrossRef](#)]
102. Melesse, A.M.; Abtew, W. *Landscape Dynamics, Soils and Hydrological Processes in Varied Climates*; Springer International Publishing: Basel, Switzerland, 2015; 839p, ISBN1 3319187872. ISBN2 9783319187877.
103. Dirmeyer, P.A.; Brubaker, K.L. Characterization of the Global Hydrologic Cycle from a Back-Trajectory Analysis of Atmospheric Water Vapor. *J. Hydrometeorol.* **2007**, *8*, 20–37. [[CrossRef](#)]
104. Trenberth, K.E. Atmospheric Moisture Recycling: Role of Advection and Local Evaporation. *J. Clim.* **1999**, *12*, 1368–1380. [[CrossRef](#)]
105. Sorí, R.; Nieto, R.; Drumond, A.; Vicente-Serrano, S.M.; Gimeno, L. The atmospheric branch of the hydrological cycle over the Indus, Ganges, and Brahmaputra river basins. *Hydrol. Earth Syst. Sci.* **2017**, *21*, 6379–6399. [[CrossRef](#)]

106. Wright, J.S.; Fu, R.; Worden, J.R.; Chakraborty, S.; Clinton, N.E.; Risi, C.; Sun, Y.; Yin, L. Rainforest-initiated wet season onset over the southern Amazon. *Proc. Natl. Acad. Sci. USA* **2017**, *114*, 8481–8486. [[CrossRef](#)] [[PubMed](#)]
107. Dos Santos, S.R.Q.; Braga, C.C.; Sansigolo, C.A.; de Araujo Ti-burtino Neves, T.T.; dos Santos, A.P.P. Droughts in the Amazon: Identification, Characterization and Dynamical Mechanisms Associated. *Am. J. Clim. Chang.* **2017**, *6*, 425–442. [[CrossRef](#)]
108. Pampuch, L.A.; Drumond, A.; Gimeno, L.; Ambrizzi, T. Anomalous patterns of SST and moisture sources in the South Atlantic Ocean associated with dry events in southeastern Brazil. *Int. J. Clim.* **2016**, *36*, 4913–4928. [[CrossRef](#)]
109. Grimm, A.M.; Tedeschi, R.G. ENSO and Extreme Rainfall Events in South America. *J. Clim.* **2009**, *22*, 1589–1609. [[CrossRef](#)]
110. Foley, J.A.; Botta, A.; Coe, M.T.; Costa, M.H. El Niño–Southern oscillation and the climate, ecosystems and rivers of Amazonia. *Glob. Biogeochem. Cycles* **2002**, *16*, 79–1–79–20. [[CrossRef](#)]



© 2018 by the authors. Licensee MDPI, Basel, Switzerland. This article is an open access article distributed under the terms and conditions of the Creative Commons Attribution (CC BY) license (<http://creativecommons.org/licenses/by/4.0/>).

Article

# The Niger River Basin Moisture Sources: A Lagrangian Analysis

Rogert Sorí <sup>1,\*</sup>, Raquel Nieto <sup>1,2</sup>, Anita Drumond <sup>1</sup> and Luis Gimeno <sup>1</sup>

<sup>1</sup> Environmental Physics Laboratory (EPhysLab), Facultad de Ciencias, Universidade de Vigo, Ourense 32004, Spain; rnieto@uvigo.es (R.N.); anitadru@uvigo.es (A.D.); l.gimeno@uvigo.es (L.G.)

<sup>2</sup> Department of Atmospheric Sciences, Institute of Astronomy, Geophysics and Atmospheric Sciences, University of São Paulo, São Paulo 05508-090, Brazil

\* Correspondence: rogert.sori@uvigo.es; Tel.: +34-988-387-208

Academic Editor: Anthony R. Lupo

Received: 23 November 2016; Accepted: 9 February 2017; Published: 14 February 2017

**Abstract:** The Niger River basin (NRB) is located in the important climatic region of the African Sahel. In this study we use the Lagrangian tridimensional model FLEXPART v9.0 to identify and characterise the moisture sources for the NRB. This method allows the integration of the budget of evaporation minus precipitation over 10-day backward trajectories, thereby identifying the origins of the air masses residing over the NRB. The analysis was performed for the 35-year period from 1980 to 2014, which allowed us to identify the main semi-annual climatological moisture sources of the NRB, for November–April (NDJFMA) (dry season) and May–October (MJJASO) (wet season), and to quantify the respective moisture uptakes. Throughout the year, the NRB main moisture sources are located on the tropical eastern North Atlantic Ocean near Africa, the tropical eastern South Atlantic Ocean in the Gulf of Guinea, in the regions surrounding the Sahel and in the Mediterranean Sea. The extents of these sources vary between dry and wet seasons. In NDJFMA two regions appear in the east of the basin, which then join up, forming a larger source to the northeast of the basin in MJJASO, when three other less important moisture sources can be seen in central-equatorial Africa, the tropical western Indian Ocean and the Persian Gulf. In NDJFMA the majority of the moisture uptake comes from the NRB itself but then, later in MJJASO, when the precipitation increases over the basin the greatest uptake of moisture occurs over the tropical eastern South Atlantic Ocean, northeast Africa and the NRB, which suggests that these are the effective sources of precipitation in the basin in overall terms. The seasonal moisture uptake quantification over the moisture sources of the NRB, reveals that largest fraction of moisture income to the basin from outside its boundaries. Despite providing moisture to the NRB the source located in the tropical eastern North Atlantic Ocean does not contribute that much to precipitation in the basin. A daily (ten-day) backward analysis shows the importance of the moisture uptake within the NRB and from near moisture sources during the first few (backward) days, while the Atlantic Ocean sources and the Mediterranean became more important during the last five (backward) days of the analysis.

**Keywords:** moisture sources; Lagrangian analysis; Niger River basin

## 1. Introduction

Several authors have investigated the moisture sources for precipitation in the Sahel and West Africa (WA) by using a range of different methods. Rainfall over any area of land has two possible sources: water vapour advected into the region from the surrounding areas, and that which is supplied by evaporation from within the same region [1]. The identification of mechanisms and sources of moisture responsible for the precipitation regimes is crucial for the understanding of the global hydrological cycle and for improving the predictive power of numerical models [2]. In fact, the

identification of moisture sources as part of the analysis of extreme events has become a major research area (e.g., for flooding and droughts), but it is also increasingly important for regional and global climatic assessments, including paleoclimatic reconstructions and future climate change scenarios [3].

Differences in Sahelian precipitation rate are primarily a consequence of the contrasting circulation, together with recycling of local evaporation and moisture advected from the tropical North Atlantic Ocean and the Gulf of Guinea [4]. Evaporation in the tropical Atlantic Ocean, WA, and Central Africa (CA) contribute about 23%, 27%, and 17% of the total rainfall in WA [1]. Precipitation recycling is defined as the contribution of local evaporation to local precipitation [5]. Utilizing a Lagrangian method, Nieto et al. [6] investigated the moisture sources for the African Sahel in five-year period (2000–2004), confirming recycling as the dominant moisture source over the Sahel. Through a quasi-isentropic back-trajectory scheme Dirmeyer et al. [7] also obtained that terrestrial evaporative source that supplied the water for precipitation is dominant in this region.

Results of van der Ent et al. [8], using a moisture recycling approach to study the complete process of continental moisture feedback also demonstrated that the Sahel region receives its moisture from three large water bodies: the Mediterranean Sea, the South Atlantic Ocean, and the Indian Ocean, and on average about 50% to 60% of the precipitation originates from continental evaporation. The same technique, based in a water accounting model of 2-D moisture tracing and 3-D moisture tracing was implemented by Keys et al. [9,10], respectively, confirming that land surface plays a dominant role in mediating variability in moisture recycling processes for the sink region of the West Sahel. Nevertheless, evaporative source regions for precipitation in the nearby located western Sahel can probably not be diagnosed adequately using the 2-D approximation due to the strong generation of vertical inhomogeneities by surface evaporation and by directional shear [11]. On the other hand, in a recent study Arnault et al. [12] describe how local evaporation in WA is not the dominant factor controlling local precipitation over this region. These authors implemented a set of two methods (tracking of tagged atmospheric water species originating from evaporation in a source region, i.e., E-tagging, and three-dimensional budgets of total and tagged atmospheric water species) developed in the weather research and forecasting (WRF) model for investigating regional precipitation recycling mechanisms. They observed that locally-evaporated water was mainly transported outside of the target domain at the lower levels. Specifically for the Niger River basin (NRB), Stohl and James. [13] utilized a Lagrangian approach for a five-year period (1999–2003), finding that about half of the moisture provided to it originates from the Atlantic Ocean and half originates from the land (including from the NRB itself). There is also a climatology of evaporative moisture sources for the NRB, as well as their seasonal variations and mean contributions in a period of 25 years available online [14]. These results were obtained through the quasi-isentropic back-trajectory scheme utilized by Dirmeyer et al. [7], and reveal the importance of the basin itself and surrounded Sahel regions providing moisture to the basin [14]. A comparison of different methodologies to study the source-receptor relationships have been provided by Gimeno et al. [3].

As discussed, studies of moisture source identification and atmospheric transport mechanisms are fundamental for understanding the nature of the precipitation. Studies of climate variability in WA show the seasonal rainfall migration during the boreal summer [15,16] and a reduction in accumulated rainfall over the last century [17–20]. These phenomena have affected stream discharges and both are considered a partial feedback of the land-cover degradation in the watershed [21]. A review of recent studies of rainfall regime in the West African Sahel by Nicholson [22] shows some recovery since the extreme dry episodes of the 1970s and 1980s, but also certain changes in the rainfall regime, such as less spatial coherence and less temporal persistence. Investigations of the moisture sources of the NRB has become particularly important if we consider that the total population of the basin is about 130 million, 70% of whom live in rural areas [23] and most of them, as well as the economies of countries in the NRB rely mainly on agriculture, pastoral systems, crop-livestock systems and fishing [24]. This work aims to perform a climatological study to identify the moisture sources of the NRB, but take into account a longer period of time, as well as consider variations of the sources between dry and rainy seasons

in the basin. Likewise, the purpose is to emphasize on the role of each source and the NRB itself providing moisture to the basin. The results will support new climatic and hydrological research in the NRB. Particularly, they will strengthen the knowledge for understanding the mechanisms associated with the rainfall variability and the occurrence of extreme weather events in this basin.

## 2. Study Area

The Niger River basin (NRB) is located in West Africa (WA) along the Sahel region (Figure 1). It is shared by nine countries and, at 4200 km in length, the Niger River itself is the third longest in Africa after the Nile and the Congo/Zaire. The Sahel is a transition zone between the Sahara desert and the wet climate of tropical Africa [25], giving the basin contrasting climatic conditions that mainly vary with latitude. According to the climatic classification of L'Hôte and Mahé [26] for WA based on annual rainfall, the NRB experiences five climatic zones with a gradual variation between deserts (arid) in the north, to transitional equatorial in the south. The mean annual precipitation ranges from less than 50 mm/year in the northern part of the basin in Algeria, increasing southwards to more than 2000 mm/year close to the river mouth in the Guinean coastal zone [27]. In WA the mean annual cycle of precipitation, is characterised by minimum values at the beginning of the year that increase month by month, reaching a peak in August, to later decrease until December [28].

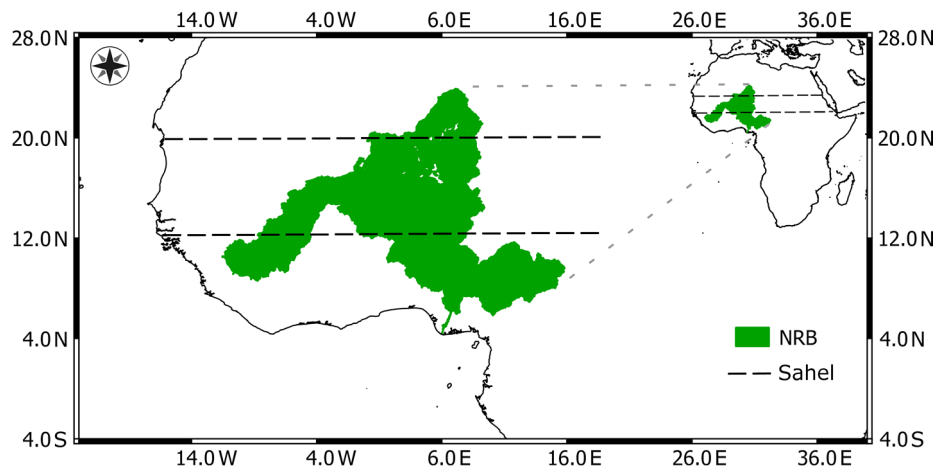


**Figure 1.** Geographical location of the Niger River Basin (green area) in West Africa.

For WA some authors consider the rainy season to be the period May–October, and the dry season to be November–April [29,30]. In fact, the maximum precipitation rate occurs from May–October and the minimum during November–April [28]. However, Andersen et al. [27] consider the periods June–November and December–May as wet and dry seasons in the basin, while Liebmann et al. [15] argue that the southern coast of WA experiences a wet season beginning in early March and its duration decreasing latitudinally to the north. During the boreal summer, an intense heat low develops over the Western Sahara [22]. This is termed the Saharan heat low (SHL) and it is the thermal response of the lower troposphere over the northern African continent to seasonal surface warming [31]. The SHL plays a pivotal role in the West African Monsoon (WAM) system in spring and summer [32]. It controls the zonal circulation of the lower half of the troposphere, particularly the westerly component of the monsoon winds and with the anticyclonic circulation around 600 hPa at the top of the heat low, it controls the speed of the African Easterly Jet (AEJ) [33]. The monsoon is longer and wetter in the southern part of the NRB [34]. In the dry season, under the influence of the Saharan high-pressure zone, the northeastward Harmattan wind brings hot, dry air and high temperatures, which last longer in the north of the basin [27].

The observed annual average precipitation varied over the period 1951–2010 over Africa, showing negative trends in some parts of the NRB [17]. The major circulation features associated with the

variability of the rainfall in the Sahel at interannual and decadal time scales are the upper-level Tropical Easterly Jet, the mid-level African Easterly Jet, and the Saharan heat low; a correlation with the intensity of the Intertropical Convergence Zone (ITCZ) (as defined by rainfall intensity) is also apparent [22]. A schematic overview of the basic surface circulation is depicted in Figure 2. It shows the sea level pressure (SLP) and winds at 1000 mb in North Africa for the seasons under study, November–April and May–October. In the dry season, high pressures observed in the north of Africa decrease with latitude and, as a result, winds flow from the northeast over the NRB towards the south, and there is a confluence of winds with those flowing from the southwest (Figure 2a). In the wet season, the surface southerly monsoon onshore flow penetrates through the rain band over the entire seasonal cycle, while the depth of the southerly surface monsoon flow undergoes some seasonal variation, being highest during the peak of the monsoon [35]. This is shown in Figure 2b: low pressures extend from the east to the West of Africa between 10° N and 25° N approximately, and winds flowing from the south turn from a southwesterly direction after crossing the equator and are dominant in the major part of the NRB until they reach its northern part, where the confluence is now located due to the weakening effect of the winds from the northeast.

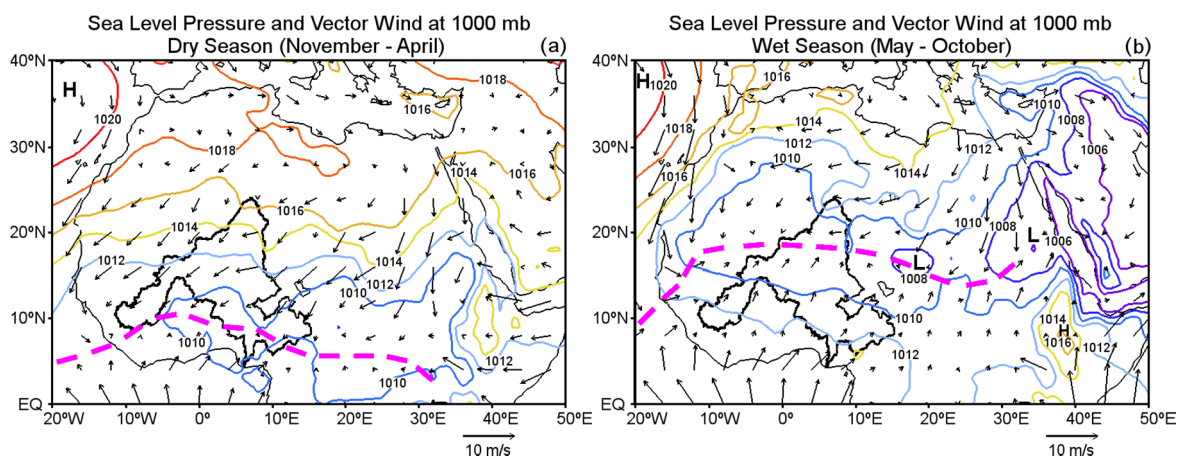


**Figure 2.** Climatological schematic diagram of mean sea level pressure (colour contours, in mb) and winds (arrows, in m/s) at 1000 mb from ERA-Interim, for the period 1980–2014 during NDJFMA (a) and MJJASO (b). The discontinued magenta line represents the confluence of winds and the black contour in West Africa indicates the boundary of the NRB.

### 3. Experiments Section

#### 3.1. Method

In this study we applied the Lagrangian particle dispersion model FLEXPART v9.0 developed by Stohl and James [13,36]. The model considers the atmosphere divided homogeneously into three-dimensional finite elements (hereafter “parcels”) over the entire globe, each representing a fraction of the total atmospheric mass [36]. This allows variations in atmospheric moisture to be obtained along backward and forward trajectories of air parcels, permitting the establishment of meaningful source-receptor relationships. In our case, a backward analysis was performed using parcels residing over the NRB, limiting the transport time to 10 days in accordance with the average residence time of water vapour in the atmosphere [37]. This way, the rate of moisture increase (through evaporation from the environment,  $e$ ) or decrease (through precipitation,  $p$ ) along the trajectory of the parcels can be calculated by changes to the specific humidity ( $q$ ) over time ( $t$ ) by Equation (1), assuming a constant mass ( $m$ ) of the particles:

$$(e - p) = m(dq/dt) \quad (1)$$

It is possible to obtain the moisture changes of all parcels in the atmospheric column over an area, obtaining the surface freshwater flux, hereafter denoted  $(E - P)$ . Nevertheless,  $q$  fluctuations along individual trajectories can occur for nonphysical reasons (e.g., because of  $q$  interpolation or trajectory errors); a limitation partly compensated among the many particles in an atmospheric column over the target area. More details about this method have been provided by Stohl and James [13,36].  $(E - P)$  is obtained from the sum of the  $(e - p)$  associated with all the particles present in the atmospheric column over the NRB. Recalling that  $(e - p)$  is proportional to the temporal variations of  $q$  in a particle during the 6-h interval. The  $(E - P)$  sign then would correspond to the prevailing  $(e - p)$  conditions associated with the particles observed in that atmospheric column during a given time interval. A region is then considered as a moisture source when  $(E - P) > 0$ , i.e., the net moisture budget of the particles tracked is favourable to the evaporation from the environment into the particles. The opposite occurs in a moisture sink, i.e., a region in which the moisture budget associated is favourable to the moisture loss by the tracked particles to the environment. For this work, to identify the moisture sources we calculated the budget of  $(E - P)$  integrated over 10 days (the mean residence time of the water vapour in the global atmosphere), meaning that  $(E - P) > 0$  or  $(E - P) < 0$  values are the result of the integrated daily  $(E - P)$  values over the 10 days. The regions in which prevailed  $(E - P) > 0$  conditions during the 10 day-period are considered moisture sources, while regions where particles lose humidity ( $(E - P) < 0$ ) are considered moisture sinks.

FLEXPART has been applied in the pursuit of similar goals in several regions of the world, including the Sahel [6], the Sahelian Sudan [38], the Orinoco River Basin [39], China [40], the Amazon River Basin [41], and several continental regions [42].

The budget of  $(E - P)$  was calculated for two semi-annual climatological periods, from November to April (NDJFMA) and from May to October (MJJASO), considered to represent the dry and rainy seasons, respectively. For both seasons the backward analysis was implemented from 1 to 10 days, and the results were then integrated over the 10 days ( $(E - P)i10$ ) to define the climatological moisture sources.

A percentile criterion was applied to the  $(E - P)i10$  field to define a threshold delimiting the spatial extent of the respective sources of moisture. The 90th percentile delimits those regions where the air masses were likely to have picked up a large amount of moisture on their transit towards the target region. In other words, the 90th percentile criteria would show the 10% grid points with the highest positive  $(E - P)i10$  values in the map. This criterion has been applied for similar purposes in Drumond et al. [41], Drumond et al. [43], and Drumond et al. [44]. The NRB itself was considered a moisture source area.

### 3.2. Data

The analyses were carried out using 35 years of data (1980–2014), ensuring that climatological results were obtained. The Lagrangian model FLEXPART is forced by the ERA Interim reanalysis datasets [45] available at 6 h intervals (00, 06, 12, and 18 UTC) at a resolution of  $1^\circ \times 1^\circ$  with 60 model layers with the top of the atmosphere located at 0.1 hPa. The ERA-Interim reanalysis achieved good progress with respect to data assimilation problems previously encountered in ERA-40, mostly related to the use of satellite data, resulting in an improved representation of the hydrological cycle, a more realistic stratospheric circulation, and better temporal consistency on a range of time-scales [45].

Datasets of precipitation in the basin from the Climatic Research Unit (CRU 3.23TS) [46] were used to calculate the annual cycle of precipitation in the NRB. This datasets available with a resolution of  $0.5^\circ \times 0.5^\circ$  were constructed from monthly observations at meteorological stations across the world's land areas [46]. To calculate the Vertically Integrated Moisture Flux (VIMF) we used datasets of the vertical integral of the eastward and northward water vapour flux from the ERA-Interim reanalysis [45] at a resolution of  $1^\circ \times 1^\circ$ .

#### 4. Results and Discussion

##### 4.1. Backward Analysis of ( $E - P$ )

The seasonal budget of ( $E - P$ ) backward-integrated using FLEXPART for the NRB from  $-1$  to  $-10$  days for the dry and wet seasons is shown in Figure 3. Areas where ( $E - P$ )  $> 0$  are considered evaporative regions and, thus, moisture sources, while regions where ( $E - P$ )  $< 0$  are moisture sinks. Over these regions is evident that the number of trajectories that coincide is high. This analysis makes it possible to identify those areas where air masses tracked backwards from the NRB take up humidity. Additionally, worth mentioning is that moisture sink regions (bluish colours) in Figure 3 could also act as moisture sources, since local evaporation could end up as precipitation over themselves or other regions. However, here FLEXPART has been used to compute the budget of ( $E - P$ ) just on air masses tracked backward in time from the NRB, thus representing the net freshwater flux into the air masses traveling to the target basin.

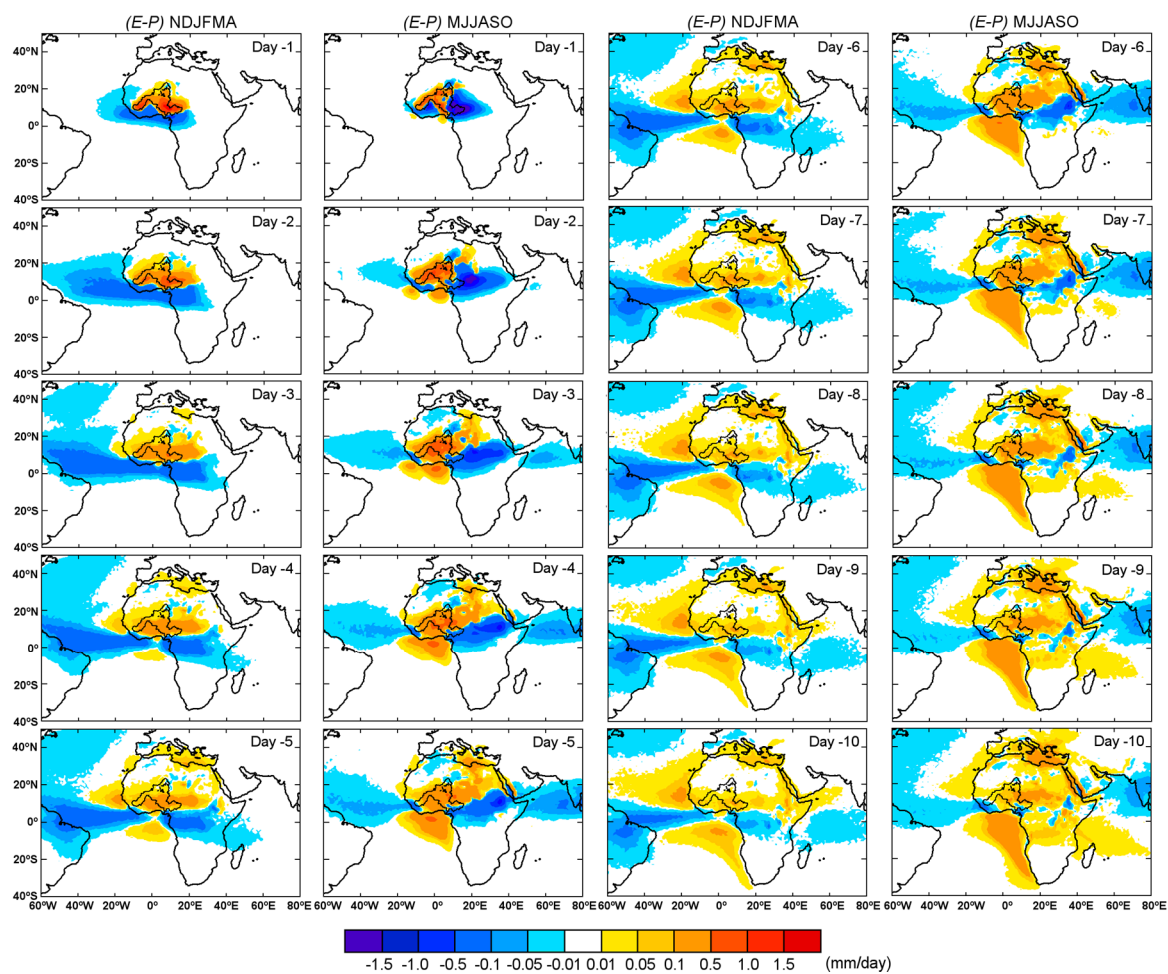


**Figure 3.** Seasonal pattern of ( $E - P$ ) backward-integrated from the Niger River Basin for days  $-1$  to  $-10$ , for dry (NDJFMA) and wet (MJJASO) seasons.

For both periods at one day backwards in time (day  $-1$ ) the NRB mainly acts as its own moisture source, but in MJJASO the eastern part of the basin and the Sahel regions that lie mostly to the east and south of the NRB act as moisture sinks, suggesting convective precipitation that typically occurs in air masses in transit to the Sahel [6]. At days 2 and 3 back in time (days  $-2$  to  $-3$ ) the pattern of ( $E - P$ ) is characterised by positive values remaining over the NRB and extending across the Sahel and North Africa, although they are also observed for MJJASO over the Gulf of Guinea in the wet

season. For these days, areas of  $(E - P) < 0$  are distributed throughout equatorial Africa and the Atlantic Ocean, but they are displaced further south in NDJFMA when the ITCZ moves to the summer hemisphere [22]. At days  $-4$  and  $-5$  the spatial pattern of  $(E - P)$  expands and both the NRB and the Sahel remain as moisture sources. The east-equatorial South Atlantic Ocean (covering the Gulf of Guinea) and the Mediterranean Sea are now moisture sources and persist throughout the remaining days of the analysis, although according to Schicker et al. [47] the western part of North Africa receives less Mediterranean rainwater than Northeast and Central Africa. Particularly on these days, the tropical-east North Atlantic Ocean becomes a much expanded moisture source in NDJFMA. For these, and all preceding days, it is commonly observed that regions where parcels lose moisture to the atmosphere before reaching the NRB are more intense around the equatorial Atlantic Ocean, Central Africa, and the Arabian Sea.

Regarding the source regions, the greatest differences observed between the  $(E - P) > 0$  areas for NDJFMA and MJJASO may be seen clearly between  $-5$  to  $-10$  days in the tropical east North Atlantic Ocean. In MJJASO the positive values in the spatial pattern are confined to the African coast but in NDJFMA they are propagated to the west until reach the Caribbean by days  $-9$  and  $-10$ . In these days it is clear that in NDJFMA uptake takes place over part of the Arabian Sea, but the opposite occurs in MJJASO when the Arabian Sea remains a moisture sink while it also becomes an important moisture source for precipitation for the Indian monsoon [48]. During the boreal summer months in the west tropical Indian Ocean between  $0^\circ$  and  $10^\circ$  S, a small region of  $(E - P) > 0$  expands to the east from day  $-6$  through to day  $-10$ , when it reaches  $20^\circ$  S.

Despite the moisture source regions varying or persisting throughout the 10 days of the analysis, part of the uptake of moisture for the NRB from these regions can fall as precipitation along the trajectories of the air masses when they move towards the target area [49]. In MJJASO when the WAM increases the rainfall in WA, the pattern of  $(E - P)$  is mostly characterised by higher values of  $(E - P) > 0$ . A common characteristic of the field of  $(E - P)$  for both seasons is the persistence of moisture contribution from the NRB itself during first few days of the backward analysis, which suggests the importance of local recycling, as previously identified as the major source of moisture for the Sahel [6].

#### 4.2. Climatological Moisture Sources Delimitation

As a means of summarising and giving proper consideration to all of the daily results, we integrated the budget of  $(E - P)$  for all 10 days backwards in time for each period, dry and wet (Figure 4). Spatial differences of resulting positive values in the budget of  $(E - P)$  confirm the importance of considering the rainfall seasonal variation in the target region to identify the moisture sources. The 90th percentile (p90) of the  $(E - P) > 0$  values is shown by the magenta line, which identifies the predominantly evaporative regions, i.e., those finally utilized as moisture sources for the NRB. These are shown more clearly in the schematic illustration in Figure 5. The p90 was calculated in a matrix for the entire globe, thus, the percentile value does not change for another domain. As commented, the boundaries of the sources delimited by the p90 values show the 10% grid points with the highest positive  $(E - P)_{i10}$  values in the map. To understand how appropriate are the boundaries of the sources delimited using this criterion, there was calculated the 80th and 95th percentiles and later plotted along with p90 over the integrated budget of  $(E - P)$  for all 10 days backwards in time, for dry and wet seasons (Supplementary Materials Figure S1). In this figure, it is easy to appreciate that between boundaries of p80 and p90,  $(E - P)_{i10} > 0$  values are low, while the threshold of p95 comprises extremely high values.

In the dry season the threshold of p90 = 0.13 mm/day (Figure 4a) defines the following boundaries of the moisture sources regions: the “tropical east north Atlantic Ocean” (NAtl), the “tropical east south Atlantic Ocean” (SAtl), the “Western Sahel” (WSah), the NRB, the “Southern Sahel” (SSah), the “Eastern Sahel” (ESah), “Eastern Africa” (EA), and the “Mediterranean” (MEDT) region that mainly comprises the Mediterranean Sea and a small part of the Northern African continent (Figure 5a). In the wet season, most of the sources selected using the threshold of p90 = 0.10 mm/day (Figure 4b)

remain the same as for the dry season, but their spatial extents change and new sources appear. It can clearly be seen that boundaries of the MEDT source are now expanded to the north over Europe, while the SATl to the south and the Natl are reduced and confined near the African coasts. To the northeast of the basin a large source (hereafter NEA) covers a wide area that even comprises part of the Red Sea. In Central Equatorial Africa a moisture source occupies a belt extending from the Atlantic to the Indian Ocean, henceforward named CEA. Other new small sources are located in the “Indian Ocean” (Ind) and the Persian Gulf (Figure 5b).

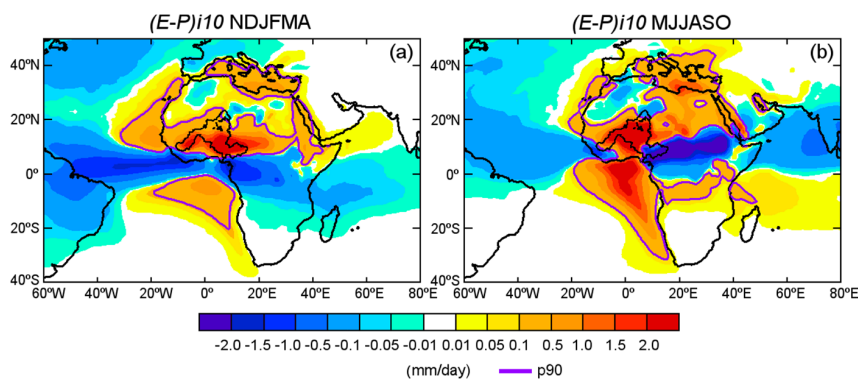


**Figure 4.** Average pattern of  $(E - P)$  backward results integrated from the Niger River Basin for all 10 days for the dry (a) and wet season (b). The magenta line represents the 90th percentile of the  $(E - P)_{i10} > 0$  values: (a)  $p90 = 0.13$  mm/day, and (b)  $p90 = 0.10$  mm/day.

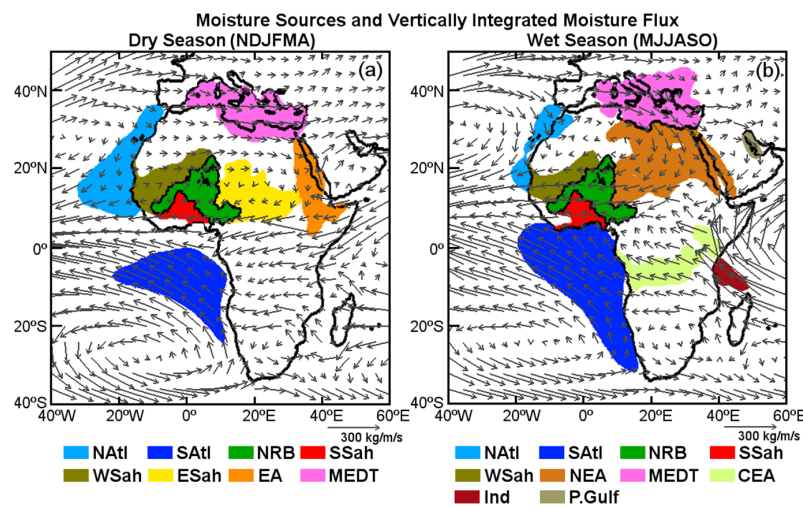


**Figure 5.** Schematic representation of moisture sources for the NRB (colour shaded areas) and average vertically integrated moisture flux (VIMF) (arrows) from ERA-Interim, for the period 1980–2014 during the dry (a) and wet (b) seasons.

A climatology of evaporative moisture sources for the NRB [14] obtained by a quasi-isentropic back-trajectory scheme highlight the importance of recycling ratio in the NRB, which agrees with our results (Figures 3 and 4). Both methods also recognise the importance on the moisture contribution to the basin from the  $(E - P) > 0$  regions represented in Figure 4. Nevertheless, our finding reflect a greatest spatial extension of the  $(E - P) > 0$  areas through the tropical-north Atlantic Ocean in the period November–April respect the period May–October, while results in the already commented climatology represent the evaporative source of the NATl extended in April–September and limited to the North African coasts in October–March. Additionally, according to Keys et al. [10] who implemented an Eulerian method for tracking moisture, the most important evaporation source regions in the ERA-I

western Sahel precipitation shed during the growing season, come from the Gulf of Guinea, the entire east-west expanse of the Sahel, the Mediterranean Sea, Central Africa, the coastal Mediterranean regions, and the Mozambique Channel. These results for the Sahel coincide greatly with those obtained in this work, but the seasonal analysis implemented in ours also reveals the seasonal spatial variability of the NRB’s moisture sources.

#### 4.3. Daily Budget of $(E - P)$ Over the Sources

The daily budgets of  $(E - P)$  over the sources, obtained in the backward experiment with FLEXPART are shown in Figure 6. Positive values represent moisture uptake while the negative values show losses of moisture. Positive  $(E - P)$  values appear whether the sum of the  $(e - p)$  associated with the parcels moving over a certain area is positive. Figure 6 shows the time series of daily  $(E - P)$  calculated backward for moisture over NRB and integrated over the different sources considered. These results show the total contribution from each source, regardless of the number of parcels identified or the sources areas. To understand these values it must be noted that source areas are not spatially of the same size and, thus, the amount of moisture uptake, or lose over them are quite scale dependent. In the dry season during the first few days backwards in time (from day  $-1$  to  $-4$ ) the most important sources accounting for  $(E - P) > 0$  values, are the NRB itself followed by ESah, SSah, and WSah (Figure 6a). Is notable that on days  $-1$  and  $-2$  over the NRB,  $(E - P) > 50$  mm/day, which reduces to a minimum ( $<10$  mm/day) on day  $-10$ . The SATl and NATl sources are moisture sinks until day  $-3$ , but then, up to day  $-10$  both become moisture sources for the NRB. Over the MEDT the moisture uptake increases after day  $-3$  (backwards), which supports the  $(E - P)$  pattern shown in Figure 3. Like the MEDT, EA becomes more important providing moisture during last few days, although it ends up being a less important source in the total daily moisture uptake for the NRB.

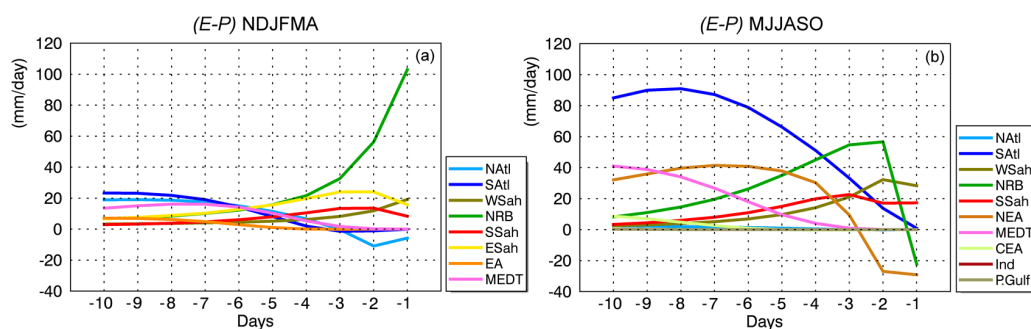


**Figure 6.** Climatological absolute daily (1–10 days) values of  $(E - P)$  integrated using a backward analysis from the NRB considering moisture sources for NDJFMA (a) and MJJASO (b) for the period 1980–2014. The acronyms of the sources regions correspond with those given in Figure 5.

In the wet season when the precipitation over the basin is greater (Figure 7), the NRB acts as a moisture sink on day  $-1$  (Figure 6b). The role of the basin changes from day  $-2$  backwards in time, when it provides humidity for itself and is the most important moisture source until day  $-3$  ( $>50$  mm/day). For SSah and WSah, in the analysis these sources provide moisture to the NRB during all 10 days, being more important during the first days. For both SSah and WSah the  $(E - P) > 0$  values decrease over the last few days of the analysis. After day  $-4$  backwards in time, and in order of importance, the highest moisture uptake takes place over the SATl and NEA. In the wet season SATl becomes the most important moisture source (from day  $-4$  to  $-10$ ) for the NRB. NEA is a moisture sink for the first two days of backwards tracking, in agreement with the pattern of  $(E - P)$  over this region shown in Figure 3 for these days. During last few days (from day  $-6$  backwards), the MEDT is an important moisture source ( $>20$  mm/day) for the NRB. Over the smaller sources of CEA, Indian Ocean, and the Persian Gulf, the air masses in transit to the NRB only gain small amounts of moisture ( $<10$  mm/day). In this season, when the rainfall is intense over the NRB (Figure 7) the moisture uptake

over all days seems to be greater than that obtained for NDJFMA, with the exception of the moisture supply by the NRB itself, which is greater for the first two days during the dry season. Additionally, the resulting  $(E - P)$  over the previously and important Natl moisture source, decreased and becomes one of the less important. As expected in both semi-annual periods NDJFMA and MJJASO, it is notable that the greatest moisture uptake during the first few days backwards in time occurs over the NRB itself, and the surrounding sources, while for the last few days it occurs over the sources furthest away.

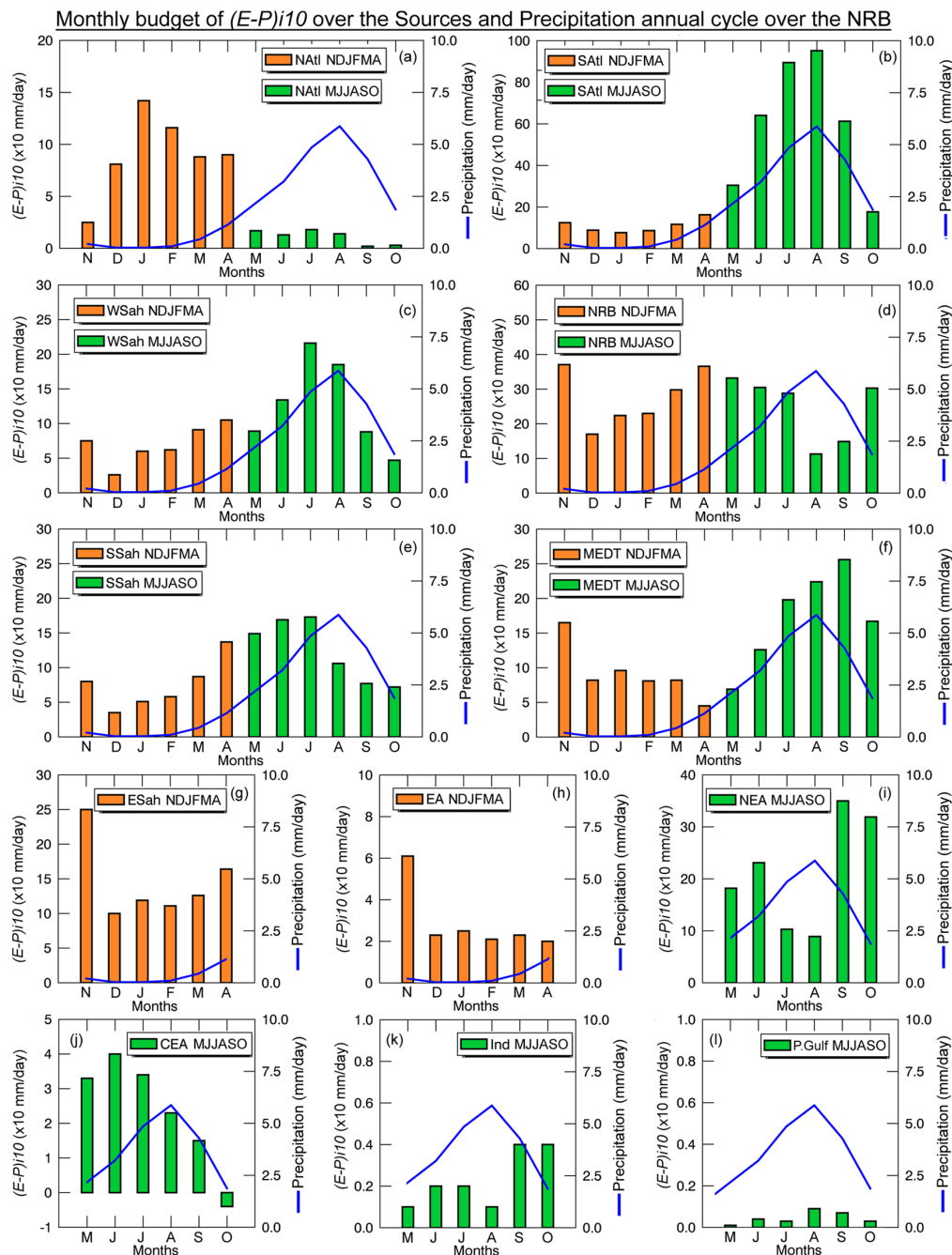


**Figure 7.** Climatological monthly  $(E - P)/10$  values backward integrated from the Niger River Basin over the sources in NDJFMA–MJJASO (bar columns in orange and green, respectively) and precipitation over the NRB (blue line). The acronyms of the sources regions correspond with those given in Figure 5, in the order from (a) to (l).  $(E - P)/10$  from FLEXPART running and precipitation from CRU, for the period 1980–2014.

#### 4.4. Monthly Budget of $(E - P)i10$ over the Sources and Precipitation in the NRB

The moisture sources identification for the Niger catchments by Stohl and James [13] did not explore, but recommended, the analysis of the seasonal and interannual variability in the moisture transport. In this work the source-receptor relationship was also assessed at a monthly scale by calculating the budget of  $(E - P)i10$  over the sources defined for each climatological season. The results are represented in Figure 7 (orange and green columns), together with the annual cycle of precipitation in the NRB (blue line). It is important to note that some of the sources change spatially between the two analysed seasons and others only appear during one of them. Hence, the two coloured bars (orange and green) serve to highlight that although the moisture sources remain within a geographical region they change spatially between NDJFMA and MJJASO (Figure 5).

The spatially-averaged monthly precipitation over the NRB in the first and last months of the year is less than 1 mm/day, but it increases from February until it reaches a maximum in August (5.9 mm/day) (Figure 7) during the African monsoon peak. To support the results in Figure 7 we calculated the mean vertically integrated moisture flux (VIMF) for November–April and May–October, and plotted in the extents of the sources (Figure 5).

Starting with the moisture sources located in the Atlantic Ocean, NATl and SATl (Figure 7a,b, respectively) play different roles over the year. Over NATl the maximum moisture uptake occurs from November to April, when this source is extended to the west over the ocean (Figure 5a), reaching a peak near 150 mm/day in January. In general during these months the VIMF carries humidity from NATl to the northern half of the NRB (Figure 5a), being slightly higher in January (Figure 8a). Climatologically, December, January, and February are the driest months in the basin (Figure 7), but the moisture uptake over NATl is at a maximum in the climatological year. From June to November when the WAM develops and affects WA, this source experiences a spatial reduction (Figure 5b) and with this, a decrease in the monthly average budget of  $(E - P)i10$  in the air masses over it. During this period, the average direction of the VIMF over this region changes to flow from the east (Figure 5b), which does not favour moisture transport from the NATl source to the basin. The monthly annual cycle of the  $(E - P)$  values over this source is clearly opposite to the precipitation cycle in the basin. These results suggest that despite providing moisture to the NRB the NATl is not an effective moisture source for precipitation here during the rainy season.

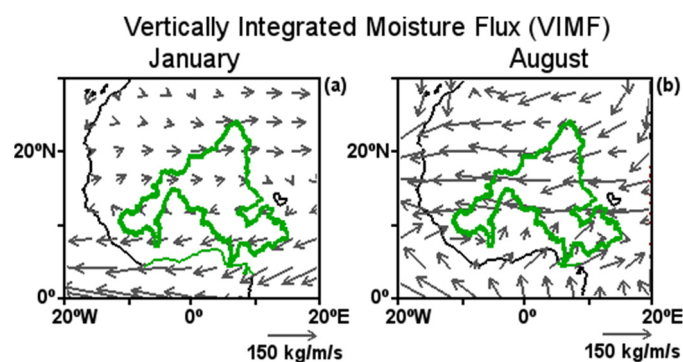


**Figure 8.** Vertically integrated moisture flux (VIMF) climatology for January (a) and August (b). Data from ERA-Interim Reanalysis for 1980–2014.

The SATl source, as might be expected due to its location predominantly south of the equator, has an  $(E - P)i10$  cycle (Figure 7b) opposite to that computed for the NATl source. The budget of  $(E - P)i10$  over the SATl source is positive during all the year and shows values increasing from the dry months until August (when reach > 900 mm/day). From June to September, when the boundaries of this source extend to the south of 30° S (Figure 5b), the moisture uptake over this source is greater than 600 mm/day. This concurs with the penetration of VIMF to the south of the NRB carrying moisture

from the Gulf of Guinea (Figure 5b), which is more appreciable in August (Figure 8b). In general the African Sahel is influenced throughout the monsoon period by southerly winds transporting moisture from the Gulf of Guinea [50]. These results are in agreement with similar findings for the NRB by Stohl and James [13]. The annual cycle of the budget of  $(E - P)i10$  over the SATl source matches the cycle of precipitation over the NRB (Figure 7b), which also agrees with previous results of Gong and Eltahir [1] who argue that moisture fluxes from the tropical Atlantic are almost in phase with rainfall in WA. The maximum precipitation in the NRB occurs in August when the maximum moisture uptake occurs from the SATl source, and less precipitation occurs when the NRB receives less moisture from this oceanic source. Contrary to Natl, this source seems to be very effective for precipitation in the NRB.

The monthly budget of  $(E - P)i10$  over WSah is always positive (Figure 7c), which means that the air masses from here that are in transit to the NRB take up humidity throughout the year. The budget reflects a quite similar cycle to the precipitation over the basin (Figure 7c), similar to SATl. From December to April the moisture uptake increases month by month, decreasing in May, but in July it reaches an annual maximum (>200 mm/day). Regarding the VIMF, it is observed over WSah coming from the west to the east in NDJFMA, carrying moisture to the NRB, and from the east to the west in NJJASO not favouring the moisture supply to the basin.

The only source to be defined without reference to spatial changes over the year is the NRB itself, which is of interest especially in view of its role in providing its own moisture supply. The NRB provides humidity to the atmospheric column in all months of the year (Figure 7d). The annual cycle of  $(E - P)i10$  is characterised by two maxima greater than 350 mm/day in November and April and a minimum in August (<120 mm/day) coinciding with the maximum precipitation rate over the basin. This behaviour confirms the important role of other sources providing moisture for precipitation in the NRB.

To the south of the NRB, the budget of  $(E - P)i10$  over the SSah source is always positive, reaching a maximum of 170 mm/day in July (Figure 7e). The precipitation in the basin seems to show a one-month lag with respect to the budget of  $(E - P)i10$  over the SSah. The VIMF appears towards the west over this region during the dry season while for the wet season it also penetrates in the source from the Gulf of Guinea (Figure 5).

The MEDT source plays a distinct role in the moisture uptake by air masses in transit to the NRB. The budget of  $(E - P)i10$ , with positive values in all months confirms the moisture uptake, which is at a maximum from July to September (Figure 7f) when the precipitation is at a maximum in the basin. Nevertheless, in November when  $(E - P)i10 > 150$  mm/day the precipitation is less than 1 mm/day. In a previous study of the NRB moisture sources, Stohl and James [13] documented that the Mediterranean air masses provide 5% of the NRB precipitation. During the wet season, on average, the VIMF over the Mediterranean region is from the west, but it then forms two branches over this source; one of these flows southwards over northeast Africa before turning westwards reaching the northern half of the NRB (Figure 5b). It is clearly appreciated in August (Figure 8b), the rainiest month in the basin. For NDJFMA it is not clear that the VIMF reaches the NRB from the MEDT source (Figure 5a), which is agreement with the decrease in the  $(E - P)i10$  over it in this season.

The ESah is a source of moisture for the NRB only during the dry season. The budget of  $(E - P)i10$  over this source remain positive during all months and is maximum in November (~250 mm/day) (Figure 7g). The other source for this season, EA, contributes with positive but smaller  $(E - P)i10$  values than those obtained over ESah, with a maximum also in November of around 60 mm/day (Figure 7h). The VIMF from the east has a low magnitude and mostly enters via the southern part of the basin (Figure 5a).

Regarding the sources that only appear in the wet season, NEA (occupying much of northeast Africa) seems to join the regions identified as moisture sources of the NRB during the dry season, ESah and EA. Air masses tracked backwards from the NRB yield a considerable amount of moisture in all months (>80 mm/day) (Figure 7i). In the wet season, the VIMF over NEA reach the basin from the east (Figure 5b). For CEA the budget of  $(E - P)i10$  is negative in October; this implies that air masses tracked

backwards from the NRB, lose rather than gain, humidity over CEA, because it acts as a moisture sink (Figure 7j). In the rest of months the budget is positive but moisture uptake over this source results much less than obtained over the previous described sources. Though from East Africa and Central Africa almost all of the evaporation is recycled regionally or transported to West Africa [8]. Over the Indian Ocean and the Persian Gulf (Figure 7k,l) the budget of  $(E - P)i10$  is positive and small; in fact, Druyan and Koster [4] previously confirmed that Indian Ocean evaporate did not precipitate at all over the Sahel. The findings of the VIMF over these sources appear to advect moisture by the southern border of the NRB (Figure 5b).

4.5. Seasonal  $(E - P)i10 > 0$  over the Sources

To summarise the role of each source of moisture for the NRB in both seasons NDJFMA and MJJASO, we calculated the total moisture uptake ( $(E - P)i10 > 0$ ) over the sources and the percentage they represent. The results are expressed in percentage terms in Figure 9. The numbers in the figure relate to inside, or to the nearest possible colour contour representing each source boundary.

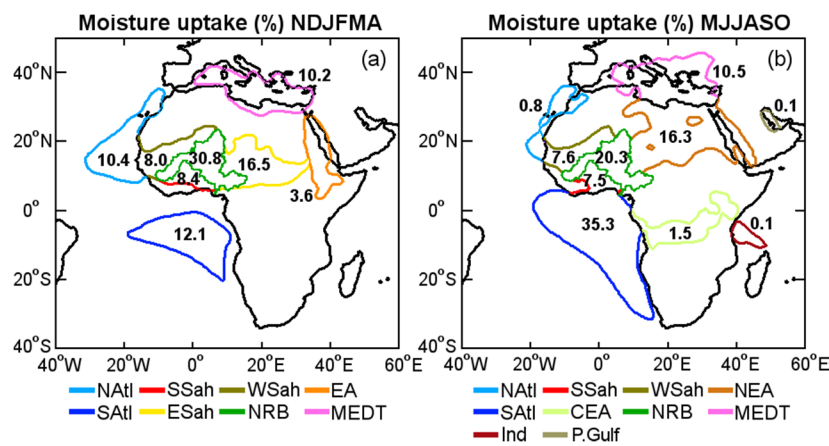


**Figure 9.** Percentage moisture uptake ( $(E - P) > 0$ ) by the NRB over the climatological sources during NDJFMA (a) and MJJASO (b). The colour contours indicates the boundaries of the moisture sources in both seasons.

In NDJFMA (Figure 9a) the NRB itself (30.8%), ESah (16.5%), SATl (12.1%), and the MEDT (10.2%) are the regions where the air masses gained the most moisture for the NRB, while the least important sources are WSah (8.0%) and EA (3.6%). In MJJASO the most important sources are SATl (35.3%), which has a greater extent in this period and the NRB (20.3%), followed by NEA (16.3%) and the MEDT (10.5%) (Figure 9b). The MEDT source (now covering part of the European Mediterranean countries) in this season increase the moisture contribution to the NRB (Figure 7f); nevertheless, it represents almost the same percentage of the total moisture uptake in both seasons. The CEA, NATl, Ind, and P.Gulf sources are the least important; here the uptake represents 1.5%, 0.8%, 0.1%, and 0.1%, respectively, of the total moisture uptake for the air masses travelling towards the NRB.

Focusing on the role of the NRB itself, its own moisture contribution is greater in NDJFMA than in MJJASO, which can be explained by the maximum precipitation seen during the wet season, which favours the loss of moisture. This supports the finding that during the WAM the precipitation in the NRB is fed by moisture transported mainly from SATl, NRB, NEA, and MEDT. These results reveal the importance of moisture contribution by the ocean, even when terrestrial surfaces represent 77% of the Western Sahel precipitation shed and oceanic surfaces comprise the remaining 23% [9]. The seasonal moisture uptake quantification over the moisture sources of the NRB, reveals that largest fraction of moisture income to the basin (69.2% in NDJFMA and 79.7% in MJJASO) comes from outside its boundaries (Figure 9).

## 5. Conclusions

The main moisture sources for the Niger River Basin were investigated during the dry and wet seasons defined at a semi-annual scale, i.e., dry (NDJFMA) and wet (MJJASO). The sources were identified using a Lagrangian approach for 35 years (1980–2014), which ensured reliable climatological results.

- The moisture sources for the NRB in both seasons are located in the tropical east North Atlantic Ocean (NAtl), the tropical east South Atlantic Ocean (SAtl), the surrounding Sahel areas, the Mediterranean region (MEDT), and the NRB itself (Figure 5). They experience differences in the spatial extension between the rainy and dry seasons in the NRB.
- The sources appear during NDJFMA, herein termed ESah and EA, seem to join together in MJJASO occupying north-east Africa (NEA). Additionally, during the wet season three moisture sources appear in central equatorial Africa (CEA), the Indian Ocean (Ind), and on the Persian Gulf (Figure 5).
- Computing the budget of  $(E - P)$  for the air masses tracked up to 10 days backwards in time from the NRB, it was found that the NRB itself, and the surrounding Sahel regions, are mainly responsible for moisture uptake during the first few days of the backwards analysis confirming, as expected from previous studies, the importance of recycling in this region. Further back in time, SAtl, NAtl, NEA, and MEDT are the most important sources (Figures 3 and 6).
- During the dry season, when the precipitation decreases over the basin (Figure 7), the main moisture sources (those where the greatest moisture uptake takes place) are the NRB itself, followed by ESah and SAtl (Figure 9a).
- In the rainy season, together with greater precipitation over the NRB (Figure 7), the  $(E - P)_{i10} > 0$  values over the NRB itself decrease (Figures 7d and 9b). In these months (May–October) the atmospheric circulation associated with the West African monsoon favours greater moisture transport to the basin from regions located to the north-east, east, and south of the basin (Figure 5b).
- The seasonal moisture uptake quantification over the moisture sources of the NRB, reveals that the largest fraction of moisture income to the basin (69.2% in NDJFMA and 79.7% in MJJASO) comes from outside its boundaries (Figure 9). This finding suggests that precipitation variability over the basin must be governed by the moisture contributions from these sources.

It is not always true that more or less moisture uptake over some sources leads to more or less precipitation over the NRB. In fact, the moisture uptake over the NAtl source is greater from November to April when the precipitation is generally less over the NRB, while the opposite tends to apply in the other months. A fact is that the amount of moisture uptake depends of the balance of  $(E - P)$  over the sources because they can act as moisture sinks, as occurs over the CEA in October. These findings suggest that NAtl is not an effective moisture source for rainfall in the NRB. On the contrary, SAtl supplies a great percentage of the total moisture uptake of the basin and exhibits the same annual cycle of the precipitation, suggesting the importance of this oceanic region in supplying moisture for rainfall in the NRB (Figure 7).

Further research to provide new insights into the hydrological cycle in the NRB is underway. This comprises the use of FLEXPART in a forward experiment from each of the sources, which will allow us to investigate the inter-annual variability of the moisture contribution to the basin and establish quantitative relationships with precipitation, including the possible impacts of different modes of climate variability and the role of the sources during drought conditions.

**Supplementary Materials:** The following are available online at [www.mdpi.com/2073-4433/8/2/38/s1](http://www.mdpi.com/2073-4433/8/2/38/s1).

**Acknowledgments:** Rogert Sorí would like to acknowledge funding by the Xunta of Galicia, Spain, in support of this doctoral research; Raquel Nieto acknowledges support from CNPq grant 314734/2014-7 provided by the Brazilian government, and Anita Drumond acknowledges the support of the Spanish Government and FEDER via the SETH (CGL2014-60849-JIN) project.

**Author Contributions:** Rogert Sorí, and Luis Gimeno designed, proposed and conducted the research; Rogert Sorí performed the experiments and analysed the data; Rogert Sorí, Raquel Nieto, Luis Gimeno and Anita Drumond wrote the paper.

**Conflicts of Interest:** The authors declare no conflict of interest. The founding sponsors had no role in the design of the study; in the collection, analyses, or interpretation of data; in the writing of the manuscript, or in the decision to publish the results.

## References

- Gong, C.; Eltahir, E.A.B. Sources of Moisture for Rainfall in West Africa. *Water Resour. Res.* **1996**, *32*, 3115–3121. [[CrossRef](#)]
- Durán-Quesada, A.M.; Gimeno, L.; Amador, J.A.; Nieto, R. Moisture sources for Central America: Identification of moisture sources using a Lagrangian analysis technique. *J. Geophys. Res.* **2010**, *115*, D05103.
- Gimeno, L.; Stohl, A.; Trigo, R.M.; Dominguez, F.; Yoshimura, K.; Yu, L.; Drumond, A.; Durán-Quesada, A.M.; Nieto, R. Oceanic and terrestrial sources of continental precipitation. *Rev. Geophys.* **2012**, *50*, RG4003. [[CrossRef](#)]
- Druyan, L.M.; Koster, R.D. Sources of Sahel Precipitation for Simulated Drought and Rainy Seasons. *J. Clim.* **1989**, *2*, 1438–1446. [[CrossRef](#)]
- Eltahir, E.A.B.; Bras, R.L. Precipitation recycling. *Rev. Geophys.* **1996**, *34*, 367–378. [[CrossRef](#)]
- Nieto, R.; Gimeno, L.; Trigo, R.M. A Lagrangian identification of major sources of Sahel moisture. *Geophys. Res. Lett.* **2006**, *33*, 1–6. [[CrossRef](#)]
- Dirmeyer, P.A.; Brubaker, K.L.; DelSole, T. Import and export of atmospheric water vapor between nations. *J. Hydrol.* **2009**, *365*, 11–22. [[CrossRef](#)]
- Van der Ent, R.J.; Savenije, H.H.G.; Schaeffli, B.; Steele-Dunne, S.C. Origin and fate of atmospheric moisture over continents. *Water Resour. Res.* **2010**, *46*, W09525. [[CrossRef](#)]
- Keys, P.W.; van der Ent, R.J.; Gordon, L.J.; Hoff, H.; Nikoli, R.; Savenije, H.H.G. Analyzing precipitationsheds to understand the vulnerability of rainfall dependent regions. *Biogeosciences* **2012**, *9*, 733–746. [[CrossRef](#)]
- Keys, P.W.; Barnes, E.A.; van der Ent, R.J.; Gordon, L.J. Variability of moisture recycling using a precipitationshed framework. *Hydrol. Earth Syst. Sci.* **2014**, *18*, 3937–3950. [[CrossRef](#)]
- Goessling, H.F.; Reick, C.H. On the “well-mixed” assumption and numerical 2-D tracing of atmospheric moisture, *Atmos. Chem. Phys.* **2013**, *13*, 5567–5585.
- Arnault, J.; Knoche, R.; Wei, J.; Kunstmann, H. Evaporation tagging and atmospheric water budget analysis with WRF: A regional precipitation recycling study for West Africa. *Water Resour. Res.* **2016**, *52*, 1544–1567. [[CrossRef](#)]
- Stohl, A.; James, P. A Lagrangian analysis of the atmospheric branch of the global water cycle: 2. Earth’s river catchments, ocean basins, and moisture transports between them. *J. Hydrometeorol.* **2005**, *6*, 961–984. [[CrossRef](#)]
- The Center for Ocean-Land-Atmosphere Studies. Available online: <http://cola.gmu.edu/wcr/river/Niger.png> (accessed on 2 February 2017).
- Liebmann, B.; Blade, I.; Kiladis, G.N.; Carvallo, L.M.V.; Senay, G.B.; Allured, D.; Leroux, S.; Funk, C. Seasonality of African Precipitation from 1996 to 2009. *J. Clim.* **2011**, *25*, 4304–4322. [[CrossRef](#)]
- Biasutti, M.; Yuter, S.E. Observed frequency and intensity of tropical precipitation from instantaneous estimates. *J. Geophys. Res. Atmos.* **2013**, *118*, 9534–9551. [[CrossRef](#)]
- Niang, I.; Ruppel, O.C.; Abdrabo, M.A.; Essel, A.; Lennard, C.; Padgham, J.; Urquhart, P. Africa. In *Climate Change 2014: Impacts, Adaptation, and Vulnerability. Part B: Regional Aspects; Contribution of Working Group II to the Fifth Assessment Report of the Intergovernmental Panel on Climate Change*; Cambridge University Press: Cambridge, UK, 2014; pp. 1199–1265.
- Nicholson, S.E.; Some, B.; Kone, B. An analysis of recent rainfall conditions in West Africa, including the rainy seasons of the 1997 El Nino and the 1998 La Nina years. *J. Clim.* **2000**, *13*, 2628–2640. [[CrossRef](#)]
- Lebel, T.; Ali, A. Recent trends in the Central and Western Sahel rainfall regime (1990–2007). *J. Hydrol.* **2009**, *375*, 52–64. [[CrossRef](#)]
- Huang, J.; Zhang, C.; Prospero, J.M. Large-scale effect of aerosols on precipitation in the West African Monsoon region. *Q. J. R. Meteorol. Soc.* **2009**, *135*, 581–594. [[CrossRef](#)]

21. Djebou, D.C.S. Integrated approach to assessing streamflow and precipitation alterations under environmental change: Application in the Niger River Basin. *J. Hydrol. Reg. Stud.* **2015**, *4*, 571–582. [[CrossRef](#)]
22. Nicholson, S.E. The West African Sahel: A Review of Recent Studies on the Rainfall Regime and Its Interannual Variability. *ISRN Meteorol.* **2013**, *2013*, 1–32. [[CrossRef](#)]
23. The Niger River Basin Authority (NBA). Executive Secretariat P.O.Box 729, Niamey (Niger). Available online: <http://www.abn.ne> (accessed on 1 November 2016).
24. Ogilvie, A.; Mahe, G.; Ward, J.; Serpantie, G.; Lemoalle, J.; Morand, P.; Barbier, B.; Diop, A.T.; Caron, A.; Namara, R.; et al. Water, agriculture and poverty in the Niger River Basin. *Water Inter.* **2010**, *35*, 594–622. [[CrossRef](#)]
25. Buontempo, C. *Sahelian Climate: Past, Current, Projections*; Sahel and Club West Africa Secretariat. Met Office Hadley Centre: London, UK, 2010; pp. 1–20.
26. L'Hôte, Y.; Mahé, G. *Afrique de l'ouest et Centrale. Carte des Précipitations Moyennes Annuelles (Période 1951–1989)*; Office de la Recherche Scientifique et Technique d'Outre-Mer (ORSTOM): Paris, France, 1996. (In French)
27. Andersen, I.; Dione, O.; Jarosewich-Holder, M.; Olivry, J.-C. *The Niger River Basin: A Vision for Sustainable Management*; World Bank: Washington, DC, USA, 2005.
28. Van der Ent, R.J. A New View on the Hydrological Cycle over Continents. Ph.D. Thesis, Delft University of Technology, Delft, The Netherlands, 2014.
29. Nicholson, S. On the question of the “recovery” of the rains in the West African Sahel. *J. Arid Environ.* **2005**, *63*, 615–641. [[CrossRef](#)]
30. Knippertz, P.; Andreas, H.F. Dry-Season Precipitation in Tropical West Africa and Its Relation to Forcing from the Extratropics. *Mon. Weather Rev.* **2008**, *136*, 3579–3596. [[CrossRef](#)]
31. Lavaysse, C.; Flamant, C.; Janicot, S.; Parker, D.J.; Lafore, J.-P.; Sultan, B.; Pelon, J. Seasonal evolution of the West African heat low: A climatological perspective. *Clim. Dyn.* **2009**, *33*, 313–330. [[CrossRef](#)]
32. Lavaysse, C.; Flamant, C.; Evan, A.; Janicot, S.; Gaetani, M. Recent climatological trend of the Saharan heat low and its impact on the West African climate. *Clim. Dyn.* **2015**. [[CrossRef](#)]
33. Sultan, B.; Janicot, S. The West African Monsoon Dynamics. Part II: The “Preonset” and “Onset” of the Summer Monsoon. *J. Clim.* **2003**, *16*, 3407–3427. [[CrossRef](#)]
34. Namara, R.E.; Barry, B.; Owusu, E.S.; Ogilvie, A. *An Overview of the Development Challenges and Constraints of the Niger Basin and Possible Intervention Strategies*; IWMI Working Paper 144; International Water Management Institute: Colombo, Sri Lanka, 2011; pp. 1–34. [[CrossRef](#)]
35. Zhang, C.; Woodworth, P.; Gu, G. The seasonal cycle in the lower troposphere over West Africa from sounding observations. *Q. J. R. Meteorol. Soc.* **2006**, *132*, 2559–2582. [[CrossRef](#)]
36. Stohl, A.; James, P. A Lagrangian analysis of the atmospheric branch of the global water cycle. Part 1: Method description, validation, and demonstration for the August 2002 flooding in central Europe. *J. Hydrometeorol.* **2004**, *5*, 656–678. [[CrossRef](#)]
37. Numaguti, A. Origin and recycling processes of precipitating water over the Eurasian continent: Experiments using an atmospheric general circulation model. *J. Geophys. Res.* **1999**, *104*, 1957–1972. [[CrossRef](#)]
38. Salih, A.A.M.; Zhang, Q.; Tjernström, M. Lagrangian tracing of Sahelian Sudan moisture sources. *J. Geophys. Res. Atmos.* **2015**, *120*, 6793–6808. [[CrossRef](#)]
39. Nieto, R.; Gallego, D.; Trigo, R.M.; Ribera, P.; Gimeno, L. Dynamic identification of moisture sources in the Orinoco basin in equatorial South America. *Hydrol. Sci. J.* **2008**, *53*, 602–617. [[CrossRef](#)]
40. Drumond, A.; Nieto, R.; Gimeno, L. Sources of moisture for China and their variations during drier and wetter conditions in 2000–2004: A Lagrangian approach. *Clim. Res.* **2011**, *50*, 215–225. [[CrossRef](#)]
41. Drumond, A.; Marengo, J.; Ambrizzi, T.; Nieto, R.; Moreira, L.; Gimeno, L. The role of the Amazon Basin moisture in the atmospheric branch of the hydrological cycle: A Lagrangian analysis. *Hydrol. Earth Syst. Sci.* **2014**, *18*, 2577–2598. [[CrossRef](#)]
42. Nieto, R.; Castillo, R.; Drumond, A.; Gimeno, L. A catalog of moisture sources for continental climatic regions. *Water Resour. Res.* **2014**, *50*, 5322–5328. [[CrossRef](#)]
43. Drumond, A.; Taboada, E.; Nieto, R.; Gimeno, L.; Vicente-Serrano, S.M.; López-Moreno, J.I. A Lagrangian analysis of the present-day sources of moisture for major ice-core sites. *Earth Syst. Dynam.* **2016**, *7*, 549–558. [[CrossRef](#)]

44. Drumond, A.; Nieto, R.; Gimeno, L. A Lagrangian approach for investigating anomalies in the moisture transport during drought episodes. *Cuad. Investig. Geogr.* **2016**, *42*, 113–125. [[CrossRef](#)]
45. Dee, D.P.; Uppala, S.M.; Simmons, A.J.; Berrisford, P.; Poli, P.; Kobayashi, S.; Andrae, U.; Balmaseda, M.A.; Balsamo, G.; Bauer, P.; et al. The ERA-Interim reanalysis: Configuration and performance of the data assimilation system. *Q. J. R. Meteorol. Soc.* **2011**, *137*, 553–597. [[CrossRef](#)]
46. Harris, I.; Jones, P.D.; Osborn, T.J.; Lister, D.H. Updated high-resolution grids of monthly climatic observations—The CRU TS3.10 Dataset. *Int. J. Climatol.* **2014**, *34*, 623–642. [[CrossRef](#)]
47. Schicker, I.; Radanovics, S.; Seibert, P. Origin and transport of Mediterranean moisture and air. *Atmos. Chem. Phys.* **2010**, *10*, 5089–5105. [[CrossRef](#)]
48. Levine, R.C.; Turner, A.G. Dependence of Indian monsoon rainfall on moisture fluxes across the Arabian Sea and the impact of coupled model sea surface temperature biases. *Clim. Dyn.* **2012**, *38*, 2167–2190. [[CrossRef](#)]
49. Drumond, A.; Nieto, R.; Hernandez, E.; Gimeno, L. A Lagrangian analysis of the variation in moisture sources related to drier and wetter conditions in regions around the Mediterranean Basin. *Nat. Hazards Earth Syst. Sci.* **2011**, *11*, 2307–2320. [[CrossRef](#)]
50. Lélé, M.I.; Leslie, L.M.; Lam, P.J. Analysis of Low-Level Atmospheric Moisture Transport Associated with the West African Monsoon. *J. Clim.* **2015**, *28*, 4414–4430. [[CrossRef](#)]



© 2017 by the authors; licensee MDPI, Basel, Switzerland. This article is an open access article distributed under the terms and conditions of the Creative Commons Attribution (CC BY) license (<http://creativecommons.org/licenses/by/4.0/>).

1 Article

# 2 Dry conditions in the Niger River Basin and the link 3 with atmospheric moisture transport from the South 4 Atlantic Ocean

5 Rogert Sorí<sup>1\*</sup>, Raquel Nieto<sup>1</sup>, Anita Drumond<sup>1</sup> and Luis Gimeno<sup>1</sup>

6 <sup>1</sup> Environmental Physics Laboratory (EPhysLab), Facultad de Ciencias, Universidade de Vigo,  
7 Ourense 32004, Spain.

8 \* Correspondence: [rogert.sori@uvigo.es](mailto:rogert.sori@uvigo.es); Tel.: +34-988-387-208

9 Received: July 2018; Accepted: date; Published: date

10 **Abstract:** Dry conditions were identified in the Niger River Basin (NRB) from 1980-2016 using the  
11 Standardised Precipitation-Evapotranspiration Index, as well as the hydrological conditions using  
12 the Standardised Streamflow Index. Dry conditions prevailed in the Niger River Basin during  
13 1982-1988, 1998-2002, and 2009-2011. Considering the seasonal precipitation cycle over the basin,  
14 those seasons affected by severe and extremely dry conditions were identified. The results showed  
15 that these conditions occurred during the dry seasons of November-April of 1982-1983, 1983-1984,  
16 and 1986-1987, and the rainy seasons of May-October of 1983, 1984, and 1987. These results  
17 revealed that droughts considerably affected the NRB in 1983, 1984, and 1987. The impact of  
18 meteorological droughts in the Niger River basins seemed shorter in the upper Niger than in the  
19 middle sectors of the basin. Considering that the South Atlantic Ocean plays a key role in the  
20 precipitation regime of West Africa and considering the importance of local recycling, the moisture  
21 contribution to precipitation over the Niger basin from the South Atlantic Ocean was computed as  
22 a climatological source along with the Niger basin itself. The results show that moisture  
23 contribution from both regions followed the annual precipitation cycle over the basin, but the  
24 contribution from the South Atlantic Ocean was greater, particularly during the rainy season.  
25 Despite the importance of the South Atlantic Ocean, its contribution to precipitation during those  
26 seasons under severe and extremely dry conditions in NRB was not always decreased. This reveals  
27 that its role is not always crucial in reducing rainfall over the basin. The Intertropical Convergence  
28 Zone position modulates the atmospheric moisture reaching the Niger basin from the southern  
29 oceanic source and possibly the recycling over the basin itself.

30 **Keywords:** Dry conditions; moisture contribution; Niger River Basin

31

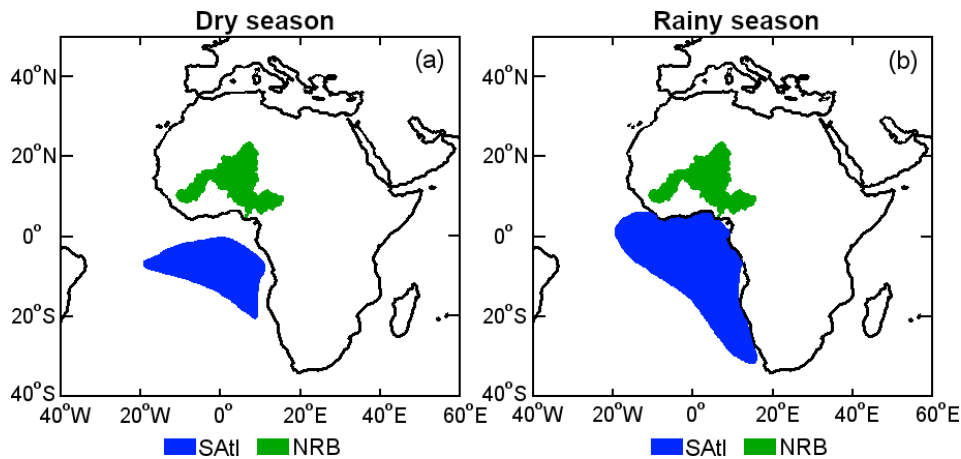
## 32 1. Introduction

33 The Niger River Basin (NRB) is located in West Africa (WA) (Figure 1) and drains to the Niger  
34 River (NR), the third largest river extending through the continent. Home to approximately 100  
35 million people, the NRB is a crucial source for the economic and social development of the region.  
36 Since the 1970s, hydro-climatic changes in the NRB have had significant impacts on the local  
37 populations [1]. It is well known that in this zone there are strong spatial as well as intra- and  
38 inter-annual variabilities in the Sahelian rainfall regime [2]. Differences in the Sahelian precipitation  
39 rates are primarily a consequence of the contrasting circulation, together with the recycling of local  
40 evaporation and moisture advected from the tropical North Atlantic Ocean and the Gulf of Guinea  
41 [3]. In WA, and particularly in the NRB, the mean annual cycle of precipitation is characterised by  
42 minimum values at the beginning of the year that increases monthly, reaching a maximum in  
43 August [4, 5]. The dry season is from November to April and the rainy season is from May to

44 October. The observed changes in the onset and cessation dates of the seasonal rains and the  
45 presence of a negative (positive) precipitation (evaporation) trend from 1941-2002 (1960-1992) are a  
46 discernible indication of climate change [6]. Nevertheless, Okpara and Tarhule [7] found the absence  
47 of a trend for the Standardised Precipitation Index (SPI), the Standardised Rainfall Anomaly Index  
48 (SAI), and the Bhalme and Mooley Drought Index (BMDI) in the Upper Niger sub-watershed during  
49 the period of 1950-2001. During the second half of 1900-2013, droughts in Africa have intensified in  
50 terms of their frequency, severity, and geospatial coverage [8], threatening the food supply of  
51 millions of people. Particularly, the semi-arid West African Sahel has experienced nearly three  
52 decades of abnormally dry conditions, starting with the drought period of 1968-1973 [9] and the  
53 most intense droughts in the early 1980s [10, 7].

54 Drought is an insidious natural hazard that results from lower than normal levels of  
55 precipitation. When this phenomenon extends along a season, or during a longer period, the  
56 precipitation is insufficient to meet the demands of human activities and the environment [11]. A  
57 better understanding of the mechanisms leading to drought occurrences and the assessment of their  
58 impacts and the responses of WA populations is indispensable for researchers and decision-makers  
59 in the current and future context of multiple socioeconomic and environmental changes, including  
60 climate change [12]. To support this, researching the factors responsible for modulating the rainfall  
61 regime is highly important. Within a river catchment area, the precipitation comes from one of three  
62 sources; moisture already in the atmosphere, the convergence of the moisture advected into the  
63 region by winds, or the evaporation of surface moisture into the atmosphere within the basin itself  
64 [13]. Applying a recycling model based on mass balance, Gong and Eltahir [14] found that  
65 evaporation from the tropical Atlantic Ocean, WA, and central Africa contributed about 23, 27, and  
66 17% of rainfall in WA, respectively; while recycling played an important role in the local  
67 precipitation amounts [15, 3]. Nevertheless, other findings argue that local evaporation in WA is not  
68 the dominant factor controlling local precipitation in this region and that the evaporated water is  
69 locally recycled as precipitation in the source area [16, 17]. Most recently, Sorí et al. [5] identified the  
70 main sources of moisture for the NRB during the dry and rainy seasons (Figure 1). These authors  
71 used the 3-dimensional FLEXPART model [18, 19] to track backward in time the air masses residing  
72 within the atmospheric column over the NRB, and along the transient identified from where the  
73 uptake of humidity occurred. This permitted them to determine the most important regions  
74 considered as moisture sources for the NRB. The eastern South Atlantic Ocean (SATl) comprising the  
75 Gulf of Guinea was determined as the most important oceanic source, and the most important  
76 among the continental and oceanic sources during the rainy season. The Sea Surface Temperature  
77 (SST) variability in the Gulf of Guinea and their implications for the spatio-temporal variability of  
78 the precipitation in WA have been widely investigated (e.g. Odekunle and Eludoyin [20]; Joly and  
79 Moldoire [21]; Ali et al., [22]; Nnamchi et al., [23]). However, the moisture uptake by air masses in  
80 transient to the NRB and the SST variability in the Guinea Gulf does not explain directly the  
81 mechanism by which the  $P$  reduces and further assessment is required.

82 The diagnosis of moisture sources has become a major research tool in the analysis of extreme  
83 events (e.g., floods [24, 25] and droughts [26, 27]) and it can be thought of as a basic tool for regional  
84 and global climatic assessments [28]. There are several methods to investigate the origin of moisture  
85 (e.g. Eulerian, Lagrangian, and isotopes) [29]. However, the Lagrangian diagnostic scheme has  
86 proved to be a powerful tool to investigate anomalous atmospheric moisture transports associated  
87 with during dry conditions in continental regions [30, 31, 32]. Considering the previous arguments,  
88 our aim was to identify the dry and wet conditions in the NRB and determine the role of the source  
89 located on the South Atlantic Ocean (SATl) (Figure 1) on the climatological moisture contribution to  
90  $P$  over the NRB and during those seasons affected by severe and extremely dry conditions from  
91 1980-2016. Additionally, we also assessed the impact of dry conditions on streamflow discharge.



92

93 **Figure 1.** Schematic representation of the NRB and the SATl climatological sources in the dry (a) and  
 94 rainy (b) seasons. Adapted from: Sorí et al. [5].

### 95 1.2 Study region

96 The NRB, located in WA, covers 7.5% of the continent and spreads over ten countries in which  
 97 the Niger River, with a total length of about 4100 km, is the third-longest river in Africa, after the  
 98 Nile and the Congo/Zaire Rivers, and the longest and largest river in WA [33]. From the standpoint  
 99 of water resources, the NRB can diagrammatically be divided into four zones with more or less  
 100 homogenous physical and geographical characteristics; the Upper Niger Basin, the Inland Delta that  
 101 is entirely situated in Mali, the Middle Niger Basin, and the Lower Niger Basin [34]. For the  
 102 approximately 100 million inhabitants of the nine countries in WA, the NRB it is a source of identity,  
 103 a route for migration, commerce, and conflict [35]. About 65% of the active WA and Sahelian  
 104 population (more than half of which are women) work in the agricultural sector and are therefore  
 105 vulnerable to climate hazards and environmental factors. Their vulnerability is further increased by  
 106 the fact that the majority of agricultural production in the sub-region is dominated by subsistence  
 107 farming almost exclusively based on rainfed agriculture and extensive animal husbandry systems  
 108 [36].  
 109

## 110 2. Materials and Methods

### 111 2.1. Methods

#### 112 2.1.1 Identification of dry and wet conditions in the NRB

113 Many drought indices have been developed and used by meteorologists and climatologists  
 114 around the world [11]. Many of them are based on traditional methods for drought assessment, such  
 115 as those derived from precipitation time series [37, 38]. In this study, we used the Standardised  
 116 Precipitation-Evapotranspiration Index (SPEI) [39] to identify dry and wet conditions in the NRB  
 117 from 1980-2016. The SPEI is based on the probability distribution of the difference between the  
 118 precipitation ( $P$ ) and the potential evapotranspiration ( $PET$ ) ( $SPEI = P - PET$ ) on 1-24 month  
 119 time-scales. For this index, the  $PET$  actually represents the Atmospheric Evaporative Demand  
 120 (AED). The term “potential” is equivalent to maximum possible level under given climatic condition  
 121 [40]. The SPEI compares the moisture deficit for a given period of time at a given location with  
 122 respect to the historical average of the cumulative moisture deficit. It is based on the same  
 123 methodology as the Standardised Precipitation Index (SPI) [41]. Thus, positive values of the SPEI  
 124 indicate above average water balance conditions (wet conditions), while negative values reveal  
 125 below normal conditions (dry conditions). The SPEI has the advantage of combining a multi-scalar  
 126 character with the capacity to include the effects of temperature variability on drought assessments  
 127 [39], and it has been widely utilized worldwide to investigate, monitor, and predict drought

128 conditions. To assess the seasonal water balance conditions in the NRB we utilized a 6-month  
 129 temporal scale for the SPEI (SPEI6) for April and October; the final month of the dry and rainy  
 130 semi-annual periods in the region, respectively. The SPEI6 in April (October) diagnoses the water  
 131 balance conditions for the six previous months (counting from the month itself), for the dry (rainy)  
 132 season similar to Drumond et al. [30] and Stagge et al. [42]. An SPEI threshold of -1.5 was used to  
 133 identify the severe and extremely dry conditions in the NRB (Table 1).  
 134

135  
 136  
 137

**Table 1.** Drought classifications based on the SPEI according to the initial definition of Mckee et al. [41] for the SPI

Conditions	Category
Extremely wet	SPEI > 2.0
Severely wet	1.5 < SPEI ≤ 2.0
Moderately wet	1.0 < SPEI ≤ 1.5
Mildly wet	0 < SPEI ≤ 1.0
Mild drought	-1.0 < SPEI < 0
Moderate drought	-1.5 < SPEI ≤ -1.0
Severe drought	-2.0 < SPEI ≤ -1.5
Extreme drought	SPEI ≤ -2.0

138

### 139 2.1.2 Identification of hydrological drought conditions

140

141 The hydrological drought conditions for the NR were quantified at the Koulikoro (12.86 °N,  
 142 7.55 °W) and Niamey (13.52 °N, 2.08 °E) gauging stations from 1980-2011 using the Standardised  
 143 Streamflow Index (SSI) [43]. Hydrological drought indices are generally based on streamflow, as this  
 144 variable essentially summarises every hydrometeorological process taking place in the watersheds  
 145 and river basins [37]. The relationship between the SPEI and SSI makes it possible to understand the  
 146 impact of climatic droughts on the hydrological conditions. The recorded data at the Koulikoro  
 147 station permitted the assessment of the hydrological drought conditions for the western part of the  
 148 NRB, in particular, the Upper Niger Basin, while the Niamey fluviometric station located in the  
 149 western-centre of the basin allowed the assessment of the middle NRB.

### 150 2.1.3 Computation of the source moisture contributions

151 Outputs from a global Lagrangian particle dispersion model FLEXPART v9.0 experiment were  
 152 used to compute the moisture contribution from the SAatl and from the same basin to the P over itself  
 153 [18, 19]. The experiment was carried on at the Environmental Physics Laboratory (EPhyslab) at the  
 154 University of Vigo. FLEXPART considers the atmosphere homogeneously divided into  
 155 approximately 2 million "particles" (or "parcels") evenly distributed over the entire globe and tracks  
 156 them backward and/or forward in time. Along the trajectories it is possible to compute the rate of  
 157 moisture increases (through evaporation from the environment,  $e$ ) or decreases (through  
 158 precipitation,  $p$ ) along the trajectory of the parcels calculated by changes in the specific humidity ( $q$ )  
 159 over time ( $t$ ) by Equation (1), assuming a constant particle mass ( $m$ ):

160

$$161 \quad (e - p) = m \left[ \frac{dq}{dt} \right] \quad (1)$$

162

163 By integrating the  $(e - p)$  values for all parcels in a vertical column over an area  $A$ , it is possible  
 164 to obtain the surface freshwater flux, hereafter denoted  $(E - P)$  in Equation (2):

165

$$166 \quad E - P \approx \frac{\sum_{k=1}^k (e-p)}{A} \quad (2)$$

167

168 where  $E$  represents the evaporation and  $P$  the precipitation per unit area ( $A$ ). As a  
169 consideration, in this calculus, the average time that water vapour resides in the atmosphere was set  
170 to 10 days [44]. The air masses residing over each source (Figure 1) were tracked forward in time.  
171 This permits the budget of the  $(E-P)$  over the NRB to be computed. Negative budget values are  
172 considered as moisture losses, while positive values are moisture gains. Along the text, the moisture  
173 losses over the NRB are assumed to be a contribution to  $P$ , and are denoted as  $|E - P|_{10} < 0$ .  
174 FLEXPART has been applied to investigations of the hydrological cycle in several river basins [19], but  
175 most extensively for the Amazon River Basin [45], the Yangtze River Basin [46], the Danube River  
176 Basin [47] and as stated, the NRB itself [5]. The model makes it possible to establish the moisture  
177 source-receptor relationship along suitably defined trajectory ensembles. This main strength is one  
178 that permitted the development of this study. Nevertheless, along with individual trajectories,  $q$   
179 fluctuations can occur for nonphysical reasons (e.g. because of  $q$  interpolation or trajectory errors), a  
180 limitation that is partially compensated for by the presence of so many particles in an atmospheric  
181 column over the target area [18].  
182

## 183 2.2. Data

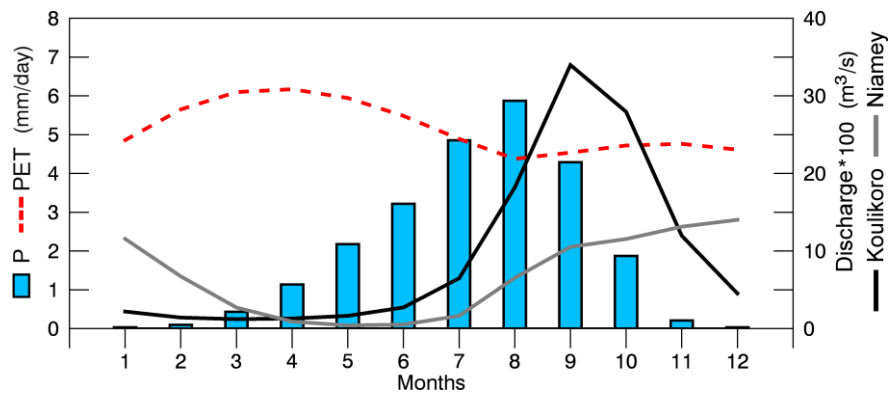
184 The analyses were carried out for a 37-year period (1980-2016), ensuring good climatological  
185 results. To compute the SPEI, we employed monthly data of the  $P$  and  $PET$  available from the  
186 Climatic Research Unit (CRU TS v. 4.01) [48] with a  $0.5^\circ$  longitude and latitude resolution. For the SSI,  
187 the discharge measurement data of the NR at the fluviometric stations located in Koulikoro and  
188 Niamey were freely provided by the Global Runoff Data Centre [49] for the period 1980-2001. This  
189 period was selected based on the longest continuous period without missing data at both locations.

190 FLEXPART uses data from the ERA-Interim reanalysis [50] every 6 h with a resolution of  $1^\circ$  in  
191 longitude and latitude on 60 vertical levels from 1000 to 0.1 hPa, with approximately 14 model levels  
192 below 1500 m and 23 below 5000 m [18, 19]. Compared with another reanalyses (such as MERRA  
193 [51] or CFRS [52]), the ERA-Interim has both a comparatively reasonable closure of the terrestrial  
194 and atmospheric water balances and a reasonable agreement with the observation datasets [53] that  
195 fits very well with the purpose of this study.  
196

## 197 3. Results and discussion

### 198 3.1 Annual cycle of $P$ , $PET$ , and NR discharge

199 The annual cycles of the  $P$  and  $PET$  in the NRB and the NR discharge data registered at the  
200 Koulikoro and Niamey hydrological station are plotted in Figure 2. The  $P$  annual cycle mean is  
201 characterised by minimum values in December-January-February, and reaches its maximum during  
202 August with 6 mm/day. After August, the  $P$  decreases and reaches a minimum value in December  
203 [4, 5]. The  $PET$ , as expected, increases when  $P$  decreases, and in August (the rainiest month)  $P$   
204 exceeds  $PET$ . At the Koulikoro hydrological station in the Upper Niger Basin (see location in Figure  
205 2) the annual cycle of the NR discharge is characterised similar to the precipitation regime, but it  
206 reflects a lag of one month showing a maximum discharge in September ( $\sim 30000 \text{ m}^3/\text{s}$ ), a month  
207 after the maximum  $P$ . In Niamey, positioned in the Middle Niger hydrological sector, the discharge  
208 volume was less than the Koulikoro station and does not reflect the same annual cycle. This could be  
209 because the  $P$  values are calculated for the entire basin and hence, could not exactly match the real  $P$   
210 values at the Niamey station. However, here, the discharge cycle seems to be modulated by the  
211 whole  $P$  after a lag of more than one month. This suggests that a similar analysis at the sub-basin  
212 scale would reveal more accurate results.



213

214

215

**Figure 2.** The annual cycle of the P and PET at the NRB and the NR discharge at the Koulikoro and Niamey stations between 1980 -2001.

216

### 3.2. Identification of the dry and wet conditions

217

218

219

220

221

222

223

224

225

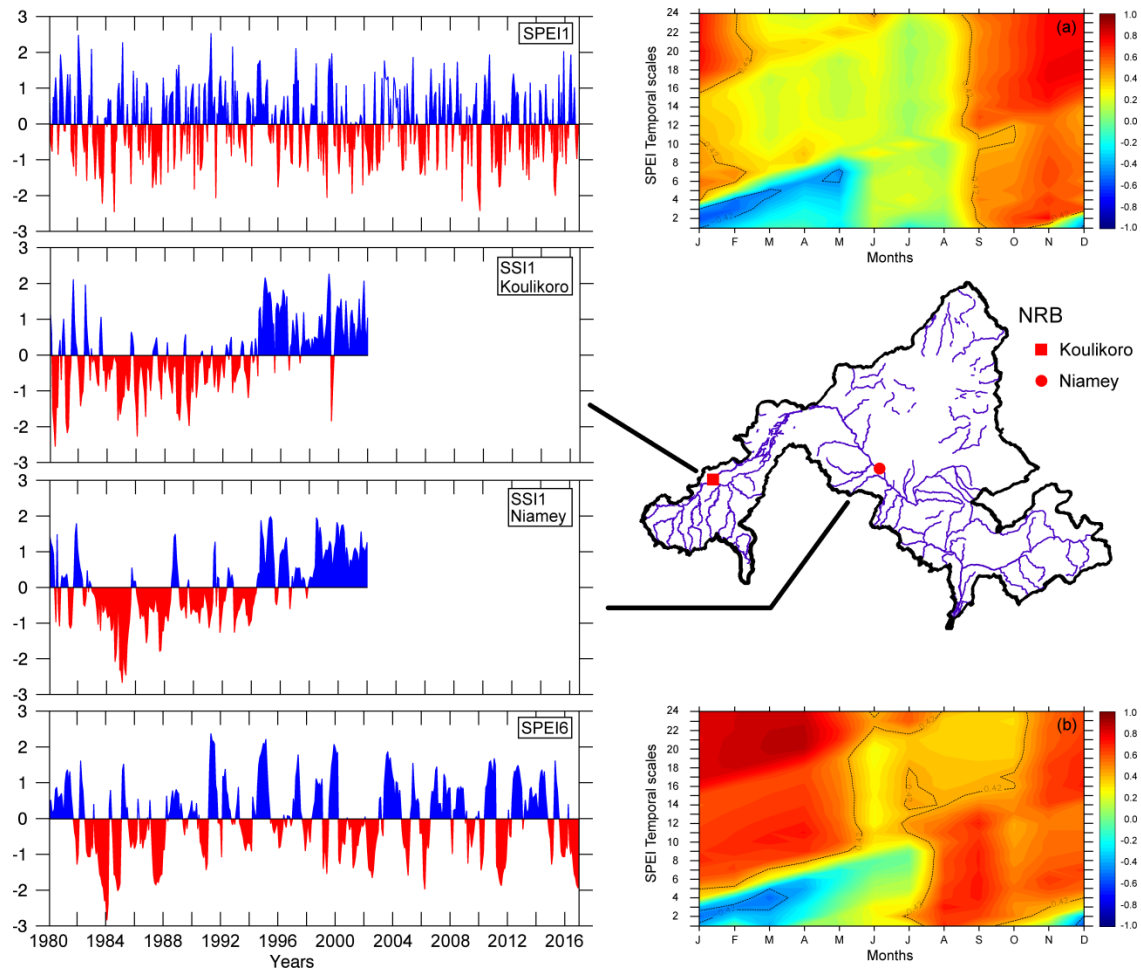
226

227

228

229

The temporal evolution of the SPEI at temporal scales of 1 and 6 months from 1980-2016 are shown in Figure 3. In addition, the SSI on a one-month temporal scale (SSI1) at hydrological stations located in Koulikoro and Niamey during 1980-2001 is also shown. According to SPEI1-6, dry conditions were more intense for the majority of 1981-1988. In particular, special attention is deserved by the 1983-1984 period that was documented as the most extreme drought that occurred in the Sahel during the last 50 years [8]. In 2010-2011, the SPEI also reached intense negative values, evidencing dry conditions in the NRB. In accordance, the SSI1 obtained at both fluviometric stations revealed the hydrological drought starting in these years but also extending an additional few months. For the 2010-2011 period, it has been documented that the Eastern Sahel and the Horn of Africa were notoriously affected by a precipitation deficit, and consequently, an intense drought [54, 8]. The SSI1 in both locations also reflects the impact of wet conditions that prevailed in the NRB from 1991-1999. Documented in other studies, from 2003 during the 2000 decade it seemed that a P recovery occurred.



230

231

232

233

**Figure 3.** Temporal evolution of the SPEI at 1-6 month temporal scales (1980-2016) and SSI 1-month temporal scale for the Koulikoro and Niamey locations (1980-2001). **a)** Monthly correlations among SSI1 in the Koulikoro and **b)** Niamey with SPEI1 to SPEI24. The black line identifies the statistically significant values.

234

235

236

237

238

239

240

241

242

243

244

245

246

247

248

249

250

251

252

253

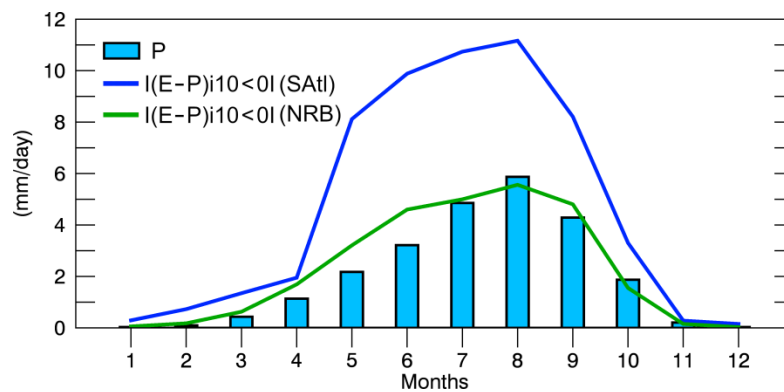
254

The SSI1 in both locations was correlated with the SPEI1 to 24 months' temporal scales (Figure 2a, b). The results were very similar to those previously described; the evolution of the hydrological regime was consistent with the meteorological rainfall deficit (excess) state over the basin. This is explained by negative correlations between the first temporal scales of the SPEI during the months characterised by less rainfall (November to April, approximately). From July and August onwards, when the  $P$  is at the annual maximum, the correlations increase from the first SPEI temporal scales and become negative in December with the SPEI1, when  $P$  is almost zero. As the dry season progresses, the correlations become negative at major time scales of the SPEI. Pearson correlations between SSI1 and different accumulation periods of the SPEI (1-24 months) showed that the hydrological responses at Koulikoro were shorter than in Niamey. It seems that the NR streamflow in Niamey during the rainy season may be more affected than Koulikoro by previous dry season water balance conditions. The Niamey fluviometric station is located in the Middle Niger. This section of the Niger receives six tributaries from Benin and Burkina Faso and the mean annual flow entering the lower Niger in Nigeria is 36 km<sup>3</sup>. With the contribution of its main tributary, the Benue River in Nigeria, and heavy rainfall, the mean annual discharge at the mouth exceeds 180 km<sup>3</sup> [55]. Authors such as Oloruntade et al. [56] applied two meteorological drought indices, the SPI and SPEI and a hydrological drought index, the Standardized Runoff Index (SRI) [57], to investigate the occurrence of droughts in the Niger-South Basin (NSB), a sub-catchment of the NRB in Nigeria, from 1970-2008. They obtained very similar results to those presented here. They also found a higher agreement between the SRI and SPEI, suggesting that hydrological droughts are more affected by temperature (warming) than precipitation (drying) in this basin.

255 3.3. Moisture contribution from the SATl and NRB

256 From each source the moisture contribution to  $P$  over the NRB was computed. The annual cycle  
 257 of  $P$  over the NRB and the  $|E - Pi10| < 0|$  over the NRB were computed in air masses forward  
 258 tracked from the SATl and the NRB itself. As expected, the maximum moisture supply occurred from  
 259 the SATl, and followed the  $P$  annual cycle. This occurs because during the peak monsoon season  
 260 (July–September), the southerly transport weakens, but the westerly transport is enhanced and  
 261 extends to 20.8 °N owing to the strengthening West African jet off the west coast [58-60]. The  
 262 moisture contribution from the basin for the  $P$  over itself is enhanced in the monsoonal months,  
 263 confirming the well documented intense recycling in WA.

264 The correlation between both the  $P$  and  $|E - Pi10| < 0|$  appear in Table 2. During the dry  
 265 season, the  $r$ -value obtained for the SATl was 0.81, while for the NRB it was 0.90. During the rainy  
 266 season, the correlations decreased to 0.60 and 0.76 for the SATl and NRB, respectively. This could be  
 267 explained because during the rainy season normally the  $P$  variability increases. Major  $r$ -values for  
 268 the correlation between the  $|E - Pi10| < 0|$  values obtained for air masses over the basin and the  $P$   
 269 over itself are easily understood to be a locally associated process. The conjunction of the  $|E - Pi10|$   
 270  $< 0|$  values from the SATl and NRB can explain 84% and 58% percent of the  $P$  values over the NRB  
 271 (see  $R^2$  in Table 2).  
 272



273

274 **Figure 4.** Annual cycle of the precipitation ( $P$ ) (light blue bars) and the moisture contribution  $|E - Pi10| < 0|$   
 275 from SATl (blue line) and the NRB (green line). Period 1980-2016.

276 **Table 2.** Monthly significant correlations ( $at p < 0.05$ ) between  $P$  and  $|E - Pi10| < 0|$  during the dry and  
 277 rainy season at the NRB from 1980-2016  
 278

Season	Moisture sources		Multiple Regression
	SATl	NRB	
	R	R	$R^2$
Dry	0.81	0.90	0.84
Rainy	0.60	0.76	0.58

279

280 3.4. Role of the sources during dry and rainy seasons under severe and extremely dry conditions

281 Utilizing the SPEI6, the seasons under severe and extremely dry and wet conditions in the NRB  
 282 (according to the SPEI threshold of  $\pm 1.5$ ) were identified. The results appear in Table 3. It is worth  
 283 mentioning that during the period under study and for different time scales the SPEI could reach  
 284 values greater than or less than those that appear in this table. Nevertheless, our aim was to focus the  
 285 analysis at the seasonal scale where the climatological moisture sources of the basin are available.  
 286 The dry season from November, 1982 to April, 1983 was affected by severely dry conditions that  
 287 which furthermore affected the 1983 rainy season, the dry season from 1983-1984, and the rainy  
 288

289 season of 1984. The 1980s have been documented as one of the driest decades in WA during the  
290 twentieth century.

291 The 1983-1984 dry season was extremely dry. During this period, a reduction in the moisture  
292 contribution from SAatl and the NRB itself occurred (Table 3). During the period from November,  
293 1982 to April, 1983, the severely dry conditions occurred together with negative anomalies on the  
294 moisture contribution from the SAatl, but the moisture contribution of the basin to P over itself was  
295 positive. For the severely dry season of 1986-1987, it seems that was a reduction in moisture from the  
296 Western Sahel, an important source during this period. For the rainy season May-October of 1983,  
297 1984, and 1987, the NRB was affected by severely dry conditions. Contrary to the expected, in the  
298 rainy season of 1983 and 1987 the moisture contribution from the SAatl source was positive.  
299 However, from the basin it was negative. Despite to being the most important NRB moisture source  
300 during the rainy season, Sorí et al. [5] found that moisture uptake from the SAatl by air masses in  
301 transit to the NRB only represented the 35.3% of the total. Thus, other sources may be responsible for  
302 the P reduction during that season. During the rainy season of 1984 the opposite occurred, there was  
303 a moisture supply reduction from the SAatl, but an increase from the basin itself; suggesting that the  
304 basin itself is not capable of increasing the P over itself without contribution from external sources.

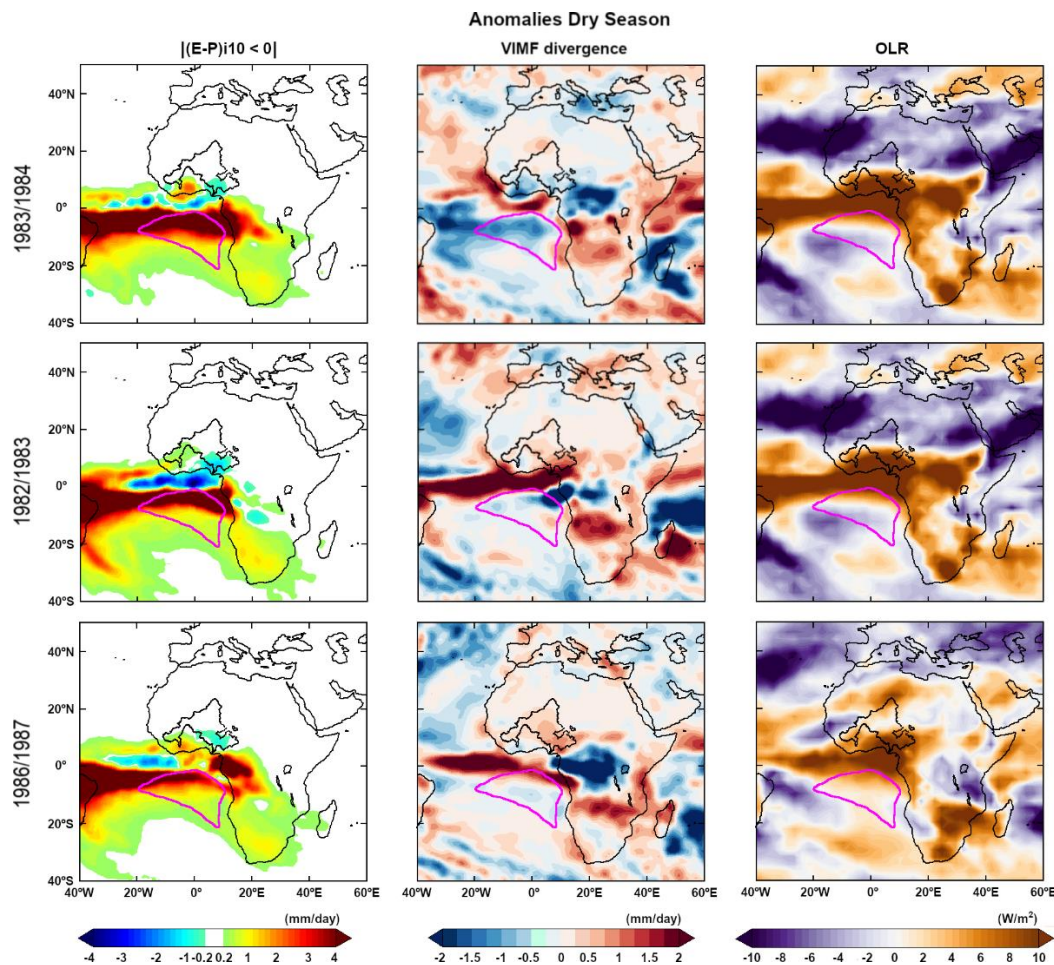
305 **Table 3.** Monthly anomalies (in mm/day) of the total  $|(E - P)/10| < 0|$  during the dry and rainy seasons  
306 affected by severe and extremely dry conditions in the NRB from 1980-2014. Numbers shaded in blue highlight  
307 the negative anomalies.  
308

Moisture sources Dry season			
Date	SPEI6 Apr	SAatl	NRB
1983/1984	-2.0	-45.0	-11.0
1982/1983	-1.92	-37.2	17.7
1986/1987	-1.57	16.0	15.6
Date	SPEI6 Oct	SAatl	NRB
1983	-1.84	120.7	-33.8
1984	-1.75	-32.8	91.3
1987	-1.75	129.0	-33.3

309

310 To support the results of Table 3, for the dry and rainy seasons the spatial anomalies of the  
311 VIMF divergence and the OLR over the 40° - 50° N and 40° W - 60° E, were calculated (Figure 5, 6).  
312 In particular, the  $|(E - P)/10| < 0|$  anomalies in air masses forward tracked from the SAatl were  
313 calculated (Figure 5, 6). For the 1982-1983 dry season (Figure 5), the  $|(E - P)/10| < 0|$  anomalies in the  
314 air masses tracked forward in time from the SAatl were positive within the basin and the most  
315 intense positive anomalies formed a longitudinal belt approximately positioned between -10° S and  
316 the Equator. The P over this region may be the most favoured by the SAatl moisture contribution.  
317 Negative  $|(E - P)/10| < 0|$  anomalies were mainly located northward of the SAatl source and to the  
318 south of the WA coast. Negative values indicate a decrease in the moisture contribution (which  
319 occurs over the NRB in this season). In accordance, over the same region positive anomalies of the  
320 VIMF divergence and the OLR were observed. This means that the atmospheric dynamics in the  
321 region do not favour vertical motion, cloud formation, and finally the P. During 1983-1984, the  
322 driest dry season, the situation was approximately the same. However, the pattern of  $|(E - P)/10| < 0|$   
323 anomalies shows most intense negative values northward the SAatl, which support that lees  
324 moisture reached the NRB. In November, 1986 to April, 1987, the pattern of  $|(E - P)/10| < 0|$   
325 anomalies were in fact very similar to those described before; however, they differed to the south  
326 of the WA coast, where the positive anomalies occurred. This suggests that during this season the  
327 moisture contribution from this source favours more the WA zone, in accordance with the positive  
328 anomalies over the NRB. In the equatorial zone, the Intertropical Convergence Zone (ITCZ) plays a  
329 key role. In November-April (the austral summer), it moves southward and a rainfall deficit occurs  
330 over the NRB. An anomalous position northward may favour the contribution of humidity from the

331 South Atlantic Ocean to WA. An important mechanism explains how positive Sea Surface  
 332 Anomalies (SST) anomalies in the South Atlantic Ocean weakened the sea level pressure gradient  
 333 between the ocean and land and hence produces a weaker ITCZ shift displaced southward during  
 334 dry years over the Sahel decreasing the rainfall over the Sahel and WA [61, 62].

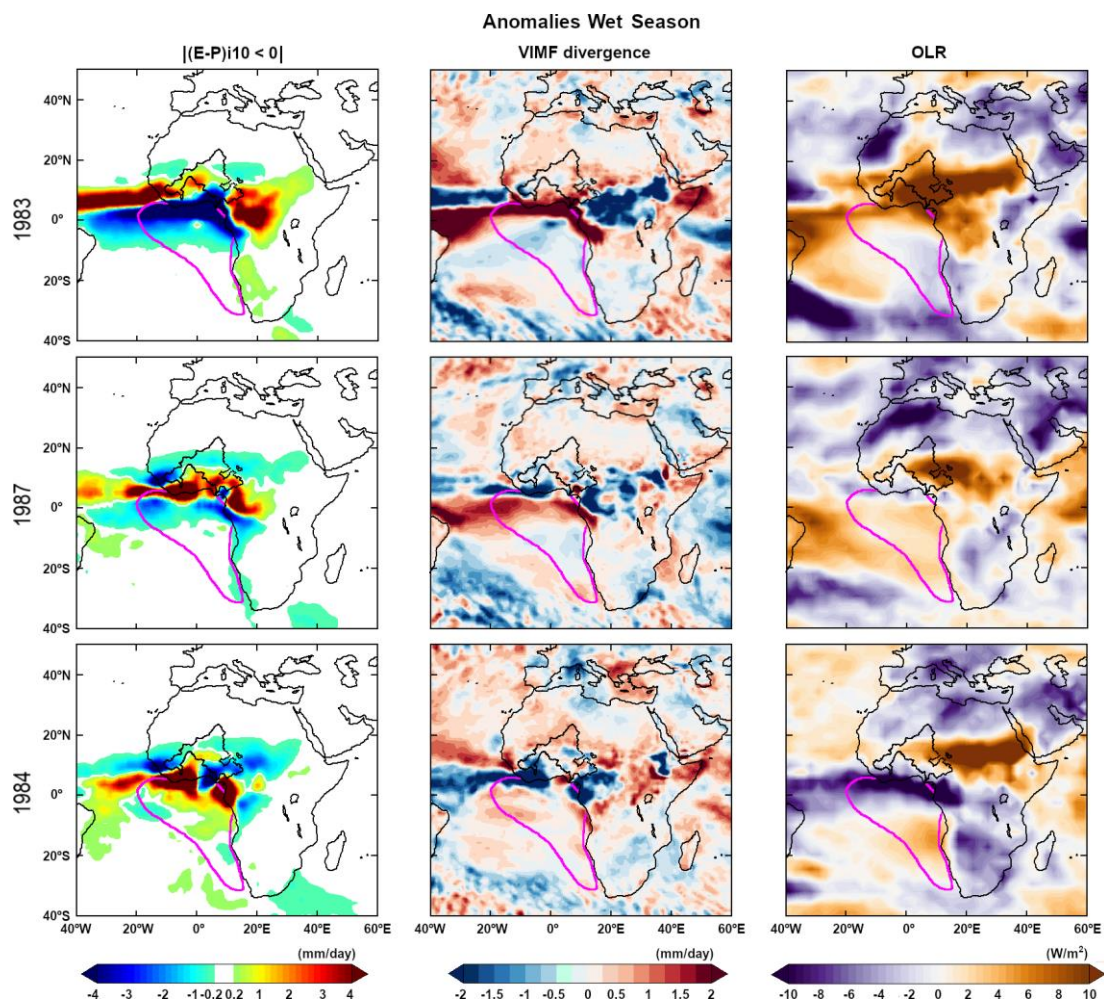


335

336 **Figure 5.** Anomalies of  $|(E - P)/10|$  on air masses tracked forward in time from SATl and the Vertically  
 337 Integrated Moisture Flux (VIMF) divergence and Outgoing Longwave Radiation (OLR). November-April  
 338 seasons under severe and extremely dry conditions according to dates listed in Table 3. The pink line represents  
 339 the boundaries of the SATl sources and the brown line represents the boundaries of the sources for the rainy  
 340 season (see Figure 1).

341 During the rainy season, the SATl source is larger and comprises the whole Gulf of Guinea  
 342 (Figure 1). As described previously, this source has been widely documented for its crucial role in  
 343 the development of WA monsoons. During the rainy season of 1983 and 1987, both affected by  
 344 severely dry conditions, the positive anomalies on the moisture contribution from the SATl mainly  
 345 occurred over the equatorial Atlantic Ocean in western and southern WA also affecting the south  
 346 half of the NRB, confirming the results in Table 3. The continental region to the southeast of the NRB  
 347 that may be part of Central Africa also benefits from moisture transported from the SATl. In both  
 348 years, the regions with positive  $|(E - P)/10|$  anomalies generally overlapped with the VIMF  
 349 divergence negative anomalies and suggests their association with the ITCZ position. The OLR  
 350 anomalies indicated there was more irradiation from the Sahel in 1983 than in 1987. Indeed, the rainy  
 351 season of 1983 was drier and cloud cover may have been lower. In both seasons, the moisture  
 352 contribution anomaly from the basin itself was negative, supporting the idea that a reduction in the  
 353 moisture income from important external moisture sources in this season such as from North East  
 354 Africa (NEA) and the Mediterranean Sea may be responsible for the  $P$  reduction. Contrary to the  
 355 observations in 1983 and 1987, in May-October of 1984 the positive anomalies of  $|(E - P)/10|$

356 covered the northern areas of the source itself and the negative anomalies prevailed inside the NRB,  
 357 confirming a negative contribution of moisture from this source to the basin. The belt of negative  
 358 anomalies of the VIMF divergence and the OLR along the Atlantic Ocean close of the WA coast  
 359 indicate that the ITCZ position that season may have been located southward with respect to the  
 360 1983 and 1987 seasons, acting as a moisture sink for moisture transported from the SATl. Further, the  
 361 increased moisture contribution from the basin itself (when it diminishes from the SATl) indicates  
 362 that during the rainy season the recycling process may be favoured if the ITCZ moves southward.  
 363 However, this should be also studied for the rainiest seasons, since some authors [63, 64] argue that  
 364 wet soil moisture conditions increase the net surface radiation and the total heat flux from the  
 365 surface. Therefore, a larger boundary layer with moist static energy (or entropy) favours the rainfall  
 366 at a local scale and the strength of the monsoon circulation at greater scales.  
 367



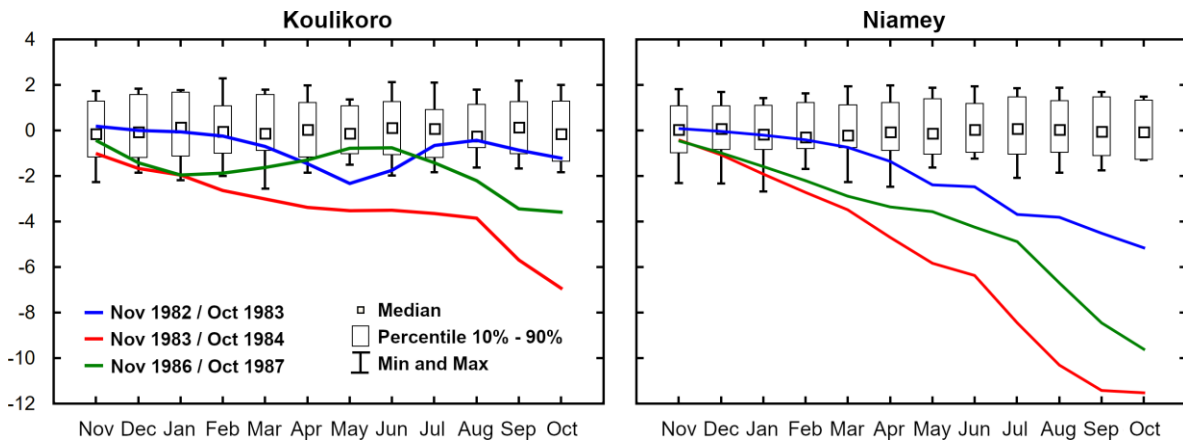
368

369 **Figure 6.** Anomalies of the  $|E - P|_{i10} < 0|$  on air masses tracked forward in time from the SATl, the  
 370 Vertically Integrated Moisture Flux (VIMF) divergence and the Outgoing Longwave Radiation (OLR).  
 371 May–October seasons under severe and extremely dry conditions according to the dates listed in Table 3. The  
 372 pink and green lines represent the boundaries of the SATl and NRB, respectively.

373 *3.5. Impact of the driest seasons on the river discharge*

374 The seasonal rainfall deficit over the NRB leading to droughts also impacts the NR discharge.  
 375 In Figure 7, some basics statistics of the SSI along the hydrological year at Koulikoro (a) and  
 376 Niamey (b) locations are presented. The temporal evolution of the median, the extreme values, and  
 377 the 10<sup>th</sup> and 90<sup>th</sup> percentiles did not show large differences, but a major variability at the Koulikoro.  
 378 Taking advantage of the coincidence that the dry and rainy seasons affected by severe and extreme  
 379 dry conditions complete a hydrological year (see dates in Table 3), the cumulative SSIs were

380 calculated from the first month of the dry season. This allows the analysis of the impact of dry  
 381 conditions on the propagation of hydrological drought from one season to another. The  
 382 accumulated SSI showed that hydrological drought conditions do not recover from negative  
 383 values to positive values at the end of the hydrological year and thus, also impact periods after  
 384 those considered. This can be easily observed for the period between November, 1983 to October,  
 385 1984, when the accumulated SSI reached more intensely negative values due to previous dry  
 386 conditions affecting the same period in 1982-1983. In Niamey, at the middle sectors of the NRB, the  
 387 impact of droughts seemed have a greater effect on the hydrological conditions.



388

389 Figure 7. Box plot diagram of the SSI at a 1-month temporal scale (SSI1) for the NRB hydrological year  
 390 (from November to October). The smaller boxes represent the median, the major boxes identify the 10<sup>th</sup>  
 391 and 90<sup>th</sup> percentiles, and the whiskers extend from the minimum to maximum SSI1 value. The colour lines  
 392 represent the evolution of the accumulated 1-month time scale SSIs.

#### 393 4. Conclusions

394 In this study, we identified the dry and also wet conditions in the NRB using the SPEI and the  
 395 hydrological streamflow conditions using the SSI from 1980-2016. The NRB was more affected by  
 396 dry conditions during 1982-1988, 1998-2002, and 2009-2011. Particularly, in 1983, 1984, and 1985 the  
 397 rainfall deficit produced the most intense dry conditions. This clearly affected the hydrological  
 398 streamflow regime. A time lag between the impact on the water balance conditions in the basin and  
 399 the hydrological regime were found to be shorter in the Upper NRB sectors than in the middle  
 400 sectors. An analysis at subbasins scale will provide more accurate results. Considering the seasonal  
 401 precipitation cycle over the Niger Basin, those seasons affected by severe and extremely dry  
 402 conditions were identified as November-April of 1982-1983, 1983-1984, and 1986-1987, and  
 403 May-October of 1983, 1984, and 1987.

404 To further investigate the possible causes of the seasons being affected by intense droughts, the  
 405 moisture contribution to precipitation over the NRB was computed from the climatological source  
 406 located in the eastern SATl considered to be an important source of moisture particularly during the  
 407 rainy season for the WA monsoon. The analysis was also performed to determine the role of the  
 408 basin itself because of the important role of recycling in WA. This was implemented using a  
 409 Lagrangian method widely employed to diagnose atmospheric moisture transport. Despite its  
 410 importance, the anomaly of the contribution of moisture from the SATl source was positive during  
 411 the 1986-1987 dry season and the rainy seasons in 1983 and 1987. In the rest of the seasons affected  
 412 by severe and extremely dry conditions, the anomalies were negative. The explanation for this  
 413 behaviour is that the ITCZ located south of the Guinean coast acts as a moisture sink for air masses  
 414 in transit from the SATl source to WA. Thus, the position of the ITCZ determines the effectiveness of  
 415 the SATl source for the NRB. Further research is ongoing to determine the role of other regions  
 416 considered as moisture sources for the Niger basin as well as to determine any possible impact of the

417 variability of climate influences such as the El Niño–Southern Oscillation, North Atlantic Oscillation,  
418 Madden-Julian Oscillation, and others on moisture transport to the NRB.  
419

420 **Author Contributions:** R.N. and L.G. designed, proposed, and conducted the research; R.S. performed the  
421 experiments; R.S., R.N., and L.G. analysed the data; R.S., R.N., L.G., and A.D. wrote the paper.

422 **Funding:** This research was funded by the Spanish Government (Ministerio de Economía, Industria y  
423 Competitividad) and the European Regional Development Fund of the European Commission (in Spanish,  
424 FEDER) through the SETH project (CGL2014-60849-JIN). This research was partially supported by Xunta de  
425 Galicia under project ED413C 2017/64 “Programa de Consolidacion e Estructuracion de Unidades de  
426 Investigacion Competitivas (Grupos de Referencia Competitiva)” co-funded by the European Regional  
427 Development Fund (FEDER).

428 **Acknowledgments:** All the authors acknowledge the anonymous reviewers and the Water Journal by financing  
429 this publication.

430 **Conflicts of Interest:** The authors declare no conflict of interest. The founding sponsors had no role in the  
431 design of the study; in the collection, analyses, or interpretation of data; in the writing of the manuscript, or in  
432 the decision to publish the results.

### 433 References

- 434 1. Oyerinde, G.T.; Hountondji, F.C.C.; Wisser, D.; Diekkruger, B.; Lawin, A.E.; Odojin, A.J.; Afouda, A.  
435 Hydro-climatic changes in the Niger basin and consistency of local perceptions. *Reg Environ Change*. **2015**,  
436 15:1627–1637, doi: 10.1007/s10113-014-0716-7.
- 437 2. Zhang, W.; Brandt, M.; Guichard, F.; Tian, Q.; Fensholt, R. Using long-term daily satellite based rainfall  
438 data (1983–2015) to analyze spatio-temporal changes in the sahelian rainfall regime. *Journal of Hydrology*.  
439 **2017**, 550, 427–440.
- 440 3. Druyan, L.M.; Koster, R.D. Sources of Sahel Precipitation for Simulated Drought and Rainy Seasons. *J.*  
441 *Clim.* **1989**, 2, 1438–1446.
- 442 4. Van der Ent, R.J. A New View on the Hydrological Cycle over Continents. Ph.D. Thesis, Delft University  
443 of Technology, Delft, The Netherlands, 2014.
- 444 5. Sorí, R.; Nieto, R.; Drumond, A.; Gimeno, L. The Niger River Basin Moisture Sources: A Lagrangian  
445 Analysis. *Atmosphere*, **2017**, 8, 38.
- 446 6. Okpara, J. N.; Tarhule, A. A.; Perumal, M. Study of Climate Change in Niger River Basin, West Africa:  
447 Reality Not a Myth. Chapter 1. In: Climate Change – Realities, Impacts Over Ice Cap, Sea Level and Risks.  
448 **2013**. <http://dx.doi.org/10.5772/55186>.
- 449 7. Okpara, J.N.; Tarhule, A. Evaluation of Drought Indices in the Niger Basin, West Africa. *Journal of*  
450 *Geography and Earth Sciences*. **2015**, 3, 2, pp. 1–32. doi: 10.15640/jges.v3n2a1.
- 451 8. Masih, I.; Maskey, S.; Mussá, F. E. F.; Trambauer, P. A review of droughts on the African continent: a  
452 geospatial and long-term perspective. *Hydrol. Earth Syst. Sci.*, **2014**, 18, 3635–3649,  
453 doi:10.5194/hess-18-3635-2014.
- 454 9. Nicholson, S. On the question of the “recovery” of the rains in the West African Sahel. *Journal of Arid*  
455 *Environments*, **2005**, 63, 615–641.
- 456 10. Nicholson, S. The West African Sahel: A Review of Recent Studies on the Rainfall Regime and Its  
457 Interannual Variability. *ISRN Meteorology*, **2013** (2013), 32 pp., <http://dx.doi.org/10.1155/2013/453521>.
- 458 11. World Meteorological Organization, **2012**: Standardized Precipitation Index User Guide (M. Svoboda, M.  
459 Hayes and D. Wood). (WMO-No. 1090), Geneva, Switzerland.
- 460 12. Gautier, D.; Denis, D.; Locatelli, B. Impacts of drought and responses of rural populations in West Africa: a  
461 systematic review. *WIREs Clim Change*, **2016**, 7:666–681. doi: 10.1002/wcc.411.
- 462 13. Trenberth, K.E. Atmospheric Moisture Recycling: Role of Advection and Local Evaporation. *J. of Climate*,  
463 **1999**, 12, 1368–1381.
- 464 14. Gong, C.; Eltahir, E.A.B. Sources of Moisture for Rainfall in West Africa. *Water Resour. Res.* **1996**, 32, 3115–  
465 3121.
- 466 15. Nieto, R.; Gimeno, L.; Trigo, R.M. A Lagrangian identification of major sources of Sahel moisture. *Geophys.*  
467 *Res. Lett.* **2006**, 33, 1–6.

- 468 16. Knoche, H. R.; Kunstmann, H. Tracking atmospheric water pathways by direct evaporation tagging: A  
469 case study for West Africa. *J. Geophys. Res. Atmos.* **2013**, *118*, 12,345–12,358, doi:10.1002/2013JD019976.
- 470 17. Arnault, J.; Knoche, R.; Wei, J.; Kunstmann, H. Evaporation tagging and atmospheric water budget  
471 analysis with WRF: A regional precipitation recycling study for West Africa. *Water Resour. Res.* **2016**, *52*,  
472 1544–1567, doi:10.1002/2015WR017704.
- 473 18. Stohl, A.; James, P. A Lagrangian analysis of the atmospheric branch of the global water cycle. Part 1:  
474 Method description, validation, and demonstration for the August 2002 flooding in central Europe. *J.*  
475 *Hydrometeorol.* **2004**, *5*, 656–678.
- 476 19. Stohl, A.; James, P. A Lagrangian analysis of the atmospheric branch of the global water cycle: 2. Earth's  
477 river catchments, ocean basins, and moisture transports between them. *J. Hydrometeorol.* **2005**, *6*, 961–984.
- 478 20. Odekunle, T.O.; Eludoyin A.O. Sea surface temperature patterns in the Gulf of Guinea: their implications  
479 for the spatio-temporal variability of precipitation in West Africa. *Int. J. Climatol.* **2008**, *28*, 1507 – 1517.
- 480 21. Joly, M.; Voldoire, A. Role of the Gulf of Guinea in the inter-annual variability of the West African  
481 monsoon: What do we learn from CMIP3 coupled simulations?. *Int. J. Climatol.* **2010**, *30*, 1843–1856.
- 482 22. Ali, K.E.; Kouadio, K.Y.; Zahiri, E.-P.; Aman, A.; Assamoi, A.P.; Bourles, B. Influence of the Gulf of Guinea  
483 Coastal and Equatorial Upwellings on the Precipitations along its Northern Coasts during the Boreal  
484 Summer Period. *Asian Journal of Applied Sciences.* **2011**, *4* (3): 271-285.
- 485 23. Nnamchi, H.C.; Li, J.; Kang, I.-S.; Kucharski, F. Simulated impacts of the South Atlantic Ocean Dipole on  
486 summer precipitation at the Guinea Coast. *Clim Dyn.* **2013**, *41*: 677.
- 487 24. Kelemen, F. D.; Ludwig, P.; Reyers, M.; Ulbrich, S.; Pinto, J. G. Evaluation of moisture sources for the  
488 Central European summer flood of May/June 2013 based on regional climate model simulations. *Tellus A:*  
489 *Dynamic Meteorology and Oceanography.* **2016**, *68*:1, 29288, doi: 10.3402/tellusa.v68.29288.
- 490 25. Ciric, D.; Nieto, R.; Ramos, A.M.; Drumond, A.; Gimeno, L. Wet Spells and Associated Moisture Sources  
491 Anomalies across Danube River Basin. *Water.* **2017**, *9*, 615.
- 492 26. Drumond, A.; Nieto, R.; Gimeno, L. A Lagrangian approach for investigating anomalies in the moisture  
493 transport during drought episodes. *Cuadernos de Investigación Geográfica.* **2016**, *42*, 113–125,  
494 <https://doi.org/10.18172/cig.2925>.
- 495 27. Sorí, R.; Nieto, R.; Drumond, A.; Vicente-Serrano, S.V.; Gimeno, L. A Lagrangian perspective of the  
496 hydrological cycle in the Congo River basin. *Earth Syst. Dynam.* **2017**, *8*, 653–675, 2017,  
497 <https://doi.org/10.5194/esd-8-653-2017>.
- 498 28. Gimeno, L.: Grand challenges in atmospheric science, *Front. Earth Sci.*, *1*, 1–5,  
499 <https://doi.org/10.3389/feart.2013.00001>, 2013.
- 500 29. Gimeno, L., Stohl, A., Trigo, R. M., Dominguez, F., Yoshimura, K., Yu, L., Drumond, A., Durán-Quesada,  
501 A. M., and Nieto, R.: Oceanic and terrestrial sources of continental precipitation. *Rev. Geophys.* **2012**, *50*,  
502 RG4003, <https://doi.org/10.1029/2012RG000389>.
- 503 30. Drumond, A.; Gimeno, L.; Nieto, R.; Trigo, R.M.; Vicente-Serrano, S.M. Drought episodes in the  
504 climatological sinks of the Mediterranean moisture source: The role of moisture transport. *Global Planet.*  
505 *Change.* **2017**, *151*, 4–14.
- 506 31. Stojanovic, M.; Drumond, A.; Nieto, R.; Gimeno, L. Moisture Transport Anomalies over the Danube River  
507 Basin during Two Drought Events: A Lagrangian Analysis. *Atmosphere.* **2017**, *8*, 193.
- 508 32. Dirmeyer, P. A.; Brubaker, K.L. Contrasting evaporative moisture sources during the drought of 1988 and  
509 the flood of 1993. *J. Geophys. Res.* **1999**, *104*(D16), 19383–19397, doi:10.1029/1999JD900222.
- 510 33. Food and Agriculture Organization of the United Nations (FAO). Irrigation potential in Africa. A basin  
511 approach. *FAO Land and Water Bulletin.* 1997, *4*.
- 512 34. Lienou, G.; Mahe, G.; Dieulin, C.; Paturel, J. E.; Bamba, F.; Sighomnou, D.; Dessouassi, R. The River Niger  
513 water availability: facing future needs and climate change. *Global Change: Facing Risks and Threats to*  
514 *Water Resources* (Proc. of the Sixth World FRIEND Conference, Fez, Morocco, October 2010). IAHS Publ.  
515 340, 2010.
- 516 35. Andersen, I.; Dione, O.; Jarosewich-Holder, M.; Olivry, J.-C. *The Niger River Basin: A Vision for Sustainable*  
517 *Management*; World Bank: Washington, DC, USA, 2005.
- 518 36. Food and Agriculture Organization of the United Nations (FAO). *Disaster Risk Management Strategy in*  
519 *West Africa and the Sahel* (2011-2013), Rome, 2011.
- 520 37. Heim Jr., R. R.: A review of twentieth-century drought indices used in the United States, *B. Am. Meteorol.*  
521 *Soc.*, *83*, 1149–1165, 2002.

- 522 38. Zargar, A.; Sadiq, R.; Naser, B.; Khan, F.I. A review of drought indices. *Environmental Reviews*. 2011. 19:  
523 333–349, doi:10.1139/A11-013.
- 524 39. Vicente-Serrano, S. M., Beguería, S., and López-Moreno, J. I.: A Multiscalar Drought Index Sensitive to  
525 Global Warming: The Standardized Precipitation Evapotranspiration Index, *J. Climate*, 23, 1696–1718,  
526 <https://doi.org/10.1175/2009JCLI2909.1>, 2010.
- 527 40. Katerji, N.; Rana, G. Crop Reference Evapotranspiration: A Discussion of the Concept, Analysis of the  
528 Process and Validation. *Water Resour Manage.* 2011, 25, 1581–1600.
- 529 41. McKee, T., Doesken, N., and Kleist, J.: The relationship of drought frequency and duration to time scales,  
530 Eighth Conference on Applied Climatology, 17–22 January, Anaheim, California, 1993.
- 531 42. Stagge, J.H.; Kingston, D.G.; Tallaksen, L.M.; Hannah, D.M. Observed drought indices show increasing  
532 divergence across Europe. *Scientific Reports*. 2017, 7, 14045, doi:10.1038/s41598-017-14283-2.
- 533 43. Vicente-Serrano, S. M., López-Moreno, J. I., Santiago, B., LorenzoLacruz, J., Azorin-Molina, C., and  
534 Morán-Tejeda, E.: Accurate computation of a streamflow drought index., *J. Hydrol. Eng.*, 17, 318–332,  
535 2012.
- 536 44. Numaguti, A. Origin and recycling processes of precipitating water over the Eurasian continent:  
537 Experiments using an atmospheric general circulation model. *J. Geophys. Res.* 1999, 104, 1957–1972.
- 538 45. Drumond, A., Marengo, J., Ambrizzi, T., Nieto, R., Moreira, L., and Gimeno, L.: The role of the Amazon  
539 Basin moisture in the atmospheric branch of the hydrological cycle: a Lagrangian analysis. *Hydrol. Earth*  
540 *Syst. Sci.* 2014, 18, 2577–2598, <https://doi.org/10.5194/hess-18-2577-2014>.
- 541 46. Bin, C.; Xiang-De, X.; Tianland, Z. Main moisture sources affecting lower Yangtze River Basin in boreal  
542 summers during 2004–2009. *Int. J. Climatol.* 2013, 33, 1035–1046.
- 543 47. Ciric, D.; Stojanovic, M.; Drumond, A.; Nieto, R.; Gimeno, L. Tracking the Origin of Moisture over the  
544 Danube River Basin Using a Lagrangian Approach. *Atmosphere*. 2016, 7, 162.
- 545 48. Harris, I.; Jones, P.D.; Osborn, T.J.; Lister, D.H. Updated high-resolution grids of monthly climatic  
546 observations—The CRU TS3.10 Dataset. *Int. J. Climatol.* 2014, 34, 623–642.
- 547 49. Global Runoff Data Centre (2017): **River Discharge Data** / Global Runoff Data Centre. Koblenz, Federal  
548 Institute of Hydrology (BfG), [2017].
- 549 50. Dee, D.P.; Uppala, S.M.; Simmons, A.J.; Berrisford, P.; Poli, P.; Kobayashi, S.; Andrae, U.; Balmaseda, M.A.;  
550 Balsamo, G.; Bauer, P.; et al. The ERA-Interim reanalysis: Configuration and performance of the data  
551 assimilation system. *Q. J. R. Meteorol. Soc.* 2011, 137, 553–597.
- 552 51. Rienecker, M.M.; Suarez, M.J.; Gelaro, R.; Todling, R.; Bacmeister, J.; Liu, E.; Bosilovich, M.G.; Schubert,  
553 S.D.; Takacs, L.; Kim, G.-K.; Bloom, S.; Chen, J.; Collins, D.; Conaty, A.; da Silva, A.; et al. MERRA: NASA's  
554 Modern-Era Retrospective Analysis for Research and Applications. *J. Climate*. 2011, 24, 3624–3648.
- 555 52. Saha, S.; Moorthi, S.; Pan, H.; Wu, X.; Wang, J.; Nadiga, S.; Tripp, P.; Kistler, R.; Woollen, J.; Behringer, D.;  
556 Liu, H.; Stokes, D.; Grumbine, R.; Gayno, G.; Wang, J.; Hou, Y.; et al. The NCEP Climate Forecast System  
557 Reanalysis. *Bull. Amer. Meteor. Soc.* 2010, 91, 1015–1058.
- 558 53. Lorenz, C. and Kunstmann, H.: The hydrological cycle in three state-of-the-art reanalyses:  
559 Intercomparison and performance analysis, *J. Hydrometeorol.*, 2012, 13, 1397–1420.
- 560 54. Dutra, E.; Magnusson, L.; Wetterhall, F.; Cloke, H.L.; Balsamo, G.; Boussetta, S.; Pappenberger, F. The  
561 2010–2011 drought in the Horn of Africa in ECMWF reanalysis and seasonal forecast products. *Int. J.*  
562 *Climatol.*, 33: 1720–1729 (2013), DOI: 10.1002/joc.3545.
- 563 55. Ogilvie, A.; Mahe, G.; Ward, J.; Serpantie, G.; Lemoalle, J.; Morand, P.; Barbier, B.; Diop, A.T.; Caron, A.;  
564 Namara, R.; et al. Water, agriculture and poverty in the Niger River Basin. *Water Inter.* 2010, 35, 594–622.
- 565 56. Oloruntadea, A.J.; Mohammad, T.A.; Ghazalib, A.H.; Wayayoka, A. Analysis of meteorological and  
566 hydrological droughts in the Niger-South Basin, Nigeria. *Global and Planetary Change*. 2017, 155, 225–233.
- 567 57. Shukla, S.; Wood, A.W. Use of a standardized runoff index for characterizing hydrologic drought. *Geophys.*  
568 *Res. Lett.* 2008, 35, 1–7.
- 569 58. Lélé, M.I.; Leslie, L.M.; Lamb, P.J. Analysis of Low-Level Atmospheric Moisture Transport Associated  
570 with the West African Monsoon. *J. of Climate*. 2015, 28, 4414–4430. doi: 10.1175/JCLI-D-14-00746.1.
- 571 59. Leslie, L.M.; Lamb, P.J. Analysis of Low-Level Atmospheric Moisture Transport Associated with the West  
572 African Monsoon. *J. of Climate*. 2015, 28, 4414–4430.
- 573 60. Zheng, X.; Eltahir, E.A.B.; Emanuel, K.A. A mechanism relating tropical Atlantic spring sea surface  
574 temperature and west African rainfall. *Q.J.R. Meteorol. Soc.* 1999, 125: 1129–1163.  
575 doi:10.1002/qj.1999.49712555604.

- 576 61. Rodríguez-Fonseca, B.; et al. Variability and Predictability of West African Droughts: A Review on the  
577 Role of Sea Surface Temperature Anomalies. *J. Clim.* **2015**, *28*, 4034–4060.
- 578 62. Janicot, S. Spatiotemporal variability of West African rainfall. Part II: Associated surface and airmass  
579 characteristics. *J. Climate*, **1992**, *5*, 499–511.
- 580 63. Eltahir, E.A.B. A Soil Moisture–Rainfall Feedback Mechanism: 1. Theory and observations. *Water Resour.*  
581 *Res.* **1998**, *34*(4), 765–776, doi:10.1029/97WR03499.
- 582 64. Zheng, X., and E. A. B. Eltahir (1998), A Soil Moisture–Rainfall Feedback Mechanism: 2. Numerical  
583 experiments, *Water Resour. Res.*, *34*(4), 777–785, doi:10.1029/97WR03497.
- 584



© 2018 by the authors. Submitted for possible open access publication under the terms and conditions of the Creative Commons Attribution (CC BY) license

587 (<http://creativecommons.org/licenses/by/4.0/>).

# 5

## Conclusions

In this thesis the principal aim was to investigate the role of the atmospheric branch of the hydrological cycle as a bridge between ocean and land evaporation and precipitation over the Negro and Madeira River Basins in the Amazon; the Congo River Basin in Central Equatorial Africa; the Niger River Basin in West Africa, and the Indus, Ganges, and Brahmaputra in the Indo-Gangetic region in Southeast Asia. These basins are located in regions characterised by monsoonal climates. The study was carried out individually for each river basin. To accomplish the aims the Lagrangian model FLEXPART was used, a robust tool used to diagnose atmospheric motion widely implemented to investigate the transport of moisture in the atmosphere. Several crucial aspects of the hydrological cycle such as the characterisation of annual cycles of precipitation, runoff, river discharge, and river water levels were also investigated. The period of analyses was heterogeneous among the study for each basin, taking into account the geographic availability of data. Afterward, the principal global sources of moisture for each basin were identified and the role of oceanic and continental sources on the moisture contribution to precipitation over the basins was determined separately. In general, the dry and wet conditions were diagnosed for each basin. Specific objectives for each basin were determined according to the location and availability of the datasets. The results obtained for each river basin, particularly, the principal results (moisture source locations, moisture contribution from the sources to the precipitation over the basin ( $(E - P) < 0$ ), dry and/or wet conditions in the basins, and the role of the sources) are listed below. However, the articles describe with the full details the specific results obtained for each basin such as the onset of the rainy season for the Negro, Madeira, Indus, Ganges,

and Brahmaputra Basins and the effectiveness of the sources for the Congo River Basin etc.

### **Congo River Basin:**

Moisture source locations: Nine regions were identified and considered to be the most important moisture sources; five continental and four oceanic. The five continental regions are located as follows: central and north-eastern Africa, the equatorial-western section of the continent on both sides of the Equator and at the river mouth, the eastern Congo River Basin along the coast of Africa from the north of Somalia and Ethiopia to approximately 20° N, and the Congo River Basin itself. The four oceanic sources are in the Red Sea, the Arabian Sea, the eastern tropical equatorial South Atlantic Ocean along the coast of Africa, and the tropical western Indian Ocean.

Moisture contribution from the sources to the precipitation over the basin  $(E - P) < 0$ : The Congo River Basin receives humidity from both hemispheres. It is remarkable that the basin itself provides more than 50% of the total atmospheric moisture contribution to precipitation. The result confirms the high evaporation recycling occurring in Central Equatorial Africa that has been well documented by other authors. Additionally, throughout the climatological year, the surrounding continental regions and the eastern tropical South Atlantic Ocean play a key role in the moisture supply. In contrast, the Red Sea that is considered a source is merely important despite its high evaporation rate.

Dry and/or wet conditions in the basins; the role of the sources: The temporal evolution of the 1- and 12-month SPEI series calculated for the Congo River Basin showed dry conditions prevailing during the periods 1980–1985, 1992–1998, and 2004–2006. The prevalence of wet conditions can be seen from 1985–1991 and from 2007–2010. During the period from 1980–2010, 1995 and 1996 were characterised by severe and extreme drought conditions, respectively, while 1982 was characterised as severely wet. The moisture contribution from the sources confirms the crucial role of the Congo River Basin in modulating the water balance within itself. During wet (dry) years, the contribution of moisture  $((E - P) < 0)$  from the Congo River Basin to precipitation over itself increased (decreased). On average, the water balance in the atmosphere over this basin was not homogenous during these years, indicating a distinct role within itself. This result

confirmed that research on the hydrological cycle should not be performed for the entire basin as a whole.

### **Indus, Ganges, and Brahmaputra River Basins:**

Moisture sources location: The principal moisture sources identified for these basins are positioned in oceanic and continental (including the basins themselves) regions. There were two main climate seasons identified for the region, the Monsoonal Precipitation Regime (MPR) period from May to October and the Westerly Precipitation Regime (WPR) that occurs from November to April. The sources are divided into continental and oceanic and named according to their geographical location. The main regions where the three basins receive moisture are the surrounding continental region and the Indian Ocean. However, in the case of the Indus River Basin the air masses uptake humidity from the eastern Mediterranean, while the Indus and Ganges Basins are the sources of humidity for the Brahmaputra River Basin. The spatial extension of the sources increases during the MPR period as expected, it is best observed in the Indian Ocean.

Moisture contribution from the sources to the precipitation over the basin ( $E - P < 0$ ): In both the WPR and the MPR periods, the moisture contribution from continental sources to precipitation over the Indus and Ganges River Basins is major from continental sources. However, moisture input occurs first during the monsoon onset from the Indian Ocean. These results suggest the importance of recycled precipitation over the basins. For the Ganges River Basin, the Bay of Bengal is the most important oceanic source during the WPR. For the Brahmaputra River Basin, the most important moisture sources in the WPR are on the continent itself and the Indian region, while in the ocean for the Bay of Bengal and the Indian Ocean. For the MPR, the Indian Ocean is the most important moisture source, and overall, the oceanic sources are the mostly responsible for the moisture loss over this basin.

Dry and/or wet conditions in the basins; the role of the sources: The longest and intense dry conditions affected the Indus River Basin from 1998–2002 and 2009. The longest period under wet conditions occurred during 1995–1996 and after 2011. In the Ganges River Basin, the 2000–2010 decade was very frequently affected by intense dry conditions, whereas from 1981–1991 by wet conditions. In the Brahmaputra River Basin in the dry conditions prevailed in 1981–1986, 2003–2010, and 2012–2015, while wet

conditions prevailed during 1987–1991, 1998, late 1999–2000, and 2007. The 6-month SPEI at the end of October (April) was used to diagnose dry and wet conditions in the basins over the MPR (WPR) season.

The roles of the sources in the moisture contribution to precipitation during severe and extremely dry and wet conditions in the basins were assessed for the WPR and MPR in composited seasons affected by severe and extremely dry and wet conditions. The composites confirmed the crucial role of the most important moisture sources (e.g. the Indian region, Indian Ocean, Bay of Bengal, and the basins themselves) in providing less (more) humidity during dry (wet) conditions in both the WPR and MPR periods.

### **Negro and Madeira River Basins**

Moisture sources locations: We divided the sources into oceanic and continental considering the origin of the air masses that uptake the major amount of humidity before arriving at the basins. The location of the oceanic sources for the Negro and Madeira River Basins are almost similar in the Tropical North and South Atlantic. Over the continent, the moisture sources of the Negro River Basin are mostly to the northeast of the basin. Conversely, the continental moisture sources of the Madeira River Basin extend into the north half of the Amazon River Basin and the north in South America. Besides, to the south of the basin are two regions considered important moisture sources.

Moisture contribution from the sources to the precipitation over the basin  $(E - P) < 0$ : For the Negro River basin, the most important moisture sources are the Tropical North and South Atlantic, but also the basin itself. The role of the oceanic sources on the moisture contributions differs across the year because they are located in different hemispheres, providing more moisture during the wintertime.

For the Madeira River Basin, the rest of the Amazon River Basin plays a crucial role on the total moisture loss over the basin. The basin itself and the Tropical North and South Atlantic are also important sources of moisture. Between the oceanic sources, the Tropical South Atlantic on average supplies more humidity to the Madeira Basin from April to November.

Dry and wet conditions; the role of the sources: The Negro River Basin was mostly affected by dry conditions from 1980–1993, 1991–1992, and from 2013–2016. Wet conditions prevailed in the period between 1996–2007. In the Madeira River Basin, the

intense and longest periods affected by dry conditions occurred approximately in 1995–1996, 1998, 2003–2005, and 2015–2016. Wet conditions in this basin were frequent and intense during 1980–1986 when the Negro Basin was affected by drought. As reported here and by several authors, there are northern-southern water budget differences and consequently, the rainfall annual cycles vary as well as the hydrological extremes. However, the impact of the El Niño phenomenon reduces the precipitation homogeneously over all of the Amazon River Basin.

### **Niger River Basin**

Moisture sources location: Throughout the year, the NRB main moisture sources are located on the tropical eastern North Atlantic Ocean near Africa, the tropical eastern South Atlantic Ocean in the Gulf of Guinea, in the regions surrounding the Sahel, and in the Mediterranean Sea. The extension of the sources changes between the dry (November–April) and rainy (May–October) seasons.

Moisture contribution from the sources to the precipitation over the basin ( $E - P$ )  $< 0$ : In this study the moisture uptake ( $E - P$ )  $> 0$  was computed over the sources by air masses in transient to the basin. In the dry season (November–April), the greatest moisture uptake takes place in the Niger River Basin itself, followed by the East Sahel and the eastern South Atlantic Ocean. In the rainy season (May–October), when the major precipitation occurs over the Niger River Basin, the ( $E - P$ )  $> 0$  values over the Niger River Basin itself decrease and the atmospheric circulation associated with the West African monsoon favours greater moisture transport to the basin from regions located to the north-east, east, and south of the basin. Particularly the moisture contribution from the source located in the eastern South Atlantic Ocean was computed.

Dry and wet conditions; the role of the sources: This assessment was conducted for the dry and rainy seasons separately through the SPEI at a temporal scale of six months obtained for April and October. The role of the South Atlantic Ocean was not homogeneous for all the seasons affected by the severe and extremely dry conditions due to the **Intertropical Convergence Zone** position. A detailed analysis will be performed in future (on-going work) to clarify the role of the rest of the sources.

More research should be done to investigate the influence of the different modes of climatic variability, and the role of the same basins as sources of moisture for remote regions. In addition, new questions arose regarding the impact of the water vapour residence time in the calculus of  $(E - P)$ .

# Appendix A: Supplementary Material

Atmosphere 2017, 6, 38; doi:10.3390/atmos8020038

S1 of S1

## Supplementary Materials: The Niger River Basin Moisture Sources: A Lagrangian Analysis

Rogert Sorí, Raquel Nieto, Anita Drumond and Luis Gimeno

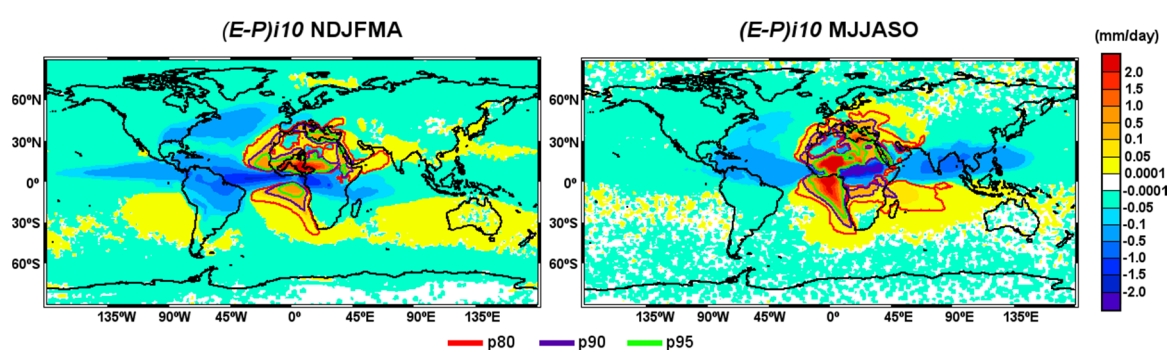


**Figure S1.** Average pattern of  $(E - P)$  backward results integrated from the Niger River Basin for all 10 days for the dry (a) and wet season (b). The lines red, purple and green represents the 80th, 90th and 95th percentile of the  $(E - P)i10 > 0$  values for every season.



© 2017 by the authors; licensee MDPI, Basel, Switzerland. This article is an open access article distributed under the terms and conditions of the Creative Commons Attribution (CC BY) license (<http://creativecommons.org/licenses/by/4.0/>).

# References

- Abramowitz, M., and Stegun, I.A. (1965). Handbook of Mathematical Functions, with Formulas, Graphs, and Mathematical Tables. Dover Publications, 1046 pp.
- Aguilar, E. et al. (2009). Changes in temperature and precipitation extremes in western central Africa, Guinea Conakry, and Zimbabwe, 1955–2006. *J. Geophys. Res.*, 114, D02115, doi: 10.1029/2008JD011010.
- Alam, J.M., and Lin, J.C. (2008). Toward a Fully Lagrangian Atmospheric Modeling System. *Mon. Wea. Rev.* 136, 4653–4667. <https://doi.org/10.1175/2008MWR2515.1>
- Allan, R.P., and Liepert, B.G. (2010). Anticipated changes in the global atmospheric water cycle. *Environ. Res. Lett.* 5, 025201, doi:10.1088/1748-9326/5/2/025201.
- Alley, W.M., (1984). The Palmer Drought Severity Index: limitations and assumptions. *J. of Climate and Applied Meteorology.* 23, 1100–1109. doi: 10.1175/1520-0450(1984)023<1100:TPDSIL>2.0.CO;2.
- Baumgartner, A., and Reichel., E. The World Water Balance. *Elsevier.*, Amsterdam, **1975**, 179 pp.
- Beguiría, S., S.M. Vicente-Serrano, and M. Angulo-Martínez, 2010: A Multiscalar Global Drought Dataset: The SPEI base: A New Gridded Product for the Analysis of Drought Variability and Impacts. *Bull. Amer. Meteor. Soc.* 91, 1351–1356. <https://doi.org/10.1175/2010BAMS2988.1>
- Beguiría, S., Vicente-Serrano, S.M., Reig, F., Latorre, B. (2014). Standardized precipitation evapotranspiration index (SPEI) revisited: parameter fitting, evapotranspiration models, tools, datasets and drought monitoring. *Int. J. Climatol.* 34, 3001-30232014, doi:10.1002/joc.3887.
- Benton, G.S., and Estoque, M.A. (1954). Water vapor transfer over the North American continent. *J. Meteorol.* 11(6), 462–477. doi:10.1175/1520-0469(1954)011<0462:WVTOTN>2.0.CO;2
- Betts, R.A. (2006). Forcings and feedbacks by land ecosystem changes on climate change. *J. Phys. IV France.* 139, 123-146. doi:10.1051/jp4:2006139009

- Bian, Q., and Lu R. (2013). Impact of sea surface temperature trend on late summer Asian rainfall in the twentieth century. *J. Geophys. Res. Atmos.* 118, 4256–4266. doi: 10.1002/jgrd.50386
- Bosilovich, M.G., and Schubert, S.D. (2002). Water vapor tracers as diagnostics of the regional hydrologic cycle. *J. Hydrometeorol.* 3, 149–165. doi:10.1175/1525-7541(2002)003<0149:WVTADO>2.0.CO;2
- Bosilovich, M. G., Sud, Y. C., Schubert, S. D., and Walker, G. K. (2003). Numerical simulation of the large-scale North American monsoon water sources. *J. Geophys. Res.* 108, 8614. <https://doi.org/10.1029/2002JD003095>.
- Brioude, J., Arnold, D., Stohl, A., Cassiani, M., Morton, D., Seibert, P., Angevine, W., Evan, S., Dingwell, A., Fast, J. D., Easter, R. C., Pisso, I., Burkhardt, J., and Wotawa, G. (2013). The Lagrangian particle dispersion model FLEXPART-WRF version 3.1. *Geosci. Model Dev.* 6, 1889-1904. <https://doi.org/10.5194/gmd-6-1889-2013>
- Brioude, J., Angevine, W.M., McKeen, S.A., and Hsie, E.-Y. (2012). Numerical uncertainty at mesoscale in a Lagrangian model in complex terrain. *Geosci. Model Dev.* 5, 1127-1136. <https://doi.org/10.5194/gmd-5-1127-2012>, 2012
- Brooks, C. E. (1928). The influence of forests on rainfall and run-off. *Q.J.R. Meteorol. Soc.* 54, 1-17. doi:10.1002/qj.49705422501
- Brubaker, K.L., Entekhabi, D., and Eagleson, P.S. (1993). Estimation of Continental Precipitation Recycling. *J. Climate.* 6, 1077–1089. [https://doi.org/10.1175/1520-0442\(1993\)006<1077:EOCPR>2.0.CO;2](https://doi.org/10.1175/1520-0442(1993)006<1077:EOCPR>2.0.CO;2)
- Brubaker, K. L., Dirmeyer, P.A., Sudradjat, A., Levy, B.S., and Bernal, F. (2001). A 36-yr climatological description of the evaporative sources of warm-season precipitation in the Mississippi River basin. *J. Hydrometeorol.* 2, 537–557. doi:10.1175/1525-7541(2001)002<0537:AYCDOT>2.0.CO;2
- Budyco, M. J. (1974). *Climate and life*. Academic Press. N.Y. 508.
- Cécé, R., Bernard, D., Brioude, J., and Zahibo, N. (2016). Microscale anthropogenic pollution modelling in a small tropical island during weak trade winds: Lagrangian particle dispersion simulations using real nested LES meteorological fields. *Atmospheric Environment.* 139, 98–112. <https://doi.org/10.1016/j.atmosenv.2016.05.028>.

- Chris, F., Peterson, P., Landsfeld, M., Pedreros, D., Verdin, J., Shukla, S., Husak, G., Rowland, J., Harrison, L., Hoell, A., and Michaelsen, J. (2015). The climate hazards infrared precipitation with stations – a new environmental record for monitoring extremes. *Scientific Data*. 2, 150066. <https://doi.org/10.1038/sdata.2015.66>
- Chowdhury, M.R. and Ward, N. (2004). Hydro-meteorological variability in the greater Ganges–Brahmaputra–Meghna basins. *Int. J. Climatol.* 24, 1495-1508. doi:10.1002/joc.1076.
- D'Abreton, P.C., and Tyson, P.D. (1995). Divergent and non-divergent water vapor transport over southern Africa during wet and dry conditions. *Meteorol. Atmos. Phys.* 55(1–2), 47–59. doi:10.1007/BF01029601
- Dansgaard, W. (1964). Stable isotopes in precipitation. *Tellus*, 16, 436–468, doi:10.1111/j.2153-3490.1964.tb00181.x.
- Dee, D.P., Uppala, S.M., Simmons, A.J., Berrisford, P., Poli, P., Kobayashi, S., Andrae, U., Balmaseda, M.A., Balsamo, G., Bauer, P., et al. (2011). The ERA-Interim reanalysis: Configuration and performance of the data assimilation system. *Q. J. R. Meteorol. Soc.* 137, 553–597. <https://doi.org/10.1002/qj.828>
- Dezfuli, A.K., and Nicholson, S.E. (2013). The Relationship of Rainfall Variability in Western Equatorial Africa to the Tropical Oceans and Atmospheric Circulation. Part II: The Boreal Autumn. *J. Climate*. 26, 66–84. <https://doi.org/10.1175/JCLI-D-11-00686.1>.
- Dirmeyer, P.A., and Brubaker, K.L. (1999). Contrasting evaporative moisture sources during the drought of 1988 and the flood of 1993. *J. Geophys. Res.* 104, 19,383–19,397. doi:10.1029/1999JD900222
- Dirmeyer, P.A., and Brubaker, K.L. (2006). Evidence for trends in the Northern Hemisphere water cycle. *Geophys. Res. Lett.* 33, L14712. doi:10.1029/2006GL026359
- Dirmeyer, P. A., K. L. Brubaker, and T. DelSole, 2009: Import and export of atmospheric water vapor between nations. *J. Hydrol.*, 365, 11–22, doi:<https://doi.org/10.1016/j.jhydrol.2008.11.016>.
- Douville, H., Conil, S., Tyteca, S., Voldoire, A. Soil moisture memory and West African monsoon predictability: artefact or reality?. *Clim Dyn* (2007) 28: 723. <https://doi.org/10.1007/s00382-006-0207-8>

- Dutta, S.K., Das, S., Kar, S.C. et al. Impact of vegetation on the simulation of seasonal monsoon rainfall over the Indian subcontinent using a regional model. *J Earth Syst Sci* (2009) 118: 413. <https://doi.org/10.1007/s12040-009-0048-z>.
- Eltahir, E. A. B. and Bras, R. L. (1996). Precipitation recycling. *Rev. Geophys.* 34, 367–378. <https://doi.org/10.1029/96RG01927>
- Eltahir, E.A.B. (1998). A soil moisture–rainfall feedback mechanism: 1. Theory and observations. *Water Resour Res.* 34(4), 765–776.
- Emanuel, K., and Zivrovic-Rothman, M. (1999). Development and Evaluation of a Convection Scheme for Use in Climate Models. *J. of Atmospheric Physics.* 56, 1766–1782.
- Forster, C., Stohl, A., and Seibert, P. (2007). Parameterization of Convective Transport in a Lagrangian Particle Dispersion Model and Its Evaluation. *J. Appl. Meteor. Climatol.* 46, 403–422. <https://doi.org/10.1175/JAM2470.1>
- Gedzelman, S.D., Rosenbaum, J.H. and Lawrence, J.R., 1989. The megalopolitan snowstorm of 11-12 February 1983: isotopic composition of the snow. *J. Atmosph. Sc.* 46: 1637-1649.
- Gedzelman, S., Lawrence, J., Gamache, J., Black, M., Hindman, E., Black, R., Dunion, J., Willoughby, H., and Zhang, X. (2003). Probing Hurricanes with Stable Isotopes of Rain and Water Vapor. *Mon. Wea. Rev.* 131, 1112–1127. [https://doi.org/10.1175/1520-0493\(2003\)131<1112:PHWSIO>2.0.CO;2](https://doi.org/10.1175/1520-0493(2003)131<1112:PHWSIO>2.0.CO;2)
- Gimeno, L., Drumond, A., Nieto, R., Trigo, R. M., and Stohl, A.: On the origin of continental precipitation, *Geophys. Res. Lett.*, 37, L13804, <https://doi.org/10.1029/2010GL043712>, 2010.
- Gimeno, L., Stohl, A., Trigo, R. M., Dominguez, F., Yoshimura, K., Yu, L., Drumond, A., Durán-Quesada, A. M., and Nieto, R.: Oceanic and terrestrial sources of continental precipitation, *Rev. Geophys.*, 50, RG4003, <https://doi.org/10.1029/2012RG000389>, 2012.
- Gimeno, L.: Grand challenges in atmospheric science, *Front. Earth Sci.*, 1, 1–5, <https://doi.org/10.3389/feart.2013.00001>, 2013.
- Gusyev, M.A., A. Hasegawa, J. Magome, D. Kuribayashi, H. Sawano and S. Lee, 2015: Drought Assessment in the Pampanga River Basin, the Philippines. Part 1: A Role of Dam Infrastructure in Historical Droughts. *Proceedings of the 21st International*

- Congress on Modelling and Simulation (MODSIM 2015), Broadbeach, Queensland, Australia.
- Haines, R.S. Kovats, D. Campbell-Lendrum, C. Corvalan, Climate change and human health: Impacts, vulnerability and public health, *Public Health*, Volume 120, Issue 7, 2006, Pages 585-596, ISSN 0033-3506, <https://doi.org/10.1016/j.puhe.2006.01.002>.
- Hartmann, H., and Buchanan, H. Trends in extreme precipitation events in the Indus River Basin and flooding in Pakistan. *Atmos. Ocean* 52, 77–91 (2014).
- Hasson, S., Lucarini, V., and Pascale, S. (2013). Hydrological cycle over South and Southeast Asian river basins as simulated by PCMDI/CMIP3 experiments. *Earth Syst. Dynam.* 4, 199–217. <https://doi.org/10.5194/esd-4-199-2013>
- Hegerl, G.C., E. Black, R.P. Allan, W.J. Ingram, D. Polson, K.E. Trenberth, R.S. Chadwick, P.A. Arkin, B.B. Sarojini, A. Becker, A. Dai, P.J. Durack, D. Easterling, H.J. Fowler, E.J. Kendon, G.J. Huffman, C. Liu, R. Marsh, M. New, T.J. Osborn, N. Skliris, P.A. Stott, P. Vidale, S.E. Wijffels, L.J. Wilcox, K.M. Willett, and X. Zhang, 2015: Challenges in Quantifying Changes in the Global Water Cycle. *Bull. Amer. Meteor. Soc.*, 96, 1097–1115, <https://doi.org/10.1175/BAMS-D-13-00212.1>.
- Hegarty, J., Draxler, R.R., Stein, A.F., Brioude, J., Mountain, M., Eluszkiewicz, J., Nehr Korn, T., Ngan, F., and Andrews, A. (2013). Evaluation of Lagrangian Particle Dispersion Models with Measurements from Controlled Tracer Releases. *J. Appl. Meteor. Climatol.* 52, 2623–2637. <https://doi.org/10.1175/JAMC-D-13-0125.1>
- Heim, R.R. (2002). A review of twentieth-century drought indices used in the United States. *Bulletin of the American Meteorological Society.* 83, 1149-1165.
- Hellwig, J., Stahl, K., Ziese, M., and Becker, A. (2018). The impact of the resolution of meteorological data sets on catchment-scale precipitation and drought studies. *Int. J. Climatol.* 1–13. doi: 10.1002/joc.5483
- Herrera-Estrada, J. E., Satoh, Y., and Sheffield, J.: Spatiotemporal dynamics of global drought, *Geophys. Res. Lett.*, 44, 2254–2263, <https://doi.org/10.1002/2016GL071768>, 2017.
- Hilker, T., Lyapustin, A.I., Tucker, C.J., Hall, F.G., Myneni, R.B., Jian-Bi, Y.W., de Moura, Y.M., Sellers, P.J. Vegetation dynamics and rainfall sensitivity of the Amazon. *Proceedings of the National Academy of Sciences* Nov 2014, 111 (45) 16041-16046; DOI: 10.1073/pnas.1404870111.

- Hu, Q., and Willson, G.D. (2000). Effects of temperature anomalies on the Palmer Drought Severity Index in the central United States. *Int. J. Climatol.* 20(15), 1899–1911. doi:10.1002/1097-0088(200012)20:15<1899::AID-JOC588>3.0.CO;2-M
- Hua, W., Zhou, L., Chen, H., Nicholson, S.E., Raghavendra, A., Jiang, Possible causes of the Central Equatorial African long-term drought. *Environ. Res. Lett.*, 11 (2016), 10.1088/1748-9326/11/12/124002.
- IPCC, 2014: Climate Change 2014: Synthesis Report. Contribution of Working Groups I, II and III to the Fifth Assessment Report of the Intergovernmental Panel on Climate Change [Core Writing Team, R.K. Pachauri and L.A. Meyer (eds.)]. IPCC, Geneva, Switzerland, 151 pp.
- James, P., Stohl, A., Forster, C., Eckhardt, S., Seibert, P., and Frank, A. (2003). A 15-year climatology of stratosphere-troposphere exchange with a Lagrangian particle dispersion model: 1. Methodology and validation. *J. Geophys. Res.* 108, 8519. doi:10.1029/2002JD002637
- Jiménez-Muñoz, J. C., Mattar, C., Barichivich, J., Santamaría-Artigas, A., Takahashi, K., Malhi, Y., Sobrino, J.A., Schrier, Gv. Record-breaking warming and extreme drought in the Amazon rainforest during the course of El Niño 2015–2016. *Scientific Reports.*, 2016, 6, 33130, <http://dx.doi.org/10.1038/srep33130>.
- Joshi, M.K. and Rai, A. (2015). Combined interplay of the Atlantic multidecadal oscillation and the interdecadal Pacific oscillation on rainfall and its extremes over Indian subcontinent. *Clim Dyn.* 44, 3339. <https://doi.org/10.1007/s00382-014-2333-z>.
- Joussaume, S., Jouzel, J., and Sadourny R. (1984). A general circulation model of water isotope cycles in the atmosphere. *Nature.* 311, 24–29, doi:10.1038/311024a0.
- Knight, J.R., Folland, C.K. and Scaife, A.A. (2006). Climate impacts of the Atlantic Multidecadal Oscillation. *Geophys. Res. Lett.* 33, L17706, doi: 10.1029/2006GL026242.
- Köppen, W. (1936). Das geographische System der Klimate, in: *Handbuch der Klimatologie*, edited by: Köppen, W. and Geiger, G., 1. C. Gebr, Borntraeger, 1–44.
- Koster, R., Jouzel, J., Souzzo, R., Russel, G., Rind, D., and Eagleson, P.S. (1986). Global sources of local precipitation as determined by the NASA/GISS GCM. *Geophys. Res. Lett.* 13, 121–124. doi:10.1029/GL013i002p00121.

- Läderach, A., and Sodemann, H. (2016). A revised picture of the atmospheric moisture residence time. *Geophys. Res. Lett.* 43, 924–933. doi:10.1002/2015GL067449
- Lake, S. (2011). *Drought and Aquatic Ecosystems: Effects and Responses*. Wiley-Blackwell Ed. 1 edition. doi:10.1002/9781444341812
- Lal, R. (1993). Challenges in Agriculture and Forest Hydrology in Humid Tropics. In: *Hydrology and Water Management in the Humid Tropics*. Hydrological research issues and strategies for water management. Edited by: Michael Bonell, Maynard M. Hufschmid and John S. Gladwell. Cambridge University Press.
- Lehner, B. and Grill, G. (2013). Global river hydrography and network routing: baseline data and new approaches to study the world's large river systems. *Hydrol. Process.* 27, 2171–2186.
- Liebmann, B., Camargo, S.J., Seth, A., Marengo, J.A., Carvalho, L.M., Allured, D., Fu, R., Vera, C.S. (2007). Onset and End of the Rainy Season in South America in Observations and the ECHAM 4.5 Atmospheric General Circulation Model. *J. Clim.* 20, 2037–2050.
- Liebmann, B., and Marengo, J. (2001). Interannual Variability of the Rainy Season and Rainfall in the Brazilian Amazon Basin. *J. Clim.* 14, 4308–4318.
- López-Moreno, J. I., Vicente-Serrano, S. M., Beguería, S., García-Ruiz, J. M., Portela, M. M., and Almeida, A. B. (2009). Downstream propagation of hydrological droughts in highly regulated transboundary rivers: The case of the Tagus River between Spain and Portugal. *Water Resour. Res.* 45(2), W02405.
- Lorenzo-Lacruz, J., Vicente-Serrano, S.M., López-Moreno, J.I., Beguería, S., García-Ruiz, J.M., and Cuadrat, J.M. (2010). The impact of droughts and water management on various hydrological systems in the headwaters of the Tagus River (central Spain). *J. Hydrol.* 386(1–4), 13–26.
- Lu, E., et al. (2014). The atmospheric anomalies associated with the drought over the Yangtze River basin during spring 2011. *J. Geophys. Res. Atmos.* 119, 5881–5894. doi:10.1002/2014JD021558.
- Marengo, J.A., Alves, L.M., Soares, W.R., Rodriguez, D.A., Camargo, H., Riveros, M.P., and Pabló, A.D. (2013). Two Contrasting Severe Seasonal Extremes in Tropical

- South America in 2012: Flood in Amazonia and Drought in Northeast Brazil. *J. Climate*. 26, 9137–9154. <https://doi.org/10.1175/JCLI-D-12-00642.1>
- Marengo, J.A. and Espinoza, J.C. (2016), Extreme seasonal droughts and floods in Amazonia: causes, trends and impacts. *Int. J. Climatol.* 36, 1033-1050. doi:10.1002/joc.4420.
- Marengo, J.A., Tomasella, J., Soares, W.R. et al. *Theor Appl Climatol* (2012) 107: 73. <https://doi.org/10.1007/s00704-011-0465-1>.
- Marshall, J. H., N. Dixon, L. Garcia-Carreras, G. M. S. Lister, D. J. Parker, P. Knippertz, and C. Birch (2013), The role of moist convection in the West African monsoon system: Insights from continental-scale convection-permitting simulations. *Geophys. Res. Lett.* 40, 1843–1849. doi: 10.1002/grl.50347.
- Massacand, A.C., Wernli, H., and Davies H.C. (1998). Heavy precipitation on the Alpine southside: An upper-level precursor. *Geophys. Res. Lett.* 25, 1435–1438, doi:10.1029/98GL50869
- McKee, T.B., Doesken, N.J., Kleist, J. (1993). The relationship of drought frequency and duration to time scales. *In: Proceedings of the Eighth Conference on Applied Climatology*. Anaheim, CA, USA, 17–22 January, pp. 179–184.
- Nalbantis, I. and Tsakiris, G. (2009). Assessment of hydrological drought revisited. *Water Resources Management*, 23(5), 881 – 897.
- Ndehedehe, C.E., Awange. J.L., Kuhn, M., Agutu, N.O., Fukuda, Y. (2017). Climate teleconnections influence on West Africa's terrestrial water storage. *Hydrological Processes*. 31, 3206–3224. <https://doi.org/10.1002/hyp.11237>
- Numaguti, A. (1999). Origin and recycling processes of precipitating water over the Eurasian continent: Experiments using an atmospheric general circulation model. *J. Geophys. Res.* 104, 1957–1972.
- Noska, R.; Misra, V. (2016). Characterizing the onset and demise of the Indian summer monsoon. *Geophys. Res. Lett.* 2016, 43, 4547–4554
- Notaro, M., G. Chen, and Z. Liu, 2011: Vegetation Feedbacks to Climate in the Global Monsoon Regions. *J. Climate*, 24, 5740–5756, <https://doi.org/10.1175/2011JCLI4237.1>.

- Pathak, A., S. Ghosh, and P. Kumar, 2014: Precipitation Recycling in the Indian Subcontinent during Summer Monsoon. *J. Hydrometeor.*, 15, 2050–2066, <https://doi.org/10.1175/JHM-D-13-0172.1>.
- Palmer, W.C. (1965). Meteorological Drought. Res. Paper No.45, 58pp., Dept. of Commerce, Washington, D.C.
- Palazzi E., and Provenzale, A. (2016) Water in the climate system. In: Provenzale A., Palazzi E., Fraedrich K. (eds) *The Fluid Dynamics of Climate*. CISM International Centre for Mechanical Sciences, vol 564. Springer, Vienna.
- Paeth, H., Fink, A.H., Pohle, S., Keis, F., Mächel, H., and Samimi, C. (2011). Meteorological characteristics and potential causes of the 2007 flood in sub-Saharan Africa. *Int. J. Climatol.* 31, 1908-1926. doi:10.1002/joc.2199
- Paul, S., Ghosh, S., Oglesby, R., Pathak, A., Chandrasekharan, A., Ramsankaran, R. Weakening of Indian Summer Monsoon Rainfall due to Changes in Land Use Land Cover (2016) *Scientific Reports*, 6, art. no. 32177. doi: 10.1038/srep32177.
- Peters T. (2016) Water Balance in Tropical Regions. In: Pancel L., Köhl M. (eds) *Tropical Forestry Handbook*. Springer, Berlin, Heidelberg. [https://doi.org/10.1007/978-3-642-54601-3\\_40](https://doi.org/10.1007/978-3-642-54601-3_40)
- Peel, M.C., Finlayson, B.L., and McMahon, T.A. (2007). Updated world map of the Köppen-Geiger climate classification. *Hydrol. Earth Syst. Sci.* 11, 1633-1644. <https://doi.org/10.5194/hess-11-1633-2007>
- Peixoto, J. P. and Oort, A. H. (1992). *Physics of Climate*, AIP-Press, New York, NY, Springer Verlag, New York Press.
- Pervez, M.S., and Henebry, G.M. (2015). Spatial and seasonal responses of precipitation in the Ganges and Brahmaputra river basins to ENSO and Indian Ocean dipole modes: implications for flooding and drought. *Nat. Hazards Earth Syst. Sci.* 15, 147-162. <https://doi.org/10.5194/nhess-15-147-2015>, 2015.
- Pokam, W.M., Djiotang, L.A.T., and Mkankam, F.K. (2012). Atmospheric water vapor transport and recycling in Equatorial Central Africa through NCEP/NCAR reanalysis data. *Clim. Dynam.* 38, 1715–1729. <https://doi.org/10.1007/s00382-011-1242-7>
- Roxy, M.K., Ritika, K., Terray, P., Murtugudde, R., Ashok, K., and Goswami, B. N. (2015). Drying of Indian subcontinent by rapid Indian Ocean warming and a

- weakening land-sea thermal gradient. *Nature Communications*. 6, 7423, 2015. <http://dx.doi.org/10.1038/ncomms8423>.
- Savenije, H. H. G. (1995a). New definitions for moisture recycling and the relationship with land-use changes in the Sahel. *J. Hydrol.* 167(1–4),57–78, doi:10.1016/0022-1694(94)02632-L.
- Savenije, H. H. G. (1995b). Does moisture feedback affect rainfall significantly?. *Phys. Chem. Earth*. 20(5–6), 507–513, doi:10.1016/S0079-1946(96)00014-6.
- Seibert, P., B. Krüger, and A. Frank. (2001). Parametrisation of convective mixing in a Lagrangian particle dispersion model. Proc. Fifth GLOREAM Workshop, Wengen, Switzerland, EUROTRAC-2, 8 pp.
- Seibert, P., Krüger, B., and Frank, A. (2002). Parametrisation of convective mixing in a Lagrangian particle dispersion model. In: Proceedings of the 5th GLOREAM Workshop, Wengen, Switzerland.
- Seibert, P., and Frank, A. (2004). Source-receptor matrix calculation with a Lagrangian particle dispersion model in backward mode. *Atmos. Chem. Phys.* 4, 51-63. <https://doi.org/10.5194/acp-4-51-2004>
- Sheil, D., and Murdiyarso, D. How Forests Attract Rain: An Examination of a New Hypothesis. *BioScience*, 2009, 59: 341–347. ISSN 0006-3568.
- Sodemann, H., and A. Stohl (2009), Asymmetries in the moisture origin of Antarctic precipitation, *Geophys. Res. Lett.*, 36, L22803, doi: 10.1029/2009GL040242.
- Sodemann, H. (2006). Tropospheric transport of water vapour Lagrangian and Eulerian perspectives. Doctoral Thesis No. 16623. 246p. Institute for Atmospheric and Climate Science (IAC), Swiss Federal Institute of Technology (ETH) Zurich. <https://doi.org/10.3929/ethz-a-005215132>
- Sohoulande Djebou, D.C., and Singh V.P. 2016. Impact of climate change on the hydrologic cycle and implications for soci-ety. *Environment and Social Psychology*, vol.1(1): 36–49. <http://dx.doi.org/10.18063/ESP.2016.01.002>.
- Spinoni, J., Naumann, G., Carrao, H., Barbosa, P., Vogt, J. (2014). World drought frequency, duration, and severity for 1951 – 2010. *Int. J. Climatol.* 34(8), 2792 – 2804.
- Starr, V.P., and Peixoto, J. P. (1958). On the global balance of water vapor and the hydrology of deserts. *Tellus*. 10(2), 189–194.

- Stohl, A., G. Wotawa, P. Seibert, and H. Kromp-Kolb (1995): Interpolation errors in wind fields as a function of spatial and temporal resolution and their impact on different types of kinematic trajectories. *J. Appl. Meteor.* 34, p. 2149-2165.
- Stohl, A., and P. Seibert (1998): Accuracy of trajectories as determined from the conservation of meteorological tracers. *Q. J. Roy. Met. Soc.* 124, p. 1465-1484.
- Stohl, A., Forster, C., Frank, A., Seibert, P., and Wotawa, G. (2005). Technical note: The Lagrangian particle dispersion model FLEXPART version 6.2. *Atmospheric Chemistry and Physics, European Geosciences Union.* 5 (9), 2461-2474. <hal-00295743>.
- Stohl, A., Forster, C., Eckhardt, S., Spichtinger, N., Huntrieser, H., Heland, J., Schlager, H., Wilhelm, S., Arnold, F., and Cooper, O. (2003). A backward modeling study of intercontinental pollution transport using aircraft measurements. *J. Geophys. Res.-Atmos.* 108, 4370. <https://doi.org/10.1029/2002JD002862>
- Stohl, A., Wernli, H., James, P., Bourqui, M., Forster, C., Liniger, M.A., Seibert, P., and Sprenger, M. (2003b). A New Perspective of Stratosphere–Troposphere Exchange. *Bull. Amer. Meteor. Soc.* 84, 1565–1574. <https://doi.org/10.1175/BAMS-84-11-1565>
- Stohl, A. and James, P. (2005). A Lagrangian analysis of the atmospheric branch of the global water cycle. Part II: Moisture transports between the Earth’s ocean basins and river catchments. *J. Hydrometeorol.* 6, 961–984. <https://doi.org/10.1175/JHM470.1>
- Stohl, A., Huntrieser, H., Richter, A., Beirle, S., Cooper, O. R., Eckhardt, S., Forster, C., James, P., Spichtinger, N., Wenig, M., Wagner, T., Burrows, J. P., and Platt, U.: Rapid intercontinental air pollution transport associated with a meteorological bomb, *Atmos. Chem. Phys.*, 3, 969-985, <https://doi.org/10.5194/acp-3-969-2003>, 2003b.
- Stohl A. and James, P. (2004). A Lagrangian analysis of the atmospheric branch of the global water cycle. Part I: Method description, validation, and demonstration for the August 2002 flooding in central Europe. *J. Hydrometeorol.* 5, 656–678. [doi:10.1175/1525-7541\(2004\)005<0656:ALAOTA>2.0.CO;2](https://doi.org/10.1175/1525-7541(2004)005<0656:ALAOTA>2.0.CO;2).
- Sturm, C., Zhang, Q., and Noone, D. (2010). An introduction to stable water isotopes in climate models: benefits of forward proxy modelling for paleoclimatology. *Clim. Past.* 6, 115-129. <https://doi.org/10.5194/cp-6-115-2010>.
- Syvitski, J.P.M., Cohen, S., Kettner, A.J., Brakenridge, G.R. (2014). How important and different are tropical rivers? - An overview. *Geomorphology.* 227, 5-17.

- Sheffield J., E. F. Wood, and M. L. Roderick (2012), Little change in global drought over the past 60 years, *Nature*, 491, 435–440, doi:10.1038/nature11575.
- Sushant, S., Balasubrami, K., Kumaraswamy, K. (2015). Spatio-temporal Analysis of Rainfall Distribution and Variability in the Twentieth Century, Over the Cauvery Basin, South India. In: Environmental Management of River Basin Ecosystems. Edit: Mu Ramkumar, K Kumaraswamy, R. Mohanraj. Springer Earth System Sciences, doi: 10.1007/978-3-319-13425-3\_2.
- Tavares, J.P.N. Interaction between vegetation and the atmosphere in cloud and rain formation in the Amazon: A review. *Estudos Avançados*. 2012, 26, 74, 219-227.
- Trewin, B. The climates of the Tropics and how they are changing. In: State of the Tropics. 2014, 39 – 52. Available online: <http://stateofthetropics.org/wp-content/uploads/Essay-1-Trewin.pdf> (accessed on 30 May 2018).
- Trenberth, K.E., Smith, L., Qian, T., Dai, A., and Fasullo, J. (2007). Estimates of the global water budget and its annual cycle using observational and model data. *J. Hydrometeorol.* 8, 758–769. doi:10.1175/JHM600.1
- Trenberth, K. E., J. T. Fasullo, and J. Mackaro (2011), Atmospheric moisture transports from ocean to land and global energy flows in reanalyses, *J. Clim.*, 24, 4907–4924, doi:10.1175/2011JCLI4171.1.
- Tsakiris, G., and Vangelis, H. (2005). Establishing a drought index incorporating evapotranspiration. *European Water*. 9(10), 3–11.
- Tschakert, P., Sagoe, R., Ofori-Darko, G., Nii Codjoe, S. Floods in the Sahel: an analysis of anomalies, memory, and anticipatory learning. *Climatic Change* (2010) 103: 471. <https://doi.org/10.1007/s10584-009-9776-y>.
- Van Loon, A.F. (2015). Hydrological drought explained. *Wiley Interdiscip. Rev. Water*. 2(4), 359–392. <https://doi.org/10.1002/wat2.1085>
- van der Ent, R. J., H. H. G. Savenije, B. Schaefli, and S. C. Steele-Dunne (2010), Origin and fate of atmospheric moisture over continents, *Water Resour. Res.*, 46, W09525, doi: 10.1029/2010WR009127.
- van der Ent, R.J., and Tuinenburg, O.A. (2017). The residence time of water in the atmosphere revisited. *Hydrol. Earth Syst. Sci.*, 21, 779-790, <https://doi.org/10.5194/hess-21-779-2017>, 2017.

- Vicente-Serrano, S.M., Beguería, S., and López-Moreno, J.I. (2010) A Multiscalar Drought Index Sensitive to Global Warming: The Standardized Precipitation Evapotranspiration Index. *J. Climate*. 23, 1696–1718, <https://doi.org/10.1175/2009JCLI2909.1>
- Vicente-Serrano, S.M., López-Moreno, J.I., Santiago, B., Lorenzo-Lacruz, J., Azorin-Molina, C., and Morán-Tejeda, E. (2012). Accurate computation of a streamflow drought index. *J. Hydrol. Eng.* 17, 318–332
- Wang, B., Liu, J., Kim, H.J., Webster, P.J., Yim, S.Y. (2012). Recent change of the global monsoon precipitation (1979–2008). *Clim Dyn.* 39, 1123–1135.
- Wernli, H. (1997). A Lagrangian-based analysis of extratropical cyclones, II, A detailed case study. *Q. J. R. Meteorol. Soc.* 123, 1677–1706. doi:10.1002/qj.49712354211.
- WMO Report 385. International Glossary of Hydrology. 2012. ISBN 978-92-63-03385-8.
- WMO & GWP (2016). Handbook of Drought Indicators and Indices (M. Svoboda and B.A. Fuchs). Integrated Drought Management Programme (IDMP), Integrated Drought Management Tools and Guidelines Series 2. Geneva. I S B N 97 8 - 9 2- 63 -1117 3 – 9.
- Wohl, E., Barros, A., Brunsell, N., Chappell, N. A., Coe, M., Giambelluca, T.: The hydrology of the humid tropics. *Nature Climate Change.*, 2012, 2(9), 655, doi: 10.1038/nclimate1556.
- Wright JS, Fu R, Worden JR, Chakraborty S, Clinton NE, Risi C, Sun Y, Yin L. A rainforest initiated wet season onset over the southern Amazon. *Proceedings of the National Academy of Sciences.* 114, 32, 8481-8486, 2017.
- Zaidman, M.D., Rees, H.G., and Young, A.R. (2002). Spatio-temporal development of streamflow droughts in north-west Europe. *Hydrol. Earth Syst. Sci.* 6, 733-751, <https://doi.org/10.5194/hess-6-733-2002>
- Zargar, A., Saquid, R., Naser, B., and Khan, F.I. (2011). A review of drought indices. *Environ. Rev.* 19, 333–349.
- Zeng, N. 2003: Drought in the Sahel *Science* 302 999–1000. *Science*, Vol. 302, Issue 5647, pp. 999-1000, DOI: 10.1126/science.1090849.

- Zheng, X. and E.A. Eltahir, 1998: The Role of Vegetation in the Dynamics of West African Monsoons. *J. Climate*, 11, 2078–2096, <https://doi.org/10.1175/1520-0442-11.8.2078>.
- Zhu, Y., Wang, W., Singh, V.P., and Liu, Y. (2016). Combined use of meteorological drought indices at multi-time scales for improving hydrological drought detection. *Sci Total Environ.* 571, 1058-68. doi:10.1016/j.scitotenv.2016.07.096